New Main Group and Rare Earth Complexes and Their Applications in the Ring-Opening Polymerisation of Cyclic Esters

Michael Gregory Cushion MSci



Thesis submitted to the University of Oxford for the degree of Doctor of Philosophy, July 2011.

The work described in this Thesis was carried out in the Chemistry Research Laboratory, University of Oxford from October 2007 to July 2011 under the supervision of Professor Philip Mountford. All work is my own unless stated to the contrary, and has not previously been submitted for any degree at this or any other university.

Michael Gregory Cushion

July 2011

Abstract

Michael Gregory Cushion Trinity 2011

Merton College D.Phil. Thesis

This Thesis describes the synthesis and characterisation of new Main Group and Rare Earth alkyl, amide, alkoxide and borohydride complexes and their use as catalysts for the ring-opening polymerisation (ROP) of ε-caprolactone and *rac*-lactide.

Chapter 1 introduces ROP from an industrial and academic perspective, as well as polymer characterisation techniques. A literature review is given, with an emphasis placed on Main Group catalysts.

Chapter 2 describes the synthesis and characterisation of new homo- and hetero-scorpionate Main Group complexes. An introduction to homo- and hetero-scorpionate ligands is given, as well as a discussion of the ε-caprolactone and *rac*-lactide ROP activity displayed by the new complexes.

Chapter 3 describes the synthesis and characterisation of new neutral and cationic Main Group borohydride complexes supported by the tris(pyrazolyl)methane and tris(pyrazolyl)hydroborate ligands. A review of borohydride complexes is also given. The ε-caprolactone and *rac*-lactide ROP activity shown by the complexes presented is also discussed.

Chapter 4 describes the synthesis and characterisation of new mono- and di-cationic yttrium complexes supported by the tris(pyrazolyl)methane and triazacyclononane ligands. An introduction to the synthesis of neutral and cationic Rare Earth complexes is given. An overview of immortal ROP is also provided. The activity of the new complexes towards the immortal ROP of *rac*-lactide is also discussed.

Chapter 5 contains experimental details and characterising data for the new complexes reported in this thesis.

CD Appendix contains .cif files for all of the new crystallographically characterised complexes.

Contents

	Declaration	i
	Abstract	ii
	Contents	iii
	Acknowledgements	vi
	Abbreviations	vii
	Notes	x
Chapter One - Introduction		1
1.0	Outline	2
1.1	Background	2
1.2	ROP Mechanisms	4
1.3	Polymer Description	6
1.4	Living Polymerisation	7
1.5	Polymer Analysis	8
1.5.1	NMR spectroscopy	8
1.5.2	Gel Permeation Chromatography	9
1.5.3	MALDI-ToF MS	10
1.6	Stereocontrol of lactide polymerisation	11
1.7	Literature review	15
1.7.1	Industrial ROP and the Development of Simple Systems	16
1.7.2	Cyclopentadienyl Based ROP Initiators	18
1.7.3	ROP Initiators with O-Donor Supporting Ligands	19
1.7.4	ROP Initiators with N,O-Donor Supporting Ligands	21
1.7.5	ROP initiators with N-donor supporting ligands	23
1.8	Summary	26
1.9	Aims and Outlook	26
2.0	References	26
Chapter Two - New Group 2 and 12 Scorpionate complexes and their activity towards the ROP of ε-caprolactone and *rac*-lactide		33
2.0	Overview	34
2.1	Introduction	34

2.2	Synthesis of Group 2 tris(pyrazolyl)meth*ane* and tris(pyrazolyl)methan*ide* complexes	38
2.3	Synthesis of Group 12 tris(pyrazolyl)methan*ide* complexes	51
2.4	Synthesis of heteroleptic zwitterionic sandwich complexes	55
2.5	Synthesis of Group 2 heteroscorpionate complexes	59
2.6	Polymerisation studies: ROP of ε-CL	61
2.7	Polymerisation studies: ROP of *rac*-LA	64
2.8	Summary and Conclusions	69
2.9	References	70

Chapter Three - Cationic and charge neutral Main Group tetrahydroborate complexes and their use in the controlled ROP of ε-caprolactone and *rac*-lactide 74

3.0	Overview	75
3.1	Introduction	75
3.2	Synthesis of cationic and charge-neutral main group tetrahydroborate tetrahydroborate complexes	82
3.3	Polymerisation studies: ROP of ε-CL	90
3.4	Polymerisation studies: ROP of *rac*-LA	93
3.5	Summary and Conclusions	111
3.6	References	112

Chapter Four – Cationic Rare Earth alkyl and alkoxide complexes and their use in the immortal ROP of *rac*-lactide 115

4.0	Overview	116
4.1	Introduction	116
4.1.1	Neutral Rare Earth Complexes	117
4.1.2	Cationic Rare Earth Complexes	119
4.1.3	Cationic ROP Catalysts	122
4.1.4	Immortal ROP	123
4.2	Synthesis of mono- and di-cationic yttrium alkyl and alkoxide complexes	127
4.3	Polymerisation studies: ROP of *rac*-LA	131

4.3.1 ROP of *rac*-LA using 24-BPh_4 and 30-$[BPh_4]_2$ 132
4.3.2 ROP of *rac*-LA using 25-$[BPh_4]_2$ and 26-$[BPh_4]_2$ 134
4.3.3 Mechanistic Studies 138
4.4 Summary and Conclusions 144
4.5 References 145

Chapter Five – Experimental details and characterising data 149

5.0 General methods and instrumentation 150
5.1 Literature preparations 151
5.2 Experimental details and characterisation data for Chapter Two 151
5.3 Experimental details and characterisation data for Chapter Three 159
5.4 Experimental details and characterisation data for Chapter Four 162
5.5 Polymerisation procedures for Chapters Two, Three and Four 167
5.6 X-ray data collection and processing parameters 168
5.7 References 174

CD Appendix

Acknowledgements

Firstly I would like to thank my supervisor, Professor Philip Mountford, for his help and support throughout the course of my studies. I've learned a lot and this has provided me with a solid foundation to build on. Also, don't worry, I'll be (relatively) clean-shaven for my viva!

I also express gratitude to the rest of the Mountford group for being pleasant to work with, and I wish them the best for the future. Thanks in particular to Matt, Lawrence, Liban, Richard and Dr. Andrew Schwarz for helping to proof read my Chapters and making many useful suggestions. Thanks must also go to Alexander Kilpatrick for being an excellent Part II student and a good guy to work with. Unfortunately I haven't been able to discuss any of your project since you worked on Chromium! We all know Calcium is a much better metal to work on (despite what Chemistry Top Trumps might say). Also, good luck to Guun with the rest of your DPhil. Keep on ROPin' in the free world.

I would also like to thank my contemporary, Robert 'Coops' Cooper, for being a good friend and also for many entertaining nights out in Oxford. It was good to have somebody else around that started at the same time as me, albeit under a different supervisor. I'm also grateful to Colin Sparrow and Dr Nick Rees for their help with mass spectroscopy and NMR. Dr Amber L. Thompson and Dr David J. Watkin also deserve special mention for helping me to collect data for many crystals.

Additionally, I am very grateful to the support provided to me throughout my life by my family and close friends at home. It hasn't always been easy but the comfort you have provided me has given me inspiration through the difficult times. That's not to say there haven't been good times too, and I'm also lucky to have shared these with you. I look forward to sharing many more. Finally, thanks must also go to Holly for everything recently. With any luck I'll be a doctor soon too.

Abbreviations

General

Å	Ångstrom
av.	average
ca.	*circa*, about
calcd	calculated
^{o}	degrees
^{o}C	degrees Celsius
d	day(s)
g	gram(s)
GPC	gel permeation chromatography
h	hour(s)
K	Kelvin
k_i	rate constant of initiation
k_p	rate constant of propagation
min	minute(s)
s	second(s)
rt	room temperature

Chemical

Ar	aryl group
Bn	benzyl
Cp	C_5H_5
Cp*	C_5Me_5
Cy	cyclohexyl
D-lactide	(*R*,*R*)-cis-3,6-dimethyl-1,4-dioxane-2,5-dione
E	generic chalcogen atom
Et	ethyl
^{i}Bu	*iso*-butyl
^{i}Pr	*iso*-propyl
^{i}PrOH	isopropyl alcohol
L	a supporting ligand (set)
L-lactide	(*S*,*S*)-cis-3,6-dimethyl-1,4-dioxane-2,5-dione
Me	methyl

Mes	2,4,6-$C_6H_2Me_3$
meso- lactide	(*R*,*S*)-cis-3,6-dimethyl-1,4-dioxane-2,5-dione
M_n	number average molecular weight
M_p	peak molecular weight
M-OR	metal alkoxide
M_w	weight average molecular weight
^{n}Bu	*n*-butyl
PDI	poly dispersity index
PET or PETE	polyethylene terephthalate
Ph	phenyl
P_m	probability of *meso*- linkages
PLA	poly(lactic acid)
PCL	poly(ε-caprolactone)
P_r	probability of racemic linkages
p-Tol	4-C_6H_4Me
py	pyridine
pz	pyrazolyl
R	generic aryl or alkyl
rac-lactide	a racemic mixture of *D*- and *L*-lactide
ROP	ring-opening polymerisation
$Sn(Oct)_2$	Tin octanoate
^{t}Bu	*tert*-butyl
THF	tetrahydrofuran
X	Generic halide

Mass Spectrometry

EI	electron impact
FI	field ionisation
m/z	mass to charge ratio
MS	mass spectrometry
MALDI-ToF MS	matrix-assisted laser desorption/ionization - time of flight mass spectrometry

Nuclear Magnetic Resonance Spectroscopy

$^{13}C\{^{1}H\}$	proton-decoupled ^{13}C
$^{11}B\{^{1}H\}$	proton-decoupled ^{11}B
app.	apparent
br	broad
COSY	correlation spectroscopy
d	doublet
HETCOR	heteronuclear correlation
HMBC	heteronuclear multiple bond correlation
HMQC	heteronuclear single quantum correlation
i	*ipso*
J	coupling constant
m	*meta*
m	multiplet
NMR	nuclear magnetic resonance
nOe	nuclear Overhauser effect
o	*ortho*
p	*para*
ppm	parts per million
q	quartet
ROESY	rotating-frame nuclear Overhauser Effect spectroscopy
s	singlet
sept	septet
t	triplet
δ	chemical shift in ppm

Infrared Spectroscopy

br	broad
FT-IR	fourier transform infrared red
IR	infrared red
m	medium
s	strong
w	weak
ν	frequency

Notes about the numbering of compounds described in this Thesis

Literature compounds described in this Thesis are numbered **1.x**, **2.x**, **3.x**, **4.x** according to the Chapter in which they first occur. The new compounds described in this Thesis are numbered **1** – **30**.

Chapter One

Introduction

1.0 Outline

This Chapter provides an introduction to the ring-opening polymerisation (ROP) of cyclic esters. Discussion will include an overview of the industrial and academic research carried out in this area. An emphasis on main group and rare earth metal catalysed ROP will be placed, with notable exceptions from other areas of the periodic table also discussed. Catalysts employing cyclopentadienyl ligands will be discussed, with a progression to post-metallocene systems, most specifically systems employing O-, N- and mixed N,O-donor ancillary ligands. An introduction to the analytical techniques used in polymer characterisation will also be presented.

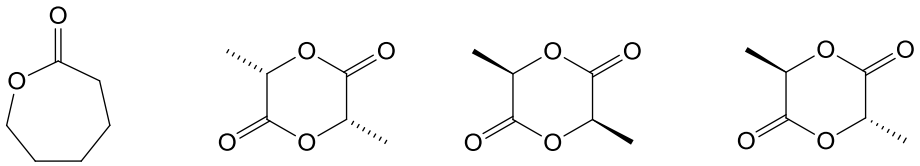
1.1 Background

Polymers derived from petrochemical resources have had a tremendous industrial impact in modern times.[1] Despite the numerous advantages presented by these materials, there are two major drawbacks. Firstly, the use of non-renewable oil based resources in their production, and secondly their non-biodegradable nature.[1, 2] As a result of this and the growing cost of crude oil, significant attention over the past three decades has turned to the synthesis of biocompatible polymers from renewable resources.

Of the extensive range of biodegradable polymers known, linear aliphatic polyesters have been the most widely studied.[1-6] Arguably the most prominent examples of this emerging class of polyesters are poly(ε-caprolactone) (PCL), poly(lactide) (PLA) and poly(glycolide) (PGA).[1] These have attracted considerable recent attention due to their biomedical and pharmaceutical applications, for example as drug delivery agents and post-operative stitches and pins.[4] PLA is also notably produced as a commodity thermoplastic in the packaging industry.[3] The remainder of this Thesis focuses on PCL and PLA.

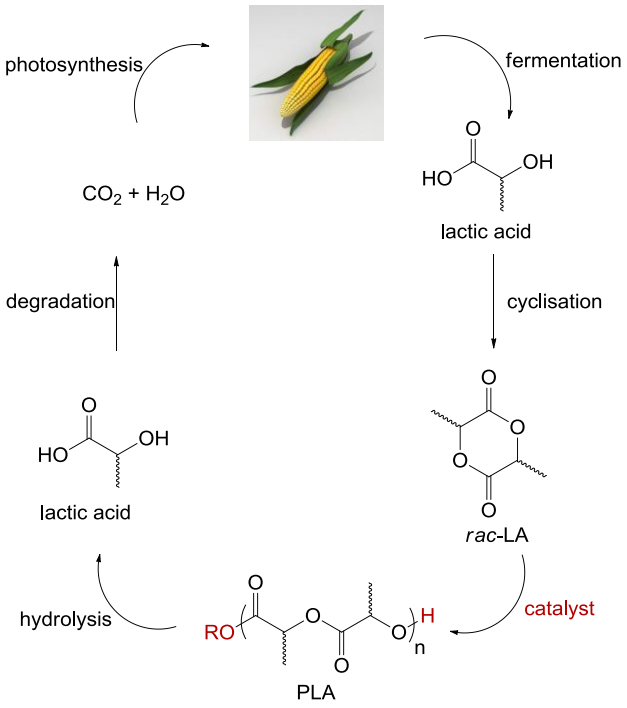
The most common and efficient method for the preparation of PCL and PLA is by the ROP of the parent cyclic monomers (the structures of which are shown in Figure 1.0). This offers a higher degree of control in terms of molecular weight and molecular weight distribution (M_w/M_n) than traditional step-growth processes (i.e. polycondensation reactions) of the appropriate α-hydroxy acids.[3]

Figure 1.0. The structures of ε-caprolactone (ε-CL) and lactide (LA).



In the case of PLA a variety of stereoregular polymer microstructures are possible, each with their own specific properties (this is discussed further in Section 1.6).[4] Therefore, interest has focussed particularly on the production of PLA, which is derived from corn, sugar beet and other annually renewable resources.[5] It should be noted at this point that ε-CL is prepared industrially by the Baeyer-Villiger oxidation of cyclohexanone with peroxyacetic acid (i.e. from non-renewable resources).[7] However, despite this, PCL is biodegradable. Millions of tonnes of cyclohexanone are produced annually (by the oxidation of cyclohexane), mainly as a precursor to nylon. The most common use of PCL is in the manufacture of speciality polyurethanes. PCL imparts good water, oil, solvent and chlorine resistance to the polyurethane produced.[7] The life cycle of PLA is shown in Figure 1.1.

Figure 1.1. The life cycle of PLA. R = initiating group (e.g. alkyl, amide, alkoxide) from the catalyst.

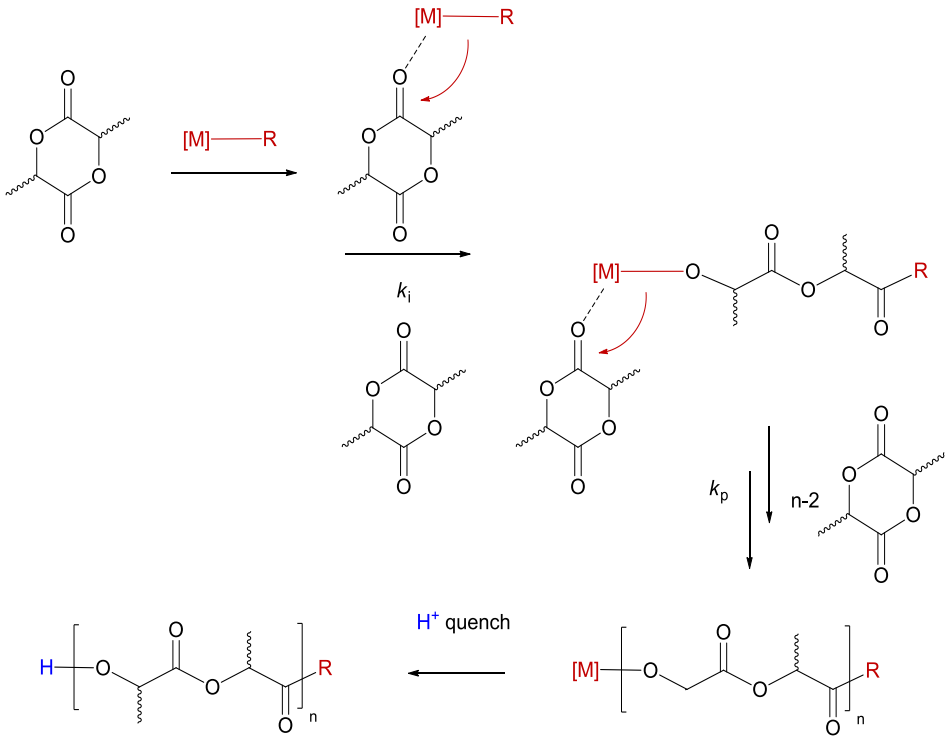


1.2 ROP Mechanisms

There are a number of known mechanisms for the ROP of CL and LA, these include: coordination-insertion, activated monomer (a description of which is given in Chapter 4), anionic, cationic, organo-catalytic and enzymatic. These are the subject of recent reviews in the area.[1-6] This Thesis focuses on coordination-insertion ROP, since this pathway is the most widely present in ROP catalysed by Main Group, transition metal and lanthanide metal complexes.[3]

The coordination-insertion mechanism proceeds by three main steps (Figure 1.2). Firstly, the carbonyl oxygen atom of the monomer coordinates to a Lewis acidic metal centre, making the carbonyl carbon more prone to nucleophilic attack. Secondly, insertion of the monomer into the M-R group of the initiator (R = typically an alkyl, amide or alkoxide group) occurs via nucleophilic attack of the R group on the carbonyl carbon of the monomer. Finally, acyl oxygen bond cleavage occurs. The coordination of subsequent monomers leads to propagation and the continuation of the cycle. Protolytic work-up liberates the polymer from the metal centre.

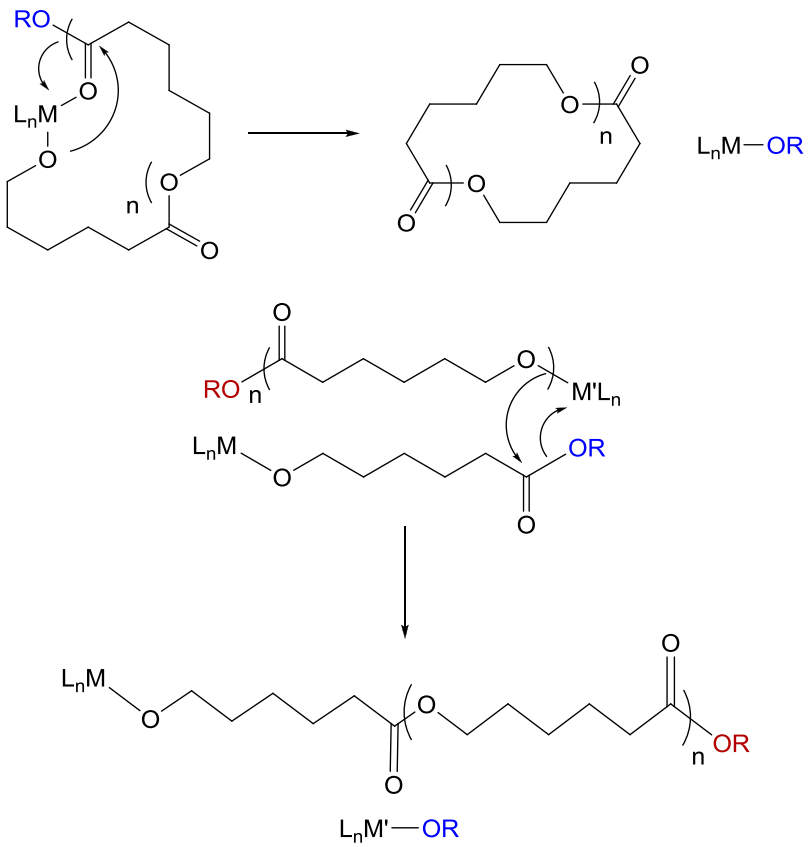
Figure 1.2. Coordination-insertion mechanism (using LA as an example). R = initiating group, e.g. alkyl, amide or alkoxide and k_i and k_p are the respective rate constants for initiation and propagation.



The majority of catalysts used for the ROP of cyclic esters suffer from a number of detrimental issues. These include inter- and intra-molecular transesterification (Figure 1.3), termination/ chain transfer reactions and a slow rate of initiation (relative to the rate of propagation). During intramolecular transesterification ('back-biting'), the non-metal bound end of growing polymer chain coordinates to the metal centre, leading to insertion and the formation of cyclic PLA units, also leading to the generation of an active species. This often leads to broad molecular weight distributions and shorter than expected polymer chains, particularly in the later stages of the polymerisation.

During intermolecular transesterification, the non-metal bound end of a growing polymer chain coordinates to a different metal centre of an adjacent polymer chain, giving rise to chain redistribution. This process also leads to the broadening of molecular weight distributions and poor control over the length of polymer chains. Similarly the presence of residual protic impurities can induce early termination reactions, and/or chain transfer.

Figure 1.3. Transesterification side reactions. Top: Intramolecular transesterification. Bottom: Intermolecular transesterification.



The degree of transesterification during a polymerisation is highly dependent on the Lewis acidity of the metal present in the catalyst, which in turn is influenced by the ancillary ligand(s) present and the nature of the initiating group.[1, 4, 8] For example Spassky *et al*. synthesised a family of Schiff-base supported aluminium complexes, finding that Schiff-base ligands with electron withdrawing substituents on the backbone produced catalysts with a greater activity and lower degree of transesterification.[9] It was proposed that the electron withdrawing substituents served to enhance the electrophilicity of the metal centre, and/or increase the polarisation of the initiating/ propagating Al-X bond.[4, 9]

Also, it was found that transesterification can occur from the onset of polymerisations with $Sn(Oct)_2$ (M_w/M_n = 2.0), whereas the less active $Al(O^iPr)_3$ showed significantly lower degrees of transesterification (M_w/M_n = 1.5) throughout the polymerisation process.[1, 10, 11] The occurrence of post-polymerisation transesterification is also possible, where the polymerisation has reached a high monomer conversion and is not quenched sufficiently quickly. This process is evident by a shortening of polymer chains and increasing molecular weight distribution at high conversions.[25]

1.3 Polymer Description

Due to the aforementioned commonly occurring side reactions, it is extremely rare for a polymer to contain chains of uniform length. For this reason, polymers are described by an average molecular weight, calculated as a number (M_n) or weight (M_w) average, alongside the distribution of molecular weights (M_w/M_n), most frequently referred to as the polydispersity index (PDI). M_n is defined by Equation 1.0, where N_i is the number of polymers having a molar mass M_i.

$$M_n = \frac{\sum N_i . M_i}{\sum N_i} \qquad \textbf{Equation 1.0}$$

Similarly, M_w is given by Equation 1.1, where W_i is the mass of polymers having a molar mass M_i.

$$M_w = \frac{\sum W_i . M_i}{\sum W_i} \qquad \textbf{Equation 1.1}$$

The PDI is given by the ratio of M_w/M_n, shown in Equation 1.2.

$$\mathrm{PDI} = \frac{M_w}{M_n} \qquad \textbf{Equation 1.2}$$

In the field of ROP, the M_n and PDI of a given polymer are the most frequently quoted values. In a perfect system the polymer chains are of uniform length and have identical M_n and M_w values, and therefore have a PDI of 1.0. However, in practice the length of polymer chains is given by a Gaussian distribution (largely due to transesterification and slow rates of initiation relative to propagation), with a bias of M_w towards higher values. Therefore, experimentally, PDI are always greater than 1.0, even for extremely well controlled systems. It follows that the further a PDI value deviates from 1.0 for a given system, the more extensive the transesterification reactions are, and/or the less well balanced the ratio of the rate of initiation to the rate of propagation is.

Generally speaking, PDI values of 1.0-1.2 are considered narrow, 1.2-1.8 moderate and 1.8 and above broad. Additionally, a comparison of experimental M_n values with calculated (based on the percentage monomer conversion) M_n is usually carried out. Thus, well controlled polymerisations usually produce polymers with narrow (1.0-1.2) PDIs and a close agreement between expected and calculated M_n values. Generally, M_n *vs* monomer conversion is monitored throughout a polymerisation and/or M_n is measured for a range of $[\text{monomer}]_0[\text{catalyst}]_0$ ratios. This is important for separating out the different (and sometimes opposing) effects of k_i/k_p or k_{tr}/k_p relative magnitudes (where k_{tr} is the rate of transesterification). These are the criteria used for the discussion of the performance of the catalysts discussed in this thesis.

1.4 Living polymerisation

'Living' polymerisations are defined by the following set of characteristics: A linear increase of M_n with monomer conversion, narrow PDI values (due to minimal transesterification side reactions or their complete absence) and the ability to undergo sequential monomer addition (i.e. the ability to form block co-polymers).[5, 6, 12] The narrow PDI values in living systems are largely due to high k_i/k_p and k_p/k_{tr} ratios.[6] Excellent examples of catalysts for living ROP are given in Chapters 3 and 4, a good example for instance is shown in Figure 3.11 in Chapter 3. In the case of highly active systems (i.e. 80-100% monomer conversion in under 2 minutes), it may not be possible to determine kinetic polymerisation profiles. In these cases, evidence for a

living polymerisation process often comes by the observation of a linear increase in M_n from a range of $[monomer]_0$:$[catalyst]_0$ ratios. A good example of this can be seen in Chapter 3 (Figure 3.8). Deviations from the aforementioned criteria of a living polymerisation are generally a consequence of a slow rate of initiation compared with propagation, and/ or extensive transesterification and termination reactions competing with propagation.

Ideally, living polymerisation leads to the production of as many growing polymer chains as there are number of initiating groups. A special case of living polymerisation exists in immortal polymerisation, where it is possible to generate more growing polymer chains than there are initiating groups. This is achieved by the addition of chain transfer reagents to the polymerisation mixture.[3] This is discussed in detail in Chapter 4.

1.5 Polymer Analysis

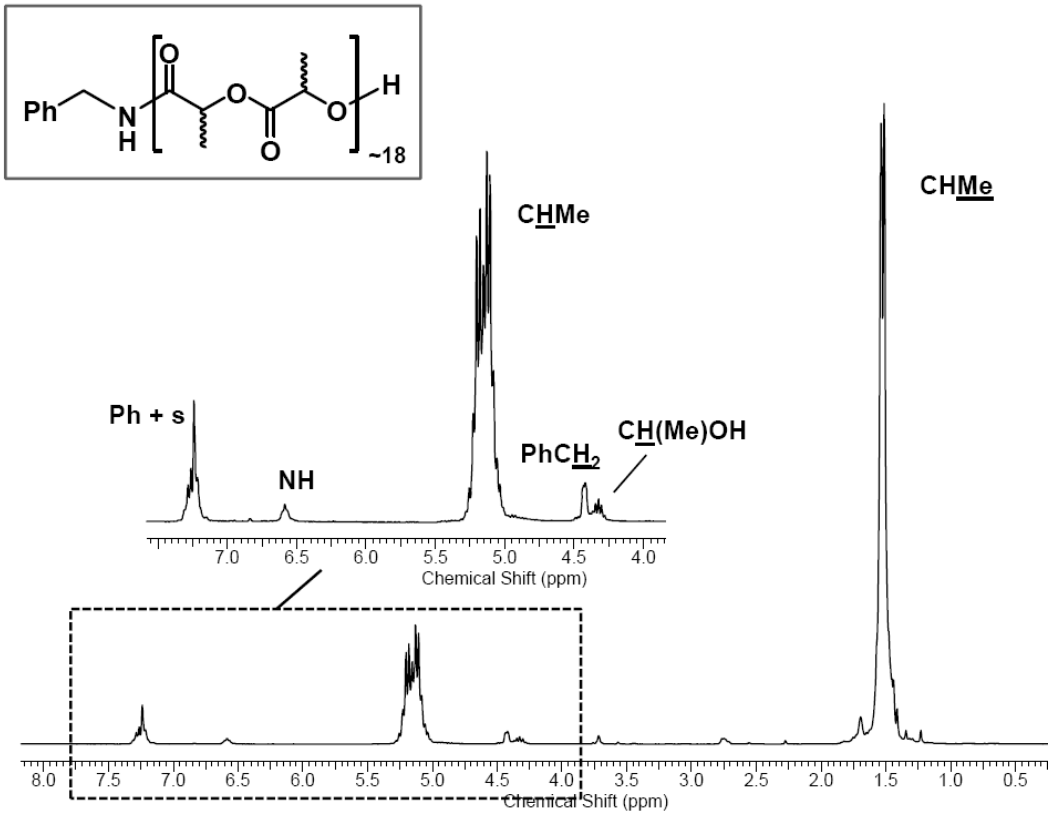
Polyesters such as PCL and PLA are characterised by a number of analytical techniques. These include: ^{1}H and ^{13}C NMR spectroscopy, gel permeation chromatography (GPC) and matrix-assisted laser desorption/ ionisation time-of-flight mass spectrometry (MALDI-ToF MS). NMR techniques generally provide information on polymer end groups (and tacticity in the case of PLA), and can also be used to determine polymer M_n (generally for M_n values less than *ca*. 2,000 g mol^{-1}) and the extent of monomer conversion. GPC analysis is used to quanitify the M_n and PDI of a given polymer sample. MALDI-ToF MS is used to determine polymer end-groups and as evidence for the presence (or lack of) transesterification. In most cases, the combination of these techniques is used to analyse polymers and investigate the polymerisation process. In some cases, DSC techniques are also used to determine the glass transition and melting points of the polymer, providing a measure of polymer crystallinity.

1.5.1 NMR Spectroscopy

In many cases, especially where high molecular weight polymers are produced, it is not possible to determine the end-group of a polymer by ^{1}H NMR. This is due to the extremely high proportion of polymer backbone resonances relative to those corresponding to the end-groups. However, using a low $[monomer]_0$:$[catalyst]_0$ ratio

often provides a solution to this (since lower ratios generally produce polymer of lower molecular weight). An example of a PLA sample with BnNH-capped end groups is shown in Figure 1.4. Additionally, in this case the M_n of the polymer sample has been determined by ^{1}H NMR (2690 g mol^{-1}). This is in excellent agreement to that measured by GPC (2660 g mol^{-1}).[13] A further drawback to this technique is that cyclic polymer backbone resonances overlap with those of linear polymer backbones.[14, 15] For this reason, it is not possible to determine the degree of transesterification using NMR techniques.

Figure 1.4. ^{1}H NMR spectrum ($CDCl_3$) of BnNH-capped PLA.[13]



1.5.2 Gel Permeation Chromatography

In this technique, polymer samples are dissolved in an organic solvent and passed through a styrene divinyl benzene copolymer column. The column is filled with porous beads of various sizes and these serve to separate the polymer chains by their hydrodynamic radius, a measure of the dynamic volume of a polymer chain based on its solution behaviour, i.e. its interactions with solvent molecules. Shorter length chains enter the pores and their path through the column is increased, whereas longer

chains pass through the column along a shorter path due to their lower degree of interaction with the pores. Therefore, shorter polymer chains have a greater retention time than longer chains. A normal distribution results and this allows a measurement of M_n, M_w and PDI.

The instrument is calibrated against linear polystyrene samples of known molecular weight and PDI. However, the hydrodynamic radius of polystyrene is very different to that of polyesters (polar polymers). Therefore, a polystyrene and polyester sample with the same M_n would have different retention times (and therefore different measured M_n values). This problem is solved by application of the appropriate Mark-Houwink corrections (K and α) for a given polymer. These constants are specific to each polymer class and so, for example, are different for PCL and PLA.[16]

The absolute molecular weight of a polymer is defined by Equation 1.3, which relates the intrinsic viscosity at infinite dilution, [η], and the molecular weight of the given polymer.

$$[\eta] = \mathrm{K}.\mathrm{M}^{\alpha} \qquad \textbf{Equation 1.3}$$

The Mark-Houwink corrections are experimentally determined by a plot of log[η] against log(M) over a large molecular weight range. Clearly, these are solvent and temperature specific. The GPC measurements reported in this Thesis were obtained by analysis in THF at 30 °C, with the appropriate corrections as previously determined for PCL[17] and PLA[18] after calibration against polystyrene standards.

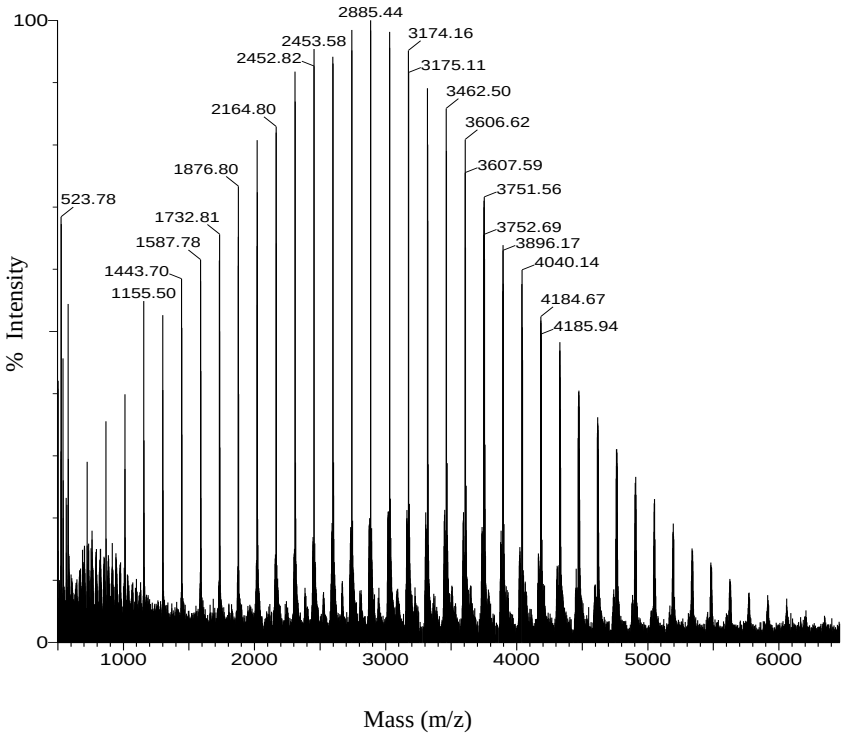
Whist GPC is an essential tool in polymer analysis for linear polymer chains, cyclic polymer units are not accurately described. Additionally, some examples in ROP literature report GPC data having not applied the Mark-Houwink corrections. This can make definitive comparisons between research originating from different origins difficult.

1.5.3 MALDI-ToF MS

In MALDI-ToF MS, polymer chains are embedded in a protective matrix, for example crystalline 4-hydroxy-3-methoxy-cinnamic acid.[19] A laser beam is then focussed on the matrix and this is ionised. The matrix then transfers some of its energy to the embedded polymer. Through this process, the polymer sample is energetically excited

but shielded from the full energy of the laser (preventing unwanted fragmentation). An added ion (for MALDI-ToF MS results in this thesis K^+) binds with the polymer molecules, forming $[polymer\text{-}K]^+$ ions. These ions then pass through a time-of-flight spectrometer where they are resolved by their mass-to-charge ratio. MALDI-ToF is used in polymer analysis as traditional vaporisation techniques used in mass spectrometry lead to unwanted ionisation and fragmentation of the polymer. An example MALDI-ToF MS spectrum of BnNH-capped PLA is shown in Figure 1.5. Also notable is the separation of peaks (144 *m*/z), which is characteristic of minimal transesterification. Contrastingly, MALDI-ToF-MS spectra from systems with significant transesterification show a peak separation of 72 *m*/*z*.

Figure 1.5. MALDI-ToF-MS spectrum of the BnNH-capped PLA. The cationisation agent used was potassium trifluoroacetate. The peak at *m/z* = 2885.4 corresponds to $[BnNH\text{-}[LA]_{14}\text{-}H + K]^+$.[13]



1.6 Stereocontrol of lactide polymerisation

Lactide exists as three diastereomers, *L*-, *D*- and *meso*-LA (see Figures 1.0 and 1.6). The epimerisation of naturally occurring *L*-LA, and subsequent separation, leads to the isolation of *D*- and *meso*-LA. The enantio-pure isomers are available commercially either as *rac*-LA (a racemic mixture) or as single enantiomers.[20] As such, there is a

range of ordered polymer microstructures (Figure 1.6). The controlled ROP of either *L*- or *D*-LA (in the absence of epimerisation), results in isotactic PLA in which all of the sterocentres are aligned along the same side of the polymer chain.[20] The ROP of *rac*-LA or *meso*-LA leads to a wider range of microstructures such as heterotactic (doubly alternating sterocentres) and isotactic PLA, in the case of *rac*-LA, and syndiotactic PLA (singly alternating sterocentres) in the case of *meso*-LA. Atactic PLA, with no ordered sterocentres, arises from epimerisation and/or a poor degree of control over tacticity.

Figure 1.6. Lactide stereoisomers and PLA microstructures.[21]

The material originally presented here is not currently available in ORA

Stereocontrol over the ROP process is important as it has a strong influence of the properties of the polymer. For example atactic PLA is amorphous and has the lowest melting point of the possible PLA microstructures.[6] Isotactic PLA is also an important target since it is highly crystalline, has excellent mechanical properties and a slow rate

of degradation. Additionally, a mixture of co-crystallised isotactic *L*-PLA and *D*-PLA has different bulk properties to that of either polymer on its own.[2] For example, this mixed PLA has a melting point up to 230 °C, approximately 50 °C higher than either *L*-PLA or *D*-PLA (heterotactic PLA has a melting point of 130 °C).[22] Therefore the best LA catalysts possess an ability to produce PLA with a degree of stereocontrol as well as the attributes listed for a good living polymerisation catalyst, for example a high k_i/k_p ratio (see also Section 1.4). Other desirable qualities include low cost and toxicity as well as minimal colour and odour.[2] In recent years, a number of such catalysts have been discovered and are the topic of many excellent reviews.[1-6] The most widely studied monomer of LA is *rac*-LA, due to its widespread availability and wider range of possible PLA microstructures.

The two methods used for the synthesis of stereoregular PLA using homogenous ROP catalysts are chain-end control and enantiomorphic site control. Chain-end control arises when the stereocentre of the last inserted monomer influences the stereochemistry of the next monomer to undergo addition. This usually occurs using achiral catalysts, generally with a significant degree of steric bulk around the metal centre. Chain-end control typically accounts for heterotactic PLA,[13, 23-27] although in some cases isotactic PLA has also been produced.[28-30] Conversely, enantiomorphic site control is induced by the chirality of the catalyst where preferential differentiation of monomer stereocentres occurs. Using such racemic systems it is possible to synthesise isotactic PLA from *rac*-LA[31-33] and syndiotactic PLA from *meso*-LA.[34, 35]

The microstructure of PLA is determined by $^{13}C\{^1H\}$ and homodecoupled ^1H NMR spectroscopy at the tetrad level and the conclusive assignments were determined by Hillmyer and Munson (Figure 1.7).[36] Homonuclear decoupling of the methyl signals of PLA decouples the methyl and methine signals of the polymer. This results in a set of singlet resonances in the range 5.15-5.25 ppm.[20] In Figure 1.7, and frequently elsewhere, '*i*' denotes and isotactic link between adjacent stereocentres (i.e. *R,R*) and '*s*' denotes a syndiotactic link between adjacent stereocentres (i.e. *S,R*). Using this notation, highly isotactic PLA has the repeating sequence *iii* at the tetrad level and, similarly, heterotactic PLA is described by the sequences *isi* and *sis*. As can be seen in Figure 1.7, PLA formed from *rac*-LA and *meso*-LA results in different sequences.

The degree of stereoregularity present in a given PLA chain is expressed as a probability, where P_r is the probability of forming a racemic link (heterotactic enrichment) and P_m is the probability of forming a *meso* link (isotactic). Hence, for the ROP of *rac*-LA, $P_r = 1.00$ and $P_m = 0.00$ for perfectly heterotactic PLA. Similarly, $P_r = 0.00$ and $P_m = 1.00$ describes perfectly isotactic PLA formed from *rac*-LA.[20] Figures 1.8 and 1.9 show good examples of the homodecoupled ^{1}H NMR spectra of isotactic, heterotactic and atactic PLA. Figure 3.15 in Chapter 3 also gives a good example of heterotactically enriched PLA.

Figure 1.7. Schematic representation of the currently accepted assignments (CH) for PLA at the tetrad level.[37]

The material originally presented here is not currently available in ORA

Figure 1.8. The methine resonances in the homonuclear decoupled ^{1}H NMR spectrum of PLA illustrating isotactic block PLA chains (a) and heterotactic PLA chains (b).[38]

The material originally presented here is not currently available in ORA

Figure 1.9. The methine resonances in the homonuclear decoupled ^{1}H NMR spectrum of PLA illustrating atactic PLA chains.[39]

The material originally presented here is not currently available in ORA

1.7 Literature Review

Over the past two decades substantial research effort has been devoted to the development of catalytic systems for the ROP of ε-CL and LA. Highly desirable systems are those that promote ROP under ambient conditions with a high activity and the control (extending to tacticity control in the case of LA). This section provides a selective overview of the varied approaches used in this area. An emphasis is based on

Main Group catalysts, since Chapters 2 and 3 focus mainly on this area. The use of these catalysts is also highly desirable due to their biologically benign nature and abundance.[23]

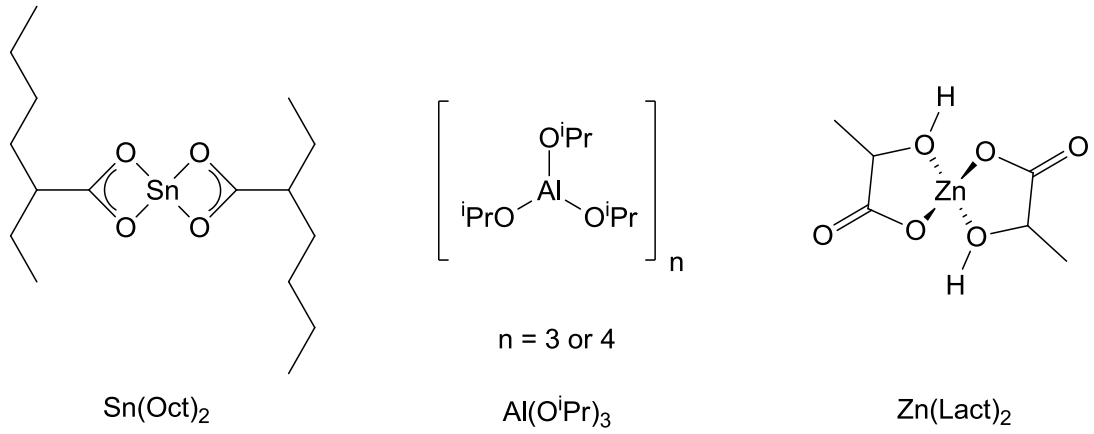
Additionally, notable examples of ROP catalysts based on metals across the periodic table are discussed. The area of ROP has been reviewed extensively on numerous occasions in the past decade and this is a reflection of the amount of widespread research existing in the area. The reader is directed to these reviews for detailed accounts.[1-6] ROP catalysts are based on many metals such as magnesium,[2, 40-43] zinc,[35, 40, 42-46] calcium,[2, 23, 24, 47-51] aluminium,[52-56] Rare Earth metals,[13, 25, 57-64] Group IV metals,[8, 14, 26, 65-68] iron,[69, 70] tin[71-73] and indium.[74, 75]

1.7.1 Industrial ROP and the Development of Simple Systems

PLA is synthesised on a 140,000 tonne scale annually by Natureworks LLC in the USA and on a smaller scale elsewhere in the EU and Japan.[6] The commonly used industrial catalyst used for the preparation of PLA is tin (II) 2-ethylhexanoate (stannous octanoate, see Figure 1.10). The advantages of this simple system are the production of high molecular weight polymer, high activity and low levels of epimerisation.[76] An additional benefit of this system is the solvent free (melt) conditions used. The monomer and catalyst are simply heated together at 180-210 °C and 95 % monomer conversion is achieved in 2.5 hours. The addition of alcohols to the process is sometimes carried out to accelerate the rate of polymerisation and/ or to form lower molecular weight polymer.[76] Also of high importance is the fact that the catalyst has been approved as a food additive by the FDA in the USA (despite being a potentially toxic Sn(II) species).[76, 77]

Despite being an approved food additive, $Sn(Oct)_2$ has been restricted from use in biomedical applications, owing to the possible retention of tin residues in the PLA formed (which could go on to form highly toxic organo-tin species).[78] For these reasons, lots of subsequent early research focussed on attempts to find a truly biocompatible homoleptic catalyst, for example $Zn(lactate)_2$ and $Al(O^iPr)_3$ (Figure 1.10).

Figure 1.10. Stannous octanoate (left), aluminium isopropoxide (middle), zinc lactate (right).



$Sn(Oct)_2$ $Al(O^iPr)_3$ $Zn(Lact)_2$

The most extensively studied homoleptic aluminium alkoxide is $Al(O^iPr)_3$,[1] which was shown to be active for the ROP of LA.[10, 54] However, this catalyst is substantially less active than $Sn(Oct)_2$, taking several days at 125-180 °C to reach high monomer conversions and also producing PLA with a lower than desired M_n.[1, 10] Furthermore, whilst the consumption of LA generally followed first order kinetics, induction periods were commonly found. This was attributed to aggregation phenomena, further complicated by the fact that $Al(O^iPr)_3$ actually exists as an equilibrium mixture of a trimer and tetramer in solution (THF).[54] An additional disadvantage of aluminium catalysts in general is that aluminium has been linked with the development of Alzheimer's disease.[1] Compared to aluminium, homoleptic zinc complexes such as zinc octanoate, zinc stearate, zinc salicylate and zinc lactate were found to be improved catalysts.[1, 6, 79, 80] For example, zinc lactate polymerised LA to moderate conversions over 24 hours under similar melt conditions (140 °C) used in the testing of $Sn(Oct)_2$.[80] However, such homoleptic zinc species were found to perform poorly compared to $Sn(Oct)_2$.[1, 6]

In related work, Feijen *et al*. tested commercially available calcium dimethoxide and found this to be an active catalyst for the ROP of *L*-LA and ε-CL in the melt at 120 °C.[81] However, the epimerisation of *L*-LA was observed and this was attributed to the formation of aggregated species. An improved system was found using *in situ* generated calcium methoxide, formed by addition of 2 equivalents of MeOH to $Ca\{N(SiMe_3)_2\}_2$ in the presence of LA.[81] This polymerised both ε-CL and *L*-LA in

THF at room temperature, with no epimerisation of *L*-LA, i.e. solely isotactic PLA was formed. In this case polymers with narrow PDIs and close to expected M_n values were observed. [81] Interestingly, the attempted isolation of the alkoxide complex in the absence of LA led to the formation of insoluble, oligomeric species. Rare earth homoleptic alkoxide complexes have also been studied for the ROP of ε-CL[82] and were also shown to have formed aggregated species in the early stages of polymerisation, evident by the observation of induction periods in the kinetic profiles.[82]

It can be seen that homoleptic polymerisation systems are generally plagued by aggregation phenomena, poor control and non-ideal kinetic polymerisation profiles. Generally, more recent academic research has focussed on the development of well-defined single site catalysts, inspired by earlier developments in polyolefin technology. The advantages of this approach are the ability to modify the Lewis acidity of a metal centre (and therefore the activity of a catalyst), as well as the selectivity of the catalyst through the manipulation of inert ancillary ligand(s).

1.7.2 Cyclopentadienyl Based ROP Initiators

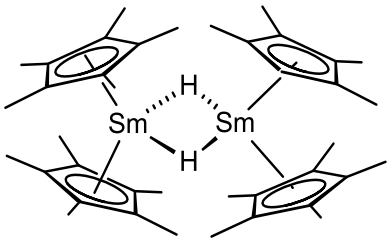
Cyclopentadienyl ligands are the most ubiquitous ancillary ligands in organometallic chemistry. Reasons for this include their relatively straightforward preparation, crystallinity and wide ranging possibilities for substitution at the ring substituents. As such there are a number of ROP catalysts with cyclopentadienyl supporting motifs (see also Chapter 3 for cyclopentadienyl borohydride complexes).

The dimeric samarium hydride complex **1.0** was prepared by Yasuda *et al.*[83] and found to be fairly active for the ROP of ε-CL at room temperature in toluene, yielding PCL with a high molecular weight and a narrow PDI (<1.1).[83] The methyl complexes $Cp^*_2M(Me)(THF)$ (M = Sm (**1.1**) and Yb (**1.2**)) were also prepared in the same study by Yasuda and were found to have a superior activity to **1.0**, attributed to the relatively high sensitivity of the latter. The lower activity of **1.2** compared to **1.1** was also thought to be due to reduction (Yb(III) to Yb(II)) during the polymerisation process, which is less favoured in the case of **1.1** (i.e. Sm(III) to Sm(II)).[31]

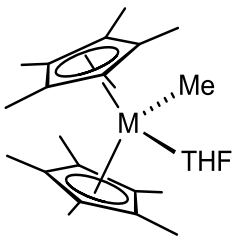
In a later study by Agarwal *et al.*,[84] the alkoxide complexes $Cp^*_2M(OR)(THF)$ (M = Sm (R = Et (**1.3**) or Yb (R = Me (**1.4**)), were synthesised alongside the dimeric

$[Cp_2Y(\mu\text{-OEt})]_2$ (**1.5**). These were tested for the ROP of ε-CL and compared with **1.1** under identical polymerisation conditions. It was found that **1.1** displayed higher activity and also gave superior control over the M_n and PDI values of the polymers formed. It was also shown through NMR studies that **1.3**-**1.5** initiated ROP by classical coordination-insertion, whereas **1.1** was shown to first form an acetal prior to an ongoing coordination-insertion mechanism.[84]

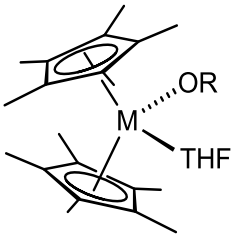
Figure 1.11. ROP catalysts supported by cyclopentadienyl based ligands.



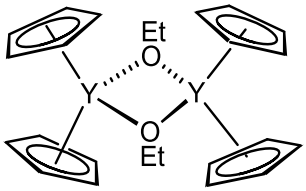
1.0



M = Sm (**1.1**) or Yb (**1.2**)



M = Sm (**1.3**, R = Et) or
Yb (**1.4**, R = Me)



1.5

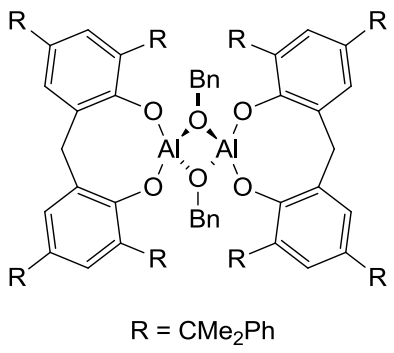
1.7.3 ROP Initiators with O-Donor Supporting Ligands

The bis(phenolates) have been studied extensively as supporting ligands for aluminium, titanium, zirconium and the rare earth metals (Figure 1.12).[52, 85-88] The aluminium bis(phenolate) **1.6** displayed a low activity for the ROP of *rac*-lactide, taking a number of days to polymerise 20-50 equivalents in refluxing toluene, although narrow polymers with narrow PDIs were yielded. The low activity of this catalyst is most likely due to its dimeric structure and significant degree of steric crowding around the metal centre.[88] The titanium bis(phenolate) **1.7** was prepared by Nakamura[87] and was active for the polymerisation of ε-CL over a period of five hours at room temperature, giving polymers with a good agreement between expected and

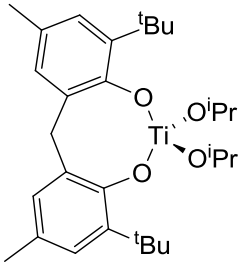
observed M_n and a narrow PDI (1.2).[87] However, no activity for the ROP of *rac*-LA was reported.

In 2008 Arnold *et al*. reported the synthesis of a family of homoleptic phosphine oxide-alkoxide complexes (see **1.8** for an example).[89] Such complexes were shown to produce isotactically enriched PLA (P_r = 0.80) from *rac*-LA at low temperature (-18 °C). The polymers produced also had a good M_n agreement and moderate PDIs (1.2-1.4).[89]

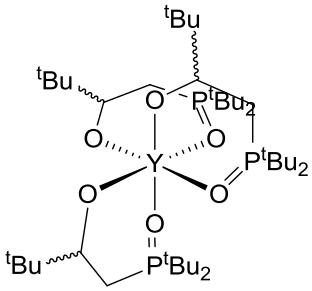
Figure 1.12. ROP catalysts supported by O-donor ligands.



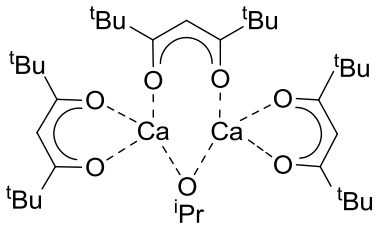
1.6



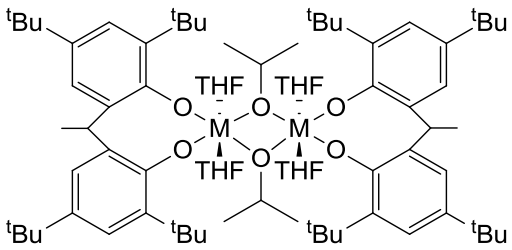
1.7



1.8



1.9



M = Nd (**1.10**) or Yb (**1.11**)

The calcium *β*-diketone complex **1.9** was prepared by Westerhausen and Feijen by protonolysis of an amide precursor with ^{i}PrOH.[90] **1.9** was shown to polymerise either ε-CL or *rac*-LA rapidly at room temperature in THF, albeit producing polymers with higher than expected M_n values and broad PDIs.[90] The dimeric neodymium and ytterbium bis(phenolate) alkoxides **1.10** and **1.11** were also shown to be active initiators for the ROP of ε-CL in toluene at room temperature over one hour (**1.10**) or up to eight hours (**1.11**). A very good M_n agreement in the polymers formed was

observed, together with narrow PDIs (1.1-1.3).[91] The extended reaction times were attributed to the dimeric nature of the complexes and the subsequently high degree of steric crowding around the metal centres (as argued in the case of **1.6**). The higher activity of **1.10** relative to **1.11** is most likely due to the larger size of the metal ion in the former.

1.7.4 ROP Initiators with N,O-Donor Supporting Ligands

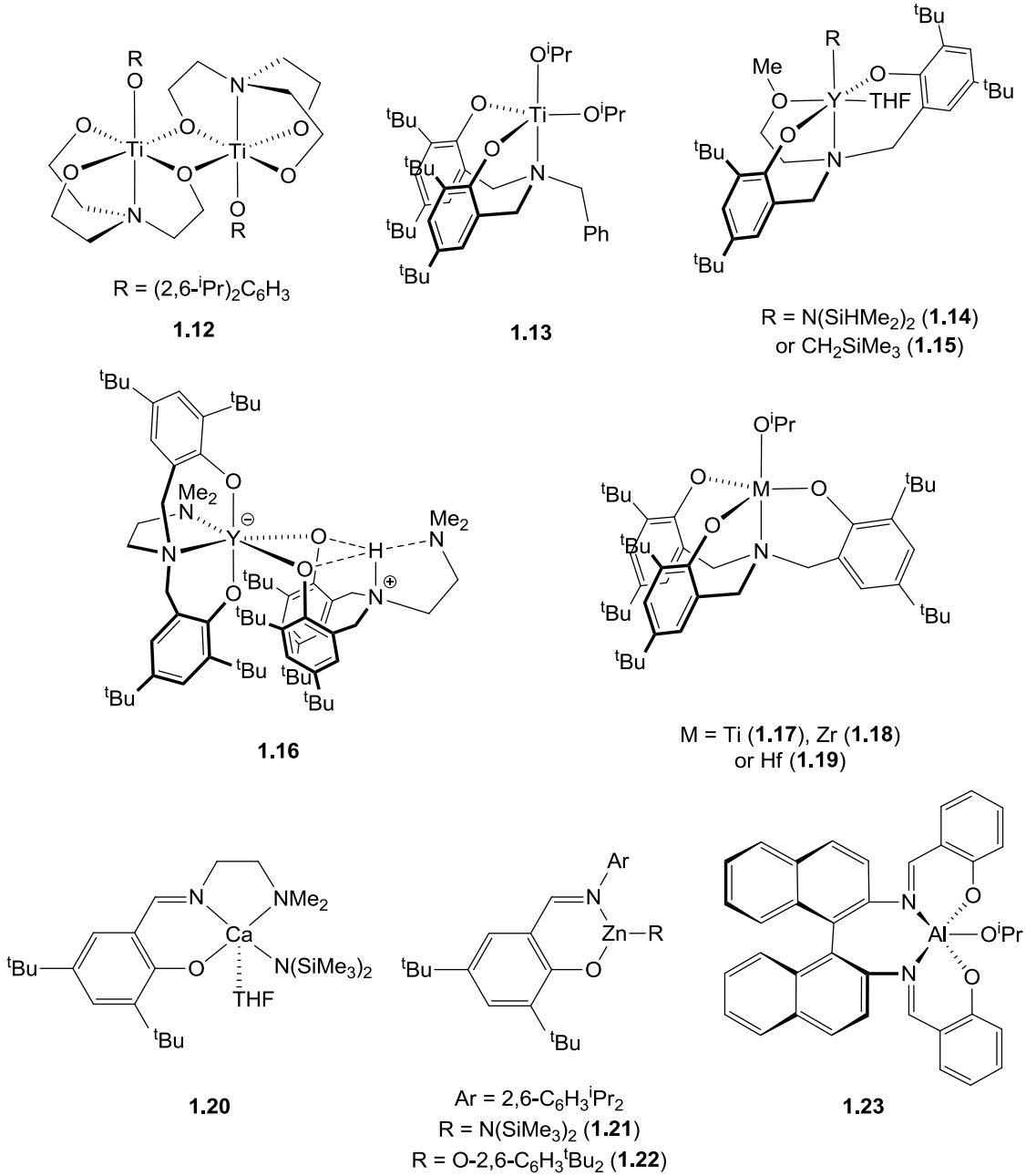
Mixed N,O-donor ligands have also been studied very successfully for the ROP of cyclic esters.[1, 20, 64] The titanatrane aryloxide complex **1.12** (Figure 1.13) was synthesised by Verkade in 2002.[68] This was shown to polymerise either *L*- or *rac*-LA over the course of 24 hours at 130 °C in the melt, yielding isotactic or atactic PLA respectively. In all cases polymers with higher than expected M_n values (approximately twice the expected value) and broad PDIs (1.8-2.0) were observed.[68]

The amine bis(phenolate) titanium bis(alkoxide) **1.13** was prepared by Davidson and co-workers in 2006 and studied for the ROP of ε-CL. **1.13** polymerised 100 equivalents of ε-CL over 24 hours at room temperature, giving a polymer M_n value consistent with two growing chains per metal centre, and a PDI of 1.2.[14] In related work by Carpentier,[27] the related amine bis(phenolate) yttrium amide (**1.14**) and alkyl (**1.15**) complexes were synthesised. These were shown to polymerise up to 500 equivalents of *rac*-LA at room temperature in THF, giving heterotactically enriched PLA (P_r = 0.80) with fairly narrow PDIs (1.2-1.4) and a good M_n agreement.[27] Carpentier later showed the capacity of this system towards the immortal polymerisation of lactide with alcohol co-initiators, yielding multiple polymer chains per metal centre alongside the aforementioned control of tacticity.[92] Subsequent and ongoing work within the Mountford group[13] has also shown the capability of the zwitterionic yttrium complex **1.16** to facilitate the immortal ROP of LA in the presence of alcohol and amine co-initiators, yielding excellent M_n control, narrow PDI values (1.0-1.1) and highly heterotactically enriched polymers (P_r values up to *ca.* 0.9).[13]

Research based on the amine phenolate ligands was later extended further by the group of Davidson[26], where notably the amine tris(phenolate) Group 4 alkoxide complexes **1.17-1.19** were synthesised. Whilst the titanium complex **1.17** produced atactic PLA in

the melt at 130 °C with a higher than expected M_n and a moderate PDI of 1.4, the zirconium (**1.18**) and hafnium (**1.19**) complexes gave highly heterotactically enriched polymer (P_r = 0.96 and 0.88 respectively) under identical conditions. The zirconium catalyst also showed excellent M_n control, whilst the hafnium catalyst gave polymer with an M_n value approximately twice that expected.[26]

Figure 1.13. ROP catalysts supported by N,O-donor ligands.



Schiff base ligands have also been used as ancillary ligands in the preparation of ROP catalysts. For example, the calcium complex **1.20** was prepared recently by Darensbourg and co-workers in 2008.[93] This was reported to polymerise up to 700 equivalents of *rac*-LA over 30 minutes at room temperature in THF, giving atactic PLA with a narrow (1.0-1.1) PDI and slightly higher than predicted M_n values. However, it was also shown that heterotactically enriched PLA could be obtained by carrying out the polymerisation at -33 °C.[93] Chisholm had previously studied the related Schiff base zinc complexes **1.21** and **1.22** for the ROP of *rac*-LA. However, they displayed low and required times of 4 and 72 hours respectively at room temperature in THF to polymerise 20 equivalents.[94] The relatively low activity of these complexes compared to **1.20** is likely to be a consequence of the smaller size of zinc(II) compared to calcium(II).

Spassky demonstrated the first stereoselective polymerisation of *rac*-LA employing methoxide complexes bearing the *(R)*-stereoisomer of the aluminium salen complex **1.23**.[33] It was shown that this complex selectively polymerised *D*-LA over *L*-LA (using *rac*-LA), forming isotactic PLA.[33] The *(R)*-stereoisomer of **1.23** was subsequently shown by Coates to give highly syndiotactically enriched PLA from *meso*-LA.[95]

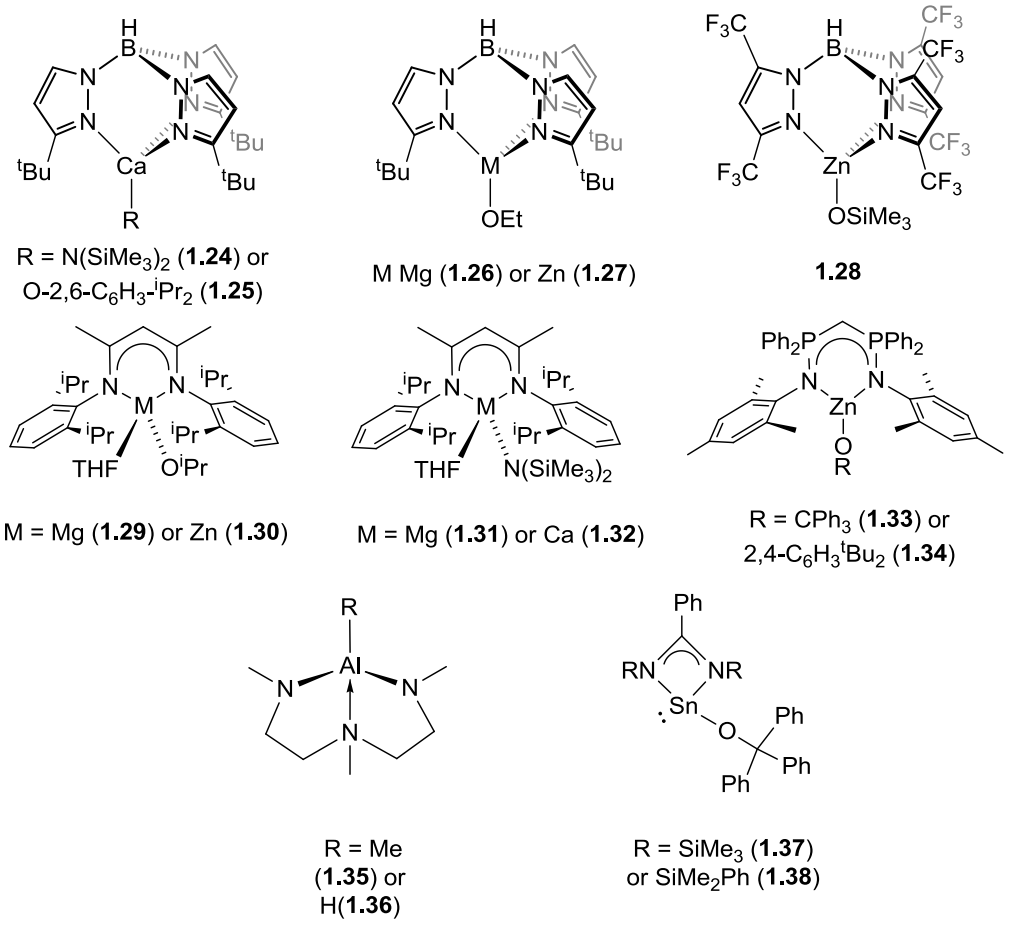
1.7.5 ROP initiators with N-donor supporting ligands

With a view to alleviating the aggregation difficulties often associated with O-donor ligands, N-donor ligands have been widely studied. With the additional substitution site available for nitrogen when compared to oxygen, it would be expected that N-donor ligands would provide a more sterically encumbering environment around a metal centre.[1]

The tris(pyrazolyl)hydroborate (Tp^R) and *β*-diketiminate ligands have been amongst the most widely exploited classes of N-donor ligands studied for ROP. The main advantages of these two ligand classes are their ease of preparation, the tuneability for substitution with bulky substituents and generally robust nature. Chisholm prepared the calcium amide and aryloxide Tp^{tBu} complexes **1.24** and **1.25**, which are amongst the most active initiators for the ROP of *rac*-LA to date, polymerising 200 equivalents at room temperature in THF in one minute (**1.24**) and five minutes (**1.25**).[24, 96]

Complex **1.24** yielded highly heterotactic PLA (P_r > 0.90) with a slightly higher than expected M_n and a broad PDI (1.74). Similar **1.25** yielded highly heterotactic PLA (P_r > 0.90) with a very similar M_n to that produced by **1.24** and a slightly narrower PDI (1.68). Both of these complexes were found to be more active than either the magnesium (**1.26**) or zinc (**1.27**) Tp^{tBu} alkoxide complexes prepared by the same group.[24, 96] The order of activity was postulated to depend on the polarity of the initiating metal oxygen bond in the order Ca > Mg > Zn, with **1.26** and **1.27** also giving polymers with narrower PDIs (approximately 1.2). The compromise between activity and control is a feature common to ROP initiators across the periodic table when employing the same ancillary ligands on different metals. The zinc siloxide complex **1.28** had earlier been prepared by Chisholm;[35] presumably it was anticipated that the presence of the CF_3 groups would enhance the Lewis acidity of the metal centre. However, it was found that this catalyst was almost inactive for the ROP of *rac*-LA at room temperature.[35]

Figure 1.14. ROP catalysts supported by N-donor ligands.



The *β*-diketiminate magnesium (**1.29**) and zinc (**1.30**) alkoxide complexes were reported by Coates in 2001[40] and were both shown to be highly active for the ROP of *rac*-LA at room temperature in CH_2Cl_2, requiring 2 minutes and 20 minutes respectively to reach high monomer conversions. Atactic PLA with a moderate PDI of 1.6 and a higher than expected M_n was formed in the case of **1.29**, whereas highly heterotactic PLA (P_r = 0.90) with a very narrow PDI (1.10) and a close to expected M_n.[40] Chisholm later reported that the *β*-diketiminate magnesium (**1.31**) and calcium (**1.32**) amides were active for the ROP of *rac*-LA.[24] Interestingly, whilst **1.31** polymerised 200 equivalents of the monomer within 5 minutes in CH_2Cl_2 at room temperature yielding heterotactic PLA (P_r = 0.90), **1.32** required 2 hours and gave atactic PLA. This is the reverse of the trend seen for the Tp^{tBu} complexes **1.25-1.27**. The unexpectedly low activity and selectivity of **1.32** was attributed to the formation of aggregated species formed during the polymerisation process.[24]

The bis(phosphinimino) zinc complexes **1.33** and **1.34** were reported by Hill in 2002.[97] Interestingly, these were both found to be inactive for the ROP of *rac*-LA at room temperature in CH_2Cl_2, unlike the high activity of the *β*-diketiminate complexes **1.29-1.32**. This was thought to be largely due to the relatively high degree of steric bulk present around the metal centre, as well as the possibility of non-innocent behaviour of the bridgehead carbon atom present in the PCP ligand. Despite this, **1.33** and **1.34** were shown to produce atactic PLA in toluene at 60 °C over a period of five and four hours, respectively.[97]

The tridentate diamidoamino aluminium complexes **1.35** and **1.36** were found to be active for the ROP of *rac*-LA in benzene at 80 °C, with the hydride complex (**1.36**) proving to be approximately twice as active as the methyl complex (**1.37**). Both catalysts produced atactic PLA with broad PDIs (1.7).[98] In other work by Tolman and Hillmyer[71], the Sn(II) amidinate complexes **1.37** and **1.38** were prepared. These were both active for the ROP of *rac*-LA, although both catalysts required a temperature of 80 °C in toluene. In both cases reasonable control was observed, producing polymers with slightly higher than expected M_n values and narrow-to-moderate PDIs (1.2-1.5).[98]

1.8 Summary

This Chapter has highlighted many important examples of research in the very active field of ROP. It can be seen that, whilst underdeveloped,[99] catalysts of the main group are amongst the most active to date. Generally it is found that calcium complexes show a greater activity than those of magnesium, which are in turn more active than those of zinc.[1, 24, 96] An extensive number of catalysts have also been prepared for the rare earth metals, Group 4 metals and tin, employing a diversity of supporting ancillary ligands bearing a range of substituents.

The activity and selectivity of a given catalyst has also been shown to generally be influenced by the choice of ancillary ligand. Hence there is a growing interest in the design and application of novel supporting ligand systems (as well as exploring new applications of existing systems). Chapters 3 and 4 provide further introductory material for borohydride based ROP catalysts and immortal ROP respectively.

1.9 Aims and Outlook

This thesis describes the synthesis, characterisation and ROP capability towards ε-CL and *rac*-LA of calcium, magnesium, zinc and yttrium N-donor ligand supported amide, alkoxide and borohydride catalysts. The solution state behaviour of the complexes synthesised will be discussed alongside solid state structural determinations that have been undertaken to elucidate the structure and bonding of the complexes presented. The study includes neutral, zwitterionic and cationic systems as well as the application of the latter towards the immortal ROP of *rac*-LA.

2.0 References

1. O. Dechy-Cabaret, B. Martin-Vaca and D. Bourissou, *Chem. Rev.*, 2004, **104**, 6147-6176.
2. C. A. Wheaton, P. G. Hayes and B. J. Ireland, *Dalton Trans.*, 2009, 4832-4846.
3. N. Ajellal, J.-F. Carpentier, C. Guillaume, S. M. Guillaume, M. Helou, V. Poirier, Y. Sarazin and A. Trifonov, *Dalton Trans.*, 2010, **39**, 8363-8376.
4. J. Wu, T. L. Yu, C. T. Chen and C. C. Lin, *Coord. Chem. Rev.*, 2006, **250**, 602-626.
5. B. J. O'Keefe, M. A. Hillmyer and W. B. Tolman, *J. Chem. Soc., Dalton Trans.*, 2001, 2215-2224.

6. R. H. Platel, L. M. Hodgson and C. K. Williams, *Polym. Rev.*, 2008, **48**, 11 - 63.
7. R. Raja and J. Meurig Thomas, *Z. Anorg. Allg. Chem.*, 2005, **631**, 2942-2946.
8. H. R. Kricheldorf, M. Berl and N. Scharnagl, *Macromolecules*, 1988, **21**, 286-293.
9. G. Montaudo, M. S. Montaudo, C. Puglisi, F. Samperi, N. Spassky, A. LeBorgne and M. Wisniewski, *Macromolecules*, 1996, **29**, 6461-6465.
10. P. Degée, P. Dubois, R. Jérŏme, S. Jacobsen and H.-G. Fritz, *Macromol. Symp.*, 1999, **144**, 289-302.
11. P. Degée, P. Dubois and R. Jérŏme, *Macromol. Symp.*, 1997, **123**, 67-84.
12. N. E. Kamber, W. Jeong, R. M. Waymouth, R. C. Pratt, B. G. G. Lohmeijer and J. L. Hedrick, *Chem. Rev.*, 2007, **107**, 5813-5840.
13. L. Clark, M. G. Cushion, H. E. Dyer, A. D. Schwarz, R. Duchateau and P. Mountford, *Chem. Commun.*, 2010, **46**, 273-275.
14. A. J. Chmura, M. G. Davidson, M. D. Jones, M. D. Lunn and M. F. Mahon, *Dalton Trans.*, 2006, 887-889.
15. Z. Zhong, P. J. Dijkstra and J. Feijen, *J. Am. Chem. Soc.*, 2003, **125**, 11291-11298.
16. A. Rudin and H. L. W. Hoegy, *J. Polym. Sci. A: Polym. Chem.*, 1972, **10**, 217-235.
17. M. Save, M. Schappacher and A. Soum, *Macromol. Chem. Phys.*, 2002, **203**, 889-899.
18. J. R. Dorgan, J. Janzen, D. M. Knauss, S. B. Hait, B. R. Limoges and M. H. Hutchinson, *J. Polym. Sci. B: Polym. Phys.*, 2005, **43**, 3100-3111.
19. R. C. Beavis, B. T. Chait and K. G. Standing, *Rapid Commun. Mass Spec.*, 1989, **3**, 436-439.
20. M. J. Stanford and A. P. Dove, *Chem. Soc. Rev.*, 2010, **39**, 486-494.
21. T. M. Ovitt and G. W. Coates, *J. Am. Chem. Soc.*, 2002, **124**, 1316-1326.
22. Y. Ikada, K. Jamshidi, H. Tsuji and S. H. Hyon, *Macromolecules*, 1987, **20**, 904.
23. M. H. Chisholm, J. Gallucci and K. Phomphrai, *Chem. Commun.*, 2003, 48-49.

24. M. H. Chisholm, J. C. Gallucci and K. Phomphrai, *Inorg. Chem.*, 2004, **43**, 6717-6725.
25. H. Dyer, S. Huijser, N. Susperregui, F. Bonnet, A. Schwarz, R. Duchateau, L. Maron and P. Mountford, *Organometallics*, 2010, 3602-3621.
26. A. J. Chmura, M. G. Davidson, C. J. Frankis, M. D. Jones and M. D. Lunn, *Chem. Commun.*, 2008, 1293-1295.
27. C. X. Cai, A. Amgoune, C. W. Lehmann and J. F. Carpentier, *Chemical Commun.*, 2004, 330-331.
28. N. Nomura, R. Ishii, M. Akakura and K. Aoi, *J. Am. Chem. Soc.*, 2002, **124**, 5938-5939.
29. T. R. Jensen, L. E. Breyfogle, M. A. Hillmyer and W. B. Tolman, *Chem. Commun.*, 2004, 2504-2505.
30. A. P. Dove, H. Li, R. C. Pratt, B. G. G. Lohmeijer, D. A. Culkin, R. M. Waymouth and J. L. Hedrick, *Chem. Commun.*, 2006, 2881-2883.
31. C. K. A. Gregson, I. J. Blackmore, V. C. Gibson, N. J. Long, E. L. Marshall and A. J. P. White, *Dalton Trans.*, 2006, 3134-3140.
32. M. H. Chisholm, N. J. Patmore and Z. Zhou, *Chem. Commun.*, 2005, 127-129.
33. N. Spassky, M. Wisniewski, C. Pluta and A. Le Borgne, *Macromol. Chem. Phys.*, 1996, **197**, 2627.
34. T. M. Ovitt and G. W. Coates, *J. Am. Chem. Soc.*, 2002, **124**, 1316-1326.
35. M. H. Chisholm, N. W. Eilerts, J. C. Huffman, S. S. Iyer, M. Pacold and K. Phomphrai, *J. Am. Chem. Soc.*, 2000, **122**, 11845-11854.
36. M. T. Zell, B. E. Padden, A. J. Paterick, K. A. M. Thakur, R. T. Kean, M. A. Hillmyer and E. J. Munson, *Macromolecules*, 2002, **35**, 7700-7707.
37. M. H. Chisholm, S. S. Iyer and M. E. Matison, *Chem. Commun.*, 1997, 1999-2000.
38. P. Hormnirun, E. L. Marshall, V. C. Gibson, A. J. P. White and D. J. Williams, *J. Am. Chem. Soc.*, 2004, **126**, 2688-2689.
39. K. A. M. Thakur, R. T. Kean, M. T. Zell, B. E. Padden and E. J. Munson, *Chem. Commun.*, 1998, 1913 - 1914.
40. B. M. Chamberlain, M. Cheng, D. R. Moore, T. M. Ovitt, E. B. Lobkovsky and G. W. Coates, *J. Am. Chem. Soc.*, 2001, **123**, 3229.

41. M. H. Chisholm and N. W. Eilerts, *Chem. Commun.*, 1996, 853-854.
42. M. H. Chisholm, J. C. Huffman and K. Phomphrai, *J. Chem. Soc., Dalton Trans.*, 2001, 222-224.
43. V. Poirier, T. Roisnel, J. F. Carpentier and Y. Sarazin, *Dalton Trans.*, 2009, 9820-9827.
44. M. Cheng, A. B. Attygalle, E. B. Lobkovsky and G. W. Coates, *J. Am. Chem. Soc.*, 1999, **121**, 11583-11584.
45. C. A. Wheaton, B. J. Ireland and P. G. Hayes, *Organometallics*, 2009, **28**, 1282-1285.
46. C. A. Wheaton and P. G. Hayes, *Chem. Commun.*, 2010, **46**, 8404-8406.
47. Z. Zhong, P. J. Dijkstra, C. Birg, M. Westerhausen and J. Feijen, *Macromolecules*, 2001, **34**, 3863-3868.
48. Y. Sarazin, V. Poirier, T. Roisnel and J. F. Carpentier, *Eur. J. Inorg. Chem.*, 2010, **2010**, 3423-3428.
49. Y. Sarazin, B. Liu, T. Roisnel, L. Maron and J. F. Carpentier, *J. Am. Chem. Soc.*, 2011, 9069-9087.
50. V. Poirier, T. Roisnel, J. F. Carpentier and Y. Sarazin, *Dalton Trans.*, 2011, **40**, 523-534.
51. M. Cushion and P. Mountford, *Chem. Commun.*, 2011, 2276-2278.
52. M. H. Chisholm, C. C. Lin, J. C. Gallucci and B. T. Ko, *Dalton Trans.*, 2003, 406-412.
53. A. Duda and S. Penczek, *Macromolecules*, 1995, **28**, 5981-5992.
54. A. Kowalski, A. Duda and S. Penczek, *Macromolecules*, 1998, **31**, 2114-2122.
55. K. Majerska and A. Duda, *J. Am. Chem. Soc.*, 2004, **126**, 1026-1027.
56. P. Hormnirun, E. L. Marshall, V. C. Gibson, A. J. P. White and D. J. Williams, *J. Am. Chem. Soc.*, 2004, **126**, 2688-2689.
57. H. E. Dyer, S. Huijser, A. D. Schwarz, C. Wang, R. Duchateau and P. Mountford, *Dalton Trans.*, 2008, 32-35.
58. F. Bonnet, A. R. Cowley and P. Mountford, *Inorg. Chem.*, 2005, **44**, 9046-9055.
59. F. Jaroschik, F. Bonnet, X. F. Le Goff, L. Ricard, F. Nief and M. Visseaux, *Dalton Trans.*, 2010, 6761-6766.

60. H. Ma and J. Okuda, *Macromolecules*, 2005, **38**, 2665.
61. D. Robert, M. Kondracka and J. Okuda, *Dalton Trans.*, 2008, 2667-2669.
62. H. Ma, T. P. Spaniol and J. Okuda, *Angew. Chem. Int. Ed.*, 2006, **45**, 7818-7821.
63. A. Amgoune, C. M. Thomas, T. Roisnel and J.-F. Carpentier, *Chem. Eur. J.*, 2005, **12**, 169.
64. M. Visseaux and F. Bonnet, *Coord. Chem. Rev.*, 2011, 374-420.
65. C. J. Chuck, M. G. Davidson, M. D. Jones, G. Kociok-Koehn, M. D. Lunn and S. Wu, *Inorg. Chem.*, 2006, **45**, 6595-6597.
66. M. G. Davidson, M. D. Jones, M. D. Lunn and M. F. Mahon, *Inorg. Chem.*, 2006, **45**, 2282-2287.
67. S. Gendler, S. Segal, I. Goldberg, Z. Goldschmidt and M. Kol, *Inorg. Chem.*, 2006, **45**, 4783-4790.
68. Y. Kim and J. G. Verkade, *Organometallics*, 2002, **21**, 2395-2399.
69. B. J. O'Keefe, L. E. Breyfogle, M. A. Hillmyer and W. B. Tolman, *J. Am. Chem. Soc.*, 2002, **124**, 4384-4393.
70. B. J. O'Keefe, M. A. Hillmyer and W. B. Tolman, *J. Chem. Soc., Dalton Trans.*, 2001, 2215.
71. K. B. Aubrecht, M. A. Hillmyer and W. B. Tolman, *Macromolecules*, 2002, **35**, 644-650.
72. M. Moller, R. Kange and J. L. Hedrick, *J. Polym. Sci. A: Polym. Chem,*, 2000, **38**, 2067-2074.
73. M. H. Chisholm, E. E. Delbridge and J. C. Gallucci, *New. J. Chem.*, 2004, **28**, 145-152.
74. A. Pietrangelo, M. A. Hillmyer and W. B. Tolman, *Chem. Commun.*, 2009, 2736-2737.
75. M. P. Blake, A. D. Schwarz and P. Mountford, *Organometallics*, 2011, **30**, 1202-1214.
76. R. E. Drumright, P. R. Gruber and D. E. Henton, *Adv. Mat.*, 2000, **12**, 1841-1846.
77. A.-C. Albertsson and I. K. Varma, *Biomacromolecules*, 2003, **4**, 1466-1486.

78. G. Schwach, J. Coudane, R. Engel and M. Vert, *Polym. Bull.*, 1996, **37**, 771-776.
79. G. Schwach, J. Coudane, R. Engel and M. Vert, *Polym. Bull.*, 1994, **32**, 617-623-623.
80. G. Schwach, J. Coudane, R. Engel and M. Vert, *Polym. Int.*, 1998, **46**, 177-182.
81. Z. Zhong, M. J. K. Ankoné, P. J. Dijkstra, C. Birg, M. Westerhausen and J. Feijen, *Polym. Bull.*, 2001, **46**, 51-57-57.
82. W. M. Stevels, M. J. K. Ankone, P. J. Dijkstra and J. Feijen, *Macromolecules*, 1996, **29**, 8296-8303.
83. M. Yamashita, Y. Takemoto, E. Ihara and H. Yasuda, *Macromolecules*, 1996, **29**, 1798-1806.
84. S. Agarwal, C. Mast, K. Dehnicke and A. Greiner, *Macromol. Rapid. Commun.*, 2000, **21**, 195.
85. M. H. Chisholm, D. Navarro-Llobet and W. J. Simonsick, *Macromolecules*, 2001, **34**, 8851-8857.
86. M. L. Hsueh, B. H. Huang, J. Wu and C. C. Lin, *Macromolecules*, 2005, **38**, 9482-9487.
87. D. Takeuchi, T. Nakamura and T. Aida, *Macromolecules*, 2000, **33**, 725-729.
88. Y. C. Liu, B. T. Ko and C. C. Lin, *Macromolecules*, 2001, **34**, 6196-6201.
89. P. L. Arnold, J. C. Buffet, R. P. Blaudeck, S. Sujecki, A. J. Blake and C. Wilson, *Angew. Chem. Int. Ed.*, 2008, **47**, 6033-6036.
90. M. Westerhausen, S. Schneiderbauer, Alexander N. Kneifel, Y. Söltl, P. Mayer, H. Nöth, Z. Zhong, Pieter J. Dijkstra and J. Feijen, *Eur. J. Inorg. Chem.*, 2003, **2003**, 3432-3439.
91. Y. Yao, X. Xu, B. Liu, Y. Zhang, Q. Shen and W. T. Wong, *Inorg. Chem.*, 2005, **44**, 5133-5140.
92. A. Amgoune, C. M . Thomas and J. F. Carpentier, *Macromol. Rapid Commun.*, 2007, **28**, 693-697.
93. D. J. Darensbourg, W. Choi, O. Karroonnirun and N. Bhuvanesh, *Macromolecules*, 2008, **41**, 3493-3502.

94. M. H. Chisholm, J. C. Gallucci, H. Zhen and J. C. Huffman, *Inorg. Chem.*, 2001, **40**, 5051-5054.
95. T. M. Ovitt and G. W. Coates, *J. Am. Chem. Soc.*, 1999, **121**, 4072.
96. M. H. Chisholm, J. Gallucci and K. Phomphrai, *Chem. Commun.*, 2003, 48-49.
97. M. S. Hill and P. B. Hitchcock, *J. Chem. Soc., Dalton Trans.*, 2002, 4694-4702.
98. N. Emig, H. Nguyen, H. Krautscheid, R. Réau, J.-B. Cazaux and G. Bertrand, *Organometallics*, 1998, **17**, 3599-3608.
99. S. Harder, *Chem. Rev.*, 2010, 3852-3876.

Chapter Two

New Group 2 and 12 Scorpionate complexes and their activity towards the ROP of ε-caprolactone and *rac*-lactide

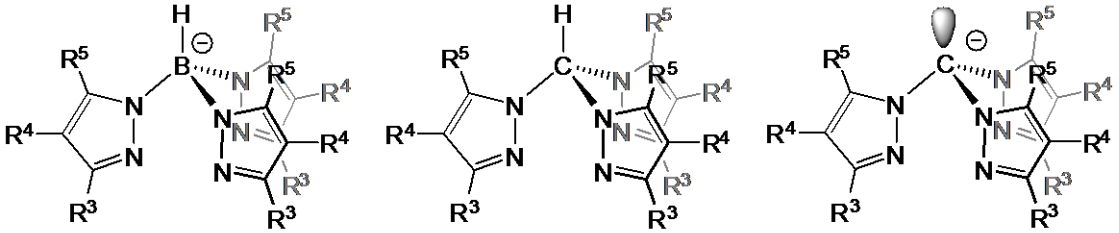
2.0 Overview

This Chapter will provide an introduction into Group 2 and 12 scorpionate complexes. An overview of the synthesis and characterisation of Group 2 and 12 neutral and zwitterionic halide and amide complexes supported by homo- and hetero-scorpionate ligands will be presented. Their solid state structures and solution behaviour will be discussed, in conjunction with their application to the ring-opening polymerisation (ROP) of cyclic esters. Comparison of the newly reported complexes and previously reported related complexes will be undertaken within the context of the solid state structures and the ROP activity and selectivity observed. The majority of this work has recently been published.[1]

2.1 Introduction

The anionic poly(pyrazolyl)borates and their neutral poly(pyrazolyl)methane counterparts are among the most widely used ligands in coordination and organometallic chemistry. Figure 2.0 depicts in general terms the tris(pyrazolyl)hydroborate (**I**) and tris(pyrazolyl)methane (**II**) homologues. The development of these and other scorpionate type ligands, and the synthesis and reactions of their complexes, have been the subject of many reviews.[2-9]

Figure 2.0. Tris(pyrazolyl)hydroborate (**I**), tris(pyrazolyl)methane (**II**) and tris(pyrazolyl)methanide (**III**) ligands.



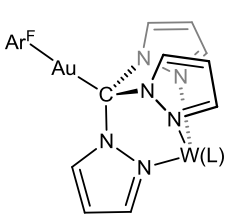
I **II** **III**

Removal of the C-bound apical proton from **II** generates the anionic tris(pyrazolyl)methan*ide* **III** (Figure 2.0). **III** is isoelectronic with the hydroborate system **I**, but features ambidentate characteristics and two possible binding sites, namely the anionic carbon or the pyrazolyl ring nitrogens.[10] Stone was the first to report a structurally authenticated derivative of tris(pyrazolyl)methanide, namely the trimetallic species **2.0** (Figure 2.1) which has an anionic $^{-}C(pz)_3$ moiety bound through both the apical carbon and all three 2-position pyrazolyl nitrogens.[11, 12] Compound **2.0** was prepared from Pt(norbornene)$(PMe_2Ph)_2$ and $Ar^FAu\{\kappa^1C, \kappa^3N\text{-}C(pz)_3\}W(CMe)(CO)_2$. The latter was not

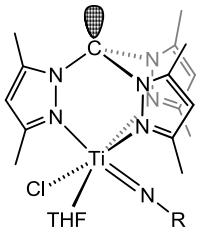
isolated but prepared *in situ* by sequential treatment of cationic $[W\{HC(pz)_3\}(CMe)(CO)_2]^+$ with NaOEt and $Au(Ar^F)(THT)$ ($Ar^F = C_6F_5$; THT = tetrahydrothiophene). Previous work in the Mountford group found that deprotonation of the apical C-H moiety of $Ti\{HC(Me_2pz)_3\}(NR)Cl_2$ with MeLi or LiN^iPr_2 in the presence of THF gave the zwitterionic species $Ti\{C(Me_2pz)_3\}(NR)Cl(THF)$ (R = ^{t}Bu (**2.1a**) or 2-$C_6H_4{}^t$Bu (**2.1b**)). These complexes, containing a formally cationic titanium, were the first structurally authenticated examples of a "naked" sp^3 hybridized carbanion.[13, 14] Direct reaction of $HC(Me_2pz)_3$ with MeLi in THF also afforded a zwitterionic carbanion-containing species, namely $Li\{C(Me_2pz)_3\}(THF)$ (**2.2**). The structural integrity of the latter was investigated in detail, both in solution and in the solid-state.[13, 15, 16]

The 5-position methyl groups of the $^-C(Me_2pz)_3$ moiety in **2.1** and **2.2** offer significant steric protection around the carbanionic centre. Compound **2.2** is nonetheless an effective reagent for delivery of the $^-C(Me_2pz)_3$ moiety: reaction of $Ti(N^tBu)Cl_2(py)_3$ with **2.2** formed $Ti\{C(Me_2pz)_3\}(N^tBu)Cl(py)$, analogous to **2.1a**,[13] and with $CuCl(PPh_3)$ or $(PPh_3)AgNO_3$ the compounds **2.3** and **2.4** were obtained, each of which possesses a κ^3*N*-$C(Me_2pz)_3$ ligand.[17] Interestingly, reaction with $AuCl(PMe_3)$ gave $Au\{\kappa^1C\text{-}C(Me_2pz)_3\}(PMe_3)$ (**2.5**),[17] a monometallic relative of the organogold complex (**2.0**) of Stone. Homoleptic first row transition metal methanide complexes have also been prepared by deprotonation of bound pyrazolylmethane ligands, namely $M\{C(Me_2pz)_3\}_2$ (M = Fe (**2.6**) or Co (**2.7**)), each of which show interesting electronic properties.[18] Mixed-sandwich complexes of ruthenium(II) containing cyclopentadienyl and tris(pyrazolyl)methane ligands have been prepared recently,[19] and zwitterionic complexes of the general formula $Ru\{C(R_2pz)_3\}Cp^{R'}$ ($Cp^{R'}$ = Cp, R = none or Me_2; $Cp^{R'}$ = Cp*, R_2 = none) are thereby made accessible.[10, 20] DFT studies of the various half-sandwich and sandwich-type complexes have supported the proposal of a localized carbanionic lone pair as depicted in Figures 2.0 and 2.1, and the electronic structures and metal charges are very similar to those of the tris(pyrazolyl)hydroborate analogues.[13, 18, 21]

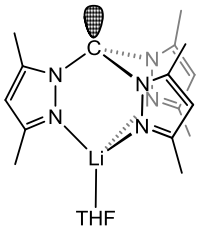
Figure 2.1. Examples of main group and transition metal tris(pyrazolyl)methanide complexes.



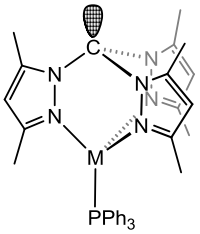
2.0 (L = PtAuAr^F (m-CMe)(CO)$_2$(PMe$_2$Ph)



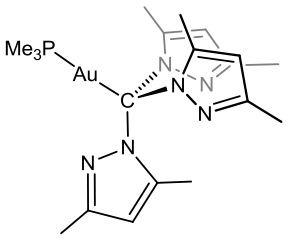
R = ^{t}Bu (**2.1a**) or 2-C$_6$H$_4$^{t}Bu (**2.1b**)



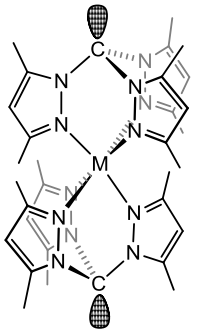
2.2



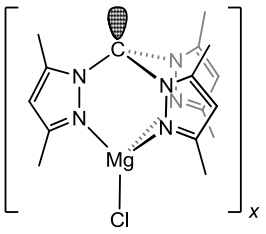
M = Cu (**2.3**) or Ag (**2.4**)



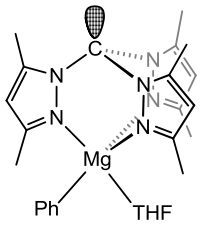
2.5



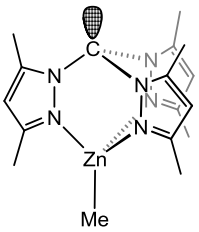
M = Fe (**2.6**), Co (**2.7**) or Mg (**2.8**)



2.9



2.10

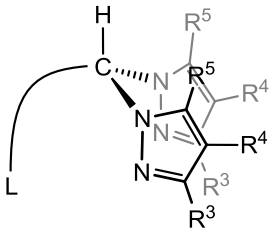


2.11

In addition to **2.2**, other main group tris(pyrazolyl)methanide complexes have been reported recently.[21] Reaction of BuMgCl with HC(Me$_2$pz)$_3$ gave the highly insoluble (and probably polymeric) [Mg{C(Me$_2$pz)$_3$}Cl]$_x$ (**2.9**). Reaction of MgBu$_2$ with HC(Me$_2$pz)$_3$ formed the magnesium sandwich complex Mg{C(Me$_2$pz)$_3$}$_2$, regardless of stoichiometry. Only on reaction with a large excess of MgPh$_2$ at low temperature, and after multiple recrystallisations, could the half-sandwich complex Mg{C(Me$_2$pz)$_3$}Ph(THF) (**2.10**) be obtained (in trace quantities). In contrast, reaction of ZnMe$_2$ with HC(Me$_2$pz)$_3$ only occurred after several days of heating to form Zn{C(Me$_2$pz)$_3$}Me (**2.11**). No reaction at all took place between ZnPh$_2$ and HC(Me$_2$pz)$_3$, and nor could a sandwich complex Zn{C(Me$_2$pz)$_3$}$_2$ (analogous to Mg{C(Me$_2$pz)$_3$}$_2$ (**2.8**)) be obtained. Detailed DFT studies of the reactions of magnesium and zinc alkyls with HC(Me$_2$pz)$_3$ were also reported.[21]

While *homoscorpionate* ligands have the same three moieties appended to the apical group (e.g., BH, CH), another important class of poly(pyrazolyl) ligands are the *heteroscorpionates.* Here one of the pyrazolyl groups has been replaced by a different C-, O-, S- or N-donor moiety (Figure 2.2).[8]

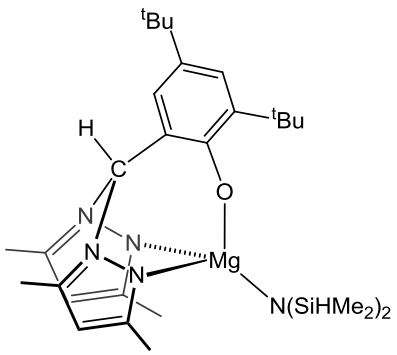
Figure 2.2. The general structure of a bis(pyrazolyl)methane (**IV**) ligand (L = C-, O-, S- or N- donor group).



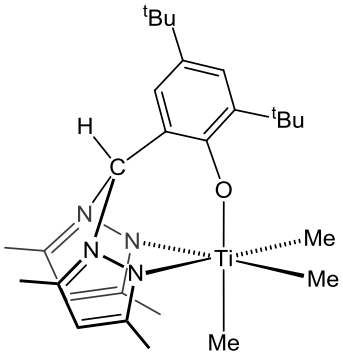
IV

While much of the early work with heteroscorpionate complexes was concerned with synthetic and structural studies, several reports have focussed more on their applications in the areas of ring-opening polymerisation of cyclic esters[22-25] (e.g. $Mg\{(Me_2pz)_2CHArO\}\{N(SiHMe_2)_2\}$ (**2.12**)[26]) and Ziegler-Natta polymerization catalysis[27] (e.g. $Ti\{(Me_2pz)_2CHArO\}Me_3$ (**2.13**, Ar = $C_6H_2{}^tBu_2$),[28] $Zr\{(Me_2pz)_2CHSiMe_2N^iPr\}(CH_2SiMe_3)_3$ (**2.14**) and $Sc\{(Me_2pz)_2CHSiMe_2N^iPr\}(CH_2SiMe_3)_2$ (**2.15**)[27]). Recently, preliminary results for Cr(III) ethylene trimerisation precatalysts **2.17** – **2.19** (Figure 2.3) featuring heteroscorpionate ligands were disclosed by Braunstein and Hor[29-31], as well as in the Mountford group (**2.20**).[32]

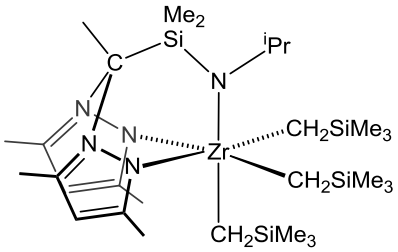
Figure 2.3. Examples of heteroscorpionate complexes used as polymerisation and ethylene trimerisation catalysts.



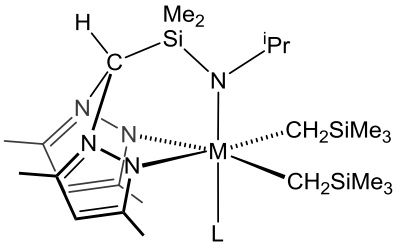
2.12



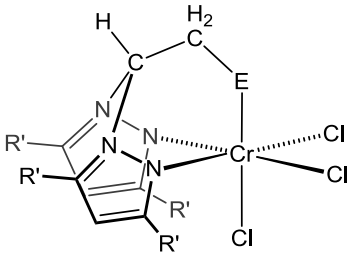
2.13



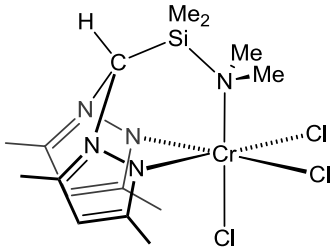
2.14



M = Sc, L = none (**2.15**)
M = Y, L = THF (**2.16**)



E = SR (**2.17**), OR (**2.18**),
N(H)CH_2Ph (**2.19**)



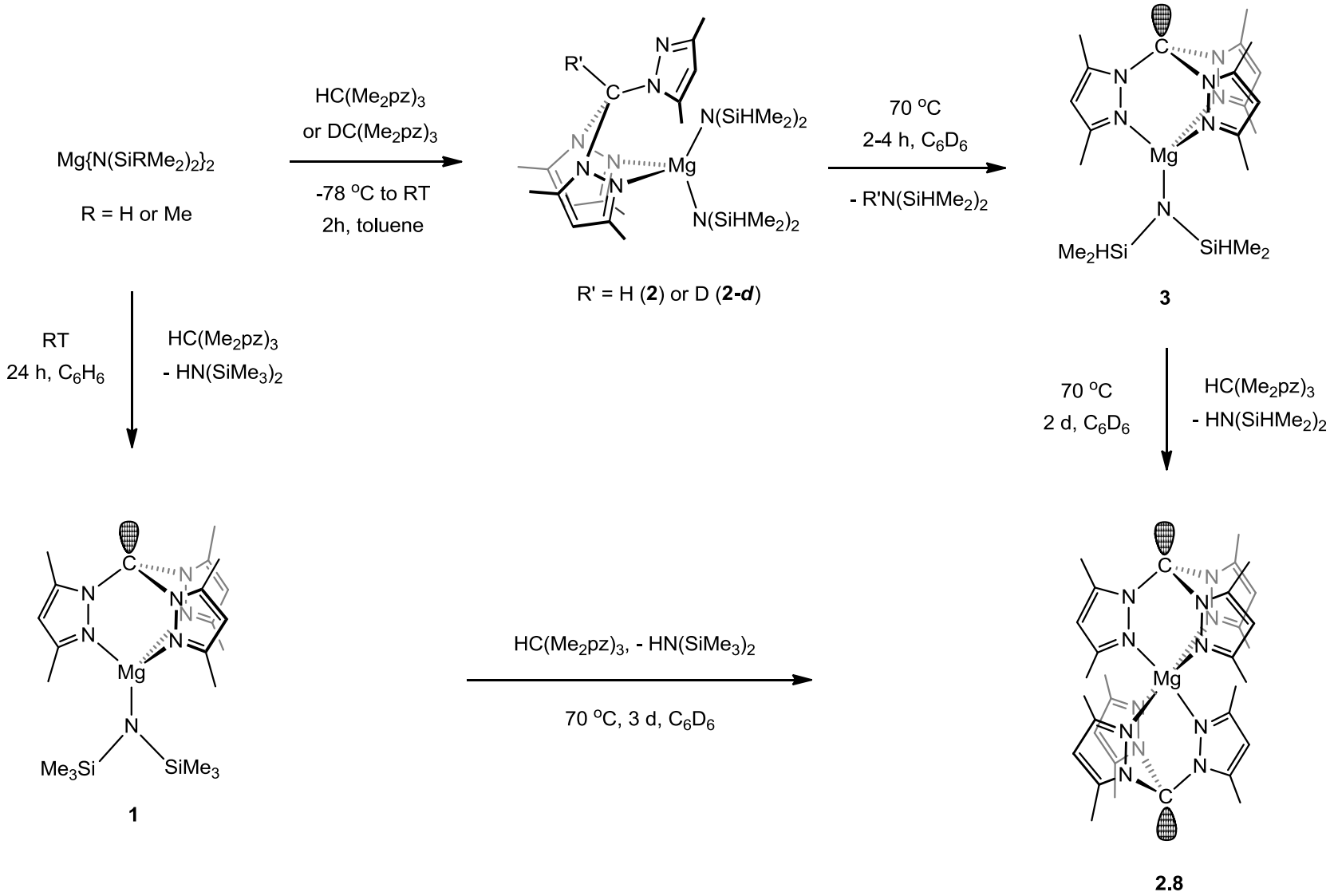
2.20

2.2 Synthesis of Group 2 tris(pyrazolyl)meth*ane* and tris(pyrazolyl)methan*ide* complexes

Scheme 2.0 summarises the reactions of $HC(Me_2pz)_3$ with $Mg\{N(SiMe_3)_2\}_2$ and the sterically less demanding $Mg\{N(SiHMe_2)_2\}_2$. The reaction with $Mg\{N(SiMe_3)_2\}_2$ proceeded smoothly at room temperature over 24 h to afford the half-sandwich compound $Mg\{C(Me_2pz)_3\}\{N(SiMe_3)_2\}$ (**1**) in 50% recrystallised yield. In contrast to the reactions of $HC(Me_2pz)_3$ with $MgBu_2$ or $MgPh_2$ (see above),[21] there was no evidence of formation of $Mg\{C(Me_2pz)_3\}_2$ (**2.8**) under these conditions. **2.8** was nonetheless obtained from $Mg\{N(SiHMe_2)_2\}_2$ or $Mg\{N(SiMe_3)_2\}_2$ by reaction with 2 equivalents. of $HC(Me_2pz)_3$ at 70 ^oC in C_6D_6 for 2 or 4 days, respectively.

The NMR spectra of **1** are consistent with the structure proposed in Scheme 2.0, assuming fast rotation about the Mg-$N(SiMe_3)_2$ bond. The solid state structure of **1** is shown in Figure 2.4 and confirms its zwitterionic nature and the presence of a cationic $\{Mg\text{-}N(SiMe_3)_2\}^+$ moiety. The approximately tetrahedral magnesium is κ^3N bound to a tris(pyrazolyl)methanide ligand featuring a naked carbanion at C(16).

Scheme 2.0. Reactions of $Mg\{N(SiRMe_2)_2\}_2$ (R = Me or H) with $HC(Me_2pz)_3$ or $DC(Me_2pz)_3$.



The Mg-N_{pz} bond lengths (avg. 2.115 Å) are reasonably comparable to those in Mg{C(Me_2pz)$_3$}Ph(THF) (avg. 2.135 Å)[21] but significantly shorter than in Mg{C(Me_2pz)$_3$}$_2$ (2.189(1) Å), consistent with the various steric factors and coordination number effects in the three compounds. The Mg-N($SiMe_3$)$_2$ distance is within the expected range.[33] The largest N_{pz}-Mg-N($SiMe_3$)$_2$ angle and longest Mg-N_{pz} bond is associated with N(3) due to steric repulsions between the C(20) and C(21) methyl groups attached to Si(2) and the C(9) methyl group. The Si(1)Me_3 group has less steric impact on the other pyrazolyl rings (containing N(1,2) and N(5,6)) as it is able to lodge into the cleft between these rings.

Figure 2.4. Displacement ellipsoid plots (20% probability) of one of the two crystallographically independent molecules of Mg{C(Me_2pz)$_3$}{N($SiMe_3$)$_2$} (**1**, left) and Mg{κ^2*N*-HC(Me_2pz)$_3$}{N($SiHMe_2$)$_2$}$_2$ (**2**, right). C-bound H atoms omitted and remaining H atoms drawn as spheres of an arbitrary radius.

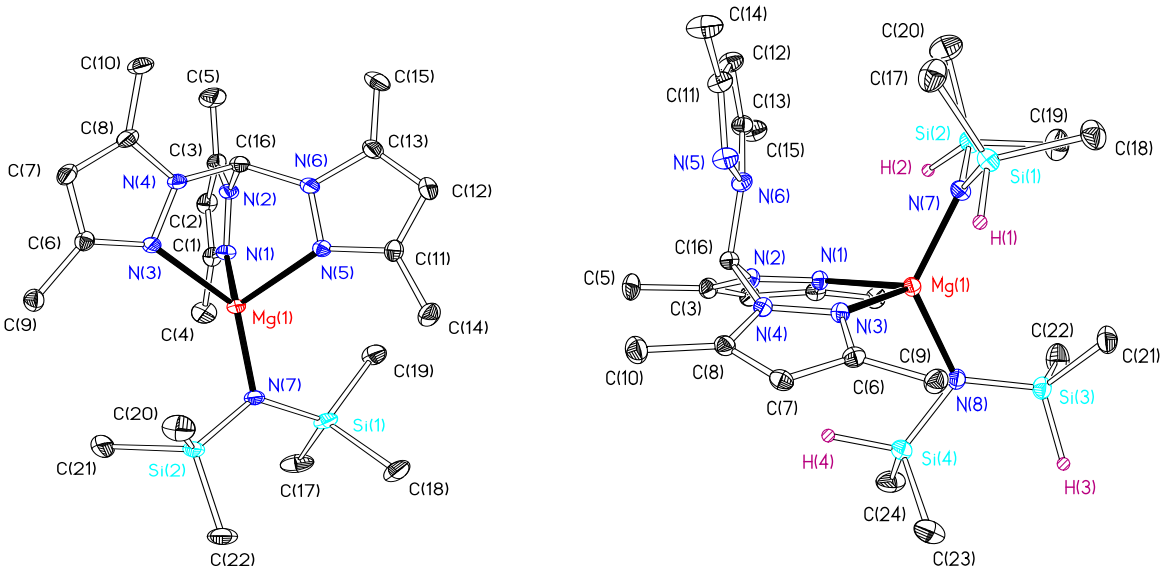


Table 2.0. Selected bond distances (Å) and angles (°) for Mg{C(Me_2pz)$_3$}{N($SiMe_3$)$_2$} (**1**).

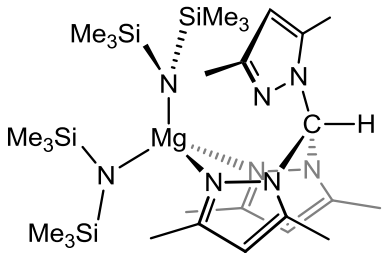
Mg(1)-N(1)	2.094(2)	N(1)-Mg(1)-N(7)	122.35(8)
Mg(1)-N(3)	2.152(2)	N(3)-Mg(1)-N(7)	136.48(8)
Mg(1)-N(5)	2.098(2)	N(5)-Mg(1)-N(7)	118.22(8)
Mg(1)-N(7)	1.987(2)		

Table 2.1. Selected bond distances (Å) and angles (°) for Mg{κ^2*N*-HC(Me$_2$pz)$_3$}-{N(SiHMe$_2$)$_2$}$_2$ (**2**).

Mg(1)-N(1)	2.147(3)	Mg(1)-N(8)	2.024(3)
Mg(1)-N(3)	2.139(3)	N(1)-Mg(1)-N(3)	87.1(1)
Mg(1)-N(7)	2.008(3)	N(7)-Mg(1)-N(8)	127.8(1)

In related work carried out in collaboration with the Breher group at the University of Karlsruhe[1] further insights into possible intermediates formed *en route* to **1** were obtained. NMR studies were performed at low temperature. HC(Me$_2$pz)$_3$ was mixed in an NMR tube with an excess of Mg{N(SiMe$_3$)$_2$}$_2$ and toluene-d_8 was condensed into the mixture. The sample was mixed and thawed at −100 °C and immediately transferred to a pre-cooled NMR probe. The initial ^{1}H NMR spectrum obtained at −100 °C is depicted in Figure 4. Several resonances for different pyrazolyl CH and methyl groups, trimethylsilyl groups as well as the apical C-H moiety were detected. Based on ROESY data, the individual resonances were assigned to the compound Mg{κ^2*N*-HC(Me$_2$pz)$_3$}{N(SiMe$_3$)$_2$}$_2$ (**2.21**) containing a κ^2*N*-HC(Me$_2$pz)$_3$ ligand.

Figure 2.5. The proposed structure of **2.21**.

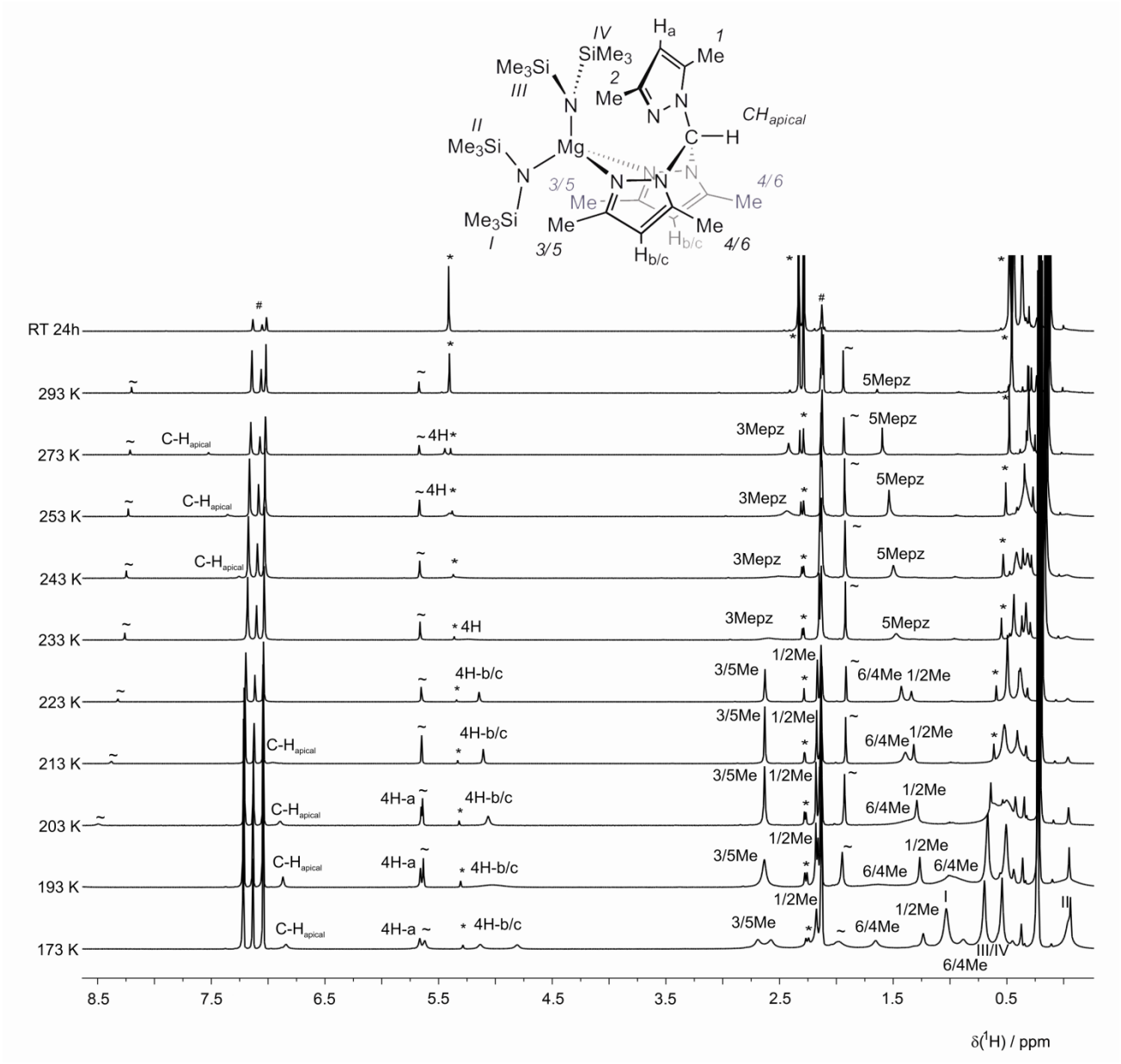


2.21

Three sets of resonances for three different Me$_2$pz groups were observed suggesting restricted rotation of the non-coordinated Me$_2$pz group. Due to this, both coordinated Me$_2$pz ligands become inequivalent (two broad pairs of signals at 2.69/2.57 and 1.65/0.88 (Me) and a pair of pyrazolyl H atoms at 5.13/4.81 ppm (CH$_{pz}$)). The non-coordinated Me$_2$pz ring shows three signals at 2.18 and 1.24 (Me) and 5.67 (CH$_{pz}$). Furthermore, four different signals for inequivalent SiMe$_3$ groups were detected at 1.03, 0.70, 0.54 and 0.06 ppm. The proposed structure of **2.21** is consistent with the structurally characterized complex **2** discussed below. Warming the sample to between −80 and −60 °C (see Figure 2.6) leads to

an exchange regime in which the two coordinated Me_2pz ligands become equivalent (free rotation of the pendant Me_2pz unit on the NMR time-scale). At higher temperatures, a second fluxional process is observed in which the two different types of Me_2pz groups are in exchange. At temperatures above 0 °C the formation of **1** and $HN(SiMe_3)_2$ is observed leading to a clean sample without any by-products after leading the sample overnight at room temperature (top trace in Figure 2.6).

Figure 2.6. Variable temperature ^1H NMR spectra of a mixture of $HC(Me_2pz)_3$ and $Mg\{N(SiMe_3)_2\}_2$ in toluene-d_8 (~ = signals of $HC(Me_2pz)_3$; * = signals of $Mg\{C(Me_2pz)_3\}\{N(SiMe_3)_2\}$ (**1**); # = residual solvent peaks of toluene).

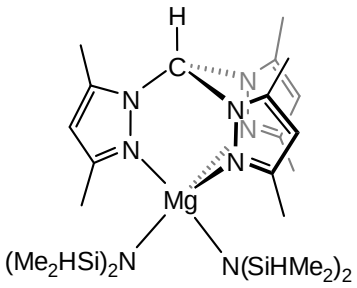


It is well-established that changing from the bulky $N(SiMe_3)_2$ to the smaller $N(SiHMe_2)_2$ can reduce steric compression within complexes and help stabilize otherwise highly

crowded complexes.[34] Therefore studies were extended to the less bulky amide $Mg\{N(SiHMe_2)_2\}_2$.[35] Indeed, reaction of $HC(Me_2pz)_3$ with $Mg\{N(SiHMe_2)_2\}_2$ at room temperature for 2 h gave the relatively stable complex $Mg\{\kappa^2N\text{-}HC(Me_2pz)_3\}\{N(SiHMe_2)_2\}_2$ (**2**) in 65% recrystallised yield. In agreement with the NMR studies on unstable **2.21**, compound **2** is an adduct between a neutral bidentate $HC(Me_2pz)_3$ and a bent $Mg\{N(SiHMe_2)_2\}_2$ moiety. κ^2N-Bound $HC(Me_2pz)_3$ ligands have been reported previously, in particular for later transition metals with d^8 valence configurations.[6] Four-coordinate compounds of the type $Mg\{N(SiMe_3)_2\}_2(L)_2$ (L = 4-NC_5H_4Me or 3,5-$NC_5H_3Me_2$) have also been structurally characterized previously.[36] The solid state structure of **2** is shown in Figure 2.4 along with selected bond distances and angles. The geometry about Mg(1) is distorted tetrahedral with the largest angle between the amide nitrogens N(7) and N(8). The Mg-N_{pz} distances (avg. 2.143 Å) are considerably shorter than those in six-coordinate $Mg\{HC(Me_2pz)_3\}Cl_2(THF)$ (avg. 2.271 Å),[21] the only other crystallographically characterized neutral $HC(Me_2pz)_3$ adduct of a Group 2 metal. The Mg-$N(SiHMe_2)_2$ distances in **2** are comparable to those in the aforementioned $Mg\{N(SiMe_3)_2\}_2(L)_2$ species.[36] The non-coordinated Me_2pz group containing N(5,6) is orthogonally orientated to both other pyrazolyl moieties due to steric factors, supporting the structure of **2.21** proposed on the basis of NMR measurements.

The NMR spectra of **2** are broad at room temperature indicative of one or more fluxional processes. Cooling to –65 °C in CD_2Cl_2 resulted in a sharp ^1H NMR spectrum consistent with the solid state structure and comparable to those obtained for **2.21**. Two sets of resonances (relative ratio 1:2) for Me_2pz groups were observed, consistent with a $\kappa^2N\text{-}HC(Me_2pz)_3$ ligand. Three broad doublets for the methyl groups of different $SiHMe_2$ groups were observed in the ratio 12H:6H:6H at –0.30, 0.01 and –0.48 ppm. These are assigned to the methyl groups of Si(1, 2) (made equivalent by the approximate C_s molecular symmetry), Si(3) and Si(4), respectively, assuming restricted rotation about Mg(1)-N(8). The low-frequency shift of the Si(4) methyl groups is due to magnetic anisotropy effects from the nearby Me_2pz rings. Warming the sample to –40 °C leads to fast exchange between $Si(3)HMe_2$ and $Si(4)HMe_2$ on the NMR timescale. Further warming to room temperature leads to an intermediate exchange regime in which the two $N(SiHMe_2)_2$ ligands and two different types of Me_2pz group are now undergoing exchange. Importantly, no exchange was found between the bound $HC(Me_2pz)_3$ ligand of **2** and free $HC(Me_2pz)_3$ purposefully added to the NMR sample, showing that the Me_2pz group exchange process is an intramolecular process.

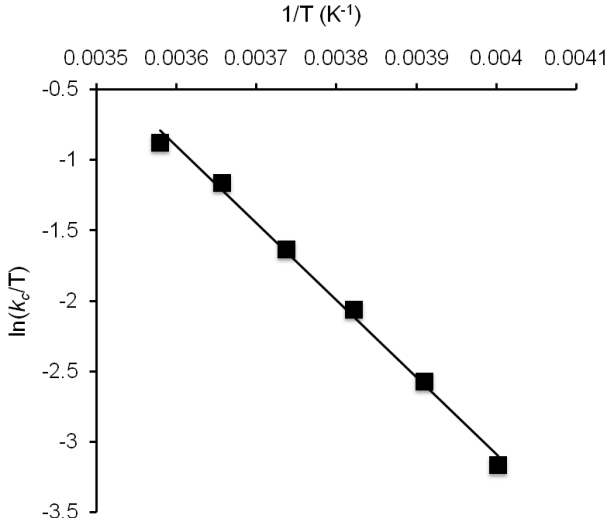
Figure 2.7. The proposed structure of **Int_exchange**.



Int_exchange

The Me_2pz group exchange process could in principle proceed either through a five-coordinate intermediate Mg{κ^3*N*-HC(Me_2pz)$_3$}{N($SiHMe_2$)$_3$}$_2$ (**Int_exchange**) or a three-coordinate alternative Mg{κ^1*N*-HC(Me_2pz)$_3$}{N($SiHMe_2$)$_3$}$_2$. The rate constants for Me_2pz group exchange were therefore determined at 6 different temperatures in the range –23 to 6 ^{o}C and the relevant Eyring plot is shown in Figure 2.8.[37] The derived activation parameters are $\Delta H^{\ddagger}$ = 46.1(1) kJ mol^{-1} and $\Delta S^{\ddagger}$ = –39(3) J mol^{-1} K^{-1} ($\Delta G^{\ddagger}_{(273K)}$ = 56.7(2) kJ mol^{-1}). The negative $\Delta S^{\ddagger}$ term is consistent with a more ordered transition state, and therefore more indicative of a five-coordinate intermediate (associative-type exchange) such as **Int_exchange**. Related exchange mechanisms are known for tris(pyrazolyl)hydroborate complexes of transition metals.[38] Structurally characterized analogues of **Int_exchange** include Mg{C(Me_2pz)$_3$}Ph(THF) (**2.21**),[21] Mg{HB(Me_2pz)$_3$}Et(THF),[39] Ca{HB(^{i}Prpz)$_3$}-{N($SiMe_3$)$_2$}(THF) (^{i}Prpz = 3-*iso*propyl pyrazolyl)[40] and Ca{C(Me_2pz)$_3$}-{N($SiMe_3$)$_2$}(THF) (**4**).

Figure 2.8. Eyring plot for Me_2pz ring exchange in Mg{κ^2*N*-HC(Me_2pz)$_3$}-{N($SiHMe_2$)$_2$}$_2$ (**2**). Derived activation parameters: $\Delta H^{\ddagger}$ = 46.1(1) kJ mol^{-1}; $\Delta S^{\ddagger}$ = -39(3) J mol^{-1} K^{-1}; $\Delta G^{\ddagger}_{(273K)}$ = 56.7(2) kJ mol^{-1}.



While **2.21** was found to lead to **1** readily at temperatures above 0 °C, the analogous conversion of **2** takes place only at higher temperatures. Heating a solution of **2** in C_6D_6 at 70 ^oC for several hours led quantitatively to the zwitterionic mono(amide) compound $Mg\{C(Me_2pz)_3\}\{N(SiHMe_2)_2\}$ (**3**, Scheme 2.0) and 1 equiv. of $HN(SiHMe_2)_2$. Compound **3** is the homologue of $Mg\{C(Me_2pz)_3\}\{N(SiMe_3)_2\}$ (**1**) and was obtained on a preparative scale directly from $HC(Me_2pz)_3$ and $Mg\{N(SiHMe_2)_2\}_2$ in 49% yield after recrystallization from toluene. The ^1H and ^{13}C NMR spectra of **1** and **3** are very similar. In particular, the carbanion carbon resonance $\underline{C}(Me_2pz)_3$ appears at 72.5 and 71.9 ppm, respectively, in the ^{13}C NMR spectra of the two compounds.

The isolation of the intermediate **2** as a relatively stable and crystalline material at room temperature, and its well-behaved conversion to **3**, provided the opportunity to probe the C–H bond breaking event that leads from pyrazolylmethane to pyrazolylmethan*ide* in the reactions of main group alkyls and amides with $HC(Me_2pz)_3$ (i.e., the formation of compounds of the type $M\{C(Me_2pz)_3\}X$ in general (Figure 2.1 and Scheme 2.0). To this end the deuterated analogue of **2**, namely $Mg\{\kappa^2\textit{N}\text{-}DC(Me_2pz)_3\}\{N(SiHMe_2)_2\}_2$, was also synthesised (**2-*d***), from $DC(Me_2pz)_3$ and $Mg\{N(SiHMe_2)_2\}_2$. Isotopomer **2-*d*** is identical to **2** except for the presence of an apical C–D in the pyrazolylmethane ligand. As for **2**, heating a solution of **2-*d*** in C_6D_6 for several hours quantitatively formed **3** (along with 1 equiv. of $DN(SiHMe_2)_2$).

Figure 2.9 shows the first order log plots for the conversion of $Mg\{\kappa^2\textit{N}\text{-}HC(Me_2pz)_3\}\{N(SiHMe_2)_2\}_2$ (**2**) and $Mg\{\kappa^2\textit{N}\text{-}DC(Me_2pz)_3\}\{N(SiHMe_2)_2\}_2$ (**2-*d***) to $Mg\{C(Me_2pz)_3\}\{N(SiHMe_2)_2\}$ (**3**) in C_6D_6 at 50 ^oC. The linear nature of the plots and near-unity R^2 values are consistent with first order, intramolecular processes. The first order rate constants are $k(H) = 2.07(1) \times 10^{-4}\ s^{-1}$ and $k(D) = 1.08(1) \times 10^{-4}\ s^{-1}$ for the protio- and deutero-systems, respectively, and show a clear primary kinetic isotope effect (KIE = $k(H)/k(D) = 1.91(2)$). Therefore the C–H (for **2**) or C–D (for **2-*d***) bond cleavage occurs in the rate-limiting step (as opposed to some other reorganisation step being critical). The magnitude of $k(H)/k(D)$ is within the usual ranges for concerted processes.[41]

Figure 2.9. First order plots for the conversion of Mg{κ^2*N*-HC(Me$_2$pz)$_3$}{N(SiHMe$_2$)$_2$}$_2$ (**2**, red circles, R^2 = 0.997) and Mg{κ^2*N*-DC(Me$_2$pz)$_3$}{N(SiHMe$_2$)$_2$}$_2$ (**2-*d***, blue squares, R^2 = 0.998) to Mg{C(Me$_2$pz)$_3$}{N(SiHMe$_2$)$_2$} (**3**) in C_6D_6 at 50 ^{o}C. I and I_0 refer to the normalized concentrations of **2** or **2-*d*** at the given time and at time = 0, respectively. *k*(H) = 2.07(1) x 10^{-4} s^{-1}; *k*(D) = 1.08(1) x 10^{-4} s^{-1}; *k*(H)/*k*(D) = 1.91(2).

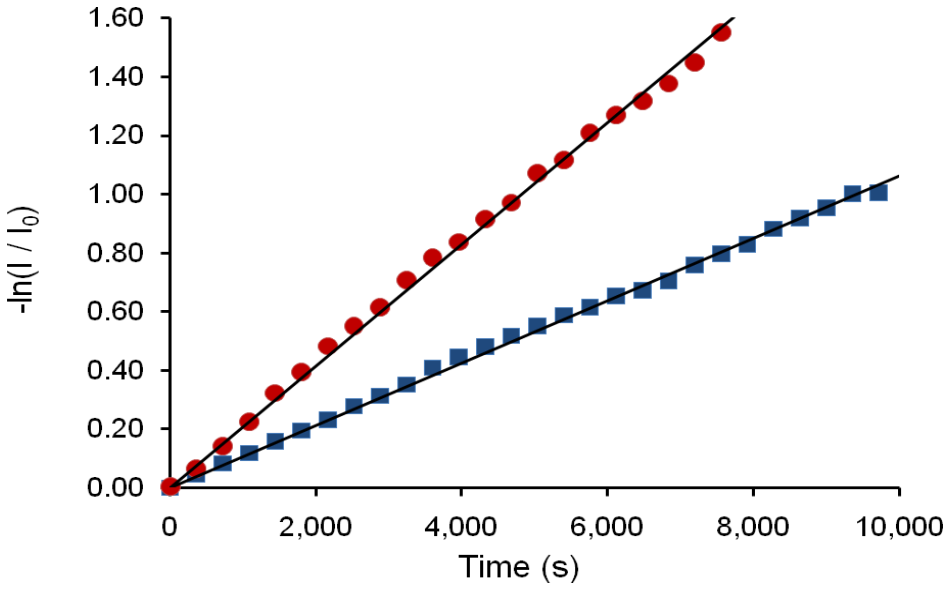
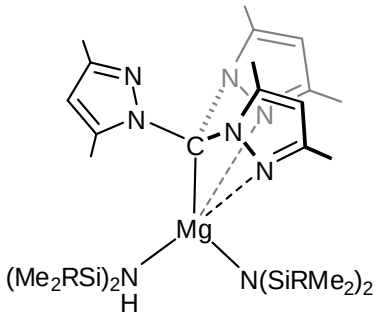


Figure 2.10. The proposed structure of **Int_C–H**



Int_C-H (R = H or Me)

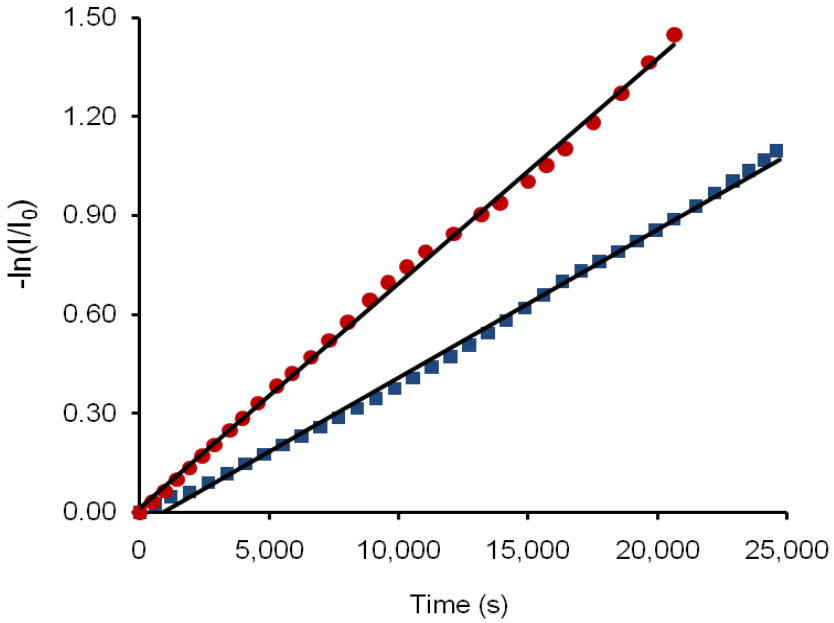
Although not detectable by NMR spectroscopy, it is proposed that the reaction coordinate leading to C–H activation (i.e., **2** → **3** and also **2.21** → **1**) is related to that suggested above for intramolecular pyrazolyl ring exchange within **2** (i.e., **Int_exchange**), but instead may proceed through a first formed intermediate of the type Mg{κ^1*C*,κ^2*N*-C(Me$_2$pz)$_3$}{N(SiRMe$_2$)$_2$}{NH(SiRMe$_2$)$_2$} (**Int_C–H**) (R = Me or H). Loss of HN(SiMe$_3$)$_2$ or HN(SiHMe$_2$)$_2$ and κ^1*C*,κ^2*N*-C(Me$_2$pz)$_3$ → κ^3*N*-C(Me$_2$pz)$_3$ rearrangement subsequently forms **1** or **3**, respectively. As mentioned in the Introduction (Section 2.2), structurally authenticated examples of C-metallated pyrazolylmethanides have been reported previously (**2.0** and **2.5**, Figure 2.1).[11, 17] The compound Cd{C(Me$_2$pz)$_3$}{κ^1*C*, κ^2*N*-C(pz)$_3$},

synthesised by collaborators, is shown by crystallography and NOESY spectra to contain a κ^1*C*, κ^2*N*-bound pyrazolylmethanide ligand. Previous DFT calculations for model compounds M{κ^1*C*-C(Me_2pz)$_3$}Me (2-coordinate; M = Mg or Zn) and M{κ^3*N*-C(Me_2pz)$_3$}Me (4-coordinate) predicted a substantial thermodynamic preference for the conversion of M{κ^1*C*-C(Me_2pz)$_3$}Me to M{κ^3*N*-C(Me_2pz)$_3$}Me (199.2 and 111.3 kJ mol^{-1} for M = Mg and Zn, respectively). The experimental observations that only **1** or **3**, rather than **Int_C–H** or its amine-free analogue, are obtained from **2.21** or **2** are consistent with these previous calculations.

As shown in Scheme 2.0, both Mg{C(Me_2pz)$_3$}{N($SiMe_3$)$_2$} (**1**) and Mg{C(Me_2pz)$_3$}{N($SiHMe_2$)$_2$} (**3**) reacted slowly with further HC(Me_2pz)$_3$ at 70 ^{o}C in C_6D_6 to form Mg{C(Me_2pz)$_3$}$_2$. Under identical conditions of temperature and concentration, the reaction time for **1** (*ca.* 3 days) was noticeably longer than for **3** (*ca.* 2 days). Since the formation of **1** from the intermediate adduct **2.21** was faster than for the less sterically encumbered system (i.e. **2** → **3**), the slower reaction of **1** with additional HC(Me_2pz)$_3$ can be attributed to a more effective steric shielding of the magnesium centre in **1** by the bulky amide (this is consistent with the faster rates of reaction of the calcium congener, see below). We were not able to detect any pre-coordination of HC(Me_2pz) to Mg{C(Me_2pz)$_3$}{N($SiRMe_2$)$_2$} (R = H or Me) when the reactions were followed on the NMR tube scale, either at low or high temperature.

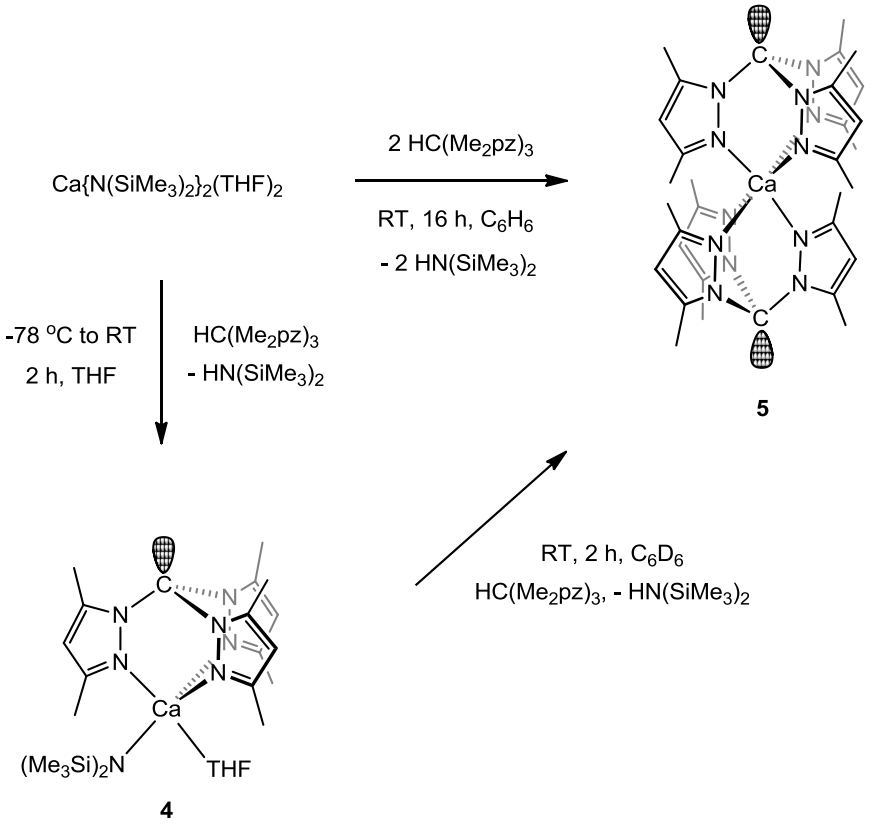
As shown in Figure 2.11, the reaction between **3** and 10 equivalents of either HC(Me_2pz) or DC(Me_2pz)$_3$ at 50 ^{o}C in C_6D_6 follows pseudo first order kinetics with observed rate constants k_{obs}(H) = 6.75(2) x 10^{-5} s^{-1} and k_{obs}(D) = 4.50(2) x 10^{-5} s^{-1}, respectively, for the consumption of **3**. The k_{obs}(H)/k_{obs}(D) value of 1.51(4) indicates a slightly reduced primary KIE for **3** → Mg{C(Me_2pz)$_3$}$_2$ compared with that for **2** → **3** (Figure 2.9), but the two KIEs are nonetheless broadly similar.

Figure 2.11. Pseudo first order plots for the reaction of Mg{C(Me$_2$pz)$_3$}{N(SiHMe$_2$)$_2$} (**3**) with an excess (10 equivalents.) of HC(Me$_2$pz)$_3$ (red circles, R^2 = 0.998) or DC(Me$_2$pz)$_3$ (blue squares, R^2 = 0.997) at 50 ^{o}C to form Mg{C(Me$_2$pz)$_3$}$_2$. I and I$_0$ refer to the normalized concentration of **3** at the given time and at time = 0, respectively. k_{obs}(H) = 6.75(2) x 10^{-5} s^{-1}; k_{obs}(D) = 4.50(2) x 10^{-5} s^{-1}; k_{obs}(H) / k_{obs}(D) = 1.51(4).



The reactions of the heavier congener Ca{N(SiMe$_3$)$_2$}$_2$(THF)$_2$ with HC(Me$_2$pz)$_3$ are summarized in Scheme 2.1. Reaction with 1 or 2 equivalents. of tris(dimethylpyrazolyl)methane afforded the 5-coordinate half-sandwich compound Ca{C(Me$_2$pz)$_3$}{N(SiMe$_3$)$_2$}(THF) (**4**) or the homoleptic analogue Ca{C(Me$_2$pz)$_3$}$_2$ (**5**) in 85% and 61% isolated yield, respectively. These are the first tris(pyrazolyl)methanide complexes of calcium. Both reactions were significantly faster than for those of Mg{N(SiRMe$_2$)$_2$}$_2$ (R = H or Me, Scheme 2.0). Compound **4** reacted readily with HC(Me$_2$pz)$_3$ in C$_6$D$_6$ to form **5** quantitatively after 2 hours at room temperature. As mentioned above, the corresponding reaction for magnesium (i.e., **1** → Mg{C(Me$_2$pz)$_3$}$_2$) required 3 days at 70 ^{o}C under otherwise identical conditions. These observations may be attributed, at least in part, to the reduced steric effects for the larger metal. The carbanion carbon resonance C(Me$_2$pz)$_3$ for **4** appears at 72.4 ppm in the ^{13}C NMR spectrum, which is very similar to the corresponding values for **1** and **3** (72.5 and 71.9 ppm, respectively) and typical for tris(pyrazolyl)methanide complexes featuring "free" carbanions.[13-15, 17-19, 21] Unfortunately, compound **5** was too insoluble to obtain a satisfactory ^{13}C NMR spectrum.

Scheme 2.1. Reactions of $Ca\{N(SiMe_3)_2\}_2(THF)_2$ with $HC(Me_2pz)_3$.



The solid state structures of $Ca\{C(Me_2pz)_3\}\{N(SiMe_3)_2\}(THF)$ (**4**) and $Ca\{C(Me_2pz)_3\}_2$ (**5**) are shown in Figure 2.12. Together with the NMR and other data, these confirm the presence of cationic calcium centers with one or two carbanionic moieties, respectively. Compound **4** has a distorted trigonal bipyramidal geometry at Ca(1). The $N(SiMe_3)_2$ ligand occupies one of the equatorial coordination sites, and the THF donor and N(1) of the $C(Me_2pz)_3$ ligand are in the axial positions. An analogous geometry was reported by Chisholm for the tris(pyrazolyl)hydroborate compound $Ca\{HB(^iPrpz)_3\}$-$\{N(SiMe_3)_2\}(THF)$.[40] The distances and angles around calcium in this complex are comparable to those in **4**. The aforementioned $Mg\{C(Me_2pz)_3\}Ph(THF)$ (**11**) also has an approximately trigonal bipyramidal geometry at magnesium with the Ph and THF ligands in equatorial and axial positions, respectively.[21] Compound **5** possesses an almost ideal D_{3d} symmetric structure and is the analogue of both $Mg\{C(Me_2pz)_3\}_2$ and the bis(hydroborate) compound $Ca\{HB(Me_2pz)_3\}_2$.[42] The average Ca-N_{pz} distance in **5** (avg. 2.448 Å, range 2.437(2) – 2.459(2) Å) is experimentally identical to that in $Ca\{HB(Me_2pz)_3\}_2$ (2.454(2) Å) as expected based on previous comparisons of homoleptic complexes of the two types of ligand (e.g., for $Mg\{C(Me_2pz)_3\}_2$ and $Mg\{HB(Me_2pz)_3\}_2$ average Mg-N_{pz} distances of 2.189 and 2.186 Å were found).[18, 21]

Figure 2.12. Displacement ellipsoid plots (20% probability) of $Ca\{C(Me_2pz)_3\}\{N(SiMe_3)_2\}(THF)$ (**4**, left) and $Ca\{C(Me_2pz)_3\}_2$ (**5**, right). H atoms omitted.

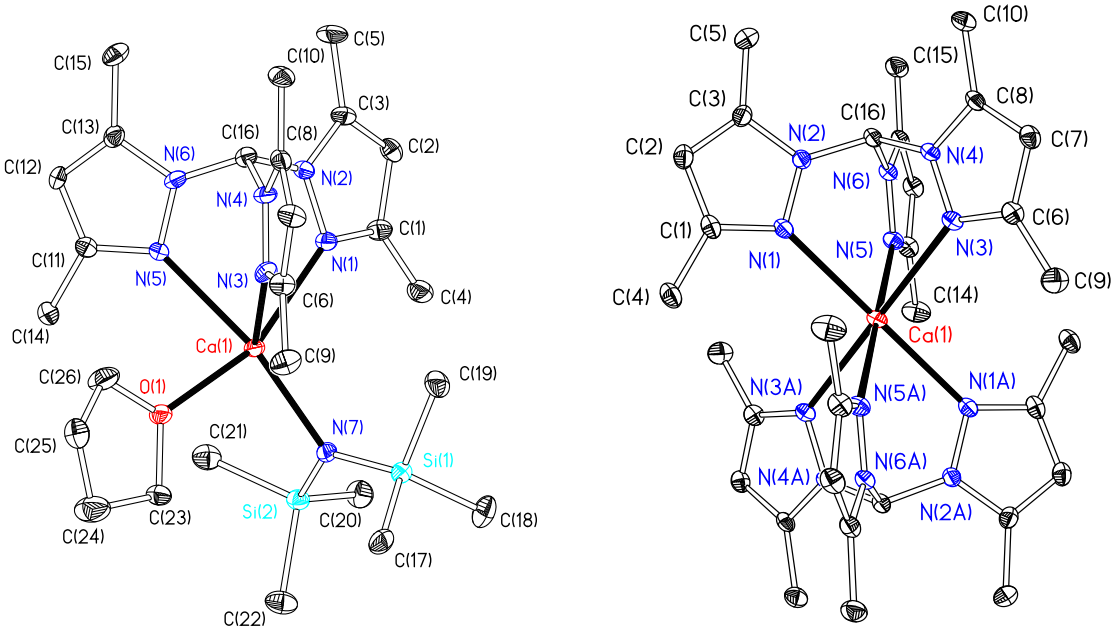


Table 2.2. Selected bond distances (Å) and angles (°) for $Ca\{C(Me_2pz)_3\}\{N(SiMe_3)_2\}$-(THF) (**4**).

Ca(1)-N(1)	2.436(7)	N(1)-Ca(1)-N(7)	104.1(2)
Ca(1)-N(3)	2.412(6)	N(3)-Ca(1)-N(7)	125.3(2)
Ca(1)-N(5)	2.454(6)	N(5)-Ca(1)-N(7)	155.9(2)
Ca(1)-N(7)	2.322(6)	O(1)-Ca(1)-N(7)	96.8(2)

Table 2.3. Selected bond distances (Å) and angles (°) for $Ca\{C(Me_2pz)_3\}_2$ (**5**).

Ca(1)-N(1)	2.4370(18)	N(1)-Ca(1)-N(3)	77.81(6)
Ca(1)-N(3)	2.4591(16)	N(1)-Ca(1)-N(5)	77.43(6)
Ca(1)-N(5)	2.448(2)	N(3)-Ca(1)-N(5)	75.48(6)

2.3 Synthesis of Group 12 tris(pyrazolyl)methan*ide* complexes

In order to develop further the chemistry of Group 12 tris(pyrazolyl)methanide complexes, the only previous example being Zn{C(Me$_2$pz)$_3$}Me (**2.11**, Figure 2.1),[21] attention was turned to the synthesis and structures of new zinc (Scheme 2.2) complexes. As stated in the Introduction, HC(Me$_2$pz)$_3$ reacts rapidly with MgR$_2$ (R = Bu or Ph) at room temperature to form homoleptic Mg{C(Me$_2$pz)$_3$}$_2$. In contrast, even on heating with an excess of ZnMe$_2$, it takes several days for the half-sandwich derivative Zn{C(Me$_2$pz)$_3$}Me (**2.11**) to form, and a homoleptic zinc analogue of Mg{C(Me$_2$pz)$_3$}$_2$ could not be obtained.[21] Unsurprisingly, therefore, the reactions of Zn{N(SiMe$_3$)$_2$}$_2$ with HC(Me$_2$pz)$_3$ yielded only trace amounts of product, even after extended periods of time (*ca.* 3 weeks) under thermally forcing conditions in refluxing hexanes. However, heating a solution of Li{C(Me$_2$pz)$_3$}(THF) (**2.2**) with anhydrous ZnCl$_2$ in THF for 24 h gave the sparingly soluble, half-sandwich complex Zn{C(Me$_2$pz)$_3$}Cl (**6**) in 40% yield after extraction into hot benzene. Subsequent reaction of **6** with NaN(SiMe$_3$)$_2$ or LiN(SiHMe$_2$)$_2$ formed Zn{C(Me$_2$pz)$_3$}{N(SiRMe$_2$)$_2$} (R = Me (**7**) or H (**8**)) in *ca*. 70% yield. The EI mass spectra of the three compounds **6** – **8** showed molecular ions with the expected isotope distributions, and the ^{13}C NMR spectra revealed resonances for the carbanion carbons C(Me$_2$pz)$_3$ in the range 71.3 – 73.0 ppm, as expected. Neither **7** nor **8** reacted with HC(Me$_2$pz)$_3$ on heating at 70 ^{o}C for 1 week in C$_6$D$_6$. Nonetheless, the homoleptic compound Zn{C(Me$_2$pz)$_3$}$_2$ (**9**) could be alternatively prepared by salt metathesis from ZnCl$_2$ and 2 equivalents of **2.2** after heating at 70 ^{o}C for 3 days. The NMR and other data for **9** are comparable to those for the magnesium and calcium analogues Mg{C(Me$_2$pz)$_3$}$_2$ and **5**.

Scheme 2.2. Synthesis of sandwich and half-sandwich zinc complexes.

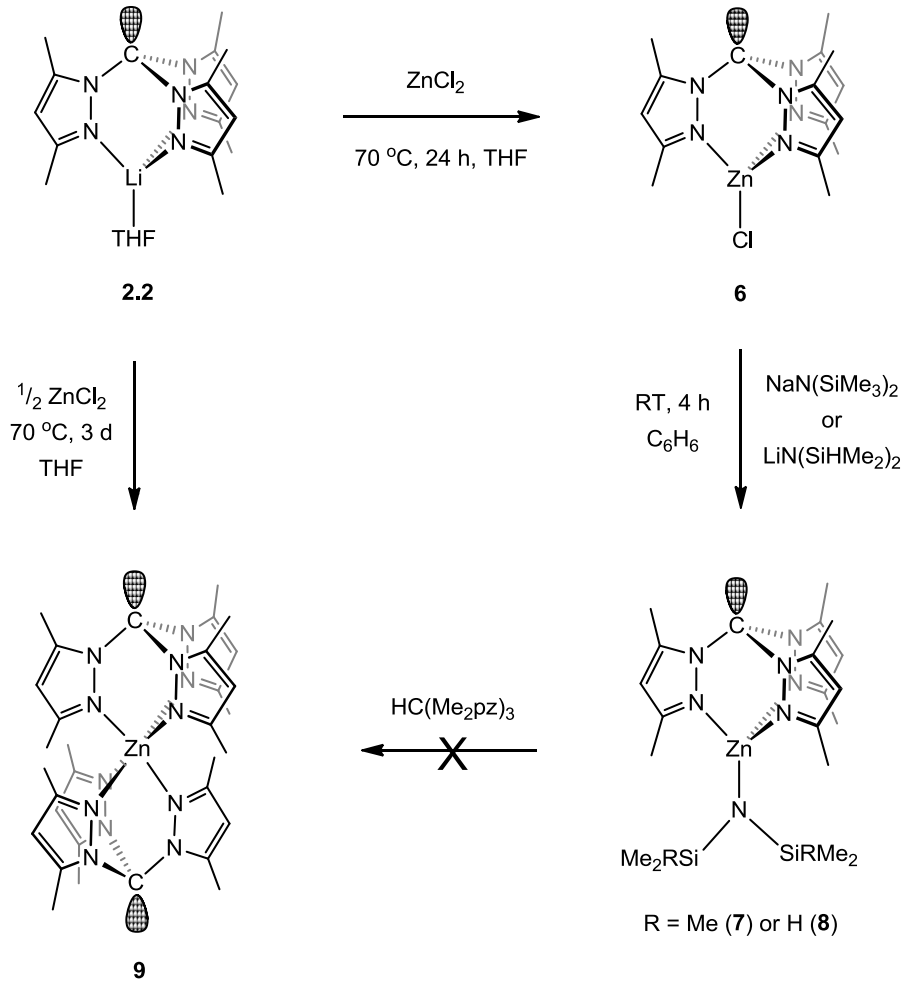


Figure 2.13 shows the solid state structures of Zn{C(Me$_2$pz)$_3$}Cl (**6**, left) and Zn{C(Me$_2$pz)$_3$}{N(SiMe$_3$)$_2$} (**7**, right); that of Zn{C(Me$_2$pz)$_3$}$_2$ (**9**) is given in Figure 2.14. The geometries around Zn(1) in **7** and **9** are analogous to those around magnesium in the analogous Mg{C(Me$_2$pz)$_3$}{N(SiMe$_3$)$_2$} (**1**) and Mg{C(Me$_2$pz)$_3$}$_2$ respectively. The M-N distances for the zinc complexes are systematically shorter as expected based on atomic radius trends.[43]

Although these are the first structurally characterized tris(pyrazolyl)methanide complexes of zinc, the structures of a large number of tris(pyrazolyl)hydroborate complexes of this element have been reported.[33] In general, the Zn-Cl, Zn-N$_{pz}$ and Zn-N(SiMe$_3$)$_2$ distances for **6** – **9** lie within the expected literature ranges.[33] The Zn-Cl and average Zn-N$_{pz}$ bond lengths in **6** are comparable to those of Zn{HB(Me$_2$pz)$_3$}Cl[44] (2.152(3) *vs.* 2.170(5), and 2.009 *vs.* 2.015 Å). Likewise, the structural data for **9** are similar to those of Zn{HB(Me$_2$pz)$_3$}$_2$[45] with average Zn-N$_{pz}$ distances of 2.162 and 2.177 Å, respectively. The dication [Zn{HC(Me$_3$pz)$_3$}$_2$]$^{2+}$ (Me$_3$pz = 3,4,5-trimethylpyrazolyl) has also been structurally characterized[46] and has an average Zn-N$_{pz}$ distance (2.166 Å) that is very similar to that of

9. Although this is at first sight surprising, it was previously found that the magnesium sandwich dication $[Mg\{HC(Me_2pz)_3\}_2]^{2+}$ has an average Mg–N_{pz} bond distance of 2.168 Å that is slightly shorter than in $Mg\{C(Me_2pz)_3\}_2$, despite the negative charge of the tris(pyrazolyl)methanide ligands in the latter.[21]

No tris(pyrazolyl)hydroborate analogue of **7** has been structurally characterized, but the Zn-$N(SiMe_3)_2$ distance of 1.913(5) Å is identical within error to the average distance (1.918 Å) for this bond in several 4-coordinate compounds containing a monoanionic N_3 donor ligand (or ligand set).[33, 47, 48] Compound **7** possesses a cationic $\{Zn\text{-}N(SiMe_3)_2\}^+$ moiety and two related (but non-zwitterionic) systems have been structurally characterized recently.[49, 50] The Zn-$N(SiMe_3)_2$ bond distance in **7** is identical within error to that in 4-coordinate $[Zn\{N(SiMe_3)_2\}(OEt_2)_3]^+$ (Zn-N = 1.907(3) Å) but longer than in $[Zn\{N(SiMe_3)_2\}\{ArNC(Me)C(Me)NAr\}]^+$ (Zn-N = 1.852(4) Å; Ar = 2,6-$C_6H_3Ph_2$) which possesses a 3-coordinate zinc cation.

Figure 2.13. Displacement ellipsoid plots (20 %) of one of the two crystallographically independent molecules of $Zn\{C(Me_2pz)_3\}Cl$ (**6**, left) and $Zn\{C(Me_2pz)_3\}\{N(SiMe_3)_2\}$ (**7**, right). H atoms omitted.

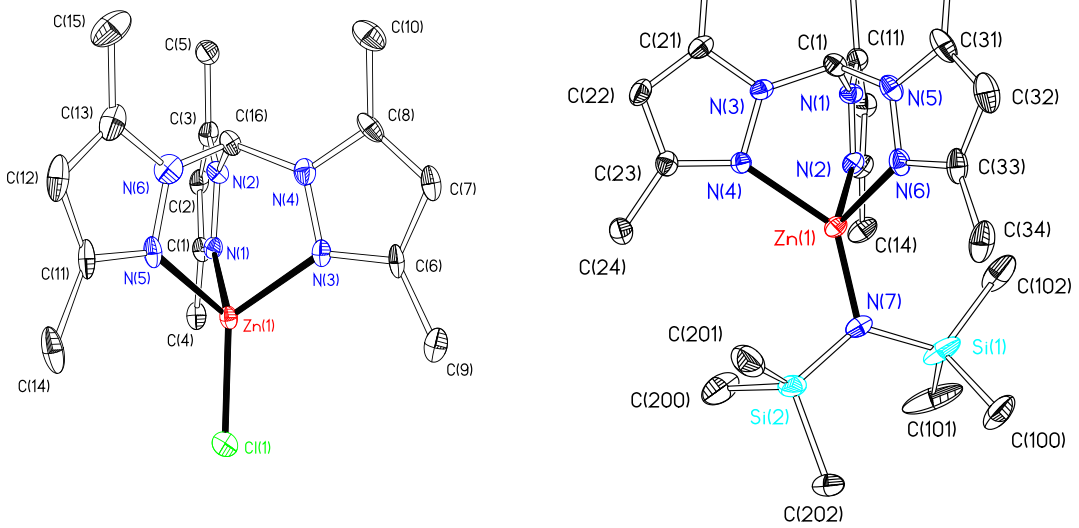


Table 2.4. Selected bond distances (Å) and angles (°) for Zn{C(Me$_2$pz)$_3$}Cl (**6**).

Zn(1)-N(1)	1.999(6)	N(1)-Zn(1)-Cl(1)	124.6(2)
Zn(1)-N(3)	2.013(6)	N(3)-Zn(1)-Cl(1)	124.9(2)
Zn(1)-N(5)	2.016(7)	N(5)-Zn(1)-Cl(1)	122.9(2)
Zn(1)-Cl(1)	2.152(3)		

Table 2.5. Selected bond distances (Å) and angles (°) for Zn{C(Me$_2$pz)$_3$}{N(SiMe$_3$)$_2$} (**7**).

Zn(1)-N(2)	2.054(4)	N(2)-Zn(1)-N(7)	123.7(2)
Zn(1)-N(4)	2.099(5)	N(4)-Zn(1)-N(7)	136.4(2)
Zn(1)-N(6)	2.039(5)	N(6)-Zn(1)-N(7)	115.7(2)
Zn(1)-N(7)	1.913(5)		

Figure 2.14. Displacement ellipsoid plot (20 %) of Zn{C(Me$_2$pz)$_3$}$_2$ (**23**).

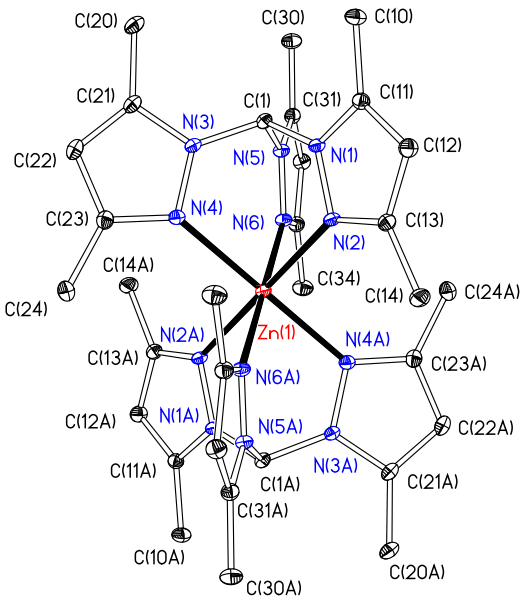


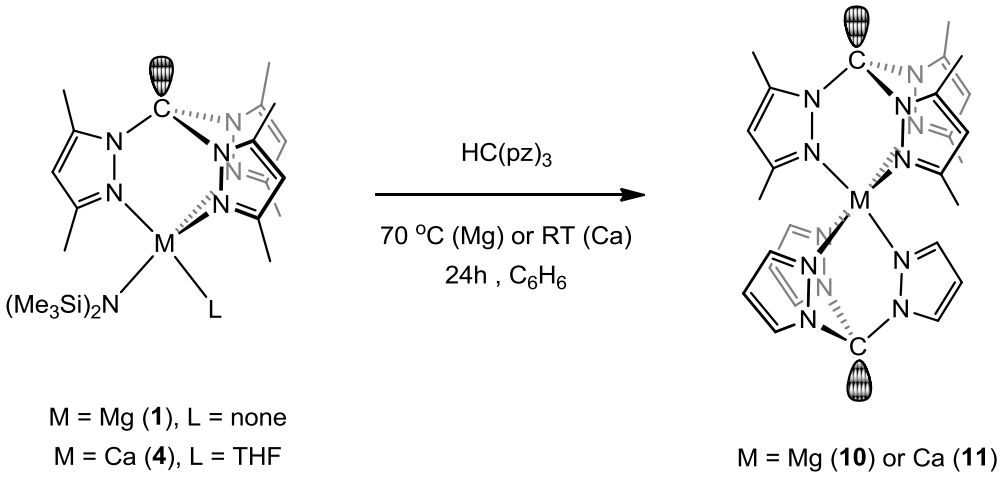
Table 2.6. Selected bond distances (Å) and angles (°) for $Zn\{C(Me_2pz)_3\}_2$ (**9**).

Zn(1)-N(2)	2.144(2)	N(2)-Zn(1)-N(4)	84.43(6)
Zn(1)-N(4)	2.180(2)	N(2)-Zn(1)-N(6)	84.40(6)
Zn(1)-N(6)	2.163(2)	N(4)-Zn(1)-N(6)	85.58(6)

2.4 Synthesis of heteroleptic zwitterionic sandwich complexes

In contrast to the successful synthesis of $Mg\{C(Me_2pz)_3\}_2$, attempts to prepare a homoleptic complex $Mg\{C(pz)_3\}_2$ from $MgBu_2$ and the "parent" $HC(pz)_3$ gave only poorly soluble materials.[21] This may be due to the several different potential coordination modes available to a sterically unconstrained tris(pyrazolyl)methanide ligand. Indeed, Stone's trimetallic compound **2.0** (Figure 2.1)[11] and $Ru\{C(pz)_3\}Cp^{R'}$ [20] are the only examples of unsubstituted tris(pyrazolyl)methanide complexes. It was therefore hoped that the already-introduced $C(Me_2pz)_3$ co-ligand in **1** or **4** would provide a sterically stabilising influence and allow the introduction of an unsubstituted tris(pyrazolyl)methanide ligand.

Equation 2.0 summarises the reactions of **1** and **4** with $HC(pz)_3$ which formed the target complexes of the composition $M\{C(Me_2pz)_3\}\{C(pz)_3\}$ (M = Mg (**10**) or Ca (**11**)) in *ca.* 55 – 75% yield. As for the corresponding reactions with $HC(Me_2pz)_3$ described above, more forcing conditions were needed for making **10** compared to **11**. The ^1H and ^{13}C NMR spectra of **10** and **11** are consistent with C_{3v} molecular symmetry and the EI mass spectra showed the expected molecular ions. Furthermore, the $^{13}C\{^1H\}$ NMR spectra of each showed resonances (assigned using the corresponding HMBC spectra) for two carbanionic carbons, namely $\underline{C}(Me_2pz)_3$ (72.1 and 72.8 ppm) and $\underline{C}(pz)_3$ (89.1 and 89.0 ppm) for **10** and **11** respectively. The difference in chemical shift between the tris(pyrazolyl)methan*ide* $\underline{C}(Me_2pz)_3$ and $\underline{C}(pz)_3$ resonances ($\Delta\delta$ = *ca.* 16.6 ppm) is somewhat larger than that between the tris(pyrazolyl)meth*ane* protio-ligands themselves ($\Delta\delta$ = 2.3 ppm; δ $H\underline{C}(Me_2pz)_3$ = 81.2 ppm; δ $H\underline{C}(pz)_3$ = 83.5 ppm). The nitrogen chemical shifts of both tris(pyrazolyl)methanide ligands $C(Me_2pz)_3$ and $C(pz)_3$ in complex **10** (indirectly measured from the $^1H,^{15}N$ gHMQC spectrum) slightly differ from each other. Closer examination of the the ^{15}N NMR cross-peaks allowed observation of the expected four nitrogen chemical shifts (δ = 232, 270 ppm ($C(Me_2pz)_3$) and 240, 278 ppm ($C(pz)_3$)), which is *a priori* consistent with the formulation of two κ^3*N*-coordinated ligands.



Equation 2.0

The solid state structure of **10** is shown in Figure 2.15 and confirms that proposed in Equation 2.0. Given the similarity of the spectroscopic data for **10** and **11** it is reasonable to assume that the two congeners have similar molecular structures. The Mg-N_{pz} distances for the $C(Me_2pz)_3$ ligand (avg. 2.169 Å) are on average shorter than for $C(pz)_3$ (avg. 2.184 Å). This is reflected in the Mg(1)···C(11) and Mg(1)···C(17) separations of 3.196(3) and 3.267(3) Å, and would be consistent with $C(Me_2pz)_3$ being the better donor (in accordance with previous studies of the donor abilities of different $HB(R_xpz)_3$ ligands).[51, 52]

Figure 2.15. Displacement ellipsoid plot (20% probability) of Mg{$C(Me_2pz)_3$}{$C(pz)_3$} (**10**). H atoms omitted.

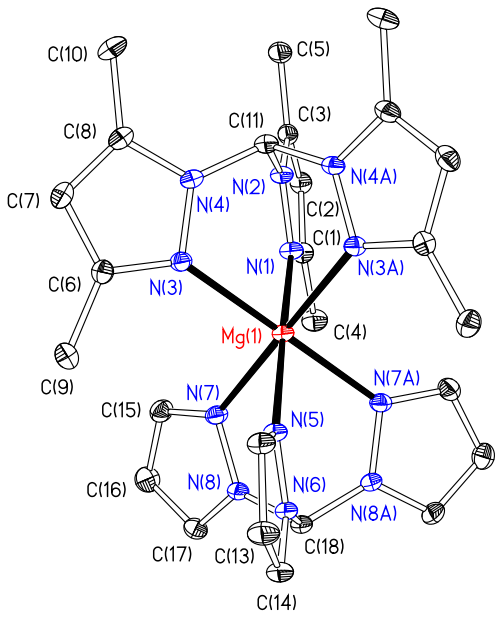
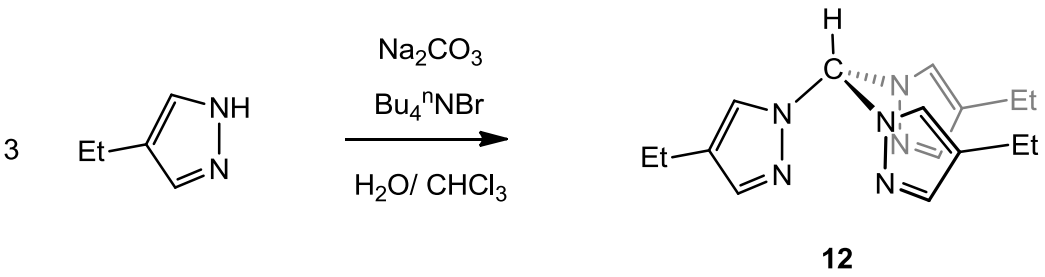


Table 2.7. Selected bond distances (Å) and angles (°) for Mg{C(Me$_2$pz)$_3$}{C(pz)$_3$} (**10**).

Mg(1)-N(1)	2.186(3)	N(1)-Mg(1)-N(3)	85.03(7)
Mg(1)-N(3)	2.1609(19)	N(3)-Mg(1)-N(3A)	84.4(1)
Mg(1)-N(5)	2.197(3)	N(5)-Mg(1)-N(7)	82.52(8)
Mg(1)-N(7)	2.177(2)	N(7)-Mg(1)-N(7A)	83.3(1)
Mg(1)··C(11)	3.196(3)		
Mg(1)···C(18)	3.267(3)		

Due to the relatively poor solubility of M{C(Me$_2$pz)$_3$}{C(pz)$_3$} (M = Mg (**10**), Ca (**11**)) and the subsequent negative consequences in polymerisation studies (e.g. inaccurate catalyst loadings and potentially reduced activity), the requirement for a {C(pz)$_3$} moiety with increased solubility became apparent. Therefore, the ligand HC(4-Etpz)$_3$ was designed and synthesised (Equation 2.1) by an analogous method used by Reger *et al*. in the synthesis of HC(Me$_2$pz)$_3$.[53] The solid state structure of **12** is shown in Figure 2.16 and confirms that proposed in Equation 2.1. The average N_{Pz}-C-N_{pz} angle of 110.8 ° shows the near perfect tetrahedral geometry around the apical C(16) atom.



12

Equation 2.1

Figure 2.16. Displacement ellipsoid plot (20% probability) of HC(4-Etpz)$_3$} **(12)**. H atoms omitted.

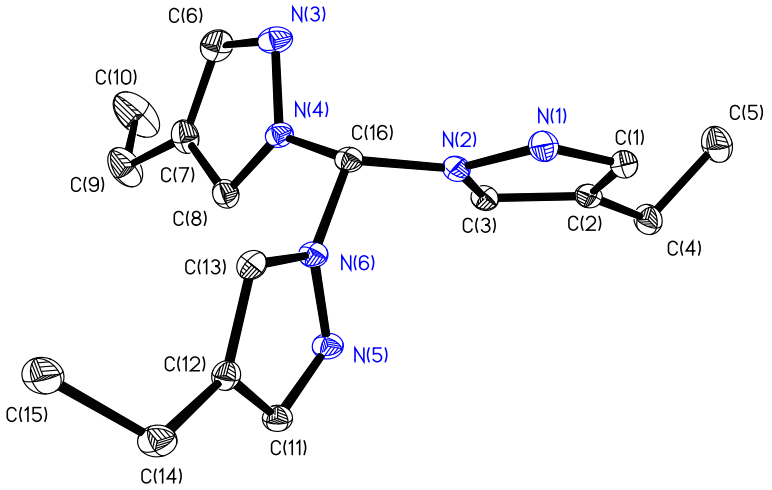
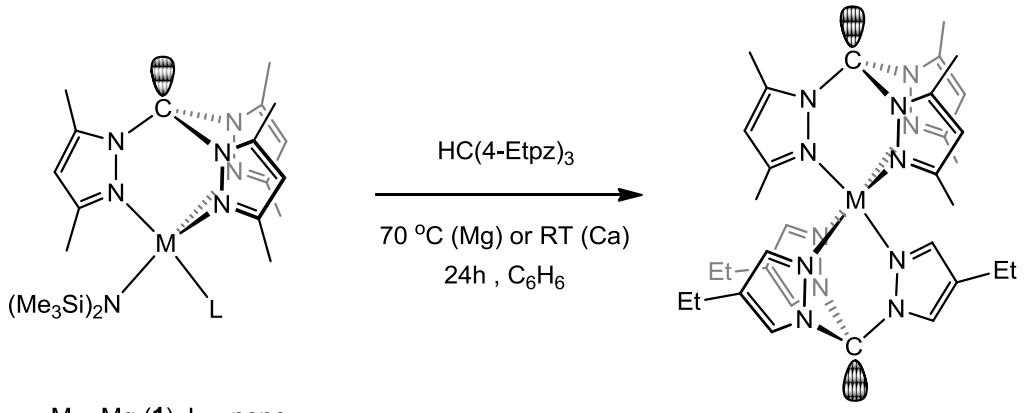


Table 2.8. Selected bond distances (Å) and angles (^{o}) for HC(4-Etpz)$_3$} (**12**).

C(16)-N(2)	1.442(2)	N(2)-C(16)-N(4)	109.91(13)
C(16)-N(4)	1.445(2)	N(2)-C(16)-N(6)	111.51(13)
C(16)-N(6)	1.449(2)	N(4)-Mg(1)-N(6)	111.08(14)

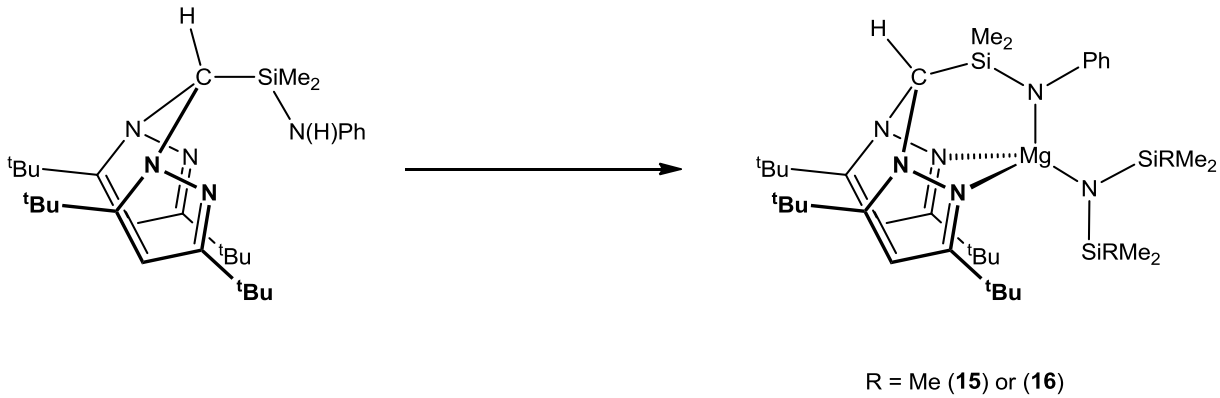
Equation 2.2 summarises the reactions of **1** and **4** with HC4-Et(pz)$_3$ which formed the target complexes of the composition M{C(Me$_2$pz)$_3$}{C(4-Etpz)$_3$} (M = Mg (**13**) or Ca (**14**)) in *ca.* 46 – 68% yield. As for the corresponding reactions with HC(Me$_2$pz)$_3$ described above, more forcing conditions were needed for making **13** compared to **14**. The ^{1}H and ^{13}C NMR spectra of **13** and **14** are consistent with C_{3v} molecular symmetry and the EI mass spectra showed the expected molecular ions. Furthermore, the ^{13}C{^{1}H} NMR spectra of each showed resonances (assigned using the corresponding HMBC spectra) for two carbanionic carbons, namely C(Me$_2$pz)$_3$ (73.1 and 73.3 ppm) and C(pz)$_3$ (90.0 and 90.8 ppm) for **13** and **14** respectively. The difference in chemical shift between the tris(pyrazolyl)methan*ide* C(Me$_2$pz)$_3$ and C(4-Etpz)$_3$ resonances ($\Delta\delta$ = *ca.* 17,2 ppm) is somewhat larger than that between the tris(pyrazolyl)meth*ane* protio-ligands themselves ($\Delta\delta$ = 2.4 ppm; δ HC(Me$_2$pz)$_3$ = 81.2 ppm; δ HC(4-Etpz)$_3$ = 83.6 ppm).



Equation 2.2

2.5 Synthesis of Group 2 heteroscorpionate complexes

Equation 2.3 summarises the reactions of $HC(^tBu_2pz)_2SiMe_2NHPh$ with $Mg\{N(SiMe_3)_2\}_2$ and the sterically less demanding $Mg\{N(SiHMe_2)_2\}_2$. The reactions with $Mg\{N(SiMe_3)_2\}_2$/ $Mg\{N(SiHMe_2)_2\}_2$ proceeded smoothly at 60 °C over 6 h and 24 h to afford the half-sandwich compounds $Mg\{HC(^tBu_2pz)_2SiMe_2NPh\}N(SiMe_3)_2$ (**15**) and $Mg\{HC(^tBu_2pz)_2SiMe_2NPh\}N(SiHMe_2)_2$ (**16**) in 49% and 53% recrystallised yields respectively. As with the reactions of $HC(Me_2pz)_3$ and $Mg\{N(SiMe_3)_2\}_2$ or $Mg\{N(SiHMe_2)_2\}_2$ (Scheme 2.0) there was no evidence of sandwich complex ($Mg\{HC(^tBu_2pz)_2SiMe_2NPh\}_2$) formation. In fact, compounds (**15**) and (**16**) were the only products of 2:1 NMR scale reactions between $HC(^tBu_2pz)_2SiMe_2NHPh$ and $Mg\{N(SiMe_3)_2\}_2$ or $Mg\{N(SiHMe_2)_2\}_2$ under identical conditions.



Equation 2.3

The NMR spectra of **15** and **16** are consistent with the structures proposed in Equation 2.3, assuming fast rotation about the Mg-$N(SiRMe_2)_2$ bonds. The solid state structures of **15** and **16** are shown in Figure 2.17. The approximately tetrahedral magnesium atoms are κ^2N

bound to a bis(pyrazolyl)methane ligand. The Mg-N_{pz} bond lengths (avg. 2.230 Å in **15** and 2.192 Å in **16)** are longer than those in Mg{$C(Me_2pz)_3$}{$N(SiMe_3)_2$} (**1**) (avg. 2.115 Å) consistent with various steric factors in the three compounds. The Mg-$N(SiRMe_3)_2$ distances are within the expected ranges.[33] The largest N-Mg-$N(SiMe_3)_2$ angle and longest Mg-N_{pz} bond in both **15** and **16** is associated with N(5) due to steric repulsions between the methyl groups attached to Si(2) and the phenyl group attached to N(5). The Si(3)Me group has less steric impact as it is able to lodge into the cleft between the pyrazolyl rings. The smaller average N_{pz}-Mg-$N(SiMe_3)_2$ angle in **16** (114.2 °) compared to that in **15** (120.4 °) is consistent with the presence of the less bulky $SiHMe_2$ group in **16** compared to the more bulky $SiMe_3$ group in **15**.

Figure 2.17. Displacement ellipsoid plot (20% probability) of Mg{$HC(^tBu_2pz)_2SiMe_2NPh$}$N(SiMe_3)_2$ (**15**, left) Mg{$HC(^tBu_2pz)_2SiMe_2NPh$}-$N(SiHMe_2)_2$ (**16**, right). C-bound H atoms omitted and remaining H atoms drawn as spheres of an arbitrary radius.

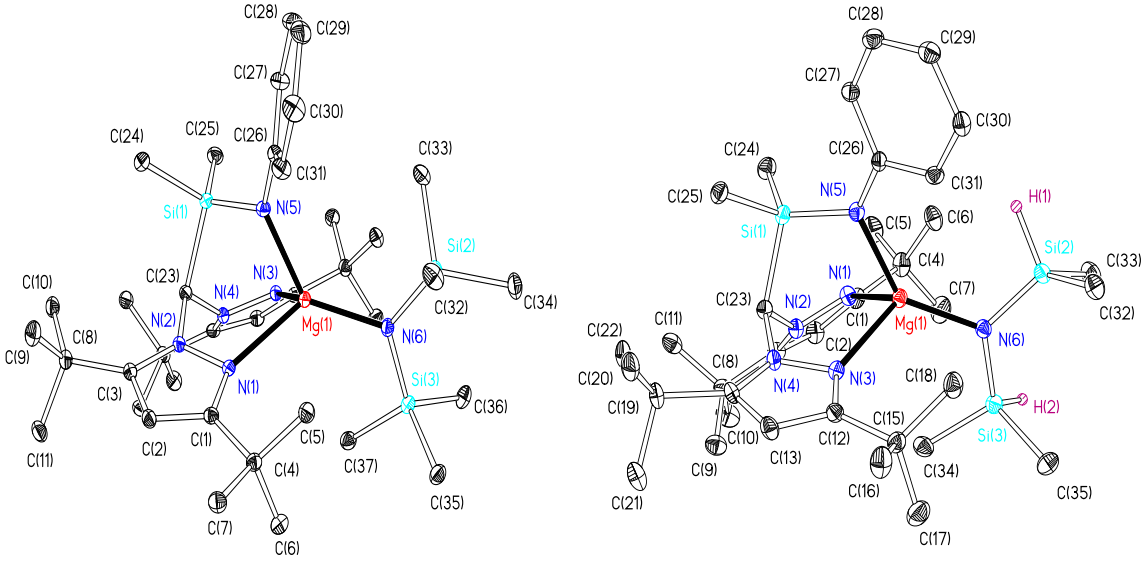


Table 2.9. Selected bond distances (Å) and angles (°) for Mg{$HC(^tBu_2pz)_2SiMe_2NPh$}$N(SiMe_3)_2$ (**15**).

Mg(1)-N(1)	2.254(2)	N(1)-Mg(1)-N(6)	123.88(8)
Mg(1)-N(3)	2.206(2)	N(3)-Mg(1)-N(6)	116.93(8)
Mg(1)-N(5)	2.023(2)	N(5)-Mg(1)-N(6)	129.76(8)
Mg(1)-N(6)	2.023(2)		

Table 2.10. Selected bond distances (Å) and angles (°) for $Mg\{HC(^tBu_2pz)_2SiMe_2NPh\}N(SiHMe_2)_2$ (**16**).

Mg(1)-N(1)	2.167(4)	N(1)-Mg(1)-N(6)	109.39(15)
Mg(1)-N(3)	2.217(4)	N(3)-Mg(1)-N(6)	119.10(15)
Mg(1)-N(5)	2.027(4)	N(5)-Mg(1)-N(6)	138.33(16)
Mg(1)-N(6)	2.002(4)		

2.6 Polymerisation studies: ROP of ε-CL

One of the aims of this work was to assess the performance of the heteroleptic homo- and hetero-scorpionate amide complexes **1, 3, 4, 7, 8, 15** and **16** for the catalytic ROP of ε-CL and *rac*-LA, in light of the success of related complexes previously discussed for similar purposes.[40, 54-57] An initial study using the seven compounds was undertaken using ε-CL owing to the relative ease of its polymerisation (compared to LA) due to the favourable release of 7-membered ring strain.

Initial studies at room temperature in THF or toluene showed the amide complexes **1, 3, 4, 7, 8, 15** and **16** to be highly active for the ROP of ε-CL, in some cases reaching full conversion in less than one minute in either solvent. The results are summarised in table 2.11. The calculated M_n values are those expected for one polymer chain growing per metal centre. All of the complexes gave a higher than expected observed M_n value by GPC, consistent with a much greater rate of propagation than rate of initiation in a coordination-insertion mechanism.[58] The observed M_n values are also for the most part in better agreement with calculated M_n for polymerisations performed in THF. This is likely to be due to the effect of THF competing with the monomer for coordination to the metal centre, thus reducing the relative rate of propagation (compared to that present in non-coordinating toluene solvent).

The PDI values for polymerisations performed in THF are also generally narrower than corresponding polymerisations performed in toluene (although these are collectively all in the moderate to very poor range). This is also likely to be a direct consequence of the coordinative nature of THF compared to toluene. Broad PDI values are well documented to be the result of intra- and intermolecular transesterification reactions.[58] It is reasonable to

assume that the presence of THF molecule bound to a metal coordination site would reduce the likelihood of 'backbiting' by a growing polymer chain at the metal centre.

Due to the viscous nature of the polymer formed and the short times involved, it was not possible to acquire full kinetic data over the course of each polymerisation, nor was it possible to collect MALDI-ToF analysis of polymer samples due to the high observed M_n values. However, the polymerisation inactivity of the complexes $Mg\{C(Me_2pz)_3\}_2$ (**2.8**), $Ca\{C(Me_2pz)_3\}_2$ (**5**) and $Zn\{C(Me_2pz)_3\}_2$ (**9**) under identical conditions rules out the possibility of ROP initiated by the carbanion present in the $C(Me_2pz)_3$ moiety of the amide catalysts. Therefore coordination-insertion has been deduced to be the most likely mechanism of polymerisation with these complexes.

Table 2.11. Solution polymerisation of ε-CL by Mg{C(Me$_2$pz)$_3$}{N(SiMe$_3$)$_2$} (**1**), Mg{C(Me$_2$pz)$_3$}{N(SiHMe$_2$)$_2$} (**3**), Ca{C(Me$_2$pz)$_3$}{N(SiMe$_3$)$_2$}(THF) (**4**), Zn{C(Me$_2$pz)$_3$}{N(SiMe$_3$)$_2$} (**7**), Zn{C(Me$_2$pz)$_3$}{N(SiHMe$_2$)$_2$} (**8**), Mg{HC(^{t}Bu$_2$pz)$_2$SiMe$_2$NPh}N(SiMe$_3$)$_2$ (**15**), Mg{HC(^{t}Bu$_2$pz)$_2$SiMe$_2$NPh}N(SiHMe$_2$)$_2$ (**16**).[a]

Catalyst	Solvent	Yield (%)[b]	Time (mins)	M_n(GPC)[c]	M_n (calcd)[d]	M_w/M_n
Mg{C(Me$_2$pz)$_3$}{N(SiMe$_3$)$_2$} (**1**)	THF	72	< 1	16,130	11,414	2.64
Mg{C(Me$_2$pz)$_3$}{N(SiMe$_3$)$_2$} (**1**)	Toluene	72	< 1	72,650	11,414	1.65
Mg{C(Me$_2$pz)$_3$}{N(SiHMe$_2$)$_2$} (**3**)	THF	78	< 1	17,230	11,414	2.94
Mg{C(Me$_2$pz)$_3$}{N(SiHMe$_2$)$_2$} (**3**)	Toluene	83	< 1	85,970	11,414	1.71
Ca{C(Me$_2$pz)$_3$}{N(SiMe$_3$)$_2$}(THF) (**4**)	THF	71	< 1	17,720	11,414	2.65
Ca{C(Me$_2$pz)$_3$}{N(SiMe$_3$)$_2$}(THF) (**4**)	Toluene	77	< 1	31,360	11,414	2.19
Zn{C(Me$_2$pz)$_3$}{N(SiMe$_3$)$_2$} (**7**)	THF	70	30	27,250	11,414	3.03
Zn{C(Me$_2$pz)$_3$}{N(SiMe$_3$)$_2$} (**7**)	Toluene	61	25	40,820	11,414	3.09
Zn{C(Me$_2$pz)$_3$}{N(SiHMe$_2$)$_2$} (**8**)	THF	68	30	16,460	11,414	5.33
Zn{C(Me$_2$pz)$_3$}{N(SiHMe$_2$)$_2$} (**8**)	Toluene	78	25	47,390	11,414	3.32
Mg{HC(^{t}Bu$_2$pz)$_2$SiMe$_2$NPh}N(SiMe$_3$)$_2$ (**15**)	THF	81	30	66,620	11,414	1.67
Mg{HC(^{t}Bu$_2$pz)$_2$SiMe$_2$NPh}N(SiMe$_3$)$_2$ (**15**)	Toluene	73	20	84,840	11,414	2.79
Mg{HC(^{t}Bu$_2$pz)$_2$SiMe$_2$NPh}N(SiHMe$_2$)$_2$ (**16**)	THF	76	25	71,450	11,414	1.86
Mg{HC(^{t}Bu$_2$pz)$_2$SiMe$_2$NPh}N(SiHMe$_2$)$_2$ (**16**)	Toluene	79	25	89,740	11,414	3.17

[a] Conditions: [ε-CL]:[catalyst] = 100:1, 3.4 mL solvent at 23 °C. See Experimental section for other details. [b] Isolated yield at 100 % NMR conversion. [c] Molecular weights (g mol^{-1}) determined from GPC using the appropriate Mark-Houwink corrections. [d] Expected M_n (g mol^{-1}) for 1 chain growing per metal centre at 100% conversion, ignoring end groups.

2.7 Polymerisation studies: ROP of *rac*-LA

Polymerisation studies were next extended to the more challenging monomer, *rac*-LA. Due to the more encouraging results with ε-CL observed using THF as a solvent, and solubility issues with some of the complexes, it was decided to focus solely on THF mediated polymerisations. The results are summarised in Table 2.12.

One of the several interesting contrasts with the ε-CL polymerisation results is that the *rac*-LA polymerisations all required elevated temperatures and extended reaction times, largely due to the unfavourable release of the stable 6-membered ring strain in *rac*-LA when compared to the less thermodynamically stable 7-membered ring strain in ε-CL. The observed M_n values are also generally in much closer agreement to the expected values for the amide catalysts (for one growing polymer chain per metal centre). However, the relatively broad PDI values are also evident in *rac*-LA polymerisations, no doubt due in part to the increased tendency of transesterification side reactions at elevated temperatures. Disappointingly, no stereochemical enrichment in the PLA polymer produced was observed.

As was the case with ε-CL polymerisations, the complexes Mg{C(Me$_2$pz)$_3$}$_2$ (**2.8**), Ca{C(Me$_2$pz)$_3$}$_2$ (**5**) and Zn{C(Me$_2$pz)$_3$}$_2$ (**9**) were all inactive for the ROP of *rac*-LA under identical polymerisation conditions, again ruling out the possibility of initiation by the carbanion present in the C(Me$_2$pz)$_3$ moiety of the amide catalysts (the activity of complexes Mg{C(Me$_2$pz)$_3$}{C(pz)$_3$} (**10**), Ca{C(Me$_2$pz)$_3$}{C(pz)$_3$} (**11**), Mg{C(Me$_2$pz)$_3$}{C(4-Etpz)$_3$} (**13**) and Ca{C(Me$_2$pz)$_3$}{C(4-Etpz)$_3$} (**14**) are discussed below).

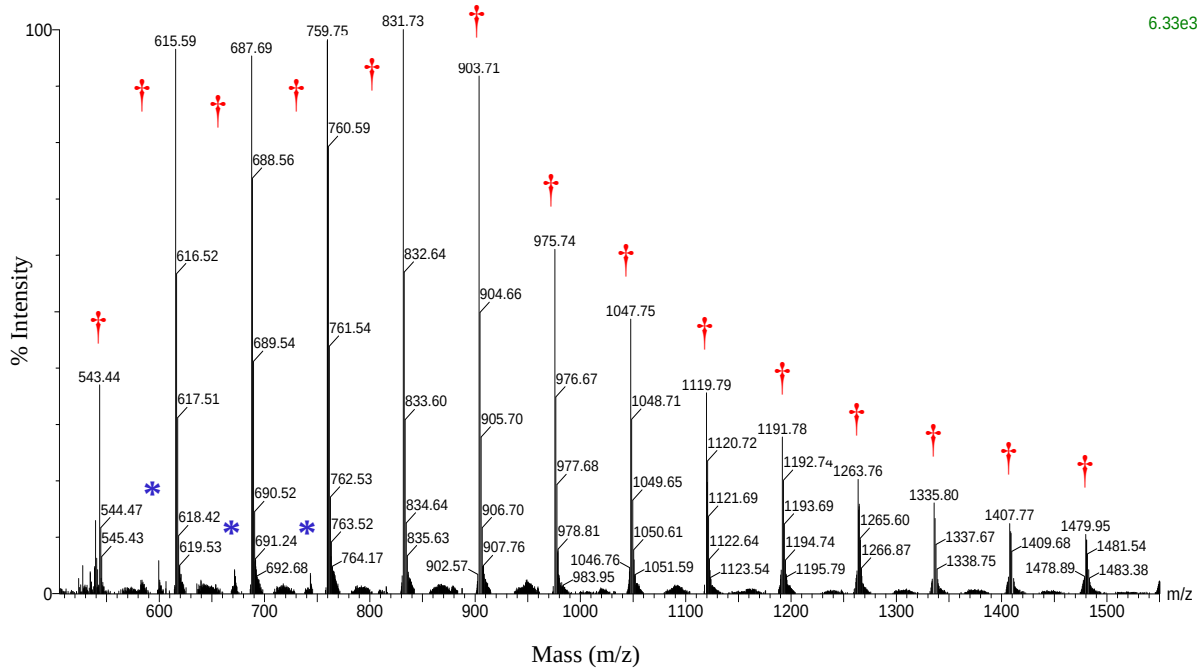
Unfortunately, quenching the polymerisations resulted mostly in hydrolysis of any potential amide end-groups that would have been formed through a coordination-insertion mechanism, and therefore it was not possible to identify these by ^{1}H NMR. However, the MALDI-ToF spectrum (Figure 2.18) obtained by analysis of a polymer produced by Mg{C(Me$_2$pz)$_3$}{N(SiHMe$_2$)$_2$} **(3)** did provide some useful information. The spectrum shows a primary distribution of integer polymer units († in Figure 2.15) with a separation of 72 *m/z* (half a lactide unit), strong evidence (along with broad PDI values) for transesterifcation side reactions leading to cyclic whole and half LA units. Also present is a minor secondary distribution (* in Figure 2.18), again with a separation of 72 *m/z*, corresponding to polymer chains with N(SiHMe$_2$)$_2$ end groups. This is consistent with the work reported by Okuda *et al*. investigating the use of rare earth bis(phenolate) amide complexes for the ROP of *rac*-lactide.[59]

Table 2.12. Solution polymerisation of *rac*-LA by Mg{C(Me$_2$pz)$_3$}{N(SiMe$_3$)$_2$} (**1**), Mg{C(Me$_2$pz)$_3$}{N(SiHMe$_2$)$_2$} (**3**), Ca{C(Me$_2$pz)$_3$}{N(SiMe$_3$)$_2$}(THF) (**4**), Zn{C(Me$_2$pz)$_3$}{N(SiMe$_3$)$_2$} (**7**), Zn{C(Me$_2$pz)$_3$}{N(SiHMe$_2$)$_2$} (**8**), Mg{HC(^{t}Bu$_2$pz)$_2$SiMe$_2$NPh}-N(SiMe$_3$)$_2$ (**15**), Mg{HC(^{t}Bu$_2$pz)$_2$SiMe$_2$NPh}N(SiHMe$_2$)$_2$ (**16**), Mg{C(Me$_2$pz)$_3$}{C(pz)$_3$} (**10**), Ca{C(Me$_2$pz)$_3$}{C(pz)$_3$} (**11**), Mg{C(Me$_2$pz)$_3$}-{C(4-Etpz)$_3$} (**13**) and Ca{C(Me$_2$pz)$_3$}{C(4-Etpz)$_3$} (**14**).[a]

Catalyst	Conversion (%)	Time (hours)[b]	M_n(GPC)[c]	M_n (calcd)[d]	M_w/M_n
Mg{C(Me$_2$pz)$_3$}{N(SiMe$_3$)$_2$} (**1**)	86	2	32,700	12,400	1.57
Mg{C(Me$_2$pz)$_3$}{N(SiHMe$_2$)$_2$} (**3**)	86	2	22,760	12,400	2.19
Ca{C(Me$_2$pz)$_3$}{N(SiMe$_3$)$_2$}(THF) (**4**)	81	2	16,520	10,590	1.21
Zn{C(Me$_2$pz)$_3$}{N(SiMe$_3$)$_2$} (**7**)	94	4	18,820	13,550	1.77
Zn{C(Me$_2$pz)$_3$}{N(SiHMe$_2$)$_2$} (**8**)	91	4	31,860	13,120	1.37
Mg{HC(^{t}Bu$_2$pz)$_2$SiMe$_2$NPh}N(SiMe$_3$)$_2$ (**15**)	89	0.75	51,480	12,799	1.45
Mg{HC(^{t}Bu$_2$pz)$_2$SiMe$_2$NPh}N(SiHMe$_2$)$_2$ (**16**)	90	1.5	55,080	12,972	1.48
Mg{C(Me$_2$pz)$_3$}{C(pz)$_3$} (**10**)	91	6	9,370	13,116	2.13
Ca{C(Me$_2$pz)$_3$}{C(pz)$_3$} (**11**)	89	6	8,460	12,828	2.90
Mg{C(Me$_2$pz)$_3$}{C(4-Etpz)$_3$} (**13**)	90	8	17,420	12,972	4.08
Ca{C(Me$_2$pz)$_3$}{C(4-Etpz)$_3$} (**14**)	92	12	12,590	13,260	3.94

[a] Conditions: [*rac*-LA]:[catalyst] = 100:1, 6.0 mL THF at 70 °C. See Experimental section for other details. [b] % conversion by ^{1}H NMR. [c] Molecular weights (g mol^{-1}) determined from GPC using the appropriate Mark-Houwink corrections. [d] Expected Mn (g mol^{-1}) for 1 chain growing per metal centre at the % conversion by ^{1}H NMR.

Figure 2.18. MALDI-ToF MS of poly(rac-LA) synthesised using Mg{C(Me$_2$pz)$_3$}{N(SiHMe$_2$)$_2$} (**3**). M_n by GPC analysis was 4,520 g mol^{-1} (from a [rac-LA]$_0$:[catalyst]$_0$ = 20:1 polymerisation). † = cyclic PLA units, * = N(SiHMe$_2$)-capped polymer.

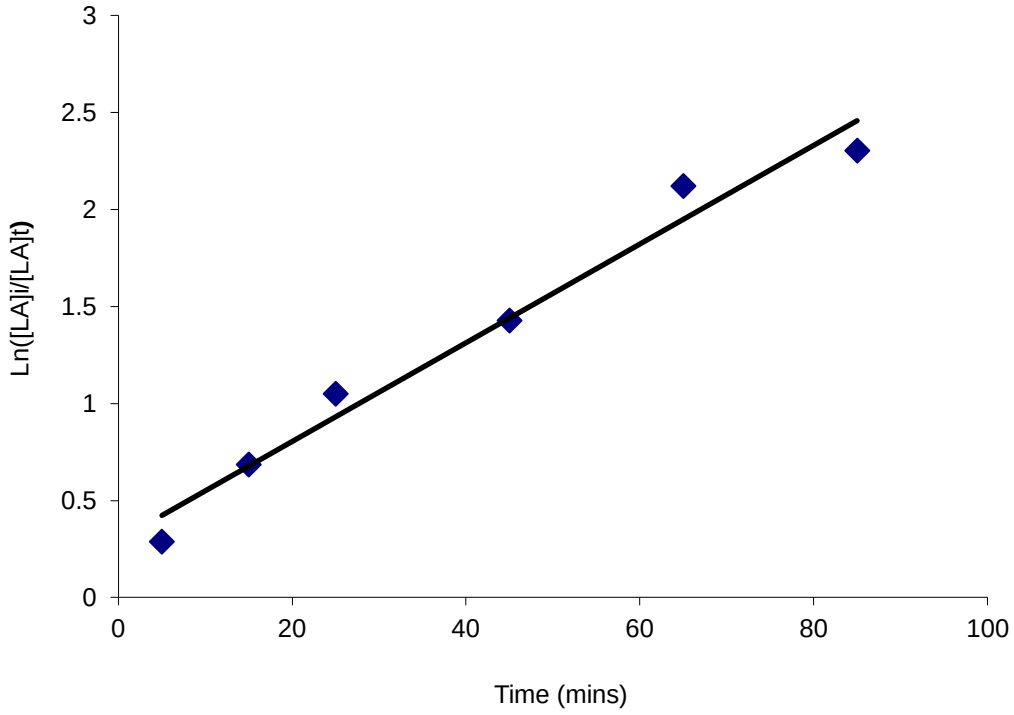


The most closely related complexes studied for the ROP of *rac*-lactide are Chisholm's (Tp^{tBu})Ca(X)(THF) (X = N(SiMe$_3$)$_2$ or O-2,6-C$_6$H$_3$^{i}Pr$_2$)[40, 57] These two complexes showed > 90% polymerisation in ~1 min at room temperature, giving polymer with *ca*. 80% heterotactic enrichment. The fact that stereochemical control was observed with Chisholm's catalysts, and not with the catalyst Ca{C(Me$_2$pz)$_3$}{N(SiMe$_3$)$_2$}(THF) (**4**) is most likely due to the presence of *tert*-butyl groups present around the metal centre in the former case promoting chain end control.

Despite the relatively poor polymerisation control shown by the complexes tested, detailed kinetics studies were carried out in some cases to investigate further the polymerisation process. Gratifyingly, despite the overall poor M_n and PDI values observed, all of the catalysts tested showed first order consumption of *rac*-LA, albeit after an initial induction period (up to approximately 20 minutes). Similar induction periods have also been observed in the ROP of cyclic esters using aluminium alkoxides[60, 61] or yttrium isopropoxides[62]. In these instances the induction period was thought to correspond to a period of ligand rearrangement around the metal centre, in order to allow the monomer access to the coordination sphere.[63] It is thought that a similar process occurs in this instance. An example plot is shown in Figure 2.19 for the catalyst Mg{HC(^{t}Bu$_2$pz)$_2$SiMe$_2$NPh}N(SiHMe$_2$)$_2$ (**16**). The measured rate constant for the

polymerisation, k_{obs} was 0.03(2) min^{-1}. This compares with a k_{obs} value of 0.04(3) min^{-1} for the related catalyst $Mg\{HC(^tBu_2pz)_2SiMe_2NPh\}N(SiMe_3)_2$ (**15**).

Figure 2.19. First order plot for *rac*-LA consumption using $Mg\{HC(^tBu_2pz)_2SiMe_2NPh\}N(SiHMe_2)_2$ (**16**).[a]



[a]Conditions [*rac*-LA_0]:[**16**] = 100:1, 6 mL THF, 70 °C, 0.1 mL aliquots taken at the given intervals. See Experimental section for other details.

The final point of interest is the polymerisation activity shown by the heteroleptic sandwich complexes $Mg\{C(Me_2pz)_3\}\{C(pz)_3\}$ (**10**), $Ca\{C(Me_2pz)_3\}\{C(pz)_3\}$ (**11**), $Mg\{C(Me_2pz)_3\}$-$\{C(4\text{-}Etpz)_3\}$ (**13**) and $Ca\{C(Me_2pz)_3\}\{C(4\text{-}Etpz)_3\}$ (**14**). Whilst it was previously noted that the complexes $Mg\{C(Me_2pz)_3\}_2$, $Ca\{C(Me_2pz)_3\}_2$ (**5**) and $Zn\{C(Me_2pz)_3\}_2$ (**9**) were all inactive for the ROP of *rac*-LA under identical polymerisation conditions, the difference between the two groups of complexes is the presence of a $C(pz)_3$ or $C(4\text{-}Etpz)_3$ moiety in the former compared to $\{C(Me_2pz)_3\}$ moieties in the latter.

It is likely that $C(pz)_3$ or $C(4\text{-}Etpz)_3$ is able to initiate ROP due to the lack of sterically hindering groups around the carbanion, compared to the degree of steric protection afforded by methyl groups in $C(Me_2pz)_3$. Also due to the absence of an amide initiating group in these catalysts a coordination-insertion mechanism centred on the metal ion cannot be envisaged. Therefore initiation through interaction with the carbanion in the $C(pz)_3$ or $C(4\text{-}Etpz)_3$ moiety and the *rac*-LA monomer is the likely possible mechanism. Further evidence supporting initiation by the carbanion, rather than by a group directly attached to the metal

centre, is the fact that in a family of related Tp^{tBu} calcium, magnesium and zinc aryloxide complexes, the observed order of *rac*-LA polymerisation activity was Ca>Mg>Zn.[40] It was postulated that this order was defined by the polarity of the initiating metal-oxygen bond. No such trend can be seen in Table 2.13 listing the data for Mg{$C(Me_2pz)_3$}{$C(pz)_3$} (**10**), Ca{$C(Me_2pz)_3$}{$C(pz)_3$} (**11**), Mg{$C(Me_2pz)_3$}-{$C(4\text{-}Etpz)_3$} (**13**) and Ca-{$C(Me_2pz)_3$}{$C(4\text{-}Etpz)_3$} (**14**).

Similarly to the amide complexes tested, polymerisations with Mg{$C(Me_2pz)_3$}{$C(pz)_3$} (**10**), Ca{$C(Me_2pz)_3$}{$C(pz)_3$} (**11**), Mg{$C(Me_2pz)_3$}{$C(4\text{-}Etpz)_3$} (**13**) and Ca-{$C(Me_2pz)_3$}{$C(4\text{-}Etpz)_3$} (**14**) all showed first order consumption of LA (after an initial induction period). The first order rate constants for these polymerisations are shown in Table 2.13.

Table 2.13. First order rate constants (k_{obs}) for *rac*-LA polymerisation by Mg{$C(Me_2pz)_3$}{$C(pz)_3$} (**10**), Ca{$C(Me_2pz)_3$}{$C(pz)_3$} (**11**), Mg{$C(Me_2pz)_3$}{$C(4\text{-}Etpz)_3$} (**13**) and Ca{$C(Me_2pz)_3$}{$C(4\text{-}Etpz)_3$} (**14**).[a]

Catalyst	k_{obs} (min^{-1})
Mg{$C(Me_2pz)_3$}{$C(pz)_3$} (**10**)	0.003(2)
Ca{$C(Me_2pz)_3$}{$C(pz)_3$} (**11**)	0.005(4)
Mg{$C(Me_2pz)_3$}{$C(4\text{-}Etpz)_3$} (**13**)	0.004(3)
Ca{$C(Me_2pz)_3$}{$C(4\text{-}Etpz)_3$} (**14**)	0.002(1)

[a] Conditions: [*rac*-LA $_0$]:[Catalyst] = 100:1, 6.0 mL THF, 70 °C.

Whilst the polymerisations all showed first order kinetics, the control of M_n with conversion was poor, i.e. non-linear growth was observed (even for the more soluble complexes Mg{$C(Me_2pz)_3$}{$C(4\text{-}Etpz)_3$} (**13**) and Ca{$C(Me_2pz)_3$}{$C(4\text{-}Etpz)_3$} (**14**). Also, MALDI-ToF spectra showed only cyclic (whole and half) PLA units. It would be expected that a nucleophilic polymerisation mechanism would show $C(4\text{-}Etpz)_3$ and $C(pz)_3$ capped PLA in MALDI-ToF spectra. However these groups would come in a very similar region to those of cyclic PLA units, therefore MALDI-ToF proved an inconclusive method.

In order to gain more insight into the polymerisation mechanism, an NMR scale experiment was carried out in which ten equivalents of *rac*-lactide were dissolved in THF-d_8 and added to one equivalent of Mg{$C(Me_2pz)_3$}{$C(4\text{-}Etpz)_3$} (**13**). The mixture was heated to 70 °C for two hours, after which time the products were analysed by ^{1}H NMR. This showed PLA,

a small amount of residual catalyst and, disappointingly, quantitative formation of HC(4-Etpz)$_3$. Therefore it is likely that the C(4-Etpz)$_3$ moiety merely acts as a base (and not a nucleophile), deprotonating a lactide monomer unit, forming an enolate and allowing for subsequent polymerisation of monomer units. The same mechanism is implied for the remaining heteroleptic sandwich complexes, although similarly conclusive evidence for the complexes Mg{C(Me$_2$pz)$_3$}{C(pz)$_3$} (**10**) and Ca{C(Me$_2$pz)$_3$}{C(pz)$_3$} (**11**) could not be obtained due to the relatively poor solubility of these complexes. The polymerisation mechanism for these four catalysts is therefore thought to be anionic and not nucleophilic. An anionic mechanism was also found for the ROP of LA using potassium *tert*-butoxide,[64] as well as primary and secondary lithium alkoxides.[65]

2.8 Summary and Conclusions

The work presented in this chapter has significantly extended the range of reported Group 2 and 12 tris(pyrazolyl)methanide complexes, primarily through the use of bulky amide metal precursors (except for in the case of zinc). By adjustment of the amide (SiMe$_3$ *vs* SiHMe$_2$) or pyrazolyl (Me$_2$pz *vs* pz) substituents, and/or the metal centres themselves new coordination modes, intermediates and fluxional processes have been observed. The diminished rates of reaction of the Group 12 amides with HC(Me$_2$pz)$_3$ parallel the results reported previously for ZnMe$_2$ and are consistent with lower bond polarities and higher metal effective nuclear charge, as analyzed previously using DFT.[21] Additional studies have shown primary kinetic isotope effects that are consistent with H/D–C(Me$_2$pz)$_3$ bond-breaking being important in the rate-determining step leading to zwitterion formation. The magnitudes of these KIEs are comparable for both sandwich and half-sandwich formation.

The amide complexes were found to be highly active for the ROP of ε-CL, although poor polymerisation control was observed, this is attributed to a much greater rate of propagation than rate of initiation in a coordination-insertion mechanism. However improved control was shown using THF rather than toluene as a solvent. For the ROP of *rac*-LA elevated temperatures were required. However, relatively poor control was again observed. The heteroleptic sandwich complexes Mg{C(Me$_2$pz)$_3$}{C(pz)$_3$} (**10**), Ca{C(Me$_2$pz)$_3$}{C(pz)$_3$} (**11**), Mg{C(Me$_2$pz)$_3$}{C(4-Etpz)$_3$} (**13**) and Ca{C(Me$_2$pz)$_3$}{C(4-Etpz)$_3$} (**14**) were also active for the ROP of *rac*-LA. However the polymerisation mechanism was shown to be more likely to be base-initiated rather than nucleophilic.

2.9 References

1. M. G. Cushion, J. Meyer, A. Heath, A. D. Schwarz, I. Fernández, F. Breher and P. Mountford, *Organometallics*, 2010, **29**, 1174-1190.
2. N. Marques, A. Sella and J. Takats, *Chem. Rev.*, 2002, **102**, 2137.
3. D. L. Reger, *Comm. Inorg. Chem.*, 1999, **21**, 1-28.
4. S. Trofimenko, *Chem. Rev.*, 1993, **93**, 943.
5. S. Trofimenko, *Scorpionates. The Coordination Chemistry of Polypyrazolylborate Ligands*, Imperial College Press, London, 1999.
6. H. R. Bigmore, S. C. Lawrence, P. Mountford and C. S. Tredget, *Dalton Trans.*, 2005, 635-651(Perspective Article review).
7. C. Pettinari and R. Pettinari, *Coord. Chem. Rev.*, 2005, **249**, 525-543.
8. C. Pettinari and R. Pettinari, *Coord. Chem. Rev.*, 2005, **249**, 663-691.
9. A. Otero, J. Fernandez-Baeza, A. Antinolo, J. Tejeda and A. Lara-Sánchez, *Dalton Trans.*, 2004, 1499-1510.
10. I. Kuzu, I. Krummenacher, J. Meyer, F. Armbruster and F. Breher, *Dalton Trans.*, 2008, 5836–5865.
11. P. K. Byers, N. Carr and F. G. A. Stone, *J. Chem. Soc., Dalton Trans.*, 1990, 3701-3708.
12. P. K. Byers and F. G. A. Stone, *J. Chem. Soc., Dalton Trans.*, 1991, 93.
13. S. C. Lawrence, M. E. G. Skinner, J. C. Green and P. Mountford, *Chem. Commun.*, 2001, 705-706.
14. H. R. Bigmore, S. R. Dubberley, M. Kranenburg, S. C. Lawrence, A. J. Sealey, J. D. Selby, M. Zuideveld, A. R. Cowley and P. Mountford, *Chem.Commun.*, 2006, 436-438.
15. F. Breher, J. Grunenberg, S. C. Lawrence, P. Mountford and H. Rüegger, *Angew. Chem. Int. Ed.*, 2004, **43**, 2521-2524.
16. I. Fernández, P. O. Burgos, F. Armbruster, I. Krummenacher and F. Breher, *Chem. Commun.*, 2009, 2586-2588.
17. I. Krummenacher, H. Rüegger and F. Breher, *Dalton Trans.*, 2006, 1073–1081.
18. I. Kuzu, I. Krummenacher, I. J. Hewitt, Y. Lan, V. Mereacre, A. K. Powell, P. Höfer, J. Harmer and F. Breher, *Chem. Eur. J.*, 2009, **15**.
19. I. Kuzu, D. Nied and F. Breher, *Eur. J. Inorg. Chem.*, 2009, 872-879.
20. I. Kuzu and F. Breher, Unpublished results.
21. H. R. Bigmore, J. Meyer, I. Krummenacher, H. Rüegger, E. Clot, P. Mountford and F. Breher, *Chem. Eur. J.*, 2008, **14**, 5918-5934.

22. L. F. Sanchez-Barba, A. Garces, M. Fajardo, C. Alonso-Moreno, J. Fernandez-Baeza, A. Otero, A. Antinolo, J. Tejeda, A. Lara-Sanchez and M. I. Lopez-Solera, *Organometallics*, 2007, **26**, 6403-6411.
23. A. Otero, Fern, J. Fernandez-Baeza, A. Antinolo, A. Lara-Sanchez, E. Martinez-Caballero, J. Tejeda, L. F. Sanchez-Barba, C. Alonso-Moreno and I. Lopez-Solera, *Organometallics*, 2008, **27**, 976-983.
24. A. Otero, J. Fernandez-Baeza, A. Lara-Sanchez, C. Alonso-Moreno, I. Marquez-Segovia, L. F. Sanchez-Barba and A. M. Rodriguez, *Angew. Chem. Int. Ed.*, 2009, **48**, 2176-2179.
25. C. Alonso-Moreno, A. Garces, L. F. Sanchez-Barba, M. Fajardo, J. Fernandez-Baeza, A. Otero, A. Lara-Sanchez, A. Antinolo, L. Broomfield, M. I. Lopez-Solera and A. M. Rodriguez, *Organometallics*, 2008, **27**, 1310-1321.
26. A. D. Schofield, M. L. Barros, M. G. Cushion, A. D. Schwarz and P. Mountford, *Dalton Trans.*, 2009, 85-96.
27. R. G. Howe, C. S. Tredget, S. C. Lawrence, S. Subongkoj, A. R. Cowley and P. Mountford, *Chem. Commun.*, 2006, 223-225.
28. S. Milione, V. Bertolasi, T. Cuenca and A. Grassi, *Organometallics*, 2005, 4915-4925.
29. J. Zhang, P. Braunstein and T. Hor, *Organometallics*, 2008, 4277-4279.
30. J. Zhang, A. Li and T. Hor, *Dalton Trans.*, 2009, 9327-9333.
31. J. Zhang, A. Li and T. Hor, *Organometallics*, 2009, 2935-2937.
32. A. F. R. Kilpatrick, S. V. Kulangara, M. G. Cushion, R. Duchateau and P. Mountford, *Dalton Trans.*, 2010, **39**, 3653-3664.
33. D. A. Fletcher, R. F. McMeeking and D. Parkin, *J. Chem. Inf. Comput. Sci.*, 1996, **36**, 746 (The United Kingdom Chemical Database Service).
34. H. D. Dyer, S. Huijser, A. D. Schwarz, C. Wang, R. Duchateau and P. Mountford, *Dalton Trans.*, 2008, 32.
35. C. Zapilko, Y. Liang and R. Anwander, *Chem. Mater.*, 2007, **19**, 3171-3176.
36. J. L. Sebestl, T. T. Nadasdi, M. J. Heeg and C. H. Winter, *Inorg. Chem.*, 1998, **37**, 1289-1294.
37. J. Sandström, *Dynamic NMR Spectroscopy*, Academic Press, London, 1992.
38. U. E. Bucher, A. Currao, R. Nesper, H. Rüegger, L. M. Venanzi and E. Younger, *Inorg. Chem.*, 1995, **34**, 66.
39. M. H. Chisholm, N. W. Eilerts, J. C. Huffman, S. S. Iyer, M. Pacold and K. Phomphrai, *J. Am. Chem. Soc.*, 2000, **122**, 11845-11854.

40. M. H. Chisholm, J. C. Gallucci and K. Phomphrai, *Inorg. Chem.*, 2004, **43**, 6717-6725.
41. K. E. Janak, in *Comprehensive Organometallic Chemistry III*, eds. R. H. Crabtree and D. M. P. Mingos, Elsevier, Oxford, Editon edn., 2006, vol. 1.
42. Y. Sohrin, M. Matsui, Y. Hata, H. Hasegawa and H. Kokusen, *Inorg. Chem.*, 1994, **33**, 4376-4383.
43. D. M. P. Mingos, *Essential Trends in Inorganic Chemistry*, Oxford University Press, Oxford, 1998.
44. P. J. Bonitatebus and W. H. Armstrong, *Chem.Commun.*, 1999, 55-56.
45. K.-W. Yang, Y.-Z. Wang, Z.-X. Huang and J. Sun, *Polyhedron*, 1997, **16**, 1297-1300.
46. C. Titze, J. Herrmann and H. Vahrenkamp, *Chem. Ber.*, 1995, **128**, 1095.
47. A. Martín, N. Martínez-Espada, M. Mena, A. Pérez-Redondo and C. Yélamos, *Inorg. Chem.*, 2006, **45**, 6901-6911.
48. M. P. Coles and P. B. Hitchcock, *Eur. J. Inorg. Chem.*, 2004, 2662-2672.
49. Y. Sarazin, M. Schormann and M. Bochmann, *Organometallics*, 2004, **23**, 3296–3302.
50. M. D. Hannant, M. Schormann, D. L. Hughes and M. Bochmann, *Inorg. Chim. Acta*, 2005, **358**, 1683-1691.
51. J. Sundermeyer, J. Putterlik and H. Pritzkow, *Chem. Ber.*, 1993, **126**, 289.
52. S. C. Dunn, P. Mountford and O. V. Shishkin, *Inorg. Chem.*, 1996, **35**, 1006.
53. D. L. Reger, T. C. Grattan, K. J. Brown, C. A. Little, J. J. S. Lamba, A. L. Rheingold and R. D. Sommer, *J. Organomet. Chem.*, 2000, **607**, 120-128.
54. M. H. Chisholm, N. W. Eilerts, J. C. Huffman, S. S. Iyer, M. Pacold and K. Phomphrai, *J. Am. Chem. Soc.*, 2000, **122**, 11845-11854.
55. M. H. Chisholm, J. C. Huffman and K. Phomphrai, *J. Chem. Soc. Dalton Trans.*, 2001, 222-224.
56. M. H. Chisholm, J. Gallucci and K. Phomphrai, *Inorg. Chem.*, 2002, **41**, 2785-2794.
57. M. H. Chisholm, J. Gallucci and K. Phomphrai, *Chem. Commun.*, 2003, 48-49.
58. H. R. Kricheldorf, M. Berl and N. Scharnagl, *Macromolecules*, 1988, **21**, 286-293.
59. H. Ma and J. Okuda, *Macromolecules*, 2005, **38**, 2665.
60. A. Duda and S. Penczek, *Macromolecules*, 1995, **28**, 5981-5992.
61. P. Dubois, N. Ropson, R. Jérôme and P. Teyssié, *Macromolecules*, 1996, **29**, 1965-1975.
62. W. M. Stevels, M. J. K. Ankone, P. J. Dijkstra and J. Feijen, *Macromolecules*, 1996, **29**, 8296-8303.

63. Z. Zhong, P. J. Dijkstra, C. Birg, M. Westerhausen and J. Feijen, *Macromolecules*, 2001, **34**, 3863-3868.

64. H. R. Kricheldorf and I. Kreiser-Saunders, *Makromol. Chem.*, 1990, **191**, 1057-1066.

65. H. R. Kricheldorf and C. Boettcher, *Makromol. Chem.*, 1993, **194**, 1665-1669.

Chapter Three

Cationic and charge-neutral Main Group tetrahydroborate complexes and their use in the controlled ROP of ε-caprolactone and *rac*-lactide

3.0 Overview

This Chapter will provide an introduction into main group borohydride catalysed ROP, with an overview of the synthesis and characterisation of borohydride complexes. Their solid state structures and solution behaviour will be discussed in conjunction with their application to the ring opening polymerisation of cyclic esters. Comparison of the newly reported complexes and previously reported related complexes will be undertaken within the context of the solid state structures and the ROP activity and selectivity observed. Some of this work has recently been published.[1]

3.1 Introduction

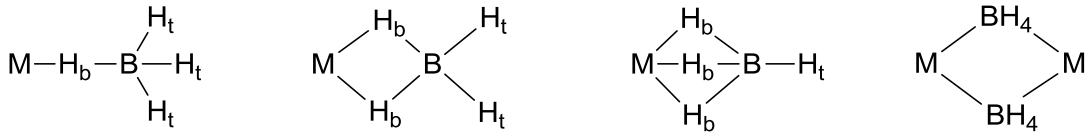
The last decade has witnessed an exponential increase in activity of the synthesis, structures, reactivity and catalytic applications of compounds of the heavier alkaline earth (Ae) metals.[2] Most of this research has centred on calcium, the ionic radius of which lies between those of yttrium and lanthanum, and which is abundant, non-toxic and inexpensive. Nonetheless, both the general solution chemistry and catalytic applications of this element remain considerably underdeveloped in relation to those of the lanthanides to which the heavier Ae elements have been compared.

The ring-opening polymerization (ROP) of cyclic esters such as ε-CL and LA to biocompatible and biodegradable polymers, viewed as potential alternatives to petroleum-derived plastics, is an area of considerable current interest.[2] Although calcium's lighter congener, magnesium, and the lanthanides are have been extensively studied for ROP, only a handful of well-defined, heteroleptic initiators of the type (L)Ca–X (X = amide or aryloxide) have been reported.[3-10] Even so, these few reports indicate superior activity of (L)Ca–X in comparison with the respective Mg analogues, signposting the considerable potential of new Ca complexes in this area.

In the last 5-8 years lanthanide tetrahydroborates,[11-15] either as "ligand-free" $Ln(BH_4)_3(THF)_x$[16-20] or heteroleptic (L)Ln(BH_4) systems,[21-26] have become well-established as effective initiators for the polymerisation of a range of cyclic esters and other monomers. However, no main group borohydride has been established in this regard.[11] Furthermore, in terms of both initiating efficiency and molecular weight control, (L)Ln–BH_4 systems are better controlled than the corresponding amides, (L)Ln–NR_2,[21] and comparable to alkoxides, (L)Ln–OR.[18] Drawing upon the potential parallels with the lanthanides, it was set out to develop main group tetrahydroborate complexes as a new class of main group initiator for the ROP of *rac*-LA.

Generally, borohydride complexes comprise at least one BH_4 anionic ligand (alkylborohydride complexes are also known but will not be discussed in this thesis); covalent borohydride complexes are well established for the transition metals,[14] lanthanides[11] and to a lesser extent the main group elements. One of the advantages of BH_4 ligands is their versatility, both in their coordination mode and their reactivity.[11] Borohydrides can adapt their hapticity to satisfy the size of the coordination sphere around a metal, adopting (most commonly) κ^3, κ^2 and κ^1 (rare) binding modes through the M(μ-H)B bridges (see Figure 3.0). In addition, a borohydride group may be connected to one metal (terminal), or up to three metal atoms (bridging). In relation to their reactivity, borohydrides can be considered as *pseudo* halides (being monoanionic and readily substituted for other groups), and can also be considered as extended hydrides, showing reactivity associated with a hydridic moiety, e.g. protonolysis and reductive polymerisations.[20, 27, 28] Since little is known about Ae borohydride complexes, the remainder of this introduction will focus on the preparation and characterisation of lanthanide borohydride complexes, given the similarities between the lanthanides and Ae elements.

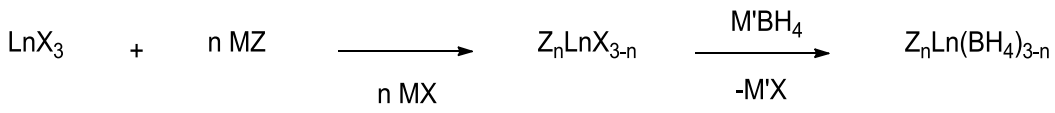
Figure 3.0. Coordination modes of tetrahydroborate ligands in monomeric and dimeric complexes



κ¹ **κ²** **κ³** **Bridging**

Several methods are known for the preparation of simple borohydride complexes, however in the context of this thesis the two most relevant are (as shown in Equations 3.0 and 3.1):

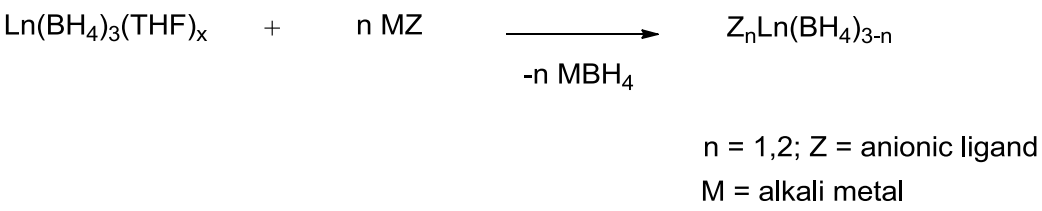
i) Substitution of a ligand (most commonly a halide) by a borohydrido anionic reagent MBH_4 (M = alkaline metal), in the final step of a synthesis, generally from a lanthanide trihalide.



X = halide; n = 1,2; Z = anionic ligand
M, M' = alkali metal

Equation 3.0

ii) Salt metathesis – replacing the trihalide with a tris(borohydride) as the starting material

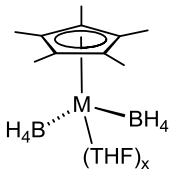


Equation 3.1

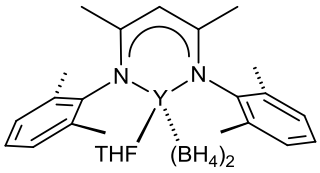
The trivalent lanthanide metallocene half-sandwich analogues **3.0** and **3.1** (Figure 3.1) were synthesised very recently by Bonnet and Visseaux through salt metathesis from the corresponding tris(borohydrides).[29, 30] Ephritikhine *et al.* had previously synthesised **3.2** using the same methodology.[31] Experimental evidence suggests that **3.2** possesses both tridentate and bidendate borohydride ligands in solution, supporting a monomeric structure. It was also shown in this work that heating **3.2** under vacuum resulted in the loss of bound THF, forming Cp*Nd$(BH_4)_2$, which gave a simple IR absorption at 2291 cm^{-1} (typical of bridging borohydride groups, see Table 3.0), indicating a polymeric structure in the solid state. The lanthanum analogue **3.1** behaved in a very similar fashion to **3.2**. It was observed that the synthesis of **3.0** was accompanied by two by-products, the sandwich complex $Cp^*_2Sc(BH_4)$ and the alkoxide half-sandwich $[Cp^*Sc(BH_4)\{\mu\text{-}O(CH_2)_3CH_3\}]_2$, the latter resulting from the ring opening of a THF molecule. Structural analysis of **3.0** and IR data showed both borohydride ligands to be tridentate.

The trivalent yttrium and samarium borohydrides **3.3** and **3.4** were synthesised recently by Cui[32] and Mountford[21] respectively. Complex **3.3** was synthesised using a one-pot method; lithiation of the β-diketimine using ^{n}BuLi was followed by *in situ* salt metathesis with yttrium tris(borohydride). Structural analysis showed that both borohydride ligands were tridentate. Similarly, reaction of the sodium diaminobis(phenoxide) $Na_2O_2N_{py}$ [$H_2O_2N_{py}$ = $(2\text{-}C_5H_4N)CH_2NCH_2\{2\text{-}HO\text{-}3,5\text{-}C_6H_2{}^tBu_2\}_2$] with samarium tris(borohydride) afforded the complex **3.4**, which was shown to be a very good initiator for the ROP of ε-CL and *rac*-LA, producing polymers with narrow PDIs and a high degree of heterotactic enrichment with the latter. Under reduced pressure it was shown that **3.4** loses the bound THF molecule, forming a phenolate-bridged species. Both this species and **3.4** were found to possess tridentate borohydride ligands.

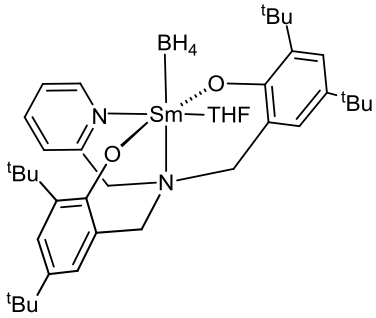
Figure 3.1. Examples of rare earth and lanthanide borohydride complexes.



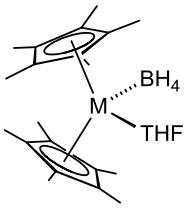
M = Sc (**3.0**, x = 1),
La (**3.1**, x = 2) or Nd (**3.2**, x = 2)



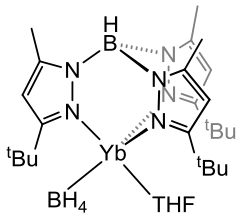
3.3



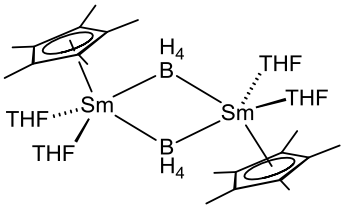
3.4



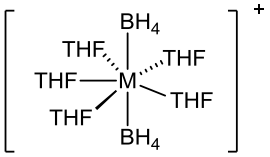
M = Y (**3.5**), Sm (**3.6**) or Lu (**3.7**)
R = H, Me, Et, ^{i}Pr or ^{t}Bu



3.8



3.9



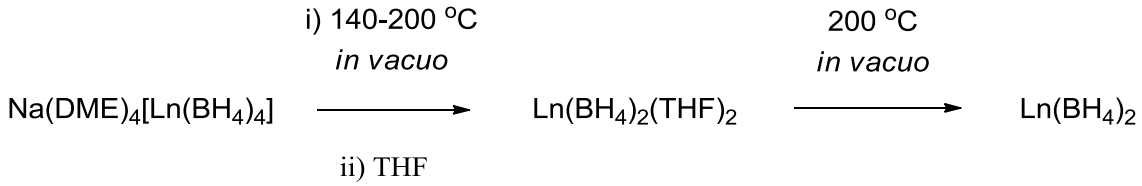
M = Y (**3.10**), La (**3.11**), Nd (**3.12**)
or Sm (**3.13**). BPh_4 anions omitted

A large family of peralkylsubstituted cyclopentadienyl borohydride metallocenes $(C_5Me_4R)_2M(BH_4)(THF)$ (M = Y (**3.5**), Sm (**3.6**) and Lu (**3.7**), R = H, Me, Et, ^{i}Pr, ^{t}Bu) was prepared in 1998 by Schumann *et al*. through reaction of the sodium salts of the cyclopentadienyl ligands with the trivalent metal chloride, followed by *in situ* reaction with sodium borohydride.[33] A mixture of tridentate and bidentate borohydride ligands were found to be present, depending on the size of the metal and the steric bulk around the cyclopentadienyl ligand.

In addition to the growing number of trivalent lanthanide borohydride complexes known, a few examples of divalent borohydride species have also been synthesised very recently. Complex **3.8** was synthesised from a salt metathesis reaction between $(Tp^{tBu,Me})Yb(I)(THF)$ and $NaBH_4$ in THF.[34] Structural analysis and IR spectroscopy revealed the borohydride ligand to be tridentate. The base free analogue of **3.8**, $(Tp^{tBu,Me})Yb(BH_4)$ was also synthesised by simply performing the reaction in acetonitrile rather than THF. Additionally

the deuterated analogue of **3.8**, ($Tp^{tBu,Me}$)Yb(BD_4), was also synthesised, and this showed isotopically shifted IR frequencies when compared to **3.8**.

A series of compounds $Ln(BH_4)_2(THF)_2$ (Ln = Sm, Eu, Yb) and their non solvated analogues $Ln(BH_4)_2$ were prepared in 1999 by thermal reduction of the $Na(DME)_4[Ln(BH_4)_4]$ precursors (Equation 3.0).[35] However, these compounds were only characterized by IR and elemental analysis.



Equation 3.2

In 2010 Bonnet and Visseaux improved the synthesis of $Sm(BH_4)_2(THF)_2$ through a high yielding comproportionation reaction between $Sm(BH_4)_3(THF)_3$ and samarium metal.[36] Structural analysis showed this complex to be polymeric with bidentate borohydride ligands bridging between adjacent metal centres. The subsequent reaction between $Sm(BH_4)_2(THF)_2$ and KCp^* yielded the complex $Cp^*Sm(BH_4)(THF)_2$ (**3.9**), which possesses two bridging borohydrides coordinated to each samarium centre in a tridentate manner. This complex has also been shown to be highly active for the ROP of ε-CL, yielding polymers with narrow PDI values.

In 2008 Okuda *et al*. synthesised the family of cationic borohydride complexes $[M(BH_4)_2(THF)_5][BPh_4]$ (M = Y (**3.10**), La (**3.11**), Nd (**3.12**) and Sm (**3.13**), by protonolysis reactions between the trivalent borohydrides and $[NEt_3H][BPh_4]$,[27] producing triethylamine, hydrogen and diborane as the side products. These complexes were also shown to be highly active for the ROP of ε-CL. However, in this instance polymers with moderate PDI values and featuring poor control of molecular weight were obtained.

As mentioned, the two foremost techniques in deciphering borohydride hapticity are single crystal X-ray diffraction and IR spectroscopy, although it should be mentioned that both ^1H and ^{11}B NMR spectroscopy are useful methods in at least detecting the presence of a borohydride. Whilst the difficulties associated with locating H atoms by X-ray diffraction are well known,[37] the location of hydrides (and borohydrides) can be reliably found using Fourier difference maps. In most cases the hapticity of the borohydride ligand in the solid state can be determined. Neutron diffraction can give more precise data. However, large single crystals are required and the facilities required are not widely available.

IR spectroscopy is used extensively in conjunction with (and solely in the absence of) X-ray diffraction to determine the hapticity of borohydride ligands.[14] For mononuclear complexes the diagnostic bands are generally found in the region 2500-1000 cm^{-1} region (Table 3.0). Both the terminal and bridging B-H stretches are found in this region for all binding modes, however the number and position of bands leave a precise fingerprint of the binding mode.

Table 3.0. IR active fundamental vibrational transitions commonly observed for mononuclear MBH_4 configurations.[14]

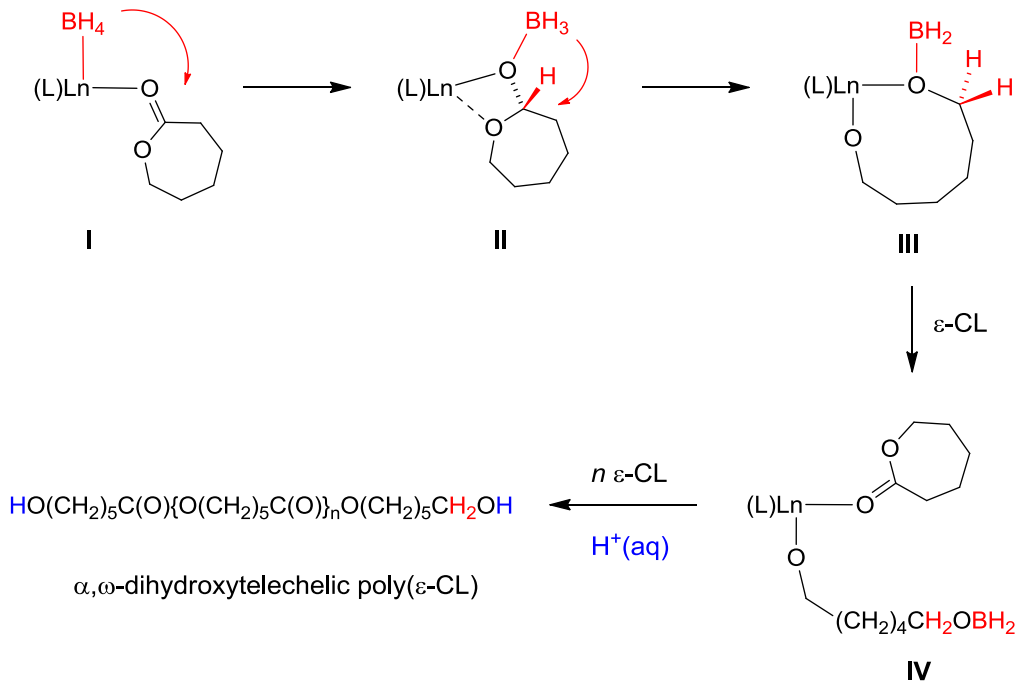
Structure	Freq, cm^{-1}	Normal Mode	Symmetry	Comments
Monodentate (**I**)	2450 – 2300	B-H_t stretching	A_1, E	Strong doublet
	~ 2000	B-H_b stretching	A_1	Strong
	~ 2000 – 1700	M-H_b stretching	A_1	Often broad
	1150 – 1000	BH_3 deformation	A_1, E	Strong band
Bidentate (**II**)	2600 – 2400	B-H_t stretching	A_1, B_1	Strong doublet (50 – 80 cm^{-1})
	2150 – 1650	B-H_b stretching	A_1, B_2	Strong band possible shoulder
	1500 – 1300	Bridge stretching	A_1	Strong band
	1200 – 1100	BH_2 deformation	B_2	Strong
Tridentate (**III**)	2600 – 2450	B-H_t stretching	A_1	Strong singlet
	2200 – 2100	B-H_b stretching	A_1, E	Doublet (50 – 80cm^{-1})
	1250 – 1150	Bridge deformation	E	Strong

As shown in Table 3.0, tridentate borohydrides give a characteristic strong singlet between 2600-2450 cm^{-1} (A_1 B-H_t stretching mode, see Figure 3.2) and a doublet between 2200-2100 cm^{-1} (A_1 and E B-H_b stretching modes). Bidentate borohydrides give a strong doublet in the range 2600-2400 cm^{-1} (A_1 and B_1 B-H_t stretching modes) and a strong band in the

range 2150-1650 cm^{-1} (A_1 and B_2 B-H_b stretching modes), as well as a strong band in the range 1500-1300 cm^{-1} (A_1 bridge stretching mode). It can also be seen that monodentate borohydrides give unique IR bands.

The initial pioneering work in the area of ROP catalysed by rare earth borohydrides was carried out by Guilleaume and co-workers focussing on $Ln(BH_4)_3(THF)_3$ (Ln = La, Nd, Sm) and $Cp^*_2Sm(BH_4)(THF)$ (**3.6**) for the ROP of ε-CL.[19, 20, 38] The ROP was shown to proceed in a living fashion with *ca.* one PCL chain forming per Ln–BH_4 group. One study has shown that the performance of these systems matches that of "$La(O^iPr)_3$" under comparable experimental conditions,[19] although this is to date the sole "head to head" performance study undertaken for borohydride *versus* more classical initiators.

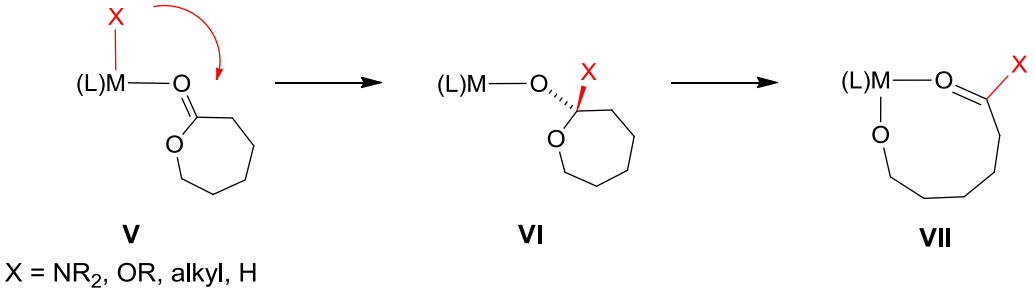
Scheme 3.0. Mechanism for the borohydride-initiated ROP of ε-CL leading to α,ω-dihydroxytelechelic PCL.[19, 24]



An important aspect of the ROP of ε-CL with (L)Ln–BH_4 complexes is the formation of α,ω-dihydroxytelechelic PCL, which is a material of importance to polyurethane chemistry. Guillaume and coworkers have established the mechanism shown in Scheme 3.0 by a combination of experimental and computational studies.[19, 24] Coordination of ε-CL to (L)Ln–BH_4 (forming **I**) is followed by hydride transfer to the carbonyl carbon and BH_3 transfer to the formally anionic oxygen (**II**). Crucially, species **II** is unable to lose BH_3 and so ring-opening only takes place *via* a further hydride transfer event which forms **III** with a fully reduced carbonyl moiety. Subsequent monomer enchainment *via* a coordination-insertion mechanism, and finally termination by protonolysis, affords the α,ω-

dihydroxytelechelic PCL. It is important to contrast this process with the usual one (Scheme 3.1) for metal-amide, alkoxide, alkyl or hydride species of the type (L)M–X. In this case, after migration of the metal-bound initiating group "X" of the adduct **V** to the carbonyl carbon of ε-CL, spontaneous ring-opening of **VI** to form **VII** occurs.[18, 19, 24, 38] The polymer subsequently formed is of the type H-[PCL]-X in which the "-X" end group arises from the (L)M-X initiator.

Scheme 3.1. Coordination-insertion mechanism for the initial ring-opening of ε-CL with metal-amide, alkoxide, alkyl or hydride species.[39-41]



However, the ROP of other cyclic esters with (L)Ln–BH_4 does not necessarily lead to α,ω-dihydroxy polymers. Guillaume has shown that the poly(TMC) formed with $Sm(BH_4)_3(THF)_3$ contains both $–CH_2OH$ and –CHO end groups,[24] while Nakayama and Shiono found that several lanthanide tris(borohydride) complexes polymerize δ-valerolactone to α,ω-dihydroxy poly(δ-VL).[42] The same authors reported that *rac*- or *L*-LA also gives α,ω-dihydroxy terminated polyesters with these initiators,[16, 24] whereas Carpentier and Trifonov, in addition to work in this Chapter,[1] found that ligand-supported borohydride initiators produce poly(*rac*-LA) with a mixture of–CH_2OH and –CHO end groups.[23, 25]

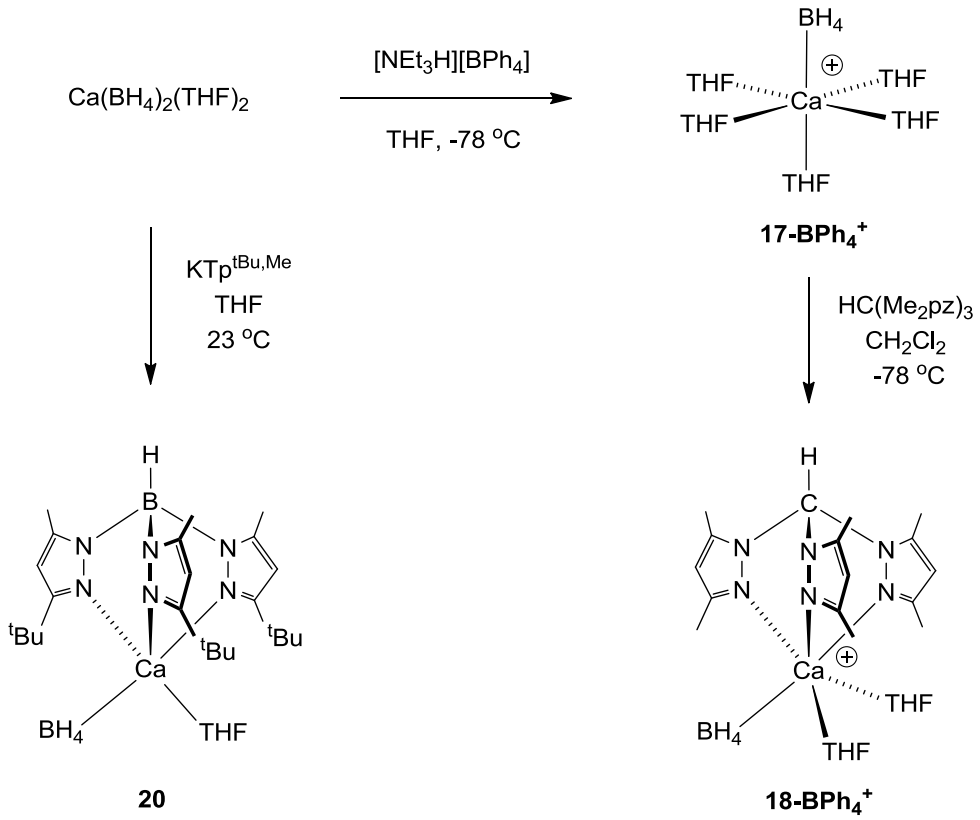
3.2 Synthesis of cationic and charge-neutral main group tetrahydroborate complexes

In light of the extensive work carried out in the preparation of lanthanide borohydride complexes and their application towards ROP,[11, 14] as well as the growing interest in the development of the chemistry of the Ae elements,[2] it was decided to investigate the synthesis and ROP applications of Ae borohydride complexes. At of the time of writing, the only Ae borohydride initiators for the ROP of cyclic esters are those presented in this Chapter.[1]

Scheme 3.2 summarizes the reactions of commercially-available $Ca(BH_4)_2(THF)_2$ with $[NEt_3H][BPh_4]$ and $KTp^{tBu,Me}$, as well as the reaction of $[Ca(BH_4)(THF)_5][BPh_4]$ (**17-BPh_4**) with $HC(Me_2pz)_3$ to give $[Ca\{HC(Me_2pz)_3\}(BH_4)(THF)_2][BPh_4]$ (**18-BPh_4**). The reaction of

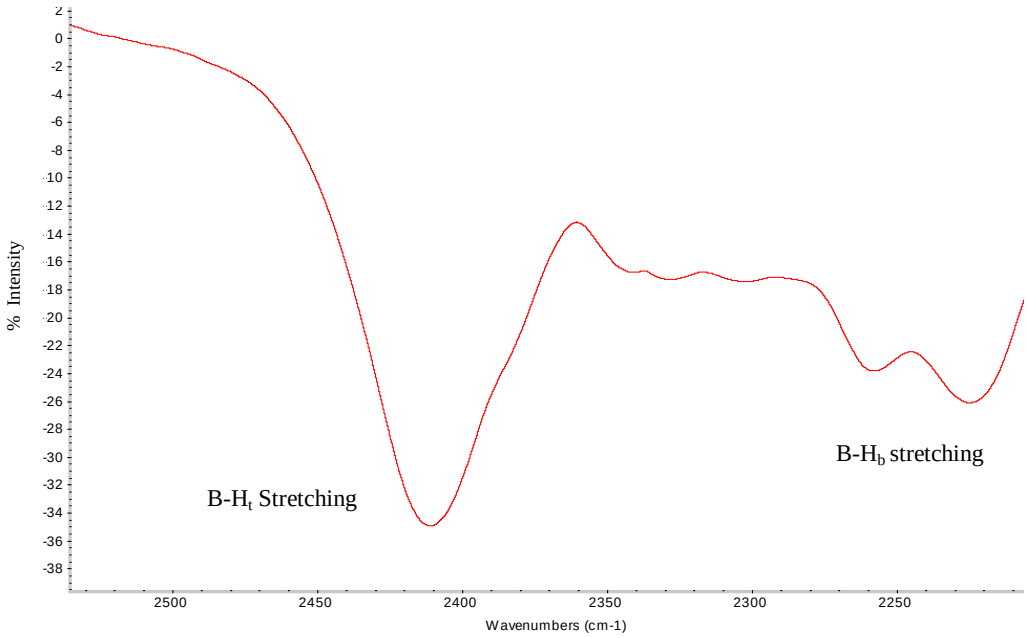
$Ca(BH_4)_2(THF)_2$ with $[NEt_3H][BPh_4]$ in THF proceeded smoothly over 2 h at -78 °C, giving **17-BPh_4** in 51% recrystallised yield.

Scheme 3.2. Synthesis of new calcium tetrahydroborate complexes. BPh_4 anions are omitted for **17-BPh_4^+** and **18-BPh_4^+**.



Using these carefully controlled temperature conditions, no formation of the dication $[Ca(THF)_6][BPh_4]_2$ was observed (as would be expected from a Schlenk-type redistribution also leading to the formation of $Ca(BH_4)_2(THF)_2$).[2] The ^1H NMR spectrum of **17-BPh_4** in CD_2Cl_2 shows a 1:1:1:1 quartet at -0.19 ppm for the BH_4 ligand ($^1J_{^1H^{11}B}$ = 82 Hz) which appears at -36.1 ppm in the $^{11}B\{^1H\}$ NMR spectrum. The THF solution IR spectrum of **17-BPh_4** (Figure 3.2) is consistent with a κ^3 bound BH_4 ligand, showing bands at 2406 ($B–H_t$ stretch), 2260cm^{-1} and 2208 cm^{-1} ($B–H_b$ stretches). Interestingly, the ^1H NMR of $Ca(BH_4)_2(THF)_2$ in CD_2Cl_2 showed a 1:1:1:1 quartet at -0.21 ppm for the BH_4 ligand ($^1J_{^1H^{11}B}$ = 82 Hz), which appears at -35.6 ppm in the $^{11}B\{^1H\}$ NMR spectrum. These shifts are almost identical to those of **17-BPh_4**. However, the THF solution IR spectrum of $Ca(BH_4)_2(THF)_2$ showed a broad multiplet centred at 2280 cm^{-1}, presumably encompassing both the $B–H_t$ and $B–H_b$ stretches of the BH_4 ligands. Therefore, whilst the comparison of NMR data for **17-BPh_4** and $Ca(BH_4)_2(THF)_2$ does not provide any insight into the potential occurrence of redistribution, the difference between the solution IR data of the two species rules out this possibility.

Figure 3.2. Borohydride region of solution (THF) IR spectrum of $[Ca(BH_4)(THF)_5][BPh_4]$ (**17-BPh$_4$**). The background has been subtracted.



Reaction of **17-BPh$_4$** with $HC(Me_2pz)_3$ in dichloromethane at -78 ^oC gave **18-BPh$_4$** in 74 % yield. The cation **18-BPh$_4$**$^+$ also possesses a κ^3 bound BH_4 ligand ($\delta(^1H)$ = 0.15 ppm ($^1J_{^1H^{11}B}$ = 82 Hz); $\delta(^{11}B)$ = -35.6 ppm in CD_2Cl_2). Again the THF solution IR spectrum is also consistent with a κ^3 bound BH_4 ligand, showing bands at 2410 (B–H_t stretch), 2270cm^{-1} and 2210 cm^{-1} (B–H_b stretches). Once again these data are different to that shown in the solution IR spectrum of $Ca(BH_4)_2(THF)_2$, ruling out the possibility of redistribution to $[Ca\{HC(Me_2pz)_3\}_2]^{2+}$ and $Ca(BH_4)_2(THF)_2$.

The solid state structures of the **17**$^+$ and **18**$^+$ are shown in Figure 3.3. The H atoms of the κ^3-BH_4 ligands were located from Fourier difference maps and positionally and isotropically refined. The only previously structurally characterized calcium tetrahydroborate compounds are $Ca(BH_4)_2(DME)_2$ (two κ^3 bound BH_4 ligands, avg. Ca···B = 2.654 Å) and $Ca_2(BH_4)_2$(diglyme)$_2$ (mixture of κ^3 and κ^2 bound BH_4 and diglyme ligands (avg. Ca···B = 2.714 and 2.878 Å)).[43, 44] The Ca···B distances of 2.610(3) and 2.581(2) Å in **17-BPh$_4$** and **18-BPh$_4$** are comparable to those of the κ^3 bound BH_4 ligands found in both of these reported complexes.

Figure 3.3. Molecular structures of $[Ca(BH_4)(THF)_5]^+$ (**17**$^+$, left) and $[HC(Me_2pz)Ca(BH_4)(THF)_2]^+$ (**18**$^+$, right). BPh_4 anions omitted. The H atoms of the κ^3-BH_4 ligands were located from Fourier difference maps and positionally and isotropically refined.

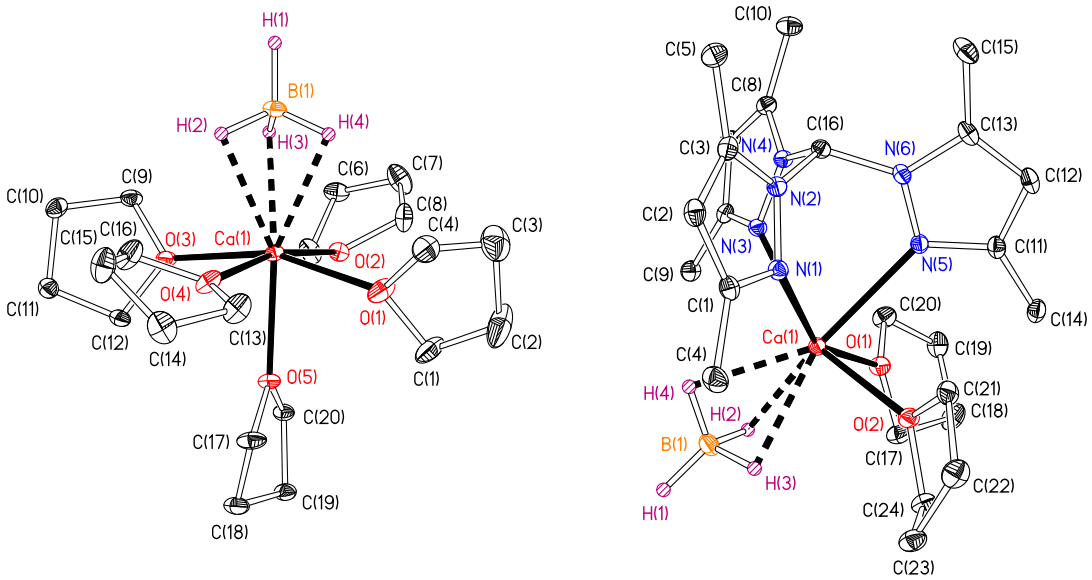


Table 3.1. Selected bond distances (Å) and angles (°) for $[Ca(BH_4)(THF)_5][BPh_4]$ (**17-BPh_4**).

Ca(1)-O(1)	2.355(2)	O(1)-Ca(1)-O(3)	161.31(9)
Ca(1)-O(5)	2.3987(19)	O(1)-Ca(1)-O(4)	84.20(10)
Ca(1) ⋯B(1)	2.601(3)	O(1)-Ca(1)-O(5)	81.40(8)
		H(1)-B(1)-H(2)	111.2(8)
		H(2)-B(1)-H(4)	108(3)

Table 3.2. Selected bond distances (Å) and angles (°) for [Ca{HC(Me_2pz)$_3$}-(BH_4)(THF)$_2$][BPh_4] (**18-BPh_4**).

Ca(1)-N(1)	2.5046(15)	N(1)- Ca(1)-O(1)	155.72(5)
Ca(1)-N(3)	2.5025(14)	N(3) -Ca(1)-O(1)	94.82(5)
Ca(1)-N(5)	2.5335(15)	N(5)-Ca(1)-O(1)	82.08(5)
Ca(1)-O(1)	2.3643(13)	N(1)- Ca(1)-O(2)	86.42(5)
Ca(1)-O(2)	2.3780(12)	N(3)- Ca(1)-O(2)	151.27(5)
Ca(1)···B(1)	2.581(2)	N(5)- Ca(1)-O(2)	80.70(5)
		H(1)-B(1)-H(2)	113.20(18)
		H(2)-B(1)-H(4)	104.60(17)

Interestingly, performing the reaction of **17-BPh_4** with HC(Me_2pz)$_3$ in THF at room temperature led to isolation of the redistribution product, [Ca{HC(Me_2pz)$_3$}$_2$][BPh_4]$_2$ (**19-[BPh_4]$_2$**), in 52 % yield. Presumably the higher temperature and presence of excess THF favours the redistribution of **18-BPh_4** to **19-[BPh_4]$_2$** and Ca(BH_4)$_2$(THF)$_2$. This was indeed evident by monitoring both the low temperature reaction in CH_2Cl_2 and the room temperature reaction in THF. The reaction solution in CH_2Cl_2 remained transparent in appearance whereas the reaction in THF led to precipitation of the less soluble (due to its dicationic nature) **19-[BPh_4]$_2$**. In fact the precipitation of the latter is likely to be an additional driving force in the formation of **19-[BPh_4]$_2$** in THF. It is noteworthy that the CH_2Cl_2 reaction led to the sole formation of **18-BPh_4**, with no evidence of the presence of **19-[BPh_4]$_2$** as a potentially competing redistribution side product. This further highlights the need for careful reaction control when synthesising organocalcium compounds in order to prevent redistribution reactions. However, this case serves to show that with care such difficulties may be overcome.

Sterically demanding tris(pyrazolyl)hydroborate ligands have been used successfully elsewhere for the preparation of heteroleptic Ae complexes.[2-4, 45-53] The most studied derivatives of these ligands possess a *tert*-butyl group in the 3-position of the ligand (i.e. close to the metal centre in a complex). The presence of these bulky groups serves to suppress unwanted redistribution reactions. For example, in the early 1990s Parkin *et* al.

reported the synthesis and solid state structures of (Tp^{tBu})Be(X) (X = Br, H or Me)[46,52] and (Tp^{tBu})Mg(X) (X = Cl, Me and ^{i}Pr)[47, 49, 54]. As mentioned in previous Chapters, Chisholm *et al*. later reported the complexes (Tp^{tBu})Ca(X) (X = $N(SiMe_3)_2$ or O-2,6-$C_6H_3{}^{i}Pr_2$)[3, 4] which were found to be extremely active initiators for the ROP of LA at room temperature. Interestingly, the attempted synthesis of (Tp^{tBu})Ca(I)(THF) from KTp^{tBu} and CaI_2 was unsuccessful,[3] presumably the bulk of the ligand was insufficient to stabilise this heteroleptic complex for the relatively large Ca^{2+} ion.

Recent work by Chisholm *et al*. led to the development of tris(pyrazolyl)hydroborate ligands with pendant methoxy substituted hemi-labile donor arms (in place of the *tert*-butyl groups seen in Tp^{tBu}).[45, 51] For example, the heteroleptic complexes (Tp^{C*})M(I) (M = Mg, Zn, Ca, Sr and Ba, Tp^{C*} = tris{3-(2-methoxy-1,1-dimethyl)pyrazolyl}hydroborate)[51] were synthesised, as well as (Tp^{C*})Ca(X) (X = $N(SiMe_3)_2$ or O-4-C_6H_4-Me).[45] Despite the steric bulk imposed by the Tp^{C*} ligand, the homoleptic compounds (Tp^{C*})$_2$M (M = Mg or Ca)[45] were also synthesised, although these species were shown to exist both in solution and the solid state as separated ion pairs, i.e. [Tp^{C*}Ca][Tp^{C*}]. Interestingly, Harder *et al*. attempted the synthesis of Tp^{tBu}Ca(H) and isolated the homoleptic calcium complex (Tp^{tBu})$_2$Ca[55] as a redistribution product. Whilst both of the Tp^{tBu} ligands are tridentate in this complex, one is κ^3 bound via the pyrazole nitrogen atoms and the other is κ^2 bound via the pyrazole nitrogen atoms and a B-H unit.[55]

($Tp^{tBu,Me}$)Ca(BH_4)(THF) (**20**, Scheme 3.2) was readily prepared at room temperature directly from Ca(BH_4)$_2$(THF)$_2$ and $KTp^{tBu,Me}$ in 65% recrystallised yield. The IR and NMR data for formally zwitterionic **20** are consistent with the structure proposed in Scheme 3.2 which is analogous to that of cationic **18-BPh$_4$** and Sella and Takats' recently reported ($Tp^{tBu,Me}$)Yb(BH_4)(THF) (**3.8**).[34] Interestingly, the fact that the unit cell parameters of the solid state structures of **20** are identical to that of **3.8** provide further evidence for the documented similarities between the Ae and lanthanide elements.[2]

^{1}H and ^{11}B NMR spectroscopy showed that **20** does not undergo redistribution to ($Tp^{tBu,Me}$)$_2$Ca and Ca(BH_4)$_2$(THF)$_2$ in THF-d_8 at room temperature or 70 ^{o}C. The stability of **20** compared to the lower temperatures required in the formation of **18-BPh$_4$** is most likely due to the increased bulk of the *tert*-butyl group of the former in the 3-position of the $Tp^{tBu,Me}$ ligand, providing additional steric stabilisation around the metal centre. The solid state structures of **19-[BPh$_4$]$_2$** and **21** are shown in Figure 3.4.

Figure 3.4. Molecular structures of $Ca\{HC(Me_2pz)_3\}_2^{2+}$ (**19**$^{2+}$, left) and $(Tp^{tBu,Me})Ca(BH_4)(THF)$ (**20**, right). BPh_4 anions for **19**$^{2+}$ omitted. The H atoms of the κ^3-BH_4 ligand were located from Fourier difference maps and positionally and isotropically refined.

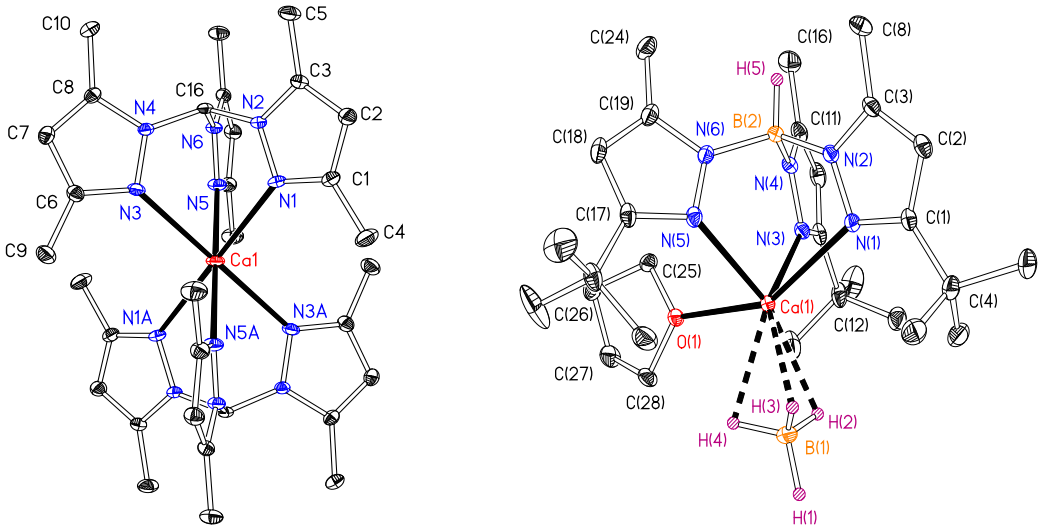


Table 3.3. Selected bond distances (Å) and angles (°) for $[Ca\{HC(Me_2pz)_3\}_2][BPh_4]_2$ (**19-[BPh$_4$]$_2$**).

Ca(1)-N(1)	2.4224(16)	N(1)-Ca(1)-N(3)	75.46(5)
Ca(1)-N(3)	2.4471(16)	N(1)-Ca(1)-N(5)	75.96(6)
Ca(1)-N(5)	2.4510(16)	N(3)-Ca(1)-N(5)	76.12(5)

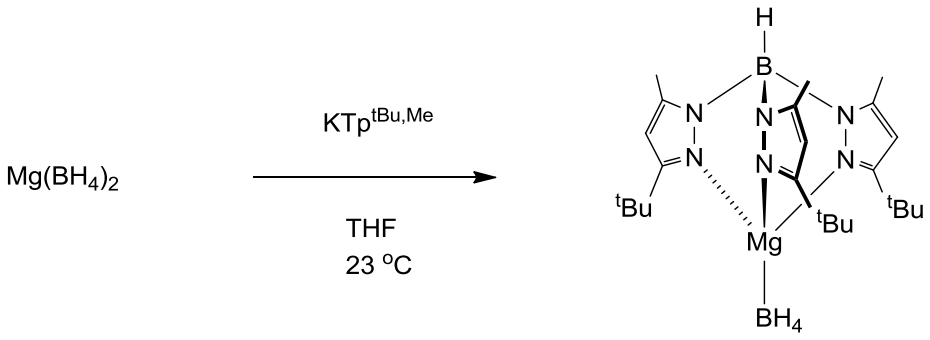
Table 3.4. Selected bond distances (Å) and angles (°) for $(Tp^{tBu,Me})Ca(BH_4)(THF)$ (**20**).

Ca(1)-N(1)	2.5053(16)	N(1)- Ca(1)-O(1)	148.97(5)
Ca(1)-N(3)	2.4256(17)	N(3) -Ca(1)-O(1)	83.63(5)
Ca(1)-N(5)	2.4307(16)	N(5)-Ca(1)-O(1)	81.75(5)
Ca(1)-O(1)	2.4291(14)	H(1)-B(1)-H(2)	112(3)
Ca(1)···B(1)	2.567(3)	H(2)-B(1)-H(4)	108(3)

The Ca···B distance of 2.654(3) Å in **20** is consistent with a κ^3-BH_4 ligand and is very similar to that observed in **17-BPh$_4$** and **18-BPh$_4$** (2.610(3) and 2.581(2) Å respectively). This distance is also very close to that (2.596(5) Å) seen in the isostructural ($Tp^{tBu,Me}$)Yb(BH_4)(THF) (**3.8**).[34] The Ca-O distance (2.4291(14) Å) is also strikingly similar to the analogous Yb-O bond distance (2.463(2) Å) in **3.8**. The solid state structure of **20** has only one coordinated THF molecule, whereas the related complex **18-BPh$_4$** has two. This is a consequence of the bulky *tert*-butyl groups around the metal centre in **20** compared to the less bulky methyl groups in the same position in **18-BPh$_4$**. The Ca-N_{pz} bond lengths in **20** (2.5053(16), 2.4256(17) and 2.4307(16) Å) are also shorter than those in **18-BPh$_4$** (2.5046(15), 2.5025(14) and 2.5335(15) Å). This is due to the monoanionic ligand in **20** compared to the neutral ligand in **18-BPh$_4$**. The Ca-N_{pz} bond lengths of **20** are longer than those of (Tp^{tBu})Ca(O-2,6-$C_6H_3{}^iPr_2$) (average 2.381 Å)[4] and slightly shorter than those in (Tp^{tBu})$_2$Ca (average 2.497 Å)[55], consistent with the various steric factors and coordination number effects in the three compounds.

The Ca-N_{pz} bond lengths in **19-[BPh$_4$]$_2$** (2.4224(16), 2.4471(16) and 2.4510(16) Å) are almost identical within error to the zwitterionic Ca{C(Me$_2$pz)$_3$}$_2$ (**5**, where the corresponding bond lengths are 2.4370(18), 2.4591(16) and 2.448(2) Å). This highlights the localised negative charge focused around the C(Me$_2$pz)$_3$ carbanion in the anionic tris(pyrazolyl)methan*ide* ligand in the zwitterionic **5**. The Ca-N_{pz} bond lengths are also shorter than those in (Tp^{tBu})$_2$Ca (average 2.497 Å)[55], due to the presence of less sterically demanding methyl groups in the 3-position of the ligand compared to the *tert*-butyl groups in (Tp^{tBu})$_2$Ca.

The magnesium analogue of **20**, ($Tp^{tBu,Me}$)Mg(BH_4) (**22**) was synthesised by an identical method (Equation 3.3) in 57% isolated yield. The IR and NMR data for formally zwitterionic **20** are consistent with the structure proposed (with a κ^3 bound BH_4 ligand) in Equation 3.2, although unfortunately it has not yet been possible to obtain diffraction-quality crystals. The absence of bound THF in **22** is a reflection of the smaller size of magnesium compared to calcium.



22

Equation 3.3

Unfortunately the reaction between $Mg(BH_4)_2$ and $[NEt_3H][BPh_4]$ at -78 °C in THF led to $[Mg(THF)_6][BPh_4]_2$ (*via* a Schlenk equilibrium also producing $Mg(BH_4)_2$) rather than the desired heteroleptic analogue of **17-BPh$_4$**, $[Mg(BH_4)(THF)_5][BPh_4]$. This was a surprising result: it was postulated that the smaller size of magnesium should make a half sandwich complex a more favoured product. The synthesis of $[Mg\{HC(Me_2pz)_3\}(BH_4)(THF)_2][BPh_4]$, the analogue of **18-BPh$_4$**, was attempted by the addition of $[NEt_3H][BPh_4]$ to a mixture of $HC(Me_2pz)_3$ and $Mg(BH_4)_2$ at -78 °C in THF. However, this again resulted in the redistribution product $[Mg\{HC(Me_2pz)_3\}_2][BPh_4]_2$. It was noted that prior to the formation of the insoluble dication, a brief period (following gas evolution) was observed where the contents of the reaction mixture remained in solution before the precipitation of $[Mg(THF)_6][BPh_4]_2$. It is thought that this may be attributed to the formation of the desired heteroleptic cation, and indeed it may be possible that use of a bulkier tris(pyrazolyl)methane ligand may result in the isolation of a desired heteroleptic cationic magnesium borohydride complex.

3.3 Polymerisation studies: ROP of ε-CL

The borohydride complexes $[Ca(BH_4)(THF)_5][BPh_4]$ (**17-BPh$_4$**), $[Ca\{HC(Me_2pz)_3\}_2][BPh_4]_2$ (**18-[BPh$_4$]$_2$**), ($Tp^{tBu,Me}$)$Ca(BH_4)(THF)$ (**20**) and ($Tp^{tBu,Me}$)$Mg(BH_4)$ (**22**) were all highly active for the ROP of ε-CL in THF at room temperature, producing α,ω–dihydroxy telechelic PCL of the form $HO(CH_2)_5C(O)$-[PCL]-$O(CH_2)_6OH$ in a matter of minutes. The formation of α,ω–dihydroxy telechelic PCL is a particular characteristic of $(L)Ln(BH_4)$-initiated ε-CL ROP and the mechanism of formation has been studied in detail experimentally and computationally (see also Scheme 3.0).[19, 24] Due to the rapid completion it was not possible to investigate the kinetic profiles of the polymerisations. Taking into consideration the aforementioned similarities between the Ae and lanthanide elements, ($Tp^{tBu,Me}$)$Yb(BH_4)(THF)$ (**3.8**) was synthesised by published

methods[34] and also tested, alongside $Ca(BH_4)_2(THF)_2$ as a control test. Similarly, these catalysts produced polymer within a number of minutes. The polymerisation results for all catalysts are summarised in Table 3.5. The time given for a particular catalyst is that taken to reach 100 % monomer conversion, as determined by ^1H NMR.

Table 3.5. Solution polymerisation of ε-CL by $[Ca(BH_4)(THF)_5][BPh_4]$ (**17-BPh$_4$**), $[Ca\{HC(Me_2pz)_3\}(BH_4)(THF)_2][BPh_4]$ (**18-BPh$_4$**), $(Tp^{tBu,Me})Ca(BH_4)(THF)$ (**20**), $(Tp^{tBu,Me})Mg(BH_4)$ (**22**), $(Tp^{tBu,Me})Yb(BH_4)(THF)$ (**3.8**) and $Ca(BH_4)_2(THF)_2$.[a]

Catalyst	Yield(%)	Time(mins)	M_n(GPC)[c]	M_n (calcd)[d]	M_w/M_n
17-BPh$_4$	84	2	39,100	22,820	1.32
18-BPh$_4$	79	2	41,820	22,820	1.35
20	81	10	17,600	22,820	1.28
22	72	10	32,240	22,820	1.31
3.8	76	10	20,600	22,820	1.30
$Ca(BH_4)_2(THF)_2$	77	2	11,560	22,820	1.28

[a] Conditions: [ε-CL]:[catalyst] = 200:1, 3.4 mL solvent at 23 °C. See Experimental section for other details. [b] Isolated yield at 100 % NMR conversion. [c] Molecular weights (g mol^{-1}) determined from GPC using the appropriate Mark-Houwink corrections. [d] Expected M_n (g mol^{-1}) for 1 chain growing per metal centre at 100% conversion.

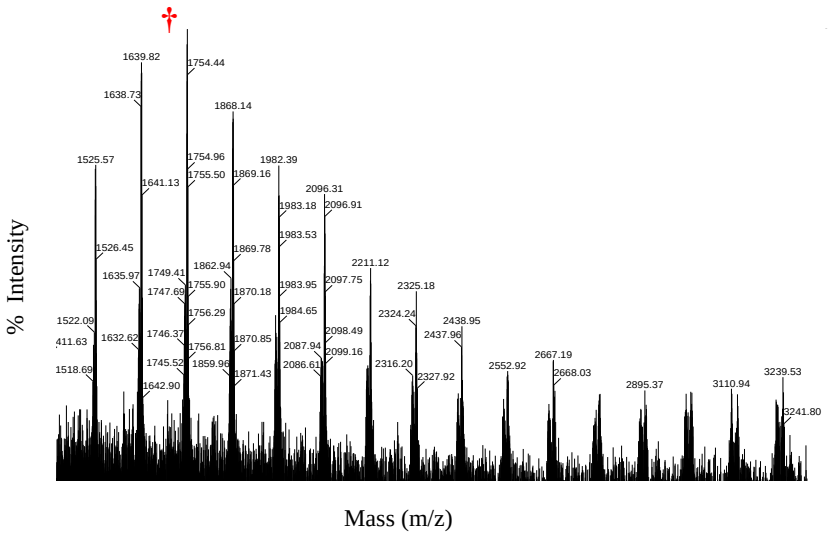
All catalysts produced polymers with narrow PDI values of approximately 1.3 and a fair agreement between measured and calculated M_n values was observed, although in most cases the measured M_n was higher than expected for the growth of one polymer chain per metal centre. This can be attributed to a fast rate of propagation relative to the rate of initiation. The similarities in the nature of the polymers produced by $(Tp^{tBu,Me})Ca(BH_4)(THF)$ (**20**) and $(Tp^{tBu,Me})Yb(BH_4)(THF)$ (**3.8**) can also be seen. Additionally, $Ca(BH_4)_2(THF)_2$ produced PCL with an M_n (11,560 g mol^{-1}) in very close agreement to that expected from two growing polymer chains per metal centre (11,410 g mol^{-1}). This result appears to rule out redistribution of either **17-BPh$_4$** or **18-BPh$_4$** under the polymerisation conditions.

No comparisons can be made with other main group borohydride complexes (since these are the first to be used in ROP studies). However, comparisons with related lanthanide borohydride complexes can be made. The most closely related complexes to $[Ca(BH_4)(THF)_5][BPh_4]$ (**17-BPh$_4$**) and $[Ca\{HC(Me_2pz)_3\}(BH_4)(THF)_2][BPh_4]$ (**18-BPh$_4$**)

are Okuda's lanthanide borohydride cations $[M(BH_4)_2(THF)_5][BPh_4]$ (M = Y (**3.10**), La (**3.11**), Nd (**3.12**) and Sm (**3.13**)). Similarly, these complexes also gave rapid gel formation for the ROP of ε-CL, giving polymers with comparable PDI values (1.3-1.4).[27] The observed M_n values of the polymers produced were also slightly higher than expected; for these catalysts two growing polymer chains per metal centre was expected and generally three to four chains were found. The most closely related catalysts to **20**, **22** and **3.8** and Chisholm's $(Tp^{tBu})M(X)(THF)_n$ (M = Ca (n = 1) or Mg (n = 2), X = $N(SiMe_3)_2$ or O-2,6-$C_6H_3{}^iPr_2$). [3, 4] However, these were not tested for ε-CL ROP.

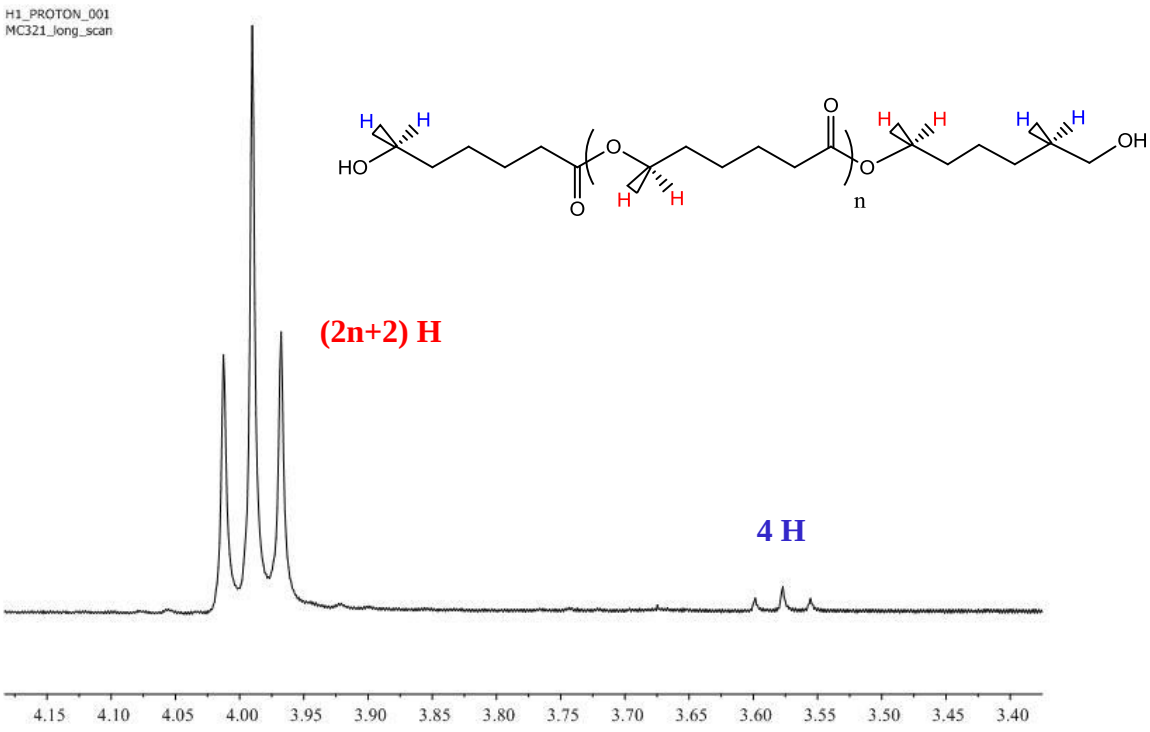
The complex $Cp^*Sm(BH_4)(THF)_2$ (**3.9**) also showed fast gel formation in the ROP of ε-CL and gave polymers with PDI values in the range 1.3-1.5 with M_n values generally in very good agreement to that expected for one chain per metal centre.[36] For example a 234:1 ratio of ε-CL:**3.9** polymerisation gave polymer with a PDI of 1.36 and an observed M_n of 20,400 (expected 22,400). The complex $Sm(O_2Npy)(BH_4)(THF)$ (**3.4**) [$H_2O_2N_{py}$ = (2-$C_5H_4N)CH_2NCH_2\{2\text{-}HO\text{-}3,5\text{-}C_6H_2{}^tBu_2\}_2$] gave PCL with a PDI of 1.8 and an observed M_n of 20,400 (expected 31,381). The broad PDI and lower than expected M_n was attributed to chain transfer events.[21] It can be seen from these comparisons that the borohydride complexes prepared in this chapter show similar activity and control (and in some cases superior) to related lanthanide borohydride initiators. MALDI-ToF-MS analysis showed α,ω–dihydroxy telechelic polymers (an example is shown in Figure 3.5), consistent with the coordination-insertion mechanism proposed for lanthanide borohydride systems outlined in Scheme 3.0.[19, 20, 38] For example, the peak at 1754.4 *m/z* († in Figure 3.5) corresponds to $HO(CH_2)_5C(O)\text{-}[PCL]_{13}\text{-}O(CH_2)_6OH$ (the calculated value is 1754.6).

Figure 3.5. MALDI-ToF MS of α,ω–dihydroxy telechelic PCL synthesised using $[Ca(BH_4)(THF)_5][BPh_4]$ (**17-BPh$_4$**). M_n by GPC analysis was 8,310 g mol^{-1} (from a [ε-CL]:[catalyst] = 20:1 polymerisation).



Additional evidence for the formation of α,ω–dihydroxy telechelic PCL was found in the ^{1}H NMR spectra of the polymers formed, showing the two C<u>H</u>$_2$CH$_2$OH end groups (right hand region in Figure 3.6). It can be seen that the number of CH$_2$OH protons in the central repeating unit of α,ω–dihydroxy telechelic PCL is dependent on the length of a polymer chain, whilst the number of terminal C<u>H</u>$_2$ protons (4) is independent. Therefore integration of the two regions in a ^{1}H NMR spectrum provides a measure of the M_n value of a polymer sample. This was measured to be 6,740 g mol^{-1} for the polymer sample shown in Figure 3.5 and in reasonable agreement with the value measured by GPC analysis (8,310 g mol^{-1}).

Figure 3.6. ^{1}H NMR spectrum ($CDCl_3$) of α,ω–dihydroxy telechelic PCL synthesised using [Ca(BH$_4$)(THF)$_5$][BPh$_4$] (**17-BPh$_4$**). M_n by GPC analysis was 8,310 g mol^{-1} ([ε -CL]$_0$:[**17-BPh$_4$**]$_0$ = 20). The relative ratio of integrals = 29.



3.4 Polymerisation studies: ROP of *rac*-LA

[Ca(BH$_4$)(THF)$_5$][BPh$_4$] (**17-BPh$_4$**) was active for the ROP of *rac*-LA at 70 ^{o}C in THF, consumption of *rac*-LA followed well-behaved first order kinetics (with a measured k_{obs} value of 0.0084(2) min^{-1}) and gave a linear M_n (GPC) *vs.* % conversion plot (Figure 3.7). The PLAs formed with this catalyst were all atactic as expected due to the absence of a supporting ligand, but had fairly narrow PDI values in the range 1.2-1.5. The gradient of the line of best fit for the M_n *vs. rac*-LA converted plot is 135(6) g mol^{-1} (% conversion)$^{-1}$ (R^2 = 0.983), very close to the expected value of 144.1. This, together with the narrow PDIs of the polymers formed, is evidence for a well controlled polymerisation process.

Figure 3.7. Data for the ROP of *rac*-LA using $[Ca(BH_4)(THF)_5][BPh_4]$ (**17-BPh$_4$**). Top: first order plot for *rac*-LA consumption; $R^2 = 0.987$, $k_{obs} = 0.0084(2)$ min^{-1}. Bottom: M_n (as measured by GPC) *vs. rac*-LA converted. The dotted line is that expected for one PLA chain per metal centre. Conditions: 6 mL THF, 70 ^oC, 4.5 hours, $[rac\text{-LA}]_0$:[**17-BPh$_4$**]$_0$ = 100. PDI values are given in parentheses.

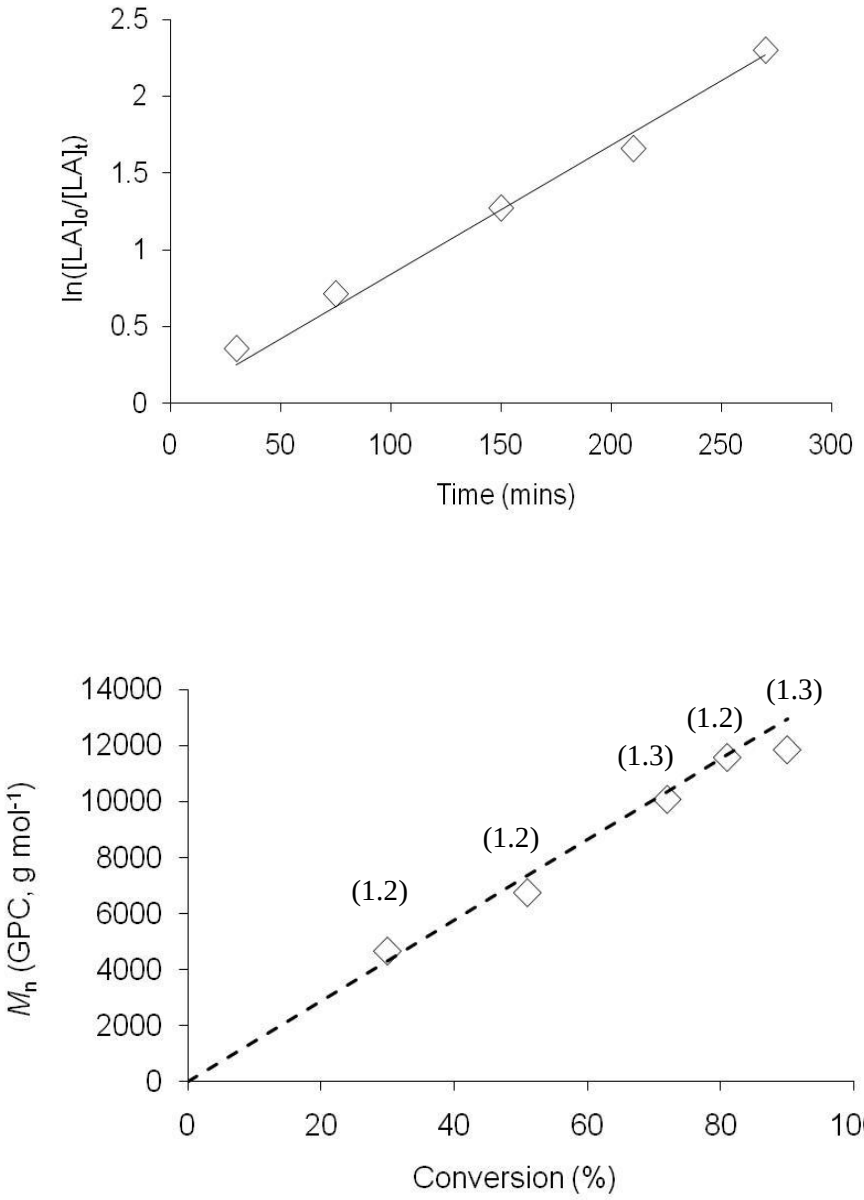
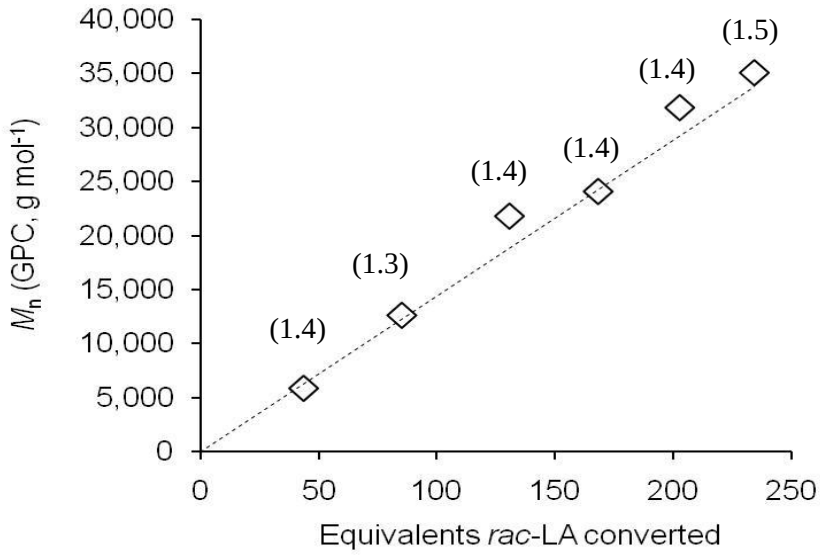


Figure 3.8 shows a plot of M_n *vs* equivalents *rac*-LA converted for $[rac\text{-LA}]_0$:[**17-BPh$_4$**]$_0$ ratios between 50 and 300. The gradient of the best-fit line was 152(3) g mol^{-1} (equivalents converted)$^{-1}$ (R^2 = 0.998) in excellent agreement with that predicted (144.1) for one PLA chain growing per Ca-BH_4 group in a living-type fashion.

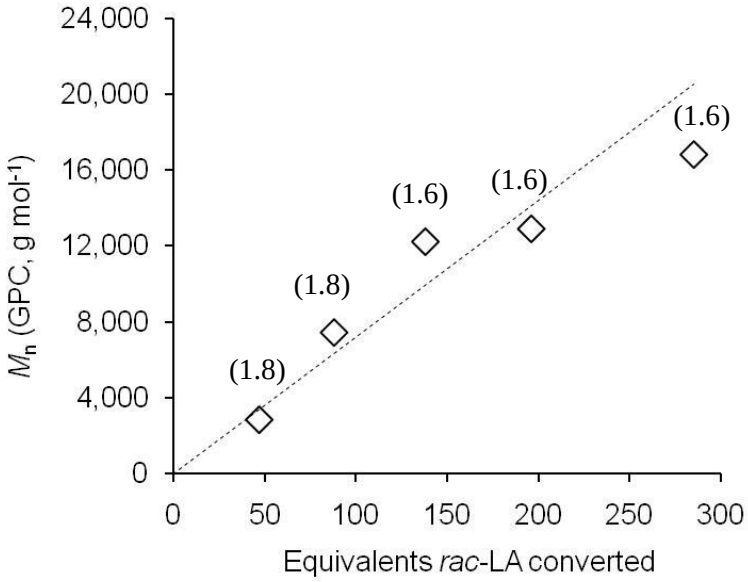
Figure 3.8. M_n (as measured by GPC) *vs.* equivalents *rac*-LA converted using $[Ca(BH_4)(THF)_5][BPh_4]$ (**17-BPh$_4$**). The dotted line is that expected for one PLA chain per BH_4 group. Conditions: 6 mL THF, 70 ^oC, 3 or 5 h, [*rac*-LA]$_0$:[**17-BPh$_4$**]$_0$ = 50, 100, 150, 200, 250, 300. PDI values are given in parentheses.



As previously discussed, it was shown by solution IR that **17-BPh$_4$** does not undergo redistribution at room temperature in THF. In order to rule out the possibility of redistribution of **17-BPh$_4$** under the polymerisation conditions (and subsequent polymerisation by $Ca(BH_4)_2(THF)_2$), the polymerisation behaviour of $Ca(BH_4)_2(THF)_2$ was studied under identical conditions to those used in the testing of **17-BPh$_4$**.

Figure 3.9 shows a plot of M_n *vs* equivalents *rac*-LA converted for [*rac*-LA]$_0$:$[Ca(BH_4)_2(THF)_2]_0$ ratios between 50 and 300. The gradient of the best-fit line was 55(10) g mol^{-1} (equivalents converted)$^{-1}$ (R^2 = 0.906), slightly lower than that predicted (72) for two PLA chains growing per borohydride group in a living-type fashion. The PDI values (1.6-1.8) of the polymers formed using $Ca(BH_4)_2(THF)_2$ are broader than those formed using **17-BPh$_4$** (1.3-1.5). Also, it has been shown that **17-BPh$_4$** produces PLA with M_n values consistent with one growing chain per metal centre, which is markedly different to the results obtained using $Ca(BH_4)_2(THF)_2$. This is strong evidence that **17-BPh$_4$** does not undergo redistribution under the polymerisation conditions. Unsurprisingly, the PLA formed using $Ca(BH_4)_2(THF)_2$ was atactic.

Figure 3.9. M_n (as measured by GPC) *vs.* equivalents *rac*-LA converted using $Ca(BH_4)_2(THF)_2$, $R^2 = 0.906$. The dotted line is that expected for two PLA chains per BH_4 group. Conditions: 6 mL THF, 70 °C, 3 or 5 h, $[rac\text{-LA}]_0:[Ca(BH_4)_2(THF)_2]_0 = 50$, 100, 150, 200, 250, 300. PDI values are given in parentheses.

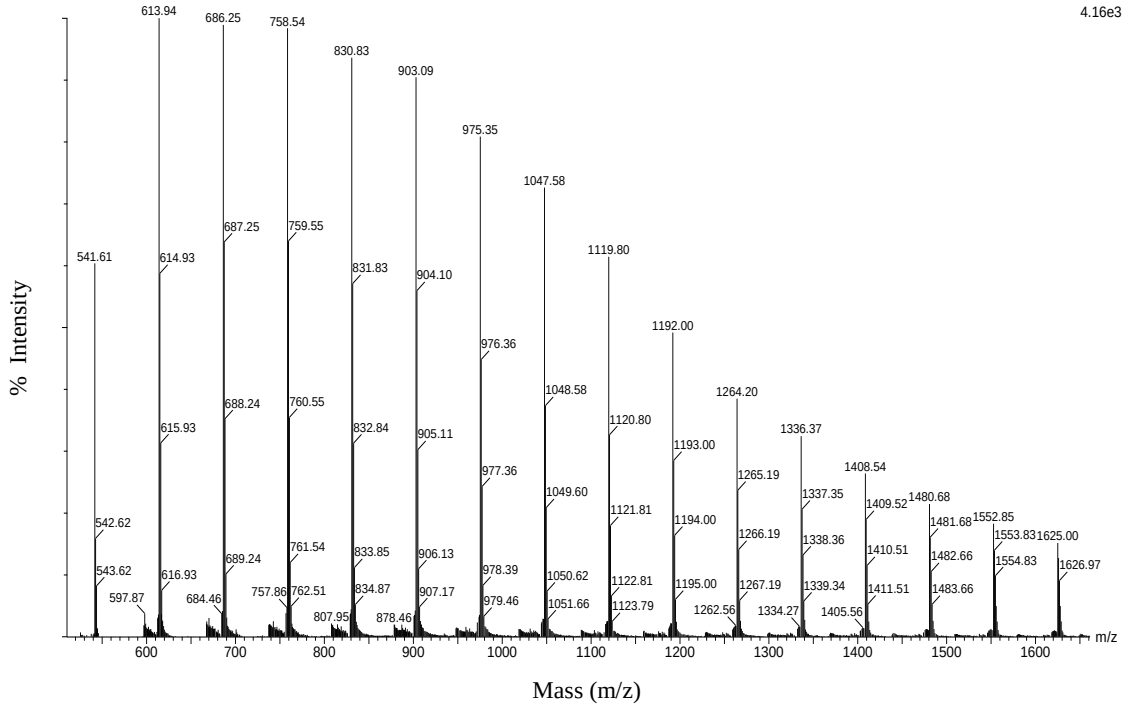


The MALDI-ToF mass spectrum of a PLA sample obtained using $[Ca(BH_4)(THF)_5][BPh_4]$ (**17-BPh_4**) is shown in Figure 3.10. The separation of integer polymer units is 72 *m/z*, consistent with transesterification side reactions. As mentioned in the introduction, the ROP of cyclic esters with borohydride initiators can lead to α,ω-dihydroxy terminated polyesters. In the case of LA, literature reports have suggested that poly(*rac*-LA) with either -CH(Me)CH_2OH or –CH(Me)CHO end groups may be formed.[16, 23, 25] The latter end group arises from protonolysis of the metal-bound "end" of the growing polymeryl chain (i.e. from the last enchained *rac*-LA), whereas the former end group arises from single reduction of one of the carbonyl groups of the first enchained *rac*-LA monomer by the initiating M–BH_4 group. A recent comprehensive experimental and theoretical study was carried out by Dyer *et al.*,[21] confirming this to be the case for a family of bis(phenolate)amine-supported samarium borohydride initiators.

However in the study by Dyer *et al.* high resolution MALDI-ToF MS techniques superior to those used for the purposes of this thesis were applied. This enabled the absolute determination of polymer end groups. The difficulty with standard MALDI-ToF MS techniques in the context of this thesis is the very similar *m/z* values predicted for polymer end groups, and their coincidence with cyclic PLA units. For example a linear polymer (n = six) chain with a –CH(Me)CH_2OH end group has a calculated *m/z* of 1050, very similar to

the calculated *m/z* of 1052 for a linear polymer chain with the same number of repeating units with a –CH(Me)CHO end group. Further complication arises when noting the calculated *m/z* of 1048 for a cyclic polymer unit consisting of seven monomer units, hence the need for higher resolution techniques when absolutely assigning polymer end groups in this case. Attempted methods to rectify this situation are discussed later in this chapter.

Figure 3.10. MALDI-ToF MS of PLA synthesised using $[Ca(BH_4)(THF)_5][BPh_4]$ (**17-BPh_4**). M_n by GPC analysis was 2,240 g mol^{-1} (from a [rac-LA]:[**17-BPh_4**]$_0$ = 20:1 polymerisation).

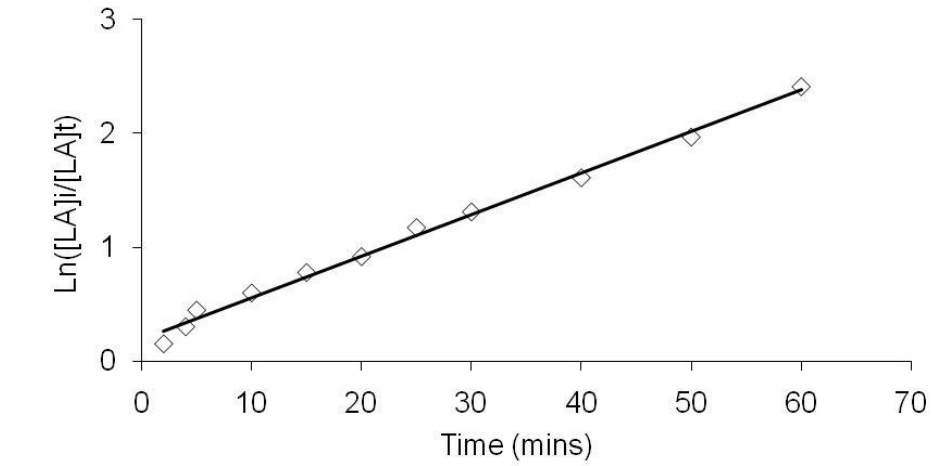


The slow ROP of *rac*-LA with **17-BPh_4** was alleviated by using **18-BPh_4**, the $HC(Me_2pz)_3$ ligand providing a better-defined coordination environment, and perhaps guarding against binuclear or extensively LA chain chelated resting states. Thus up to 250 equivalents of *rac*-LA could be converted at room temperature within two hours with PDI values generally between 1.2 and 1.4. The consumption of *rac*-LA followed first order kinetics (with a measured k_{obs} value of 0.037(1) min^{-1}) and gave a linear M_n (GPC) *vs.* % conversion plot (Figure 3.11).

Interestingly, the rate plot in Figure 3.11 appears to have two linear stages (the first ending after approximately five minutes). This effect has been observed elsewhere[56, 57] and is thought to be a result of the equilibrium between aggregated and monomeric polymeryl species.[57] It is assumed that propagation only occurs from the latter and that monomeric active species are stabilised by an excess amount of monomer. Therefore, at low conversions the concentration of such species is high, accordingly the apparent rate

of polymerisation is high also. At higher conversions the equilibrium is shifted in the favour of aggregated species and therefore the apparent rate of polymerisation decreases. Such behaviour may also explain the higher than expected M_n values seen throughout the polymerisation. Generally the experimental M_n values are twice the expected value for one growing polymer chain per metal centre. This is consistent with a small proportion of the catalyst becoming active species, as would be the case for an equilibrium between aggregated and monomeric polymeryl species. This poor control is refelected in the fact that the gradient of the line of best fit for the M_n *vs. rac*-LA converted plot is 304(7) g mol^{-1} (% conversion)$^{-1}$ (R^2 = 0.992, see also Figure 3.11), approximately twice the expected value of 144.1.

Figure 3.11. Data for the ROP of *rac*-LA using [Ca{HC(Me$_2$pz)$_3$}(BH$_4$)(THF)$_2$][BPh$_4$] (**18-BPh$_4$**). Top: first order plot for *rac*-LA consumption; R^2 = 0.994, k_{obs} = 0.037(1) min^{-1}. Bottom: M_n (as measured by GPC) *vs. rac*-LA converted. The dotted line is that expected for one PLA chain per metal centre. Conditions: 6 mL THF, RT, 1 hour, [*rac*-LA]$_0$:[**18-BPh$_4$**]$_0$ = 100. PDI values are given in parentheses.



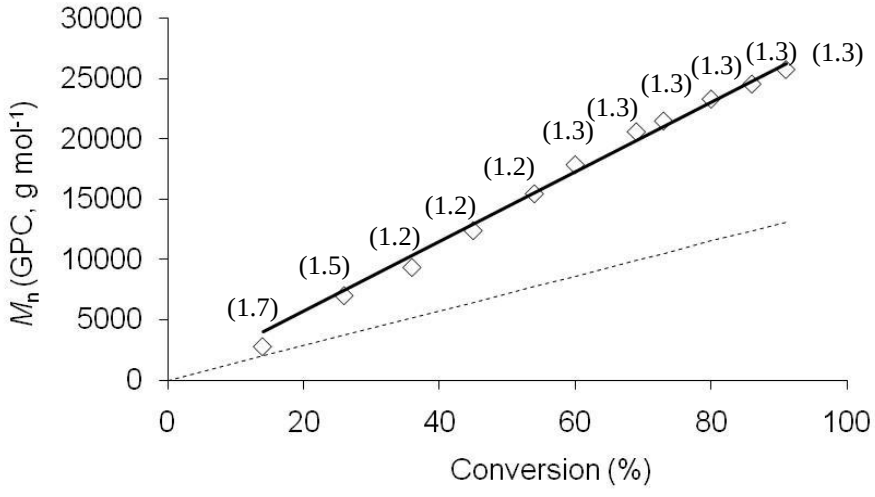
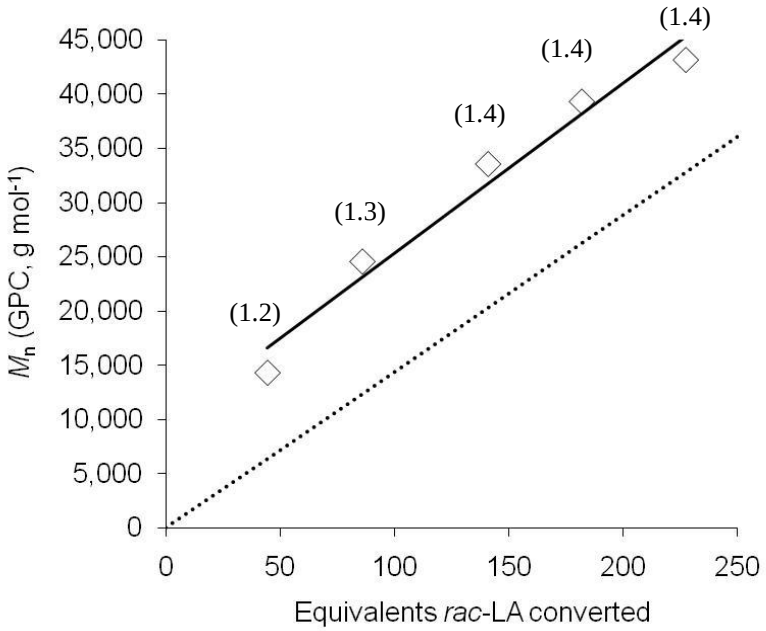


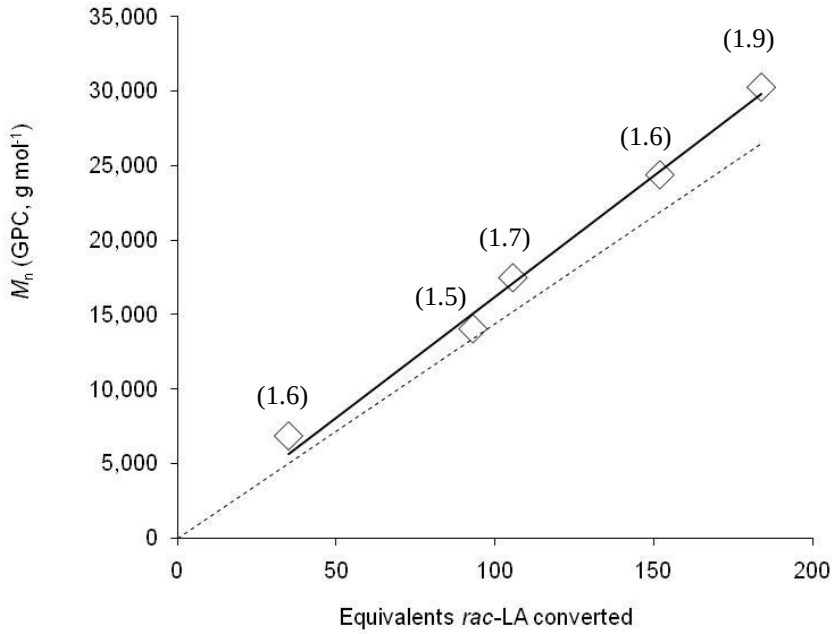
Figure 3.12 shows a plot of M_n *vs.* equivalents *rac*-LA converted for [*rac*-LA]$_0$:[**18-BPh$_4$**]$_0$ ratios between 50 and 250. The gradient of the best-fit line was 157(11) g mol^{-1} (equivalents converted)$^{-1}$ (R^2 = 0.982), in excellent agreement with that predicted (144.1) for one PLA chain, but in general the M_n values were once again higher (1.5 to 2 times) than expected. Nonetheless, it is clear that the slow *rac*-LA ROP rates typically associated with cationic initiators[7, 58] can be alleviated with the appropriate supporting ligand, thus offering considerable potential for further development. In fact the only other example of a cationic initiator for the ROP of *rac*-LA was introduced very recently by Wheaton and Hayes.[59] The MALDI-ToF mass spectrum of a PLA sample obtained using **18-BPh$_4$** is very similar to that obtained using **17-BPh$_4$**, showing a separation of integer polymer units of 72 *m/z*. Similarly, all of the polymers produced using **18-BPh$_4$** were atactic.

Figure 3.12. M_n (as measured by GPC) *vs.* equivalents *rac*-LA converted using [Ca{HC(Me$_2$pz)$_3$}(BH$_4$)(THF)$_2$][BPh$_4$] (**18-BPh$_4$**). The dotted line is that expected for one PLA chain per BH$_4$ group. Conditions: 6 mL THF, RT, 2 hours, [*rac*-LA]$_0$:[**18-BPh$_4$**]$_0$ = 50, 100, 150, 200, 250. PDI values are given in parentheses.



Gratifyingly, (Tp^{tBu,Me})Ca(BH$_4$)(THF) (**20**) is also a very efficient initiator for the ROP of *rac*-LA either at room temperature or -20 ^{o}C. For example, with [*rac*-LA]$_0$:[**20**]$_0$ = 200, >90% conversion was achieved within 5 mins at both temperatures. Figure 3.13 shows a plot of experimental M_n *vs.* equivalents *rac*-LA converted for [*rac*-LA]$_0$:[**3**]$_0$ ratios between 50 and 200 at -20 ^{o}C.

Figure 3.13. M_n (as measured by GPC) *vs.* equivalents *rac*-LA converted using ($Tp^{tBu,Me}$)Ca(BH_4)(THF) (**20**). The dotted line is that expected for one PLA chain per BH_4 group. Conditions: 6 mL THF, -20 °C, 5 minutes, [*rac*-LA]$_0$:[**20**]$_0$ = 40, 100, 120, 160, 200. PDI values are given in parentheses.



The gradient of the best-fit line is 162(4) g mol^{-1} (equivalents converted)$^{-1}$ (R^2 = 0.998), in very good agreement with that predicted (144.1 g mol^{-1} (equivalents converted)$^{-1}$) for one PLA chain growing per Ca–BH_4 group of **20** in a living-type fashion. The corresponding plot for ROP at RT was also linear (Figure 3.14) but the gradient of the best-fit line was 239(7) g mol^{-1} (equivalents converted)$^{-1}$ (R^2 = 0.996), indicating less optimal control of the relative rates of initiation and propagation for this very active system.

Tetrad analysis of the C<u>H</u>(Me)O region of the selectively homonuclear decoupled ^{1}H NMR spectra of the PLA samples formed with **20** revealed heterotactically-enriched polymer with high P_r values of 0.88-0.90 at -20 °C (*ca*. 0.80 at RT), an example spectrum is shown in Figure 3.15. The stereochemical enrichment present in the polymer samples arises from a chain-end control process (rather than enatiomorphic site control typically seen with chiral catalysts). The bulk of the *tert*-butyl groups in the 3- position of the ligand clearly favour the addition of consecutive monomer units with opposite chirality (i.e. *D*-LA followed by *L*-LA), especially at low temperature where the lowered thermal motion reduces the probability of steroerrors.

The degree of heterotactic enrichment is similar to that found by Chisholm *et al.* when using (Tp^{tBu})Ca(X) (X = $N(SiMe_3)_2$ or O-2,6-$C_6H_3{}^iPr_2$) (P_r = 0.9),[3, 4] and in contrast to the atactic PLA formed with the bulky calcium β-diketiminate complex

(BDI)Ca{N(SiMe$_3$)$_2$}(THF) (BDI = CH-[CMeN-(2,6-^{i}Pr$_2$C$_6$H$_3$)]$_2$).[3] The moderate to broad PDI values of the PLA formed using **20** both at -20 ^{o}C and room temperature (1.5-1.9) are also comparable to those found using the aforementioned tris(pyrazolyl)borate complexes prepared by Chisholm *et al.* (1.7).[3, 4] The MALDI-ToF mass spectrum of a PLA sample obtained using **20** is very similar to that obtained using **17-BPh$_4$** and **18-BPh$_4$**, showing a separation of integer polymer units of 72 *m/z*.

Figure 3.14. M_n (as measured by GPC) *vs.* equivalents *rac*-LA converted using ($Tp^{tBu,Me}$)Ca(BH$_4$)(THF) (**20**). Conditions: 6 mL THF, RT, 5 minutes, [*rac*-LA]$_0$:[**20**]$_0$ = 40, 80, 100, 120, 160, 200. PDI values are given in parentheses.

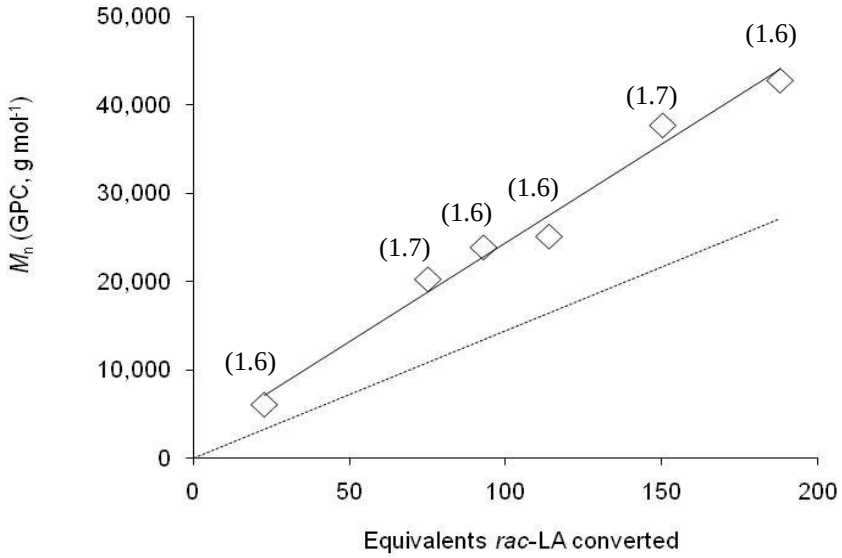
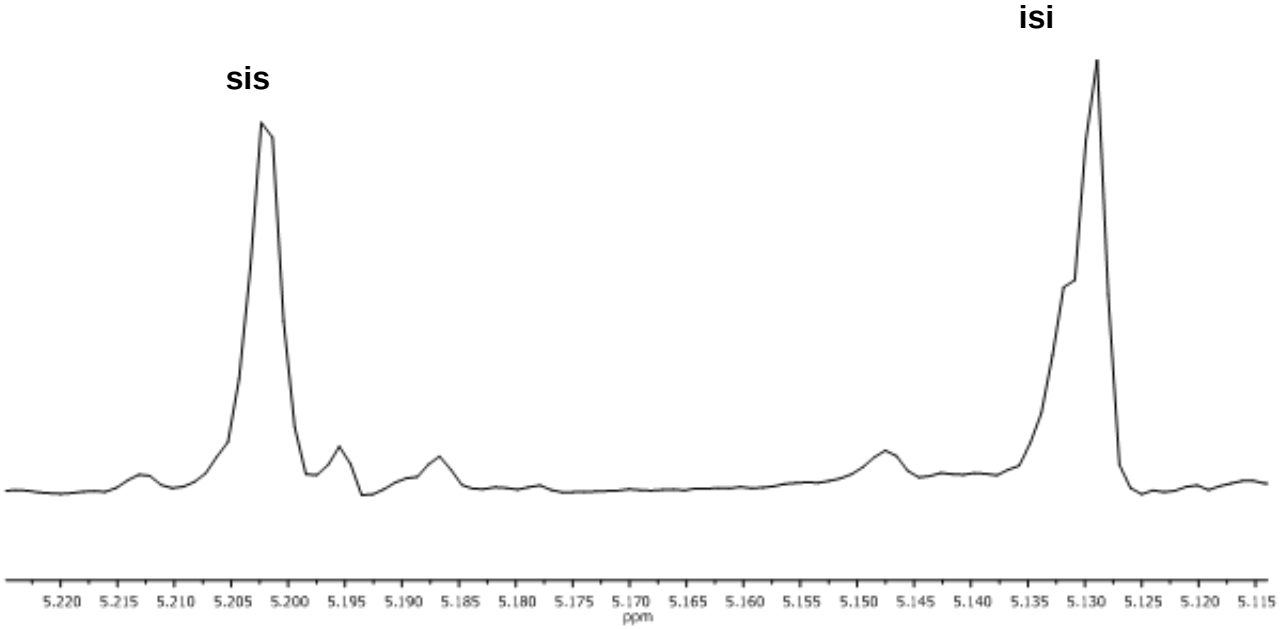


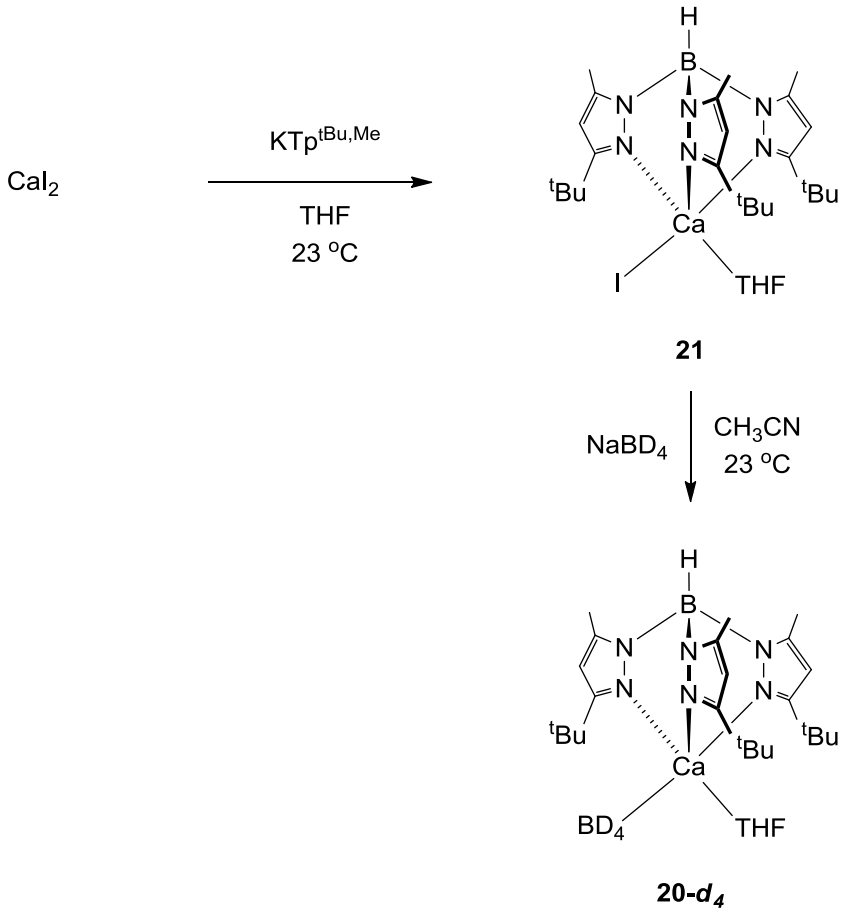
Figure 3.15. CH(Me)O region of the homonuclear decoupled ^{1}H NMR spectrum of PLA formed using **20** (P_r = 0.90) at -20 ^{o}C.



In order to gain more information on the PLA end groups seen for polymers prepared using **17-BPh$_4$**, **18-BPh$_4$** and **20**, the deuterated analogue of the latter was prepared, ($Tp^{tBu,Me}$)Ca(BD_4)(THF) (**20-*d*$_4$**). Through the use of a BD_4 initiator in place of a BH_4 initiator, the PLA end groups CH(Me)CD_2OH or –CH(Me)CDO, instead of CH(Me)CH_2OH or –CH(Me)CHO would be expected. It was postulated that the increased polymer mass would result in easier interpretation of MALDI-ToF spectra (with the previously mentioned difficulties of overlapping peaks in mind). ^{2}H NMR would also be used as a polymer analysis tool.

Initially it was intended to synthesise all three deuterated analogues from $Ca(BD_4)_2(THF)_2$. However, the attempted synthesis of this precursor from CaI_2 and $NaBD_4$ proved non-trivial, resulting in only the monosubstituted product $Ca(BD_4)I(THF)_2$ regardless of stoichiometry and temperature. The complex ($Tp^{tBu,Me}$)Yb(BD_4)(THF)[34] had previously been prepared by reaction of ($Tp^{tBu,Me}$)Yb(I)(THF) with $NaBD_4$. Following this approach the synthesis of **20-*d*$_4$** from ($Tp^{tBu,Me}$)Ca(I)(THF) (**21**) was similarly successful.

Scheme 3.3. Synthesis of ($Tp^{tBu,Me}$)Ca(I)(THF) (**21**) and ($Tp^{tBu,Me}$)Ca(BD_4)(THF) (**20-*d*$_4$**).



($Tp^{tBu,Me}$)Ca(I)(THF) (**21**) was readily prepared at room temperature directly from CaI_2 and $KTp^{tBu,Me}$ in 71% recrystallised yield. The IR and NMR data for formally zwitterionic **21** are consistent with the structure proposed in Scheme 3.3 which is analogous to that of Takats' reported ($Tp^{tBu,Me}$)Yb(I)(THF).[60] Unlike the identical unit cell parameters seen between **20** and **3.8**, in this case the unit cell parameters of **21** are not identical to that of ($Tp^{tBu,Me}$)Yb(I)(THF).

Figure 3.16. Molecular structure of ($Tp^{tBu,Me}$)Ca(I)(THF) (**21**). C-bound H atoms omitted and remaining H atoms drawn as spheres of an arbitrary radius.

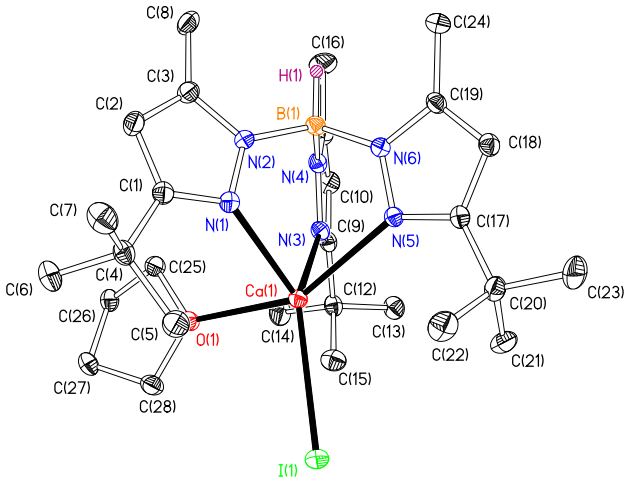


Table 3.6. Selected bond distances (Å) and angles (°) for ($Tp^{tBu,Me}$)Ca(I)(THF) (**21**).

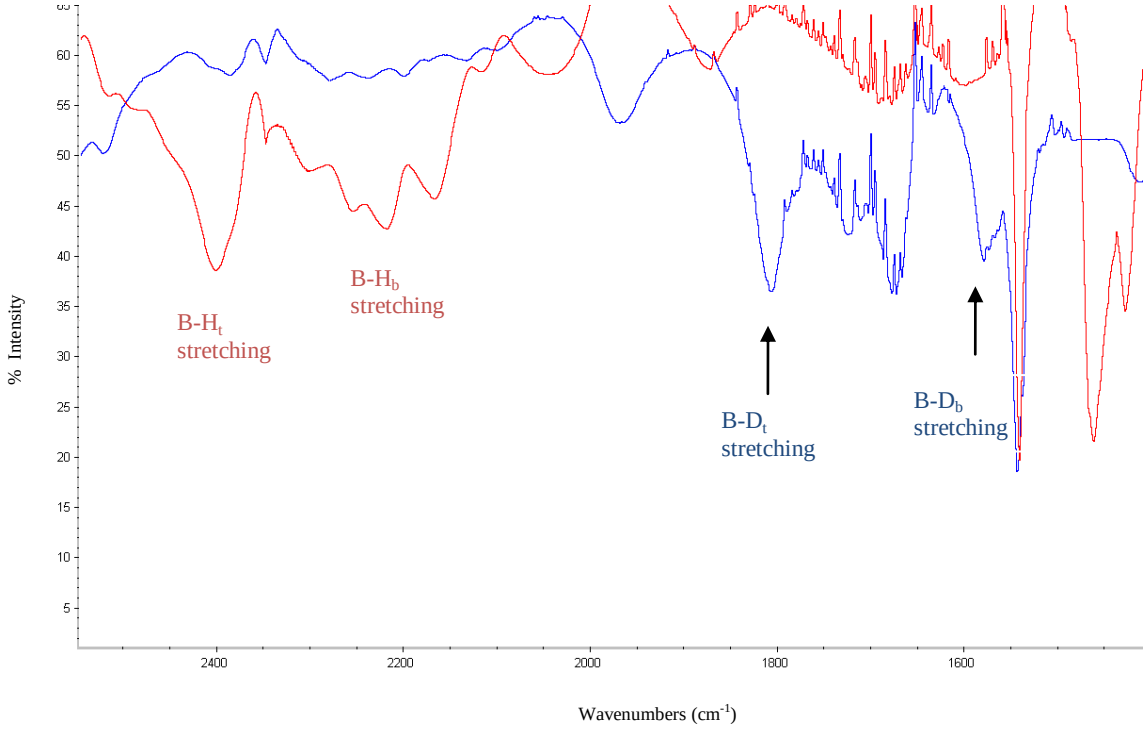
Ca(1)-N(1)	2.413(3)	N(1)- Ca(1)-O(1)	82.10(10)
Ca(1)-N(3)	2.440(3)	N(3) -Ca(1)-O(1)	85.09(9)
Ca(1)-N(5)	2.471(3)	N(5)-Ca(1)-O(1)	152.62(10)
Ca(1)-O(1)	2.402(2)	N(1)- Ca(1)-I(1)	134.70(8)
Ca(1)-I(1)	3.0281(7)	N(3)- Ca(1)-I(1)	131.71(8)
		N(5)- Ca(1)-I(1)	117.26(7)

The Ca-I distance of 3.0281(7) Å is very close to that of 3.0536(8) Å seen in the isostructural ($Tp^{tBu,Me}$)Yb(I)(THF).[60] The Ca-O distance (2.402(2) Å) is also very similar to the analogous Yb-O bond distance (2.447(6) Å) seen in ($Tp^{tBu,Me}$)Yb(I)(THF), as are the average Ca-N_{pz} bond lengths (2.44 Å, *c.f.* 2.45 Å in ($Tp^{tBu,Me}$)Yb(I)(THF)). The Ca-O

distance is slightly shorter in **21** than **20** (2.4291(14) Å). This is a consequence of the borohydride ligand in **20** possessing greater steric bulk than the iodide ligand in **21**. The average Ca-N_{pz} bond lengths in **21** are nonetheless comparable to those in **20** (2.45 Å).

($Tp^{tBu,Me}$)Ca(BD_4)(THF) (**20-*d*$_4$**) was readily prepared at room temperature directly from **20** and $NaBD_4$ in 58% recrystallised yield. The solution IR spectrum (THF) of **20-*d*$_4$** is shown along with that of **20** in Figure 3.17.

Figure 3.17. Borohydride region of solution (THF) IR spectra of ($Tp^{tBu,Me}$)Ca(BH_4)(THF) (**20**, red trace) and ($Tp^{tBu,Me}$)Ca(BD_4)(THF) (**20-*d*$_4$**, blue trace). The background has been subtracted.



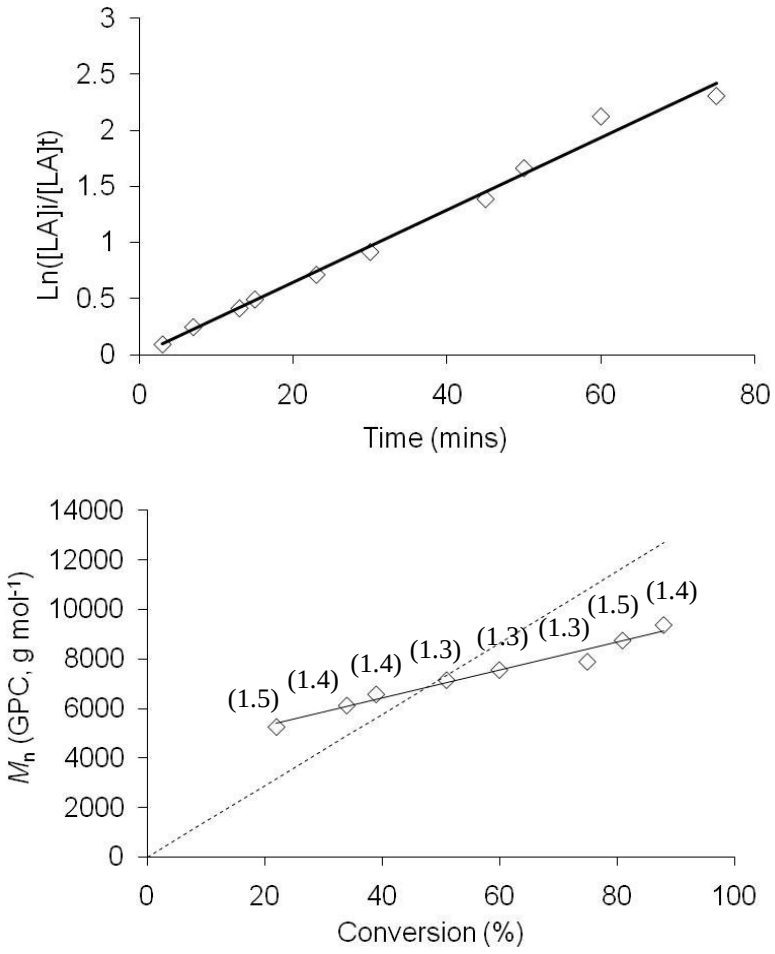
The BH_4 stretching region of the IR spectrum of **20** shows bands at 2416, 2223cm^{-1} and 2174 cm^{-1}. The first band corresponds to the B–H_t stretch of the BH_4 ligand while the other two correspond to the B–H_b stretches. The corresponding **20-*d*$_4$** isotopomer showed the expected isotope shifts in the IR spectrum, 1807 (s, B-D_t of BD_4, ν_H/ν_D = 1.34) and 1543 (s, B-D_b of BD_4); ν_H/ν_D = 1.41, the other B–H_b stretch was hidden under the subtraction artefact. The ^{1}H and ^{11}B NMR spectra of **20** and **20-*d*$_4$** are identical (the BH_4 ligand of **20** was not visible by ^{1}H NMR spectroscopy).

Whilst the ^{2}H NMR spectrum showed the presence of C$\underline{D}_2$OH protons of α,ω-dihydroxytelechelic PCL prepared using **20-*d*$_4$** in an identical position to that seen in the ^{1}H NMR spectrum of polymer prepared using **20**, the MALDI-ToF spectra of both polymers were apparently identical. Unfortunately the resolution of the MALDI-ToF spectra were not

good enough to resolve deuterium and proton capped polymers. This was unfortunately also the case for PLA samples as it was not possible to resolve $CH(Me)CH_2OH$ or -CH(Me)CHO end groups from cyclic PLA units. Despite this it is likely that *rac*-LA and ε-CL are polymerised by the same coordination-insertion mechanism for this family of catalysts, as evidenced by generally good levels of control over the M_n and PDIs of the polymers formed.

Despite the similarities observed between ($Tp^{tBu,Me}$)Ca(BH_4)(THF) (**20**) and ($Tp^{tBu,Me}$)Yb(BH_4)(THF) (**3.8**) for the ROP of ε-CL, **3.8** was a much slower initiator for the ROP of *rac*-LA than **20**, and in fact required a temperature of 70 °C. The polymerisation followed first order monomer consumption (Figure 3.18) and took 75 minutes to reach 90 % conversion (with a measured k_{obs} value of 0.032(2) min^{-1}).

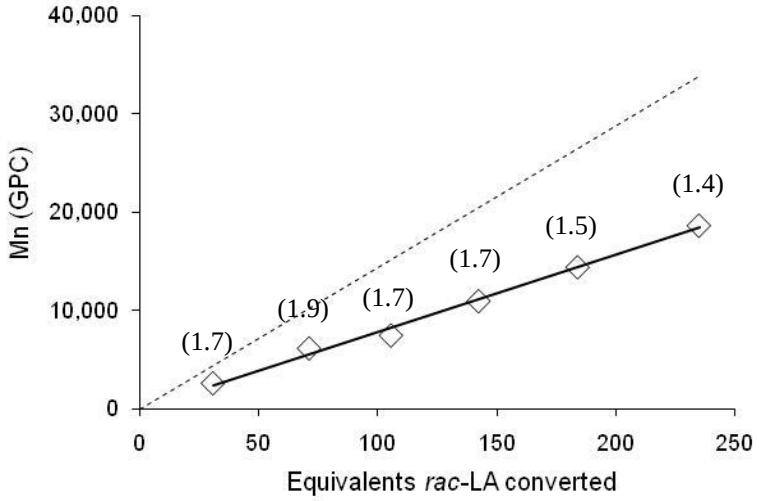
Figure 3.18. Data for the ROP of *rac*-LA using ($Tp^{tBu,Me}$)Yb(BH_4)(THF) (**3.8**). Top: first order plot for *rac*-LA consumption; R^2 = 0.990, k_{obs} = 0.032(2) min^{-1}. Bottom: M_n (as measured by GPC) *vs.* *rac*-LA converted. The dotted line is that expected for one PLA chain per metal centre. Conditions: 6 mL THF, 70 °C, 75 mins, [*rac*-LA]$_0$:[**3.8**]$_0$ = 100. PDI values are given in parentheses.



The M_n *vs. rac*-LA converted plot in Figure 3.18 shows initally higher than expected M_n values, followed by a levelling off period. At high conversions, the M_n values are slightly lower than expected. This trend is most likely due to the increasing degree of transesterifcation as the polymerisation proceeds. This poor behaviour is refelected in the fact that the gradient of the line of best fit for the M_n *vs. rac*-LA converted plot is 56(4) g mol^{-1} (% conversion)$^{-1}$ (R^2 = 0.970), less than half of the expected value (144.1) for one PLA chain growing per Yb–BH_4 group of **3.8** in a living-type fashion. Despite this poor control of M_n, the PDIs of the PLA formed were moderate (1.3-1.5).

Figure 3.19 shows a plot of experimental M_n *vs.* equivalents *rac*-LA converted for [*rac*-LA]$_0$:[**3.8**]$_0$ ratios between 50 and 250. The gradient of the best-fit line is 78(3) g mol^{-1} (equivalents converted)$^{-1}$ (R^2 = 0.994), approximately half of that predicted (144.1). For low equivalent polymerisations, the M_n values are fairly close to the expected values for one chain growing per metal centre. Using higher equivalents of monomer, the M_n values fall below the expected values. This is a similar trend to that observed in Figure 3.18 for the M_n *vs. rac*-LA converted plot. For the PLA samples discussed in Figure 3.19, a slight degree of heterotactic enrichment was found (P_r average = 0.70). This is lower than that seen in PLA prepared using **20** and can be attributed the higher temperature polymerisation conditions required using **3.8**.

Figure 3.19. M_n (as measured by GPC) *vs.* equivalents *rac*-LA converted using ($Tp^{tBu,Me}$)Yb(BH_4)(THF) (**3.8**). Conditions: 6 mL THF, 70 ^oC, 60 minutes, [*rac*-LA]$_0$:[**3.8**]$_0$ = 40, 80, 120, 160, 200, 250. PDI values are given in parentheses.

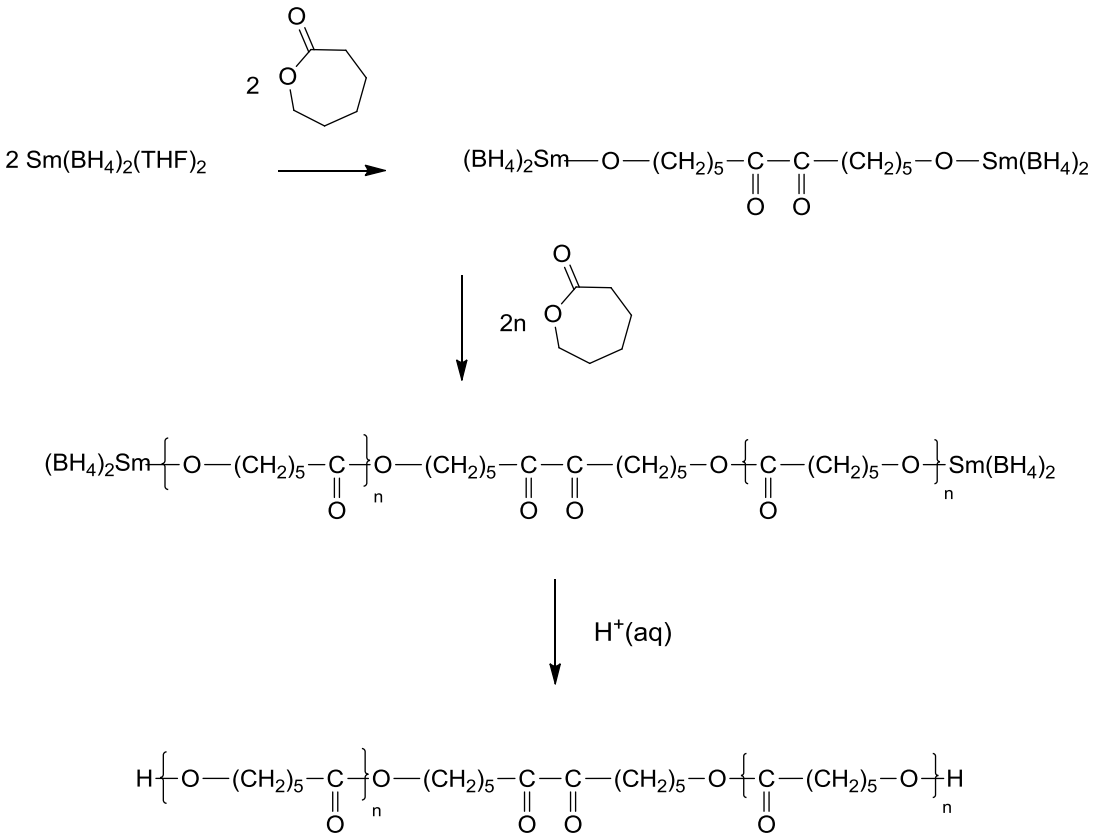


The MALDI-ToF mass spectrum of a PLA sample obtained using **3.8** is very similar to that seen previously showing a separation of integer polymer units of 72 *m/z*. It was surprising that **3.8** behaved so differently to **20** given the aforementioned similarities between the two

complexes. However, such differences are not unprecedented.[2, 61] For example, Harder *et al.* recently reported the different stereoselectivity shown towards the polymerisation of styrene by otherwise isomorphous calcium and ytterbium benzyl complexes.[61] It was shown that the ytterbium centre remained divalent throughout the polymerisation process, i.e. an oxidative mechanism was ruled out. The differences in the results shown were credited to small changes of metal-ligand bonding between the calcium and ytterbium complexes.[2, 61] However, generally the most obvious difference between calcium and ytterbium is the viable trivalent oxidation state for the latter.

Evans *et al.* showed that a series of samarium(II) compounds initiated the ROP of ε-CL by an oxidative pathway involving samarium(III).[62] More recently, Bonnet and co-workers speculated that the ROP of ε-CL using $Sm(BH_4)_2(THF)_2$ proceeded by two competing pathways:[36] the established coordination-insertion mechanism shown in Scheme 3.0 and an oxidative process involving trivalent samarium (Scheme 3.4).

Scheme 3.4. The oxidative mechanism of polymerisation of ε-CL proposed by Bonnet *et al.*[36]



It was argued that the mechanism in operation depended on the [ε-CL]:[catalyst] ratio; at low monomer to catalyst ratios (e.g. 116:1) the observed M_n values were consistent with one polymer chain growing per two metal centres, i.e. the observed M_n values were twice that

expected for one growing polymer chain per metal centre. In such situations it was argued that an oxidation pathway became prominent. At moderate monomer to catalyst ratios (e.g. 232:1) M_n values were consistent with one chain per metal centre, and therefore coordination-insertion (with initiation by only one of the borohydride groups) was thought to be the prominent mechanism. At larger monomer to catalyst ratios (e.g. 464:1) the growth of three polymer chains per metal centre was observed and it was argued that both mechanisms could be in operation. However no DFT study was carried out in parallel to the experimental work, and therefore the feasibility of an oxidative mechanism was not determined.

Presumably, if true, a similar oxidative mechanism with ytterbium catalysts is also possible, and also may apply to *rac*-LA as well as ε-CL. However, it has been shown that PLA prepared using **3.8** generally has a lower than expected M_n value, whereas M_n values twice that expected would be shown by a similar oxidative mechanism. Additionally, the PCL prepared using **3.8** had an M_n (20,600 g mol^{-1}), very close to the predicted value for one growing polymer chain per metal centre (22,820).

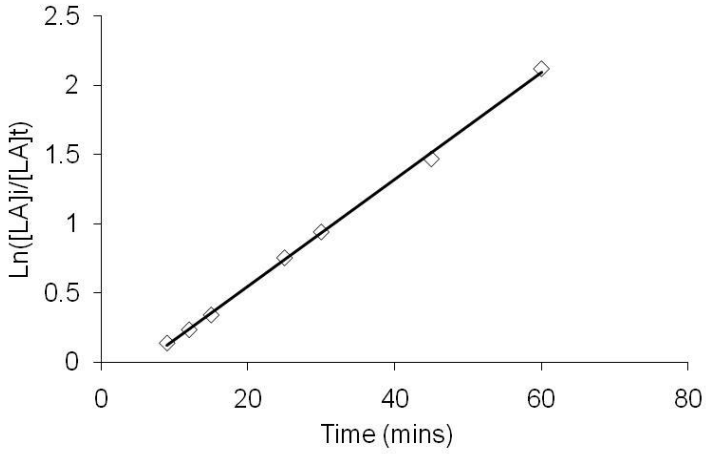
In order to probe further the likelihood of an oxidative mechanism in the case of **3.8**, Takats' previously reported complex, ($Tp^{tBu,Me}$)Yb(I)(THF) was synthesised by published methods.[60] With no initiating group available for coordination-insertion, any activity shown by this complex could be argued to be due to an oxidative mechanism. However, under identical polymerisation conditions used in the testing of **3.8** (and in fact for extended time periods), ($Tp^{tBu,Me}$)Yb(I)(THF) was shown to be inactive for the polymerisation of either ε-CL or *rac*-LA. It is also noteworthy that $Sm(I)_2(THF)_2$ was shown to be active for the ROP of ε-CL in THF by Evans *et al*.[62] The polymerisation conditions used in this case (refluxing THF), are very similar to those used in the testing of ($Tp^{tBu,Me}$)Yb(I)(THF) for *rac*-LA. Therefore an oxidative pathway seems to be highly unlikely in the case of polymerisations with **3.8**.

($Tp^{tBu,Me}$)Mg(BH_4) (**22**) was also a much slower initiator for the ROP of *rac*-LA than **20**, and also required a temperature of 70 ^oC, although heterotactically enriched polymer with P_r values averaging 0.65 were seen. The decreased enrichment when compared to polymers prepared using **20** is once more attributed to the higher temperature polymerisation conditions. The polymerisation followed first order monomer consumption and took 60 minutes to reach 88 % conversion (with a measured k_{obs} value of 0.0039(6) min^{-1}, Figure 3.20). The first order rate plot shows an induction period up to 10 minutes. As mentioned in Chapter 2, induction periods have been observed

elsewhere.[9, 63-65] It is thought that an induction period occurs due to a period of ligand rearrangement around the metal centre, in order to allow the monomer access to the coordination sphere.[57]

The M_n of the PLA formed during the polymerisation process is slightly below that expected for one growing polymer chain per metal centre at low conversions. At higher conversions the M_n of the PLA formed is significantly lower, most likely due to transesterification side reactions. This poor control is refelected in the fact that the gradient of the line of best fit for the M_n *vs. rac*-LA converted plot is 40(4) g mol^{-1} (% conversion)$^{-1}$ (R^2 = 0.945), less than a third of the expected value (144.1) for one PLA chain growing per Mg–BH_4 group of **22** in a living-type fashion. Despite this poor control of M_n, the PDIs of the PLA formed were quite narrow (1.1-1.3).

Figure 3.20. Data for the ROP of *rac*-LA using ($Tp^{tBu,Me}$)Mg(BH_4) (**22**). Top: first order plot for *rac*-LA consumption; R^2 = 0.999, k_{obs} = 0.039(6) min^{-1}. Bottom: M_n (as measured by GPC) *vs. rac*-LA converted. The dotted line is that expected for one PLA chain per metal centre. Conditions: 6 mL THF, 70 ^oC, 60 mins, [*rac*-LA]$_0$:[**22**]$_0$ = 100. PDI values are given in parentheses.



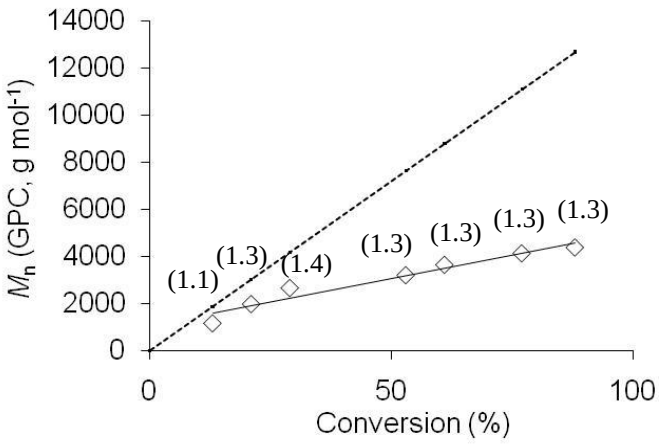
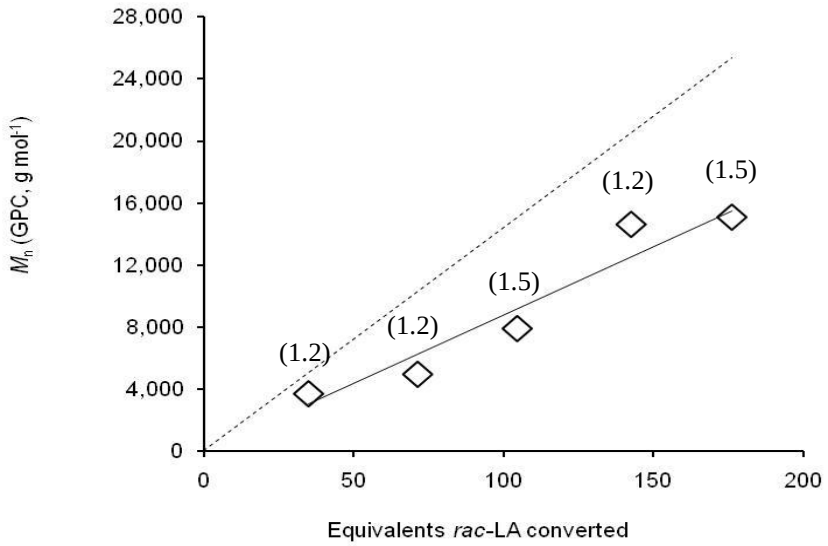


Figure 3.21 shows a plot of experimental M_n *vs.* equivalents *rac*-LA converted for [*rac*-LA]$_0$:[**3.8**]$_0$ ratios between 50 and 250. The gradient of the best-fit line is 92(15) g mol^{-1} (equivalents converted)$^{-1}$ (R^2 = 0.927) lower than that predicted (144.1 g mol^{-1} (equiv. converted)$^{-1}$) for one PLA chain growing per Mg–BH_4 group of **22** in a living-type fashion. This is consistent with the M_n *vs. rac*-LA converted plot shown in Figure 3.20 and is most likely due to the occurrence of extensive transesterification.

Figure 3.21. M_n (as measured by GPC) *vs.* equivalents *rac*-LA converted using ($Tp^{tBu,Me}$)Mg(BH_4) (**22**). Conditions: 6 mL THF, 70 °C, 60 minutes, [*rac*-LA]$_0$:[**3.8**]$_0$ = 40, 80, 120, 160, 200. PDI values are given in parentheses.



The reduced activity of **22** compared to **20** is a consequence of the reduced size of magnesium compared to calcium. Clearly the rate of initiation is slower for **22** than **20**, therefore the relative ratio with the rate of propagation would be expected to be higher for **22** than **20**. This could also explain similar behaviour shown by **3.8**. The MALDI-ToF mass spectrum of a PLA sample obtained using **22** is very similar to that seen previously showing a separation of integer polymer units of 72 *m/z*. This is also strong evidence for transesterification.

The overall performance of **22** is disappointing when compared to related heteroleptic magnesium complexes used for the ROP of LA. For example, the complex (BDI)MgN(^{i}PrO)(THF) (BDI = CH-[CMeN-(2,6-^{i}Pr$_2$C$_6$H$_3$)]$_2$), prepared by Coates in 2001, polymerised 200 equivalents of *rac*-LA at room temperature within 2 minutes. The PLA formed was atactic, and had a higher than expected M_n (64,000 g mol^{-1} compared to the expected value of 28,800).[66] Interestingly, the complex (BDI)MgN{N(SiMe$_3$)$_2$}(THF) (BDI = CH-[CMeN-(2,6-^{i}Pr$_2$C$_6$H$_3$)]$_2$) gave highly hetereotactic PLA (P_r = 0.90) in just 5 minutes

at room temperature.[3] The closely related complex (Tp^{tBu})Mg(OEt), originally prepared by Parkin[54], was shown by Chisholm to polymerise 200 equivalents of *rac*-LA at room temperature in 1 hour, although further details were not given.[4] One possible explanation for the contrastingly poor activity and control shown by **22** is the possible formation of aggregated species.

The activity of and selectivity of the borohydride complexes **17-BPh$_4$**, **18-BPh$_4$** and **20** is comparable to the best lanthanide systems reported (although the first report by Mountford and co-workers was only published in 2005).[26] For example, the complex Sm(O_2N_{py})(BH_4)(THF) (**3.4**) [$H_2O_2N_{py}$ = (2-C_5H_4N)CH_2NCH_2{2-HO-3,5-$C_6H_2{}^tBu_2$}$_2$] polymerised 200 equivalents of *rac*-LA at room temperature in THF, giving heterotactic PLA (P_r = 0.84), an M_n of 14,400 (expected 18,160) and a PDI of 1.51.[21]

3.5 Summary and Conclusions

The work presented in this chapter has developed cationic and charge neutral tetrahydroborates as a new type of ROP initiator for the Ae elements. Compounds **17-BPh$_4$** and **18-BPh$_4$** are also the first reported cationic main group tetrahydroborates. The new tetrahydroborates were readily prepared using protonolysis-substitution or salt elimination protocols and extensions to different ancillary ligands and the other Ae elements (e.g. strontium) should be readily achieved. The ROP performance for **17-BPh$_4$**, **18-BPh$_4$** and **20** equals or exceeds that found previously for initiators based on the heavier Ae elements. The heterotactic enrichment and molecular weight control achieved with **20** surpasses those of the best (L)Ln(BH_4) systems so far reported. These catalysts also show vast improvement compared to those presented in Chapter 2.

Additionally the first comparison between calcium and ytterbium for ROP has been made. Continuing work in the Mountford group is underway to further explain the differences in activity observed. Whilst it was not possible to conclusively prove a coordination-insertion mechanism in the case of the ROP of *rac*-LA, extended work with high resolution MALDI-ToF MS and DFT studies should provide further insight. These synthetic and ROP advances are expected to provide the impetus and basis for further progress in these areas.

3.6 References

1. M. Cushion and P. Mountford, *Chem. Commun.*, 2011, 2276-2278.
2. S. Harder, *Chem. Rev.*, 2010, 3852-3876.
3. M. H. Chisholm, J. C. Gallucci and K. Phomphrai, *Inorg. Chem.*, 2004, **43**, 6717-6725.
4. M. H. Chisholm, J. Gallucci and K. Phomphrai, *Chem. Commun.*, 2003, 48-49.
5. V. Poirier, T. Roisnel, J.-F. Carpentier and Y. Sarazin, *Dalton Trans.*, 2009, 9820-9827.
6. D. J. Darensbourg, W. Choi, O. Karroonnirun and N. Bhuvanesh, *Macromolecules*, 2008, **41**, 3493-3502.
7. Y. Sarazin, V. Poirier, T. Roisnel and J. F. Carpentier, *Eur. J. Inorg. Chem.*, 2010, **2010**, 3423-3428.
8. H.-Y. Chen, H.-Y. Tang and C.-C. Lin, *Polymer*, 2007, **48**, 2257-2262.
9. Z. Zhong, P. J. Dijkstra, C. Birg, M. Westerhausen and J. Feijen, *Macromolecules*, 2001, **34**, 3863-3868.
10. J. L. Espartero, I. Rashkov, S. M. Li, N. Manolova and M. Vert, *Macromolecules*, 1996, **29**, 3535-3539.
11. M. Visseaux and F. Bonnet, *Coord. Chem. Rev.*, 2011, 374-420.
12. S. Orimo, Y. Nakamori, J. Eliseo, A. Zuttel and C. Jensen, *Chem. Rev.*, 2007, 4111-4132.
13. S. Aldridge and A. Downs, *Chem. Rev.*, 2001, 3305-3365.
14. T. Marks and J. Kolb, *Chem. Rev.*, 1977, 263-293.
15. Y. Shen, Z. Shen, Y. Zhang and K. Yao, *Macromolecules*, 1996, **29**, 8289-8295.
16. Y. Nakayama, K. Sasaki, N. Watanabe, Z. Cai and T. Shiono, *Polymer*, 2009, **50**, 4788-4793.
17. I. Palard, M. Schappacher, B. Belloncle, A. Soum and S. Guillaume, *Chem. Eur. J.*, 2007, 1511-1521.
18. I. Palard, M. Schappacher, A. Soum and S. Guillaume, *Polym. Int.*, 2006, 1132-1137.
19. I. Palard, A. Soum and S. Guillaume, *Macromolecules*, 2005, 6888-6894.
20. S. M. Guillaume, M. Schappacher and A. Soum, *Macromolecules*, 2003, **36**, 54-60.
21. H. Dyer, S. Huijser, N. Susperregui, F. Bonnet, A. Schwarz, R. Duchateau, L. Maron and P. Mountford, *Organometallics*, 2010, 3602-3621.
22. J. Jenter, P. Roesky, N. Ajellal, S. Guillaume, N. Susperregui and L. Maron, *Chem. Eur. J.*, 2010, 4629-4638.

23. T. V. Mahrova, G. K. Fukin, A. V. Cherkasov, A. A. Trifonov, N. Ajellal and J.-F. Carpentier, *Inorg. Chem.*, 2009, **48**, 4258-4266.
24. N. Barros, P. Mountford, S. M. Guillaume and L. Maron, *Chem. Eur. J.*, 2008, **14**, 5507-5518.
25. G. G. Skvortsov, M. V. Yakovenko, P. M. Castro, G. K. Fukin, A. V. Cherkasov, J.-F. Carpentier and A. A. Trifonov, *Eur. J. Inorg. Chem.*, 2007, **2007**, 3260-3267.
26. F. Bonnet, A. R. Cowley and P. Mountford, *Inorg. Chem.*, 2005, **44**, 9046-9055.
27. D. Robert, M. Kondracka and J. Okuda, *Dalton Trans.*, 2008, 2667-2669.
28. F. Jaroschik, F. Bonnet, X. F. L. Goff, L. Ricard, F. Nief and M. Visseaux, *Dalton Trans.*, 2010, 6761-6766.
29. F. Bonnet, C. Violante, P. Roussel, A. Mortreux and M. Visseaux, *Chem. Commun.*, 2009, 3380-3382.
30. A. Valente, P. Zinck, A. Mortreux and M. Visseaux, *Macromol. Rap. Commun.*, 2009, 528-531.
31. S. Cendrowski-Guillaume, M. Lance, M. Nierlich and M. Ephritikhine, *Organometallics*, 2000, 3257-3259.
32. D. Chen, X. Zhang, S. Xu, H. Song and B. Wang, *Organometallics*, 2010, 3418-3430.
33. H. Schumann, M. Keitsch, J. Demtschuk and S. Muhle, *Z. Anorg. Allg. Chem.*, 1998, 1811-1818.
34. K. O. Saliu, G. H. Maunder, M. J. Ferguson, A. Sella and J. Takats, *Inorg. Chim. Acta*, 2009, **362**, 4616-4622.
35. V. Makhaev and A. Borisov, *Rus. J. Inorg. Chem.*, 1999, 1411-1413.
36. F. Jaroschik, F. Bonnet, X. F. L. Goff, L. Ricard, F. Nief and M. Visseaux, *Dalton Trans.*, 2010, **39**, 6761-6766.
37. Z. Dawoodi, M. L. H. Green, V. S. B. Mtetwa, C. K. Prout, A. J. Schultz, J. M. Williams and T. F. Koetzle, *J. Chem. Soc., Dalton Trans.*, 1986, 1629.
38. I. Palard, A. Soum and S. M. Guillaume, *Chem. Eur. J.*, 2004, **10**, 4054-4062.
39. M. Labet and W. Thielemans, *Chem. Soc. Rev.*, 2009, **38**, 3484-3504.
40. R. H. Platel, L. M. Hodgson and C. K. Williams, *Polym. Rev.*, 2008, **48**, 11-63.
41. O. Dechy-Cabaret, B. Martin-Vaca and D. Bourissou, *Chem. Rev.*, 2004, **104**, 6147-6176.
42. Y. Nakayama, K. Sasaki, N. Watanabe, Z. Cai and T. Shiono, *Polymer*, 2009, **50**, 4788-4793.
43. E. Hanecker, J. Moll and H. Noth, *Z. Naturforsch. B*, 1984, 424-430.

44. E. Lobkovskii, A. Chekhlov, M. Levicheva and L. Titov, *Koord. Khim.*, 1988, 543-550.
45. M. H. Chisholm, J. C. Gallucci, G. Yaman and T. Young, *Chem. Commun.*, 2009, 1828-1830.
46. R. Han and G. Parkin, *Inorg. Chem.*, 1992, **31**, 983-988.
47. R. Han and G. Parkin, *J. Am. Chem. Soc.*, 1990, **112**, 3662-3663.
48. A. Looney and G. Parkin, *Polyhedron*, 1990, **9**, 265 - 276.
49. R. Han and G. Parkin, *Organometallics*, 1991, **10**, 1010-1020.
50. J. L. Kisko, T. Fillebeen, T. Hascall and G. Parkin, *J. Organomet. Chem.*, 2000, **596**, 22-26.
51. M. H. Chisholm, J. C. Gallucci and G. Yaman, *Dalton Trans.*, 2009, 368-374.
52. R. Han and G. Parkin, *Inorg. Chem.*, 1993, **32**, 4968-4970.
53. M. H. Chisholm, J. C. Gallucci and G. Yaman, *Chem. Commun.*, 2006, 1872-1874.
54. R. Han and G. Parkin, *J. Am. Chem. Soc.*, 1992, **114**, 748-757.
55. S. Harder and J. Brettar, *Angew. Chem. Int. Ed.*, 2006, **45**, 3474-3478.
56. K. B. Aubrecht, M. A. Hillmyer and W. B. Tolman, *Macromolecules*, 2002, **35**, 644-650.
57. H. Ma and J. Okuda, *Macromolecules*, 2005, **38**, 2665.
58. L. Clark, M. G. Cushion, H. E. Dyer, A. D. Schwarz, R. Duchateau and P. Mountford, *Chem. Commun.*, 2010, **46**, 273-275.
59. C. A. Wheaton and P. G. Hayes, *Chem. Commun.*, 2010, **46**, 8404-8406.
60. L. Hasinoff, J. Takats, X. W. Zhang, A. H. Bond and R. D. Rogers, *J. Am. Chem. Soc.*, 1994, **116**, 8833-8834.
61. S. Harder, *Angew. Chem. Int. Ed.*, 2004, **43**, 2714-2718.
62. W. J. Evans and H. Katsumata, *Macromolecules*, 1994, **27**, 2330.
63. A. Duda and S. Penczek, *Macromolecules*, 1995, **28**, 5981-5992.
64. P. Dubois, N. Ropson, R. Jérôme and P. Teyssié, *Macromolecules*, 1996, **29**, 1965-1975.
65. W. M. Stevels, M. J. K. Ankone, P. J. Dijkstra and J. Feijen, *Macromolecules*, 1996, **29**, 8296-8303.
66. B. M. Chamberlain, M. Cheng, D. R. Moore, T. M. Ovitt, E. B. Lobkovsky and G. W. Coates, *J. Am. Chem. Soc.*, 2001, **123**, 3229-3238.

Chapter Four

Cationic Rare Earth alkyl and alkoxide complexes and their use in the immortal ROP of *rac*-lactide

4.0 Overview

This Chapter will provide an introduction into rare earth complexes (with an emphasis on cationic complexes) and their application towards polymerisation. An overview of the synthesis and characterisation of rare earth complexes will be presented. Their solid state structures and solution behaviour will be discussed, in conjunction with their application to the ring opening polymerisation of cyclic esters. An introduction to immortal ROP will also be given. Comparison of the newly reported complexes and related complexes will be undertaken within the context of the solid state structures and the ROP activity and selectivity observed. Some of this work has recently been published.[1]

4.1 Introduction

Until recently the organometallic chemistry of the rare earth metals has been underdeveloped in comparison to the later transition metals, and has been largely dominated by the ubiquitous cyclopentadienyl ligand. The recent renewal in interest in post-metallocene organometallic complexes of the rare earth metals is in part related to recent reports describing their use as pre-catalysts for olefin polymerisation[2-5] and well defined initiators for the polymerisation of cyclic esters.[6-13]

One of the major contributing factors to the relative lack of organometallic rare earth chemistry is the synthetic challenge associated with the preparation of monomeric, well-defined complexes. Rare earth metals are highly Lewis acidic and therefore have a tendency to form bridged, oligomeric structures.[14] It is not a coincidence that this Lewis acidity is also the driving force behind growing interest in the use of rare earth complexes in polymerisation catalysis. Additionally rare earth metal complexes are prone to ligand redistribution reactions and also have a tendency to form 'ate' complexes in the presence of alkali metal halides.[11]

A successful supporting ligand must fulfil a number of criteria. Firstly, the ligand must possess a degree of steric bulk sufficient to stabilise the formation of monomeric complexes, whilst the remaining coordination sphere of the metal must be large enough to conduct substrate coordination and subsequent transformations necessary for catalytic activity. Furthermore, the supporting ligand should not present any competing sites of reactivity. Aside from the cyclopentadienyl ligand and its substituted derivatives, the most commonly used ligands in post-metallocene rare earth chemistry possess 'hard' O or N based polydentate ligands.

4.1.1 Neutral Rare Earth Complexes

As mentioned, early organometallic rare earth chemistry was largely focussed around the cyclopentadienyl ligand framework. The first organometallic rare earth complexes, Cp_3M (M = Sc or Y) were prepared by Wilkinson and Birmingham in 1956 by the reaction between the trivalent metal chloride and NaCp in THF.[15] Despite this early discovery, organometallic rare earth chemistry remained relatively unexplored until the 1970s, by this time the necessary advances in analytical techniques and experimental methods had been made to prepare and study a wider range of these extremely air and moisture sensitive complexes.[16] The subsequent fast expansion of the preparation of bis(cyclopentadienyl) rare earth complexes has been the subject of excellent reviews[16-18] and will not be extensively discussed here, other than highlighting a few key examples.

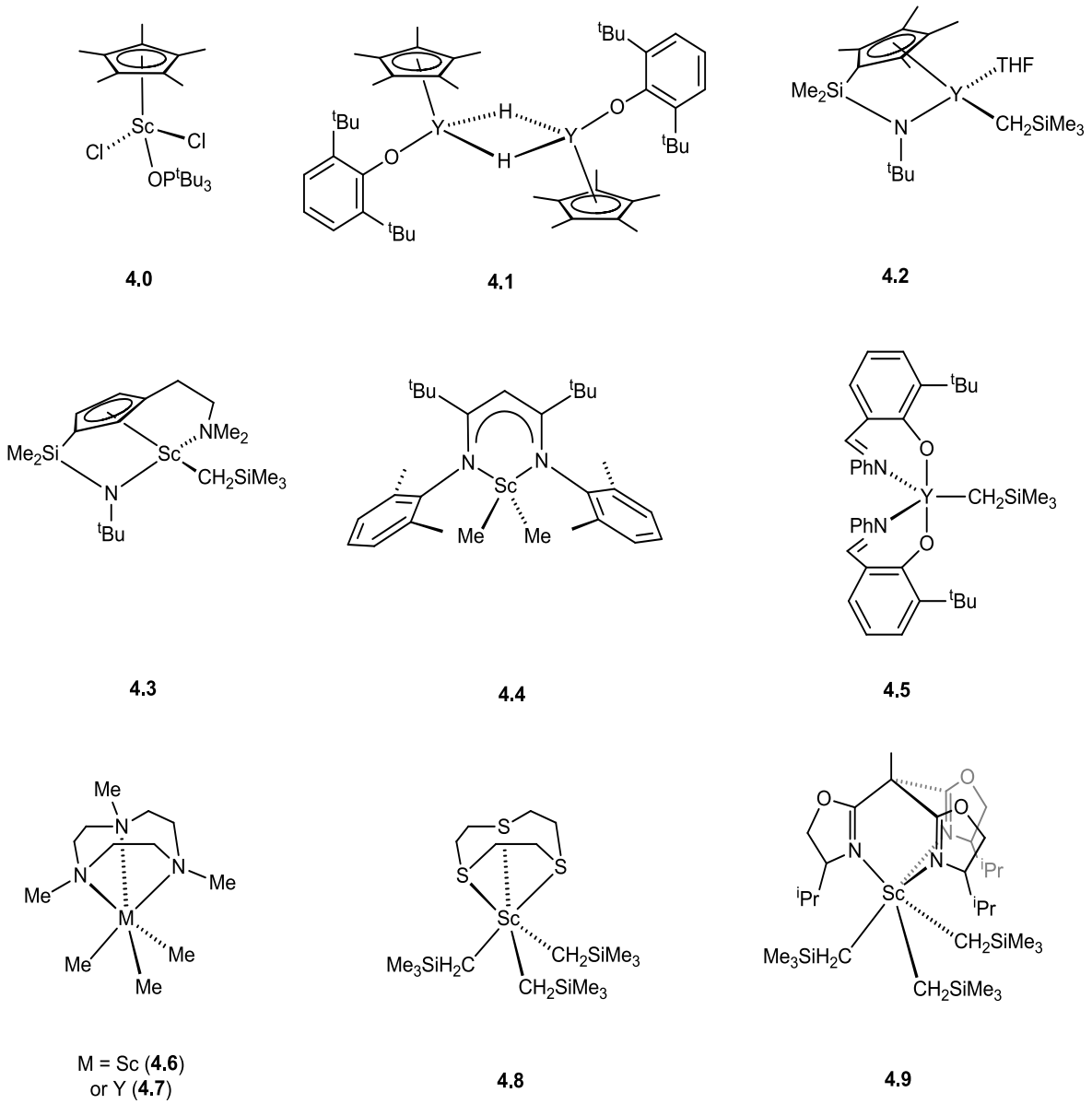
In 1970 Coutts and co-workers reported the first example of a scandium bis(cyclopentadienyl) complex, $[Cp_2Sc(\mu\text{-}Cl)]_2$, prepared by the reaction between the $ScCl_3$ and NaCp.[19] In subsequent work by Atwood and Smith the solid state structure was obtained showing this complex to be dimeric.[20, 21] Manzer later reported the solid state structure of the monomeric $Cp_2ScCl(THF)$[22], presumably the presence of a bound THF molecule stabilises the monomeric structure. Later work reported the preparation of the yttrium analogues $[Cp_2Y(\mu\text{-}Cl)]_2$[23] and $Cp_2YCl(THF)$[24] by similar synthetic methods. Reaction of these complexes with alkali metal and Grignard reagents has led to a large number of scandium and yttrium bis(cyclopentadienyl) derivatives including alkyls, aluminates, alkoxides and borohydrides.[16-18]

In comparison to the extensive research carried out on bis(cyclopentadienyl) rare earth complexes and their derivatives, there has been relatively little reported work on mono(cyclopentadienyl) rare earth complexes. This area has been a subject of an extensive recent review[25] and this thesis only serves to highlight noteworthy examples. The main reason for the relatively few known mono(cyclopentadienyl) rare earth complexes is the increased difficulty in their handling and preparation, owing much to a more exposed metal centre prone to Lewis base complexation and increased air and moisture sensitivity.

Piers *et al*. showed that mono(cyclopentadienyl) such as $Cp^*Sc(OP^tBu_3)Cl_2$ (**4.0** in Figure 4.0) can be synthesised with the incorporation of another bulky ligand.[26] Alkylation of **4.0** with MeLi yields the compounds $Cp^*Sc(OP^tBu_3)Me_2$ which, when treated with $BAr^F{}_3$, gave the ion pair $[Cp^*Sc(OP^tBu_3)Me][MeBAr^F{}_3]$.[26] The dimeric hydride complex $[Cp^*Y(OAr)(\mu\text{-}H)]_2$ (**4.1**) was prepared by hydrogenation of the parent alkyl complex

$Cp^*Y(OAr)(CH_2SiMe_3)$ and demonstrated reactivity with a range of unsaturated substrates.[27]

Figure 4.0. Rare earth complexes supported by cyclopentadienyl and post-metallocene ligands



4.0 **4.1** **4.2**

4.3 **4.4** **4.5**

M = Sc (**4.6**) or Y (**4.7**) **4.8** **4.9**

Another approach used to saturate the metal coordination sphere is the use of linked donor-cyclopentadienyl ligands. The most commonly used donor arms are amide groups,[25] and these constrained geometry systems were originally developed for Group 4 metals. The first rare earth constrained geometry systems were prepared by Bercaw[28] in 1994 and subsequent work by Okuda focused on the preparation of a family of related catalysts.[29-32] An example is the complex $(C_5Me_4SiMe_2NCMe_2NC^tBu)Y(CH_2SiMe_3)(THF)$ (**4.2**) which was shown to be a good catalyst for the polymerisation of ethylene and styrene as well as hydrosilylation.[29-32] Further work by Piers *et al*. led to the development of $\{C_5H_3$(3-

$CH_2CH_2NMe_2)SiMe_2N^tBu\}Sc(CH_2SiMe_3)$ (**4.3**),[33] which is also an active ethylene polymerisation catalyst.

The past 10-15 years have seen a rapid increase in the number and variety of non-cyclopentadienyl based ligands used to support rare earth metals. This area has been the subject of a number of recent reviews.[5, 34, 35] Good examples are the *β*-diketiminate scandium complex (**4.4**)[36] and $Y\{O\text{-}2,6\text{-}C_6H_3(^tBu)CHNPh\}_2(CH_2SiMe_3)$[37] (**4.5**), both prepared by Piers *et al.* The former was shown be highly active in the polymerisation of ethylene and the latter was active for the ROP of ε-CL.

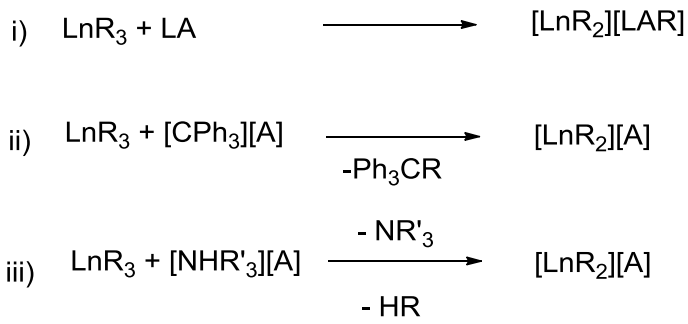
In 1997 Bercaw *et al.* reported the synthesis of the organoscandium and organoyttrium complexes $M(Me_3[9]aneN_3)Me_3$ (M = Sc (**4.6**) or Y(**4.7**)).[38] The reactivity of these complexes towards small, unsaturated molecules was investigated and the scandium complex was found to be proficient for the polymerisation of ethylene in the presence of a co-catalyst. Recently in the Mountford group the bulky neosilyl homologues $M(Me_3[9]aneN_3)(CH_2SiMe_3)_3$ (M = Sc or Y) were prepared and the scandium complex was found to be a highly active precatalyst for ethylene polymerisation.[39, 40] The solid state structure of the yttrium catalyst was subsequently reported by Hessen.[41] The first rare earth organometallic complex supported by an all-sulfur donor ligand, $Sc([9]aneS_3)(CH_2SiMe_3)_3$ (**4.8**), was recently prepared by Mountford *et al.*[42] This is the sulfur analogue of the $Me_3[9]aneN_3$ complex **4.6** and was also a highly active precatalyst for the polymerisation of ethylene. The neutral '*tris*-ox' scandium alkyl complex (**4.9**) was recently reported by Gade *et al.*[3] and was shown to be a highly active pre-catalyst for the stereospecific polymerisation of 1-hexene.

4.1.2 Cationic Rare Earth Complexes

The chemistry of the rare earth metals is dominated by neutral and anionic species.[16] More recently, however, thanks to the development of post-metallocene rare earth precatalysts for the polymerisation of olefins, cationic species have been receiving increasing interest.[2, 43] In general, when used as catalysts for the polymerisation of olefins, cationic rare earth complexes are generated in *situ* and are not isolated. Due to the high Lewis acidity of the cationic rare earth metal centres, coupled with the presence of nucleophilic alkyl groups these complexes are synthetically challenging to prepare and isolate.

Cationic rare earth alkyl complexes are most commonly prepared *via* one of three main synthetic methods (Equation 4.0): i) alkyl group abstraction by strong Lewis acids; ii) alkyl

group abstraction by trityl cation; iii) alkyl group protonation by Brønsted acids, the conjugate bases of which are usually poor Lewis bases.



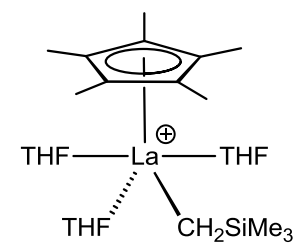
Ln = rare earth metal; LA = Lewis Acid; A = anion, R = hydrocarbyl

Equation 4.0

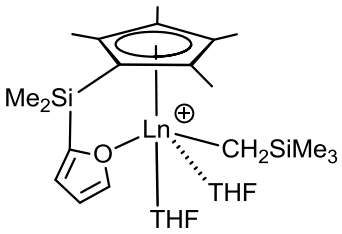
The first example of a cationic rare earth complex, $[Cp^*La\{CH(SiMe_3)_2\}(\mu\text{-}Ph)_2BPh_2]$, was reported by Schaverien in 1992.[44] This was synthesised by the protonolysis reaction between $Cp^*La\{CH(SiMe_3)_2\}_2$ and $[NHMe_2Ph][BPh_4]$ in good yield. The addition of three equivalents of THF to a toluene solution of this complex led to irreversible displacement of the BPh_4 anion and the formation of $[Cp^*La\{CH(SiMe_3)_2\}(THF)_3][BPh_4]$ (**4.10** in Figure 4.1).[44] Okuda *et al.* later reported the *in situ* synthesis of the furyl-substituted cyclopentadienyl complexes $[\{\eta^5\text{:}\eta^1\text{-}C_5Me_4SiMe_2(C_4H_3O\text{-}2)\}Ln(CH_2SiMe_3)(THF)_x]$-$[BPh_3(CH_2SiMe_3)]$ (Ln = Y (**4.11**) or Lu (**4.12**)).[45] As mentioned previously Piers *et al.* prepared the complex $[Cp^*Sc(OP^tBu_3)Me][MeBAr^F{}_3]$ (**4.13**) by the reaction of $Cp^*Sc(OP^tBu_3)Me_2$ with $BAr^F{}_3$.[26]

Evans reported in 1990 that oxidation of the divalent complex $Cp^*{}_2Sm(THF)_2$ with $AgBPh_4$ in THF led to the formation of the trivalent samarium cationic complex $[Cp^*{}_2Sm(THF)_2][BPh_4]$ (**4.14**)[46] whilst performing the reaction in toluene formed $[Cp^*{}_2Sm\}(\mu\text{-}Ph)_2BPh_2]$.[47] A unique example of an yttrium mono(cyclopentadienyl) dication, $[Y(\eta^5C_5Me_4SiMe_3)(THF)_4][BPh_4]_2$ (**4.15**), was synthesised by Okuda *et al*. by reaction of $Y(\eta^5C_5Me_4SiMe_3)_4(\mu\text{-}H)_4(\mu_3\text{-}H)_4(THF)_2$ with an excess of $[NEt_3H][BPh_4]$ in THF.[48] Additionally, Arnold and co-workers have recently reported the *in situ* generation of the cationic Sm ion pair $[Cp^*Sm\{\eta^3\text{-}ArNC(Me)CHC(Me)NAr\}(\mu\text{-}Me)BAr^F{}_3]$ (**4.16**)[49] and Berg *et al.* generated the yttrium complex, $[Y(MAC)(CH_2SiMe_3)][BAr^F{}_3(CH_2SiMe_3)]$ (MAC = deprotonated aza-18-crown-6) (**4.17**) *in situ*.[50]

Figure 4.1. Cationic rare earth complexes supported by cyclopentadienyl and post-metallocene ligands (anion(s) = BPh_4^- unless otherwise specified).

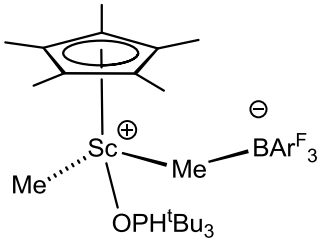


4.10

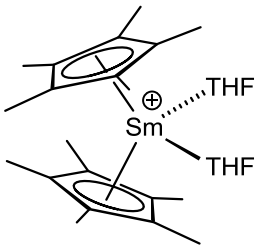


Anion = $BPh_3CH_2SiMe_3^-$

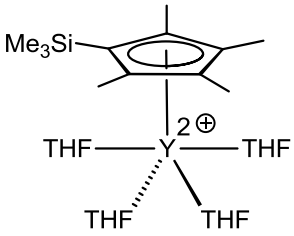
M = Y (**4.11**) or Lu (**4.12**)



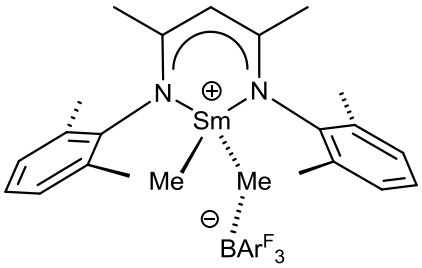
4.13



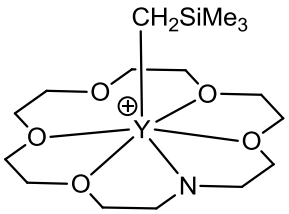
4.14



4.15

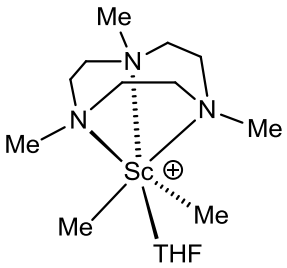


4.16



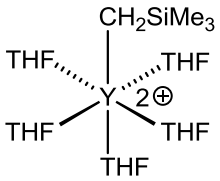
Anion = $BAr^F_3CH_2SiMe_3^-$

4.17



Anion = $BAr^F_4^-$

4.18



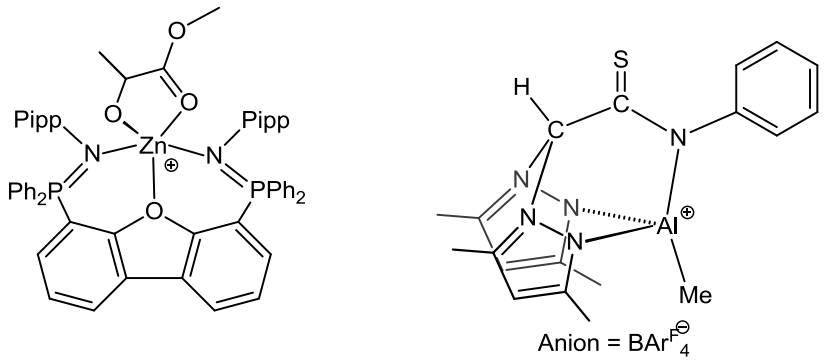
4.19

Bercaw *et al*. prepared the scandium monocationic complex $[Sc(Me_3[9]aneN_3)Me_2(THF)][BAr^F_4]$ (**4.18**)[38] by reaction of $Sc(Me_3[9]aneN_3)Me_3$ with $[PhNMe_2H][BAr^F_4]$ in THF, however the Sc-Me resonance of the cation was not detected and in the absence of a solid state structure it was postulated that a liquid lattice had formed.[38, 43] Okuda *et al.* also reported that treatment of a THF solution of the yttrium tris(alkyl)complex $[Y(CH_2SiMe_3)_3(THF)_2]$ with 2 equivalents of $[NEt_3H][BPh_4]$ or $[PhNMe_2H][BPh_4]$ gave the dicationic alkyl complex $[Y(CH_2SiMe_3)(THF)_5]_2[BPh_4]$ (**4.19**).[51]

4.1.3 Cationic ROP Catalysts

Rare earth mono- and di-cationic alkyl complexes are well-known Ziegler-type catalysts for olefin polymerisation.[43] However, despite extensive studies of neutral rare earth complexes for the ROP of LA,[11, 52] there are only a handful of reported cationic ROP catalysts (for any metal)[1, 53-58], although this is a rapidly expanding field. The cationic zinc lactate complex **4.20** (Figure 4.2) was reported by Hayes and Wheaton in 2010.[58] **4.20** is a highly active initiator for the ROP of *rac*-LA at ambient temperature in CH_2Cl_2, giving 90 % conversion of 200 equivalents in 50 minutes and slightly heterotactically enriched polymer (P_r = 0.63).[58]

Figure 4.2. Cationic ROP catalysts (anion(s) = BPh_4 unless otherwise specified).



4.20 **4.21**

18-BPh$_4$

In 2011 Otero *et al.* prepared the heteroscorpionate complex [HC(Me_2pz)HCCSN(Ph)Al-Me][BPh_4] (**4.21**),[56] which proved to be a very well controlled (but low activity) initiator for the ROP of ε-CL. PCL with an observed M_n of 19,950 g mol^{-1} (expected 24,900) and a narrow PDI of 1.26 was produced.[56]

The complex [Ca{HC(Me_2pz)$_3$}(BH_4)(THF)$_2$][BPh_4] (**18-BPh$_4$**)[55] was discussed in the previous chapter and was shown to be a good initiator for the ROP of ε-CL and *rac*-LA.

Very recently Carpentier *et al.* reported a family of base-free cationic Ae complexes [{2-[(1,4,7,10-tetraoxa-13-azacyclopentadecan-13-yl)methyl]-4,6-di-*tert*-butylphenol}M][X] (M = Zn (**4.22**); Mg (**4.23**); Ca (**4.24**); Sr (**4.25**) or Ba, (**4.26**) and X = $H_2N[BAr^F{}_3]_2$).[53, 59] These were shown to be very active in the presence of chain transfer reagents (^{i}PrOH, BnOH and in some cases $BnNH_2$) for the immortal ROP of *L*-LA, producing polymers with narrow to moderate PDIs and M_n values close to those expected.[53, 59]

In principle, two ROP mechanisms for cationic complexes can be envisaged: classical coordination-insertion and activated chain end (ACE).[53, 60] ACE differs from coordination-insertion in that the nucleophilic group attached to the metal centre (the initiating group in coordination-insertion) is not transferred to the monomer. Instead, propagation occurs through an activated (cationic) ring-opened monomer unit bound to the metal centre.[60] The complexes **4.20** and **18-BPh$_4$** are both thought to facilitate the ROP of LA by a coordination-insertion mechanism,[55, 58] whereas **4.21** has been postulated to operate by an ACE mechanism.[56] The complexes **4.22-4.26** (with no nucleophilic metal-bound group available for coordination-insertion) were reported to operate by an activated monomer mechanism (this is described in Section 4.1.4).[53, 59]

4.1.4 Immortal ROP

ROP reactions catalysed by metal complexes usually proceed in a 'living' fashion (as outlined in the introduction); there are ideally as many growing polymer chains as there are initiating groups. Whilst often successful, living polymerisation does have disadvantages, namely low catalytic productivity and potentially large contamination of the polymer with catalyst residues.[54]

The so-called 'immortal' ROP (*i*-ROP) provides an alternative to classical living ROP. This process involves a two component system, a catalyst and an external nucleophile that acts both as an initiator and a chain transfer agent (CTA). In *i*-ROP the number of growing polymer chains exceeds the number of initiating groups presented by the catalyst. This technique was first introduced by Inoue *et al*. in the 1980s for the ROP of epoxides and cyclic esters with aluminium porphyrin alkoxide catalysts in conjunction with alcohol CTAs.[61] Since then catalyst systems based on other metals (e.g. Mg, Ca, Fe, Zn, Sn and Y) have been successfully studied for *i*-ROP.[1, 53, 59, 62-66]

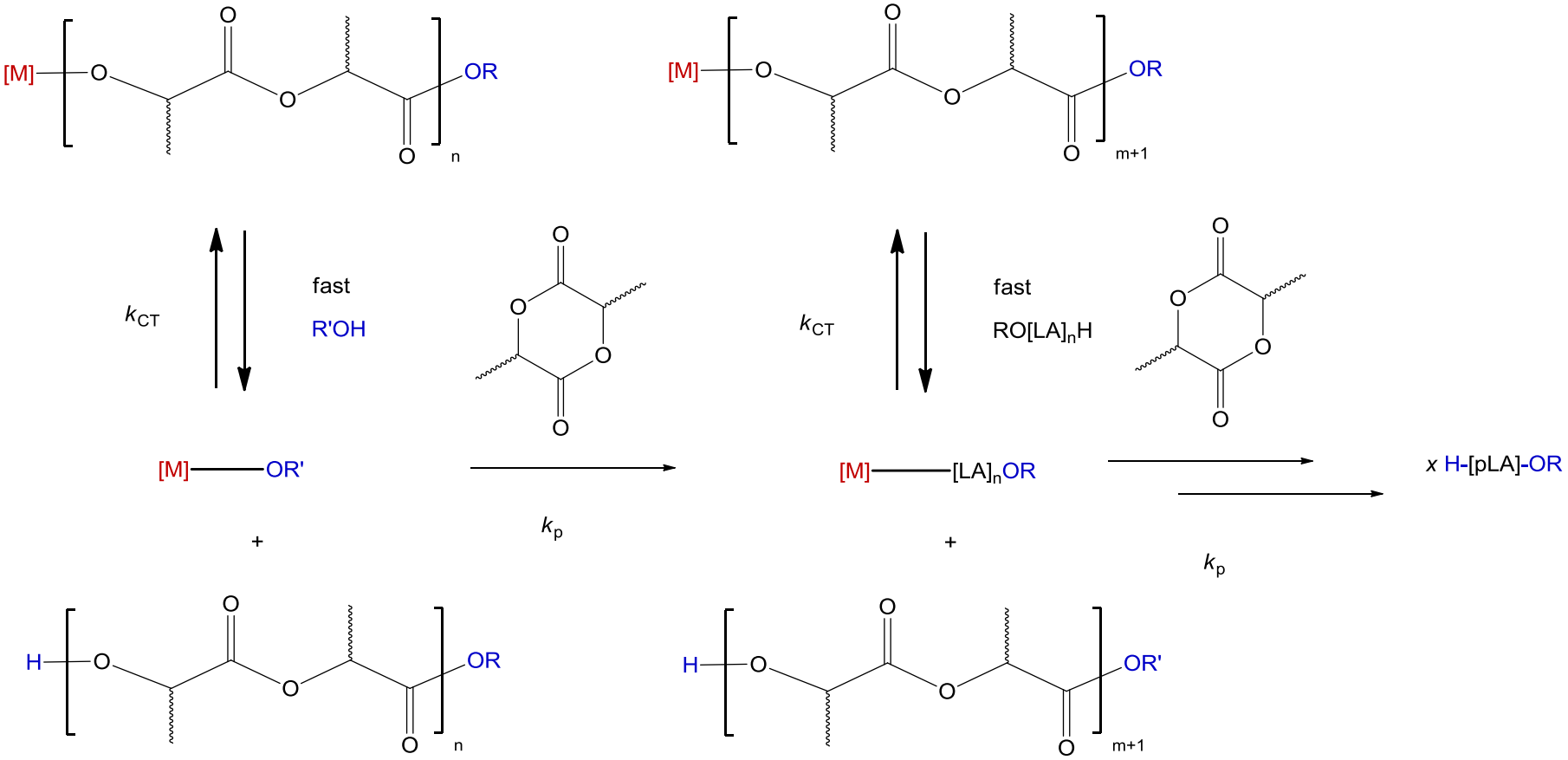
As is necessary for classical living polymerisation, for *i*-ROP to occur the rate of initiation must proceed faster than the rate of propagation and irreversible termination reactions (i.e. the formation of cyclic polymer units) must be minimal. Additionally, the rate of reversible

chain transfer reactions must be greater than the rate of propagation, leading to polymers with narrow PDIs.[54] Two mechanisms have been documented in metal initiated *i*-ROP: one based on coordination-insertion (Scheme 4.0) and a second known as an activated monomer mechanism (Scheme 4.1).

In the coordination-insertion mechanism, most typically involving a catalyst of the type (L)M-Nu (Nu = initiating group such as alkoxide, amide or borohydride), a preliminary step exists resulting in the *in situ* formation of the initiating species (L)M-OR (except where Nu and OR are homologous) occurs.[54] This newly formed species undergoes coordination-insertion of the first monomer unit, leading to the propagating species (L)M-[PLA]-OR.

The growing polymer chain undergoes rapid exchange with other protic species, initially CTA molecules, introduced in excess in the reaction medium that rapidly convert to "dormant" (metal free) polymer chains. Thus, species active for propagation for some time do reversibly convert back and forth to inactive species. This rapid growing/dormant interconversion cycle continues over the entire course of the polymerisation process. Any active species bearing a (L)M–O(alkoxide) bond can bring about the propagation and any HO-terminated polymer can behave as the CTA. The rate of this transfer process is the decisive factor in molecular weight control. Finally, termination of living (L)M-[PLA]-OR species gives the H-[PLA]-OR polymer.

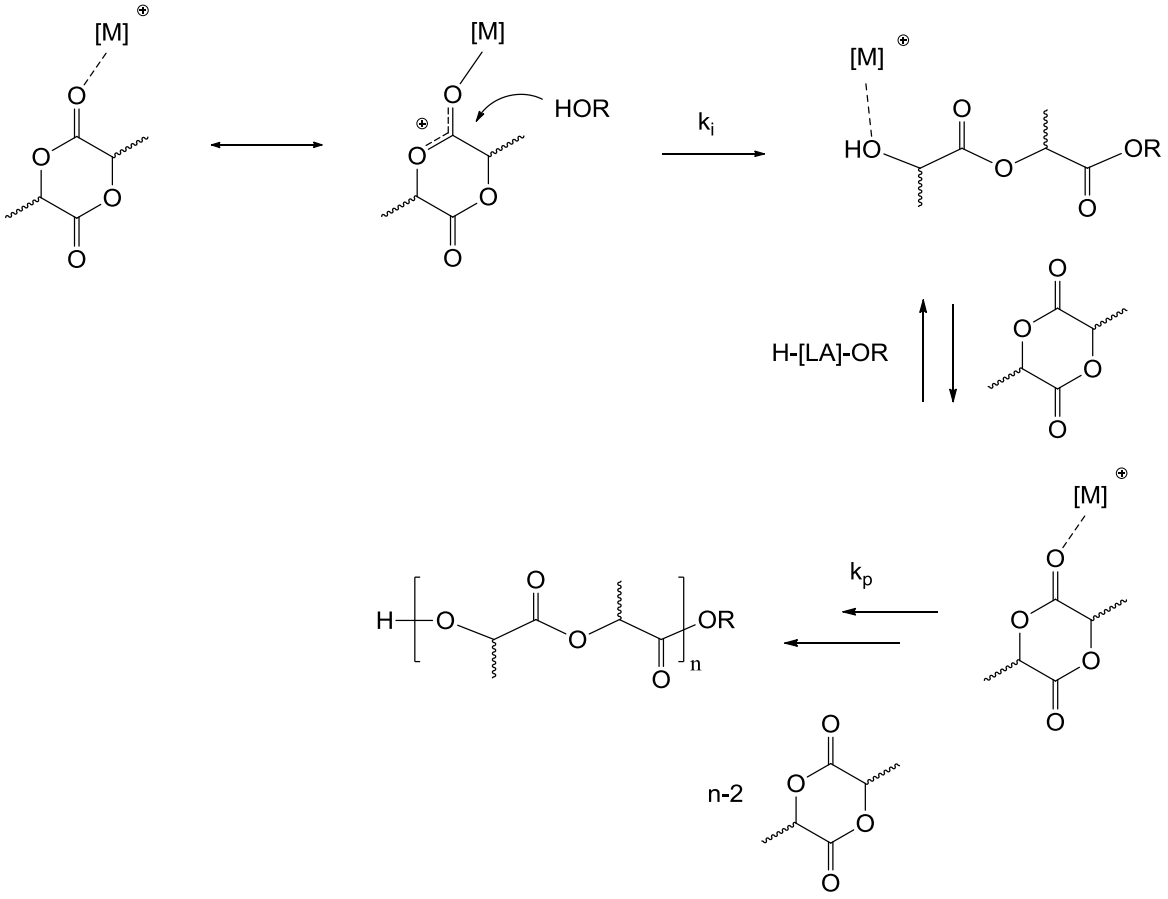
Scheme 4.0. The coordination-insertion mechanism for the *i*-ROP of LA.[54]



R'OH = alcohol or another growing chain RO[LA]$_m$H

On the other hand, *i*-ROP systems commonly based on simple Lewis acidic metal salts (e.g. triflates) usually proceed by the aforementioned activated monomer mechanism (depicted in Scheme 4.1). The Lewis acidic metal center first activates the monomer upon coordination to its carbonyl oxygen. The external protic nucleophilic additive, commonly an alcohol, then initiates the polymerisation upon attack of the electrophilic carbon atom of the carbonyl group, which results in the ring-opening of the monomer *via* oxygen-acyl bond cleavage.

Scheme 4.1. The activated monomer mechanism for the *i*-ROP of LA.[54]



The CTA and hydroxy end-capped macromolecules H-[PLA]-OR eventually produced during the process all behave as external nucleophiles. These hydroxy end-capped polymers are involved in exchange and/or transfer reaction equilibria as "active" (coordinated to the metal center) and "dormant" species. Again, as long as these transfer equilibria are rapid enough compared to the initiation and subsequent propagation steps, the *i*-ROP remains controlled. This implies that all the aforementioned end-capped polymer chains exhibit the same reactivity, so that they are all progressively transformed into higher molar weight products by iterative incorporation of monomer units.

This activated monomer mechanism differs from the coordination-insertion mechanism in that the nucleophile involved in the first ring-opening event is an external molecule, independent from the catalyst, whilst in coordination-insertion the nucleophile is inherent to the active catalyst (starting as a bound initiating group).[54] Accordingly, in both mechanisms the M_n is directly proportional to the monomer-to-CTA ratio. Despite the existence of the previously mentioned neutral systems for *i*-ROP, to date only a handful of examples for cationic systems have been reported.[1, 53, 59]

4.2 Synthesis of mono- and di-cationic yttrium alkyl and alkoxide complexes.

The monocationic complexes $Y\{HC(Me_2pz)_3\}(CH_2SiMe_3)_2(THF)][BAr^F{}_4]$, $[Y\{HC(Me_2pz)_3\}(O^iPr)_2(THF)][BAr^F{}_4]$, $[Y(Me_3[9]aneN_3)(CH_2SiMe_3)_2(THF)][BAr^F{}_4]$ were previously synthesised in the Mountford group.[67, 68] These were all shown to be active catalysts for the ROP of ε-CL in THF at RT, producing PCL with moderate-to-broad PDIs and M_n values reasonably close to that expected.[67] Inspired by this and the relatively small number of cationic ROP catalysts, it was decided to synthesise a related family of cationic yttrium catalysts and assess any potential activity towards the ROP of LA.

Scheme 4.2 summarises the reactions of $Y(CH_2SiMe_3)_3(THF)_2$ with one or two equivalents of $[NEt_3H][BPh_4]$ and $HC(Me_2pz)_3$ and subsequent reactions with ^{i}PrOH. The reaction of $Y(CH_2SiMe_3)_3(THF)_2$ with one or two equivalents of $[NEt_3H][BPh_4]$ followed by the addition of $HC(Me_2pz)_3$ in THF at -78 ^{o}C proceeded smoothly, giving the alkyl cations $[Y\{HC(Me_2pz)_3\}(CH_2SiMe_3)_2(THF)][BPh_4]$ (**23-BPh$_4$**) and $[Y\{HC(Me_2pz)_3\}(CH_2SiMe_3)(THF)_3][BPh_4]_2$ (**25-[BPh$_4$]$_2$**) in 78 and 77 % recrystallised yields respectively. **23-BPh$_4$** and **25-[BPh$_4$]$_2$** reacted with two and one equivalents of ^{i}PrOH respectively at room temperature in CH_2Cl_2 to give the isopropoxide cations $[Y\{HC(Me_2pz)_3\}(O^iPr)_2(THF)][BPh_4]$ (**24-BPh$_4$**) and $[Y\{HC(Me_2pz)_3\}(O^iPr)(THF)_3][BPh_4]_2$ (**26-[BPh$_4$]$_2$**) in 79 and 67 % recrystallised yields.

The NMR spectra of **23-BPh$_4$**, **24-BPh$_4$**, **25-[BPh$_4$]$_2$** and **26-[BPh$_4$]$_2$** are consistent with the structures proposed in Scheme 4.2. The monocationic complexes **23-BPh$_4$** and **24-BPh$_4$** have an approximate octahedral geometry around the yttrium centre, whereas the dicationic complexes **25-[BPh$_4$]$_2$** and **26-[BPh$_4$]$_2$** have an approximate pentagonal bipyramidal geometry around the yttrium centre (this can also be seen in the solid state structure of **26^{2+}** shown in Figure 4.3). In all cases, two sets of resonances (relative ratio 1:1) for Me_2pz groups were observed, consistent with a κ^3*N*-$HC(Me_2pz)_3$ ligand.

The alkyl complexes **23-BPh$_4$** and **25-[BPh$_4$]$_2$** both showed a sharp singlet ($\delta(^1H)$ = -0.15; $\delta(^{13}C)$ = 4.1 and $\delta(^1H)$ = -0.19; $\delta(^{13}C)$ = 3.9 ppm respectively) and a doublet ($\delta(^1H)$ = -0.43

(J_{HY} = 2.8 Hz); δ(^{13}C) = 38.7 (J_{CY} = 49 Hz) and δ(^{1}H) = -0.19 (J_{HY} = 2.9 Hz); δ(^{13}C) = 47.8 (J_{CY} = 40 Hz) ppm) in CD_2Cl_2, corresponding to the $SiMe_3$ and CH_2 resonances respectively. The other notable differences between the NMR spectra of the two complexes are the difference in relative intensities for the bound THF molecules and non-coordinating BPh_4^- anions. Similar differences can be seen between the NMR spectra of the mono- and di-cationic alkoxide complexes **23-BPh$_4$** and **25-[BPh$_4$]$_2$**.

Scheme 4.2. Synthesis of new HC(Me$_2$pz)$_3$ supported mono- and di-cationic yttrium alkyl and alkoxide complexes. BPh_4^- anions are omitted.

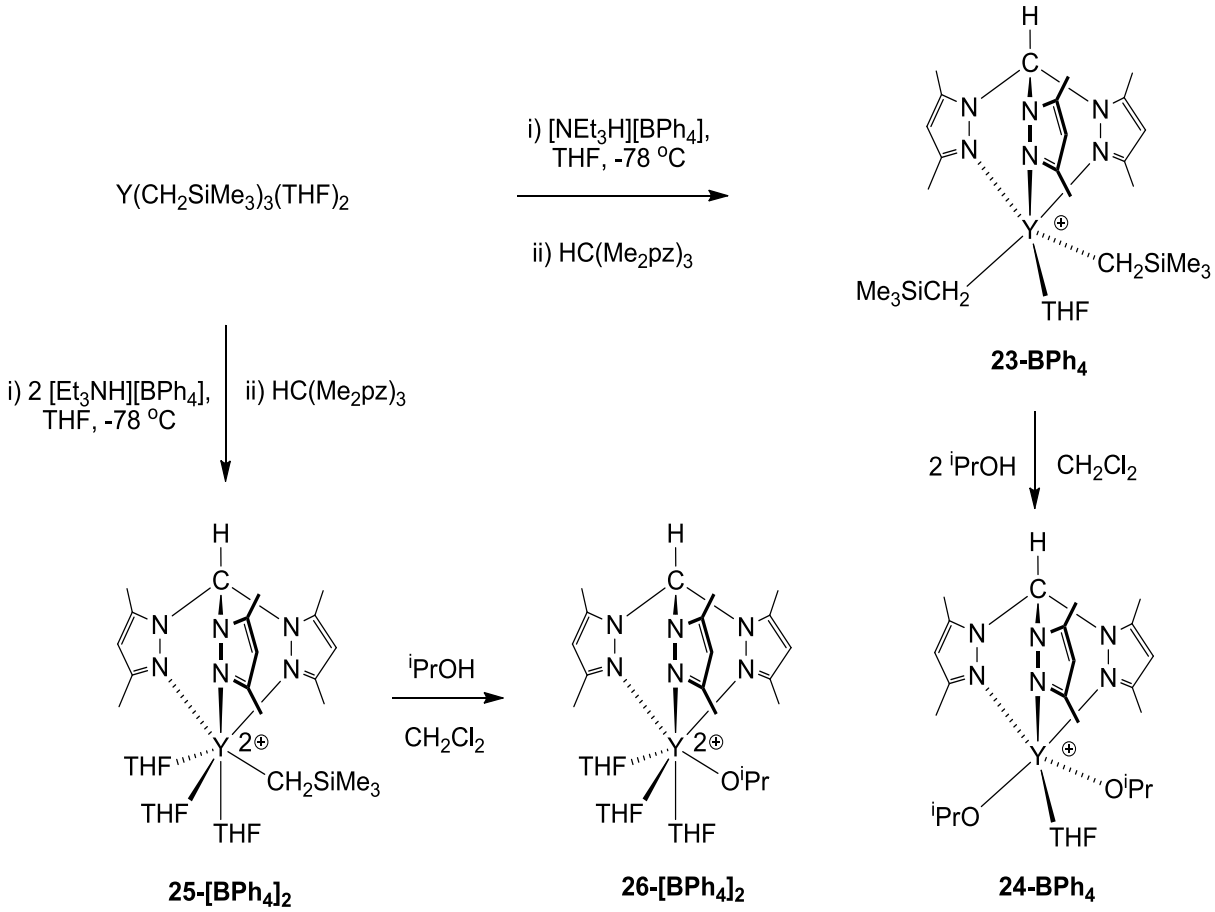


Figure 4.3. Molecular structure of $[Y\{HC(Me_2pz)_3\}(O^iPr)(THF)_3]^{2+}$ (**26**$^{2+}$). BPh_4^- anions omitted.

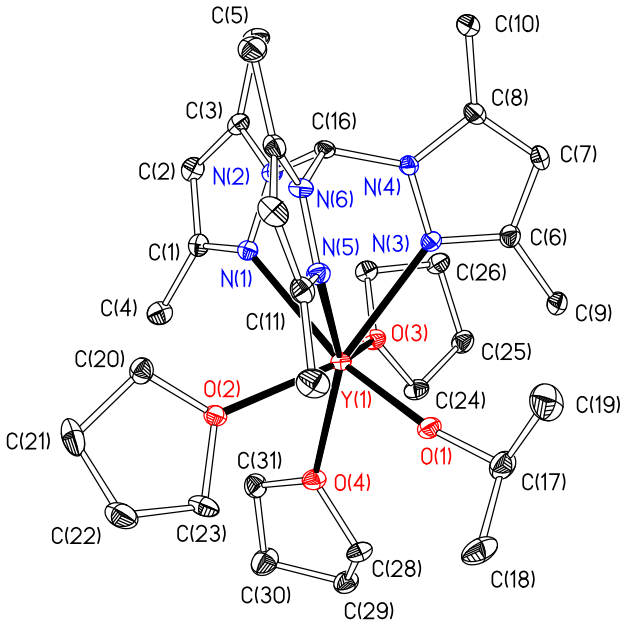


Table 3.0. Selected bond distances (Å) and angles (°) for $[Y\{HC(Me_2pz)_3\}(O^iPr)(THF)_3][BPh_4]_2$ (**26-[BPh$_4$]$_2$**).

Y(1)-O(1)	1.998(3)	O(1)-Y(1)-N(1)	161.68(10)
Y(1)-O(2)	2.391(3)	O(1)-Y(1)-N(3)	90.49(11)
Y(1)-O(3)	2.438(3)	O(1)-Y(1)-N(5)	91.04(11)
Y(1)-O(4)	2.416(3)	O(1)-Y(1)-O(2)	103.55(10)
Y(1)-N(1)	2.519(3)	O(1)-Y(1)-O(3)	110.26(11)
Y(1)-N(3)	2.500(3)	O(1)-Y(1)-O(4)	85.41(10)
Y(1)-N(5)	2.501(3)		

$[Y\{HC(Me_2pz)_3\}(O^iPr)(THF)_3][BPh_4]_2$ (**26-[BPh$_4$]$_2$**) has a distorted pentagonal bipyramidal geometry with the central 7-coordinate yttrium dication supported by a κ^3*N* bound $HC(Me_2pz)_3$ ligand. The Y-N(1) and Y-O(1) bonds occupy apical positions, with all other Y-bonded groups occupying equatorial positions. This is evident from the Y-N(1) bond length (2.519(3) Å), which is notably longer than the Y-N(3) or Y-N(5) bond lengths (2.500(3) and 2.501(3) Å respectively). The Y-O(1) bond distance of 1.998(3) Å is very close to the Y-alkoxide bond length of 1.9990(16) Å found in Okuda's

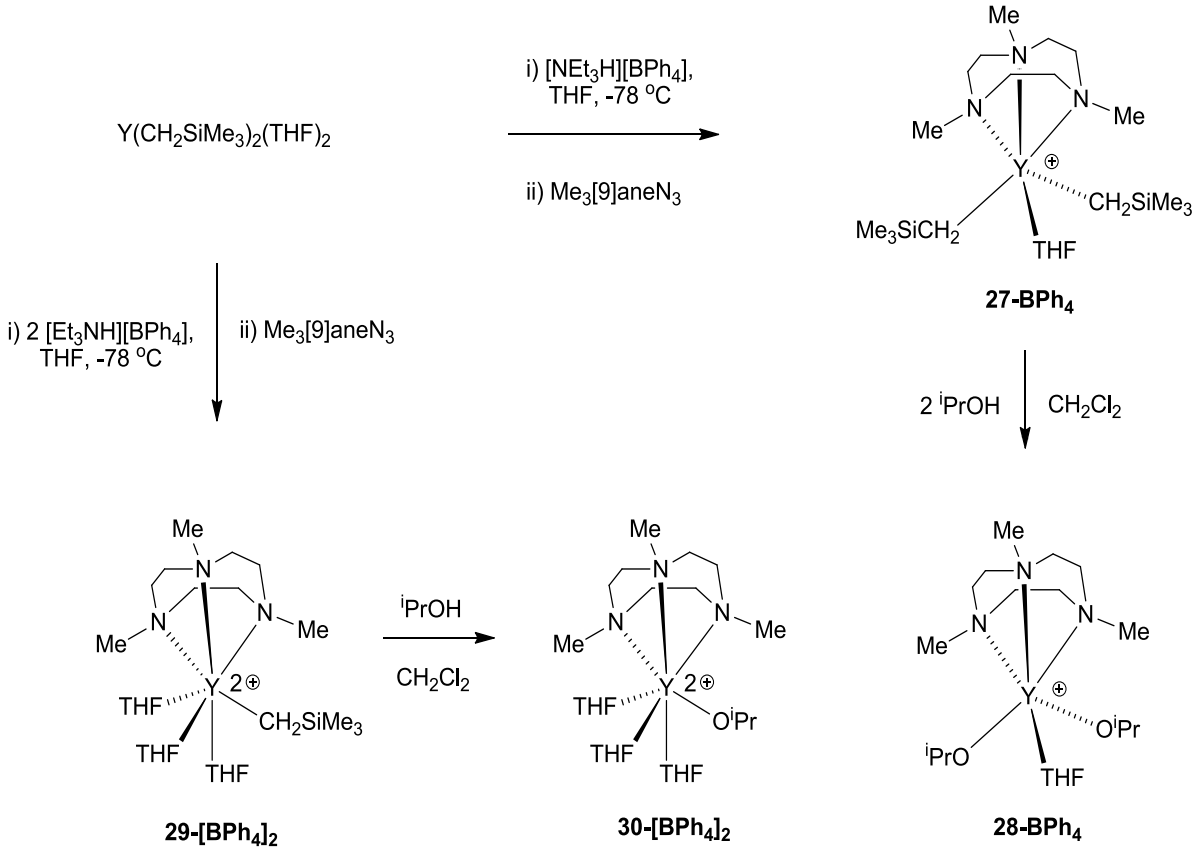
$[Y(OCMePh_2)(THF)_5][BPh_4]_2$.[69] In addition the Y-O(1) distance is similar (though a little shorter) to the Y-siloxide distance (2.0705(15) Å) found in $[Y\{OSi(O^tBu)_3\}(THF)_6][BPh_4]_2$.[70] The Y-O(THF) distances in **26-[BPh$_4$]$_2$** are also comparable to those found in the complex $[Y(Cl)(OCMe_3)(THF)_5][BPh_4]$ (2.391(5)–2.422(5) Å) reported by Evans.[71] The Y-N_{pz} bond distances found in **26-[BPh$_4$]$_2$** are substantially shorter than those found in the neutral $Y(HCMe_2pz)_3(CH_2SiMe_3)_3$ (2.601(2), 2.563(2) and 2.596(2) Å),[40] most likely a consequence of the dicationic nature of **26^{2+}.**

Scheme 4.3 summarises the reactions of $Y(CH_2SiMe_3)_3(THF)_2$ with one or two equivalents of $[NEt_3H][BPh_4]$ and $Me_3[9]aneN_3$ and subsequent reactions with ^{i}PrOH. The reaction of $Y(CH_2SiMe_3)_3(THF)_2$ with one or two equivalents of $[NEt_3H][BPh_4]$ followed by the addition of $Me_3[9]aneN_3$ in THF at -78 ^{o}C proceeded smoothly, giving the alkyl cations $[Y(Me_3[9]aneN_3)(CH_2SiMe_3)_2(THF)][BPh_4]$ (**27-BPh$_4$**) and $[Y(Me_3[9]aneN_3)(CH_2SiMe_3)$-$(THF)_3][BPh_4]_2$ (**29-[BPh$_4$]$_2$**) in 71 and 68 % recrystallised yields respectively. **27-BPh$_4$** and **29-[BPh$_4$]$_2$** reacted with two and one equivalents of ^{i}PrOH respectively at room temperature in CH_2Cl_2 to give the isopropoxide cations $[Y(Me_3[9]aneN_3)(O^iPr)_2(THF)][BPh_4]$ **(28-BPh$_4$)** and $[Y(Me_3[9]aneN_3)(O^iPr)$-$(THF)_3][BPh_4]_2$ (**30-[BPh$_4$]$_2$**) in 62 and 63 % recrystallised yields.

The NMR spectra of **27-BPh$_4$**, **28-BPh$_4$**, **29-[BPh$_4$]$_2$** and **30-[BPh$_4$]$_2$** are consistent with the structures proposed in Scheme 4.3. Similarly to the $HC(Me_2pz)_3$ supported cations, the monocationic complexes **27-BPh$_4$** and **28-BPh$_4$** have an approximate octahedral geometry around the yttrium centre, whereas the dicationic complexes **29-[BPh$_4$]$_2$** and **30-[BPh$_4$]$_2$** have an approximate pentagonal bipyramidal geometry around the yttrium centre. Unfortunately repeated attempts to grow diffraction-quality crystals were unsuccessful.

In all cases, the NMR spectra were consistent with a κ^3*N*-($Me_3[9]aneN_3$) ligand. Two sets of resonances (relative ratio 1:2) for the NMe_2 groups were observed, the first set corresponding to an NMe_2 group *trans* to bound THF molecule(s) and the second corresponding to NMe_2 groups *trans* to CH_2SiMe_3 group(s). The "up" and "down" (with respect to the metal) ring methylene protons appear as mutually coupled second-order multiplets consistent with the macrocycle being κ^3 bound to the MR (R = $(O^iPr)_n$ or $(CH_2SiMe_3)_n$, n = 1 or 2) fragment. The relative intensites of the R groups, bound THF molecules and BPh_4 anions were consistent with the mono- or di-cationic nature of the complexes.

Scheme 4.3. Synthesis of new $Me_3[9]aneN_3$ supported mono- and di-cationic yttrium alkyl and alkoxide complexes. BPh_4^- anions are omitted.



4.3 Polymerisation studies: ROP of *rac*-LA.

Initial studies showed that all of the complexes $[Y\{HC(Me_2pz)_3\}(CH_2SiMe_3)_2(THF)][BPh_4]$ (**23-BPh$_4$**), $[Y\{HC(Me_2pz)_3\}(O^iPr)_2(THF)][BPh_4]$ (**24-BPh$_4$**), $[Y\{HC(Me_2pz)_3\}(CH_2SiMe_3)(THF)_3][BPh_4]_2$ (**25-[BPh$_4$]$_2$**), $[Y\{HC(Me_2pz)_3\}(O^iPr)(THF)_3][BPh_4]_2$ (**26-[BPh$_4$]$_2$**), $[Y(Me_3[9]aneN_3)(CH_2SiMe_3)_2(THF)][BPh_4]$ (**27-BPh$_4$**), $[Y(Me_3[9]aneN_3)(O^iPr)_2(THF)][BPh_4]$ (**28-BPh$_4$**), $[Y(Me_3[9]aneN_3)(CH_2SiMe_3)(THF)_3][BPh_4]_2$ (**29-[BPh$_4$]$_2$**) and $[Y(Me_3[9]aneN_3)(O^iPr)(THF)_3][BPh_4]_2$ (**30-[BPh$_4$]$_2$**) were active for the ROP of *rac*-LA in preliminary tests. However, an elevated temperature of 70 ^oC in THF was required in all cases. Detrimental issues such as poor solubility and extreme sensitivity (especially in the case of $Me_3[9]aneN_3$ cations) limited the scope of polymerisations carried out. Detailed studies for the ROP of *rac*-LA using **24-BPh$_4$**, **25-[BPh$_4$]$_2$**, **26-[BPh$_4$]$_2$** and **30-[BPh$_4$]$_2$** will be presented.

4.3.1 ROP of *rac*-LA using 24-BPh_4 and 30-$[BPh_4]_2$.

The consumption of *rac*-LA followed first order kinetics with both the monocationic complex [Y{HC(Me_2pz)$_3$}(O^iPr)$_2$(THF)][BPh_4] (**24-BPh_4**) and the dicationic complex [Y(Me_3[9]aneN_3)(O^iPr)(THF)$_3$][BPh_4]$_2$ (**30-$[BPh_4]_2$**), taking 3-4 hours for the polymerisation to approach 90 % in both cases. The first order rate constants (k_{obs}) were similar for both catalysts (0.012(9) and 0.010(3) min^{-1} for **24-BPh_4** and **30-$[BPh_4]_2$** respectively). The gradients of the lines of best fit for the polymerisations in both cases (75(3) and 138(4) g mol^{-1} (equivalents converted)$^{-1}$ for (**24-BPh_4**) and (**30-$[BPh_4]_2$**) respectively), were close to the expected values (72 and 144 g mol^{-1} (equivalents converted)$^{-1}$). Additionally the polymers had M_n values close to those expected (see Figures 4.4 and 4.5), and moderate PDI values (1.2-1.4), although there was no stereochemical enrichment obtained.

Both **24-BPh_4** and **30-$[BPh_4]_2$** also showed first order consumption of *rac*-LA in the presence of 5 equivalents of ^{i}PrOH (see also Figures 4.4 and 4.5), showing evidence of the growth of multiple chains per metal centre (7 in the case of **24-BPh_4** and 6 in the case of **30-$[BPh_4]_2$**). The gradients of the lines of best fit for the polymerisations in both cases (19(1) and 29(2) g mol^{-1} (equivalents converted)$^{-1}$ for (**24-BPh_4**) and (**30-$[BPh_4]_2$**) respectively), were close to the expected values (20.6 and 24.0 g mol^{-1} (equivalents converted)$^{-1}$). Once more the M_n values observed were in excellent agreement to those expected, and the PDIs were narrow (1.2-1.4). Interestingly, the first order rate constants for both sets of polymerisations were identical within error (0.011(4) and 0.012(3) min^{-1} for **24-BPh_4** and **30-$[BPh_4]_2$** respectively) to those measured for polymerisations in the absence of ^{i}PrOH (0.012(9) and 0.010(3) min^{-1}), implying a zero order dependence on [^{i}PrOH] of the rate of polymerisation. The implications of this are discussed in detail later in this chapter for polymerisations using [Y{HC(Me_2pz)$_3$}(CH_2SiMe_3)(THF)$_3$][BPh_4]$_2$ (**25-$[BPh_4]_2$**) and [Y{HC(Me_2pz)$_3$}(O^iPr)(THF)$_3$][BPh_4]$_2$ (**26-$[BPh_4]_2$**).

Figure 4.4. M_n vs. conversion for the ROP of *rac*-LA using **24-BPh$_4$** (i) without ^{i}PrOH (black diamonds) and (ii) with 5 equiv. ^{i}PrOH (red squares). The upper dotted line is that predicted for 2 PLA chains per **24**$^+$, the lower for 7 chains per **24**$^{2+}$. Conditions: 6 mL THF, 70 ^{o}C, 3 hours, [*rac*-LA]$_0$:[**24-BPh$_4$**]$_0$ = 100.

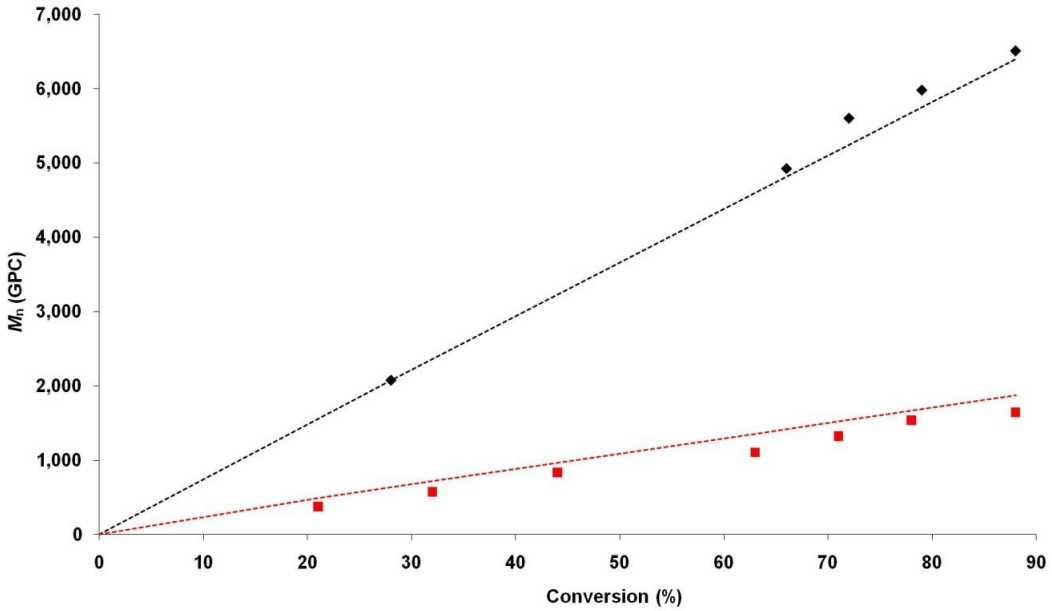
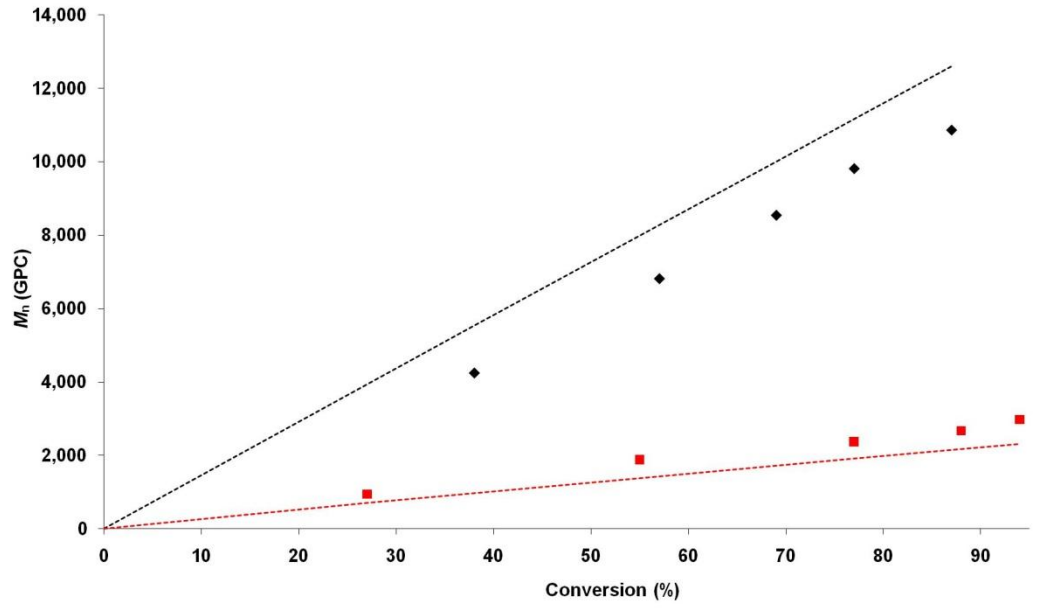


Figure 4.5. M_n vs. conversion for the ROP of *rac*-LA using **30-[BPh$_4$]$_2$** (i) without ^{i}PrOH (black diamonds) and (ii) with 5 equiv. ^{i}PrOH (red squares). The upper dotted line is that predicted for 1 PLA chain per **30**$^{2+}$, the lower for 6 chains per **30**$^{2+}$. Conditions: 6 mL THF, 70 ^{o}C, 4 hours, [*rac*-LA]$_0$:[**30-[BPh$_4$]$_2$**]$_0$ = 100.



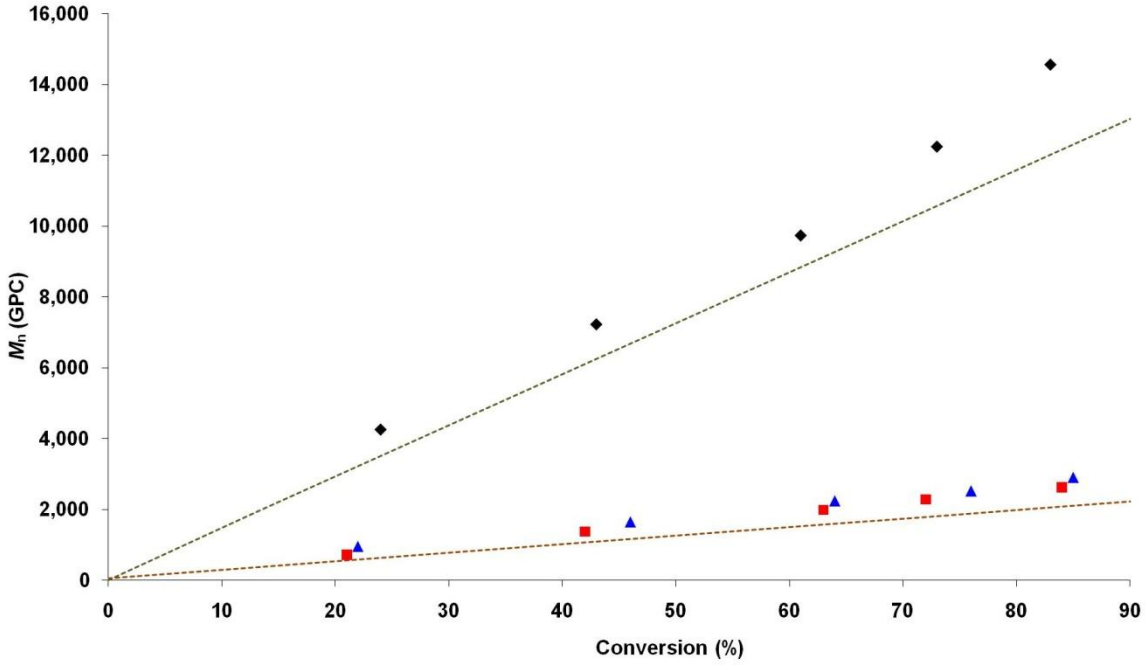
4.3.2 ROP of *rac*-LA using 25-$[BPh_4]_2$ and 26-$[BPh_4]_2$.

Building upon these initial results, polymerisation studies were extended to the $HC(Me_2pz)_3$ dicationic complexes $[Y\{HC(Me_2pz)_3\}(CH_2SiMe_3)(THF)_3][BPh_4]_2$ (**25-$[BPh_4]_2$**) and $[Y\{HC(Me_2pz)_3\}(O^iPr)(THF)_3][BPh_4]_2$ (**26-$[BPh_4]_2$**).

The consumption of *rac*-LA followed first order kinetics with both **25-$[BPh_4]_2$** and **26-$[BPh_4]_2$**, taking approximately 12 hours for the polymerisation to approach 90 % conversion. The first order rate constants (k_{obs}) were identical within error for both catalysts (0.0027(4) (**25-$[BPh_4]_2$**) and 0.0027(2) min^{-1} (**26-$[BPh_4]_2$**)). The identical rate constants suggest the presence of the same propagating species in both cases. Despite the extended times required (most likely due to the dicationic nature of the catalysts and subsequent propagating species), the polymerisations were well controlled. It is notable that polymerisations using **25-$[BPh_4]_2$** and **26-$[BPh_4]_2$** are both significantly slower than those using **30-$[BPh_4]_2$**. This is most likely due to the difference between the face capping ligand used ($HC(Me_2pz)_3$ *vs.* $Me_3[9]aneN_3$) and is discussed further towards the end of this Chapter. Figures 4.6 and 4.7 show that chain growth proceeded in a linear manner with the observed M_n values being very close to those predicted with either one or six (in the presence of ^iPrOH or $BnNH_2$ CTAs) polymer chains per metal.

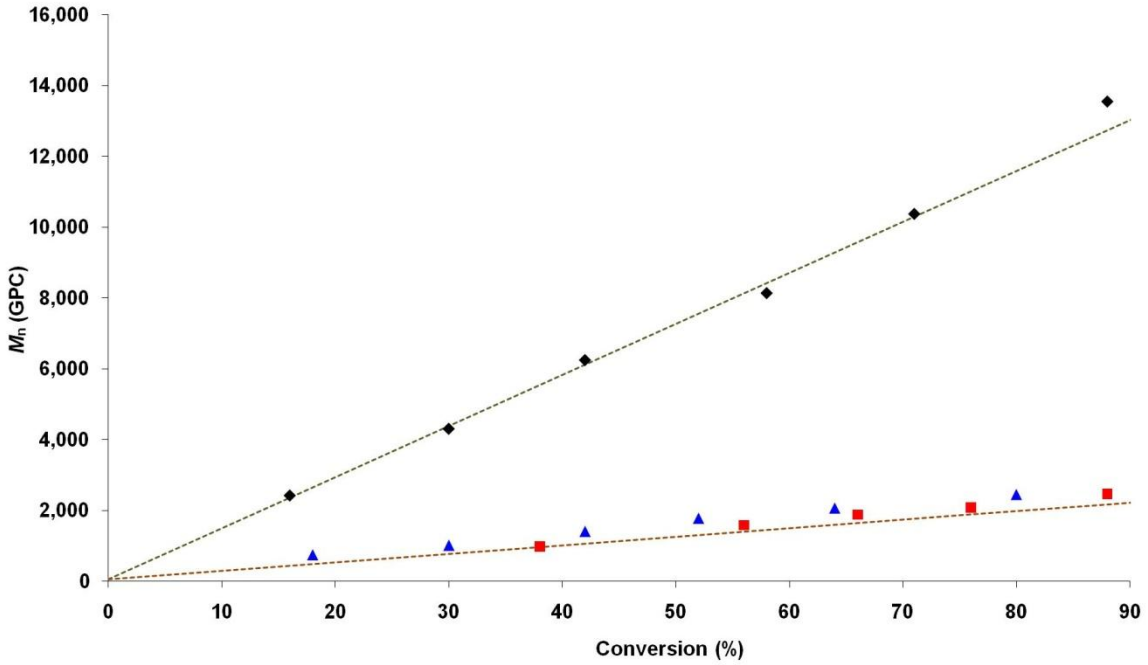
The gradient of the line of best fit for the polymerisation with no CTA using **25-$[BPh_4]_2$** was 170(10) g mol^{-1} (equivalents converted)$^{-1}$, in reasonable agreement with the expected value of 144 g mol^{-1} (equivalents converted)$^{-1}$. Together with the good agreement between expected and observed M_n values and the fairly narrow (average 1.40) PDI values this indicates a well controlled, living polymerisation process. Additionally it can be seen that the agreement between expected and observed M_n values using both ^iPrOH and $BnNH_2$ as CTAs is very good. The gradients of the lines of best fit are 30(1) and 31(1) g mol^{-1} (equivs. converted)$^{-1}$ respectively, very close to the expected value of 29 g mol^{-1} (equivs. converted)$^{-1}$. The average PDI values of the polymers obtained using both CTAs were quite narrow (1.30). It also noteworthy that the first order rate constants (k_{obs}) for polymerisations with both CTAs (0.0028(6) (^iPrOH) and 0.003(1) ($BnNH_2$) min^{-1}) were identical within error to the first order rate constant for the polymerisation with no added CTA (0.0027(4) min^{-1}).

Figure 4.6. M_n vs. conversion for the ROP of rac-LA using **25-[BPh$_4$]$_2$** (i) without ^{i}PrOH or $BnNH_2$ (black diamonds); (ii) with 5 equiv. ^{i}PrOH (red squares); (iii) with 5 equiv. $BnNH_2$ (blue triangles). The upper dotted line is that predicted for 1 PLA chain per **25**$^{2+}$, the lower for 6 chains per **25**$^{2+}$. Conditions: 6 mL THF, 70 ^{o}C, 12 hours, [*rac*-LA]$_0$:[**25-[BPh$_4$]$_2$**]$_0$ = 100.



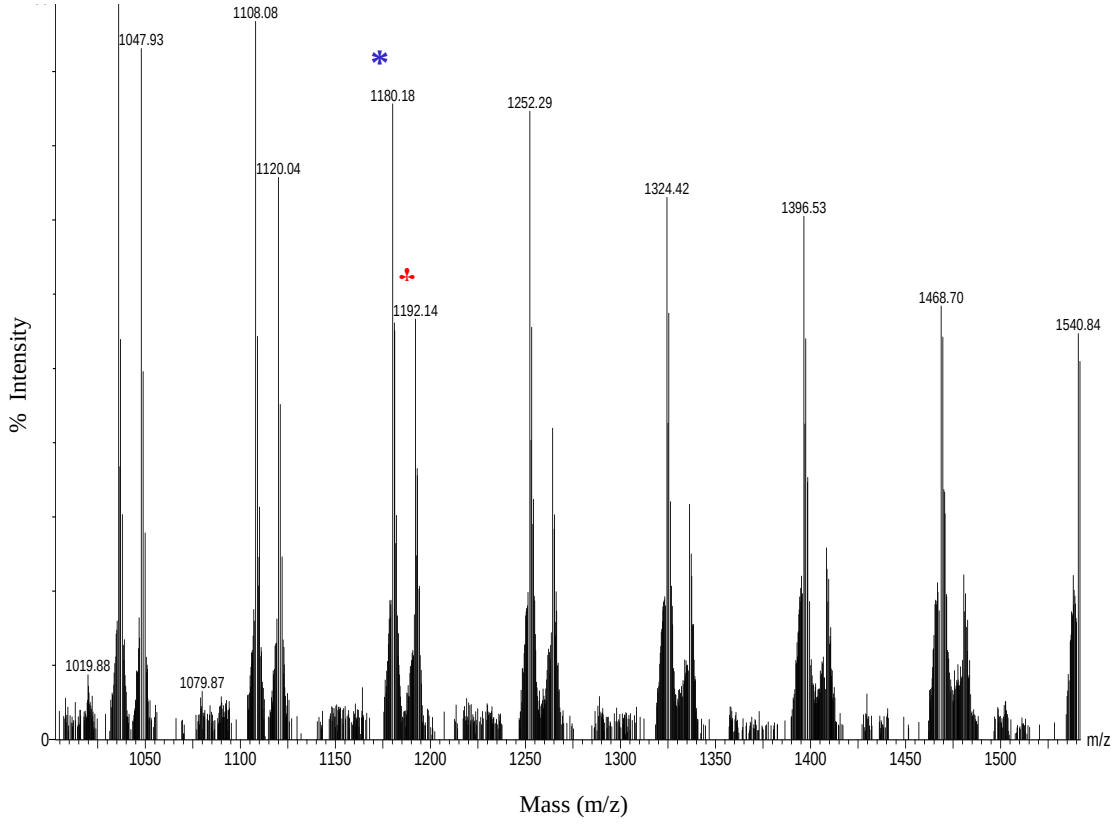
Similarly, the gradient of the line of best fit for the polymerisation with no CTA using **26-[BPh$_4$]$_2$** was 152(10) g mol^{-1} (equivs. converted)$^{-1}$, in very good agreement with the expected value of 144 g mol^{-1} (equivs. converted)$^{-1}$ and in closer agreement than that observed with **25-[BPh$_4$]$_2$** (170(10) g mol^{-1} (equivs. converted)$^{-1}$ Excellent agreement between expected and observed M_n values was found and the PDI values (1.2-1.3) were very narrow. Once more it can be seen that the agreement between expected and observed M_n values using both ^{i}PrOH and $BnNH_2$ as CTAs is very good. The gradients of the lines of best fit are 29(1) and 28(1) g mol^{-1} (equivs. converted)$^{-1}$ respectively, identical within error to the expected value of 29 g mol^{-1} (equivs. converted)$^{-1}$. The average PDI values of the polymers obtained using both CTAs were also narrow (1.2-1.3). As was the case with **25-[BPh$_4$]$_2$**, the first order rate constants (k_{obs}) for polymerisations with both CTAs (0.0029(5) (^{i}PrOH) and 0.0028(4) ($BnNH_2$) min^{-1}) were identical within error to the first order rate constant for the polymerisation with no CTA (0.0027(2) min^{-1}).

Figure 4.7. M_n vs. conversion for the ROP of *rac*-LA using **26-[BPh$_4$]$_2$** (i) without ^{i}PrOH or $BnNH_2$ (black diamonds); (ii) with 5 equiv. ^{i}PrOH (red squares); (iii) with 5 equiv. $BnNH_2$ (blue triangles). The upper dotted line is that predicted for 1 PLA chain per **26**$^{2+}$, the lower for 6 chains per **26**$^{2+}$. Conditions: 6 mL THF, 70 ^{o}C, 12 hours, [*rac*-LA]$_0$:[**26-[BPh$_4$]$_2$**]$_0$ = 100.



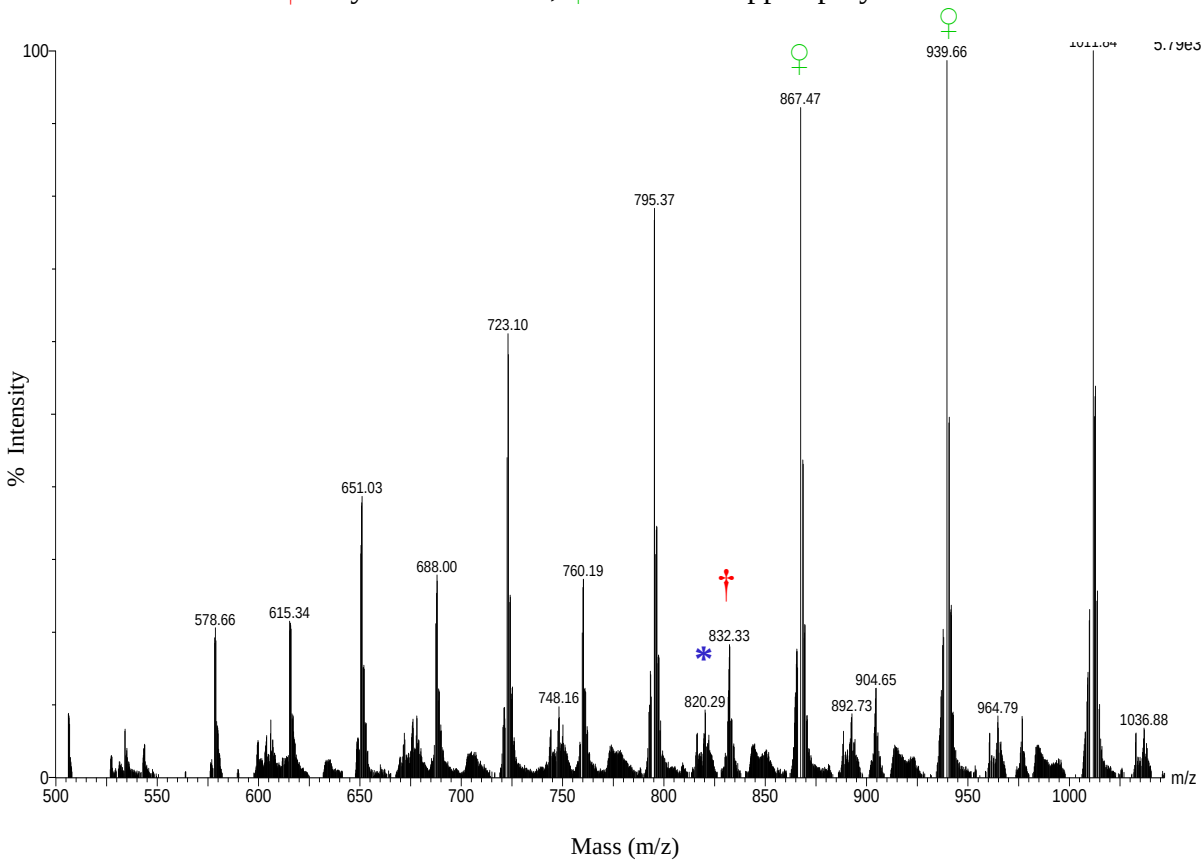
The MALDI-ToF MS and ^{1}H NMR spectra of polymers formed using **25-[BPh$_4$]$_2$** and **26-[BPh$_4$]$_2$** with ^{i}PrOH as a CTA showed the expected ^{i}PrO-chain end groups (an example MALDI-ToF mass spectrum is shown in Figure 4.8). As seen with the previous systems described in chapters two and three, the separation of peaks was 72 *m/z* units, consistent with a degree of transesterification in the polymerisation process. This is not surprising given the extended reaction times and elevated temperatures required. However, the good control and close M_n agreement between observed and expected values are a good indication of the probable minor extent of the occurrence of these processes. The major distribution in the MALDI-ToF spectrum shown in Figure 4.8 corresponds to ^{i}PrO-chain end groups, whilst the minor distribution corresponds to cyclic PLA units formed by intramolecular transesterification. Whilst the intensity of the two distributions appears very similar, this is due to the fact that the formation of lower molecular weight cyclic units is probably favoured over larger cyclic units, and therefore a low molecular weight sample would contain a higher concentration of them than a higher molecular weight sample. This is evident by the 'tailing off' of the secondary distribution at higher *m/z* values.

Figure 4.8. MALDI-ToF MS of ^{i}PrO-chain end capped PLA synthesised using [Y{HC(Me$_2$pz)$_3$}(O^{i}Pr)(THF)$_3$][BPh$_4$]$_2$ (**26-[BPh$_4$]$_2$**) and ^{i}PrOH as a CTA. M_n by GPC analysis was 3,100 g mol^{-1} (from an aliquot taken at 60 minutes). * = ^{i}PrO-capped polymer, † = cyclic PLA units.



Similarly the MALDI-ToF MS and ^{1}H NMR spectra of polymers formed using **25-[BPh$_4$]$_2$** and **26-[BPh$_4$]$_2$** with BnNH$_2$ as a CTA showed the expected BnNH-chain end groups (an example MALDI-ToF spectrum is shown in Figure 4.9). The spectrum shown corresponds to polymer prepared using **26-[BPh$_4$]$_2$** and shows a major distribution corresponding to BnNH-capped polymer units alongside a minor cyclic unit distribution and a second minor distribution corresponding to ^{i}PrO-terminated chains, arising from the ^{i}PrO end groups originally attached to **26-[BPh$_4$]$_2$**. Once again there is a peak separation of 72 *m/z* consistent with transesterification side reactions.

Figure 4.9. MALDI-ToF MS of BnNH-chain end capped PLA synthesised using [Y{HC(Me$_2$pz)$_3$}(O^{i}Pr)(THF)$_3$][BPh$_4$]$_2$ (**26-[BPh$_4$]$_2$**) and BnNH$_2$ as a CTA. M_n by GPC analysis was 1,520 g mol^{-1} (from an aliquot taken at 60 minutes). * = ^{i}PrO-capped polymer, † = cyclic PLA units, ♀ = BnNH-capped polymer.



4.3.3 Mechanistic Studies.

Holding the [*rac*-LA]:[BnNH$_2$] constant at 100:3 and varying the equivalents of **26-[BPh$_4$]$_2$** from 1 to 4 allowed the order in [Y]$_0$ to be determined (Figure 4.10). The rate constants for [*rac*-LA]:[BnNH$_2$]:[Y]$_0$ ([Y]$_0$ = 1, 2, 3 or 4) were measured to be 0.0027(2), 0.006(1), 0.009(2) and 0.013(2) min^{-1} respectively, consistent with a first order dependence in [Y]$_0$. Furthermore, the plot of -ln(k_{obs}) against -ln(equivalents Y) (Figure 4.11) had a gradient of 1.02(2), confirming the first order dependence of k_{obs} on [Y]$_0$. Additionally, the end point M_n values for the polymerisations were measured to be 3170, 3140, 3210 and 3270 (for [Y]$_0$ = 1, 2, 3 or 4 respectively), showing that the M_n of the resultant polymer is independent of [Y]$_0$ and dependent on [*rac*-LA]:[BnNH$_2$]$_0$ only. This indicates that the rate of propagation is slower than the rate of chain transfer and therefore the rate of chain transfer is not involved in the rate determining step.

Figure 4.10. First order rate plots for the ROP of 100 equivalents of *rac*-LA in the presence of 3 equivalents of $BnNH_2$ and 4 (red squares), 3 (blue triangles), 2 (green circles) and 1 (black squares) equivalents of **26-[BPh_4]$_2$**. Observed first order rate constants are 0.0027(2), 0.006(1), 0.009(2) and 0.013(2) min^{-1} respectively. Conditions: 6 mL THF, 70 ^oC, 3-12 hours, [*rac*-LA]$_0$:[**26-[BPh_4]$_2$**]$_0$ = 100.

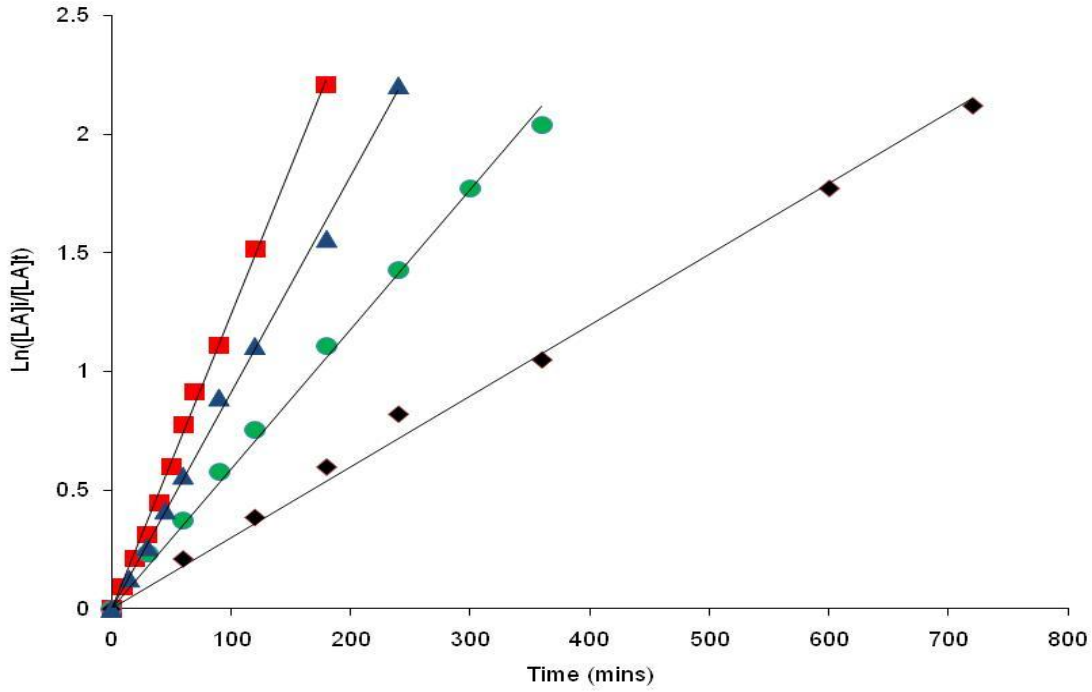
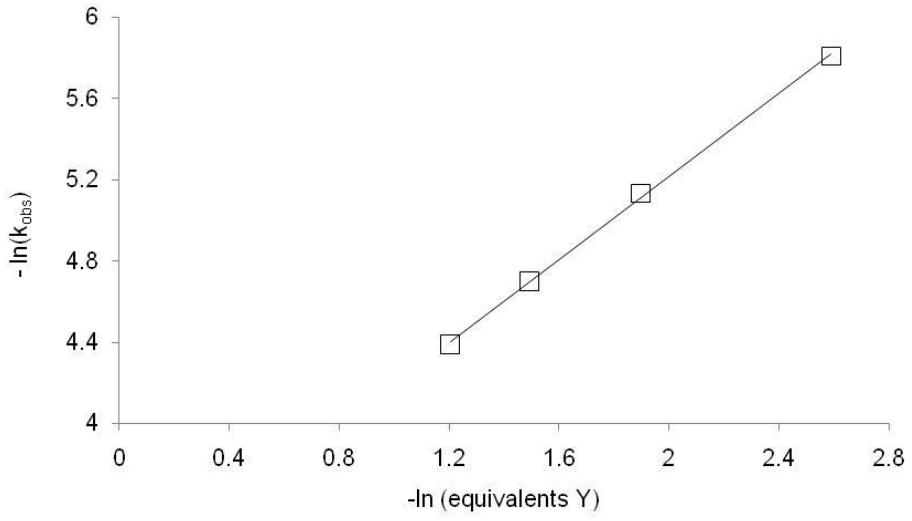


Figure 4.11. A plot of -ln(k_{obs}) against -ln(equivalents Y) for the ROP of 100 equivalents of *rac*-LA in the presence of 3 equivalents of $BnNH_2$ and 1-4 equivalents of **26-[BPh_4]$_2$**. The gradient of the line of best fit was 1.02(2), R^2 = 0.999.



In order to determine the order in LA, a second series of kinetics experiments were carried out. Holding the $[Y]_0$:$[BnNH_2]$ constant at 1:3 and varying the equivalents of *rac*-LA from 100 to 250 allowed the order in [*rac*-LA] to be determined (Figure 4.12). The rate constants for [*rac*-LA]:$[BnNH_2]$:$[Y]_0$ ([*rac*-LA] = 100, 150, 200 or 250) were measured to be 0.0027(2), 0.004(1), 0.006(3) and 0.008(2) min^{-1} respectively, consistent with a first order dependence in [*rac*-LA]. Additionally, the plot of -ln(k_{obs}) against -ln(equivalents *rac*-LA) (Figure 4.13) had a gradient of 1.04(1), confirming the first order dependence of k_{obs} on [*rac*-LA].

Figure 4.12. First order rate plots for the ROP of different equivalents of *rac*-LA (250 (red squares), 200 (blue triangles), 150 (green circles) and 100 (black squares)) using one equivalent of **26-$[BPh_4]_2$** and three equivalents of $BnNH_2$. Observed first order rate constants are 0.0027(2), 0.004(1), 0.006(3) and 0.008(2) min^{-1} respectively. Conditions: 6mL THF, 70°C, 3-12 hours.

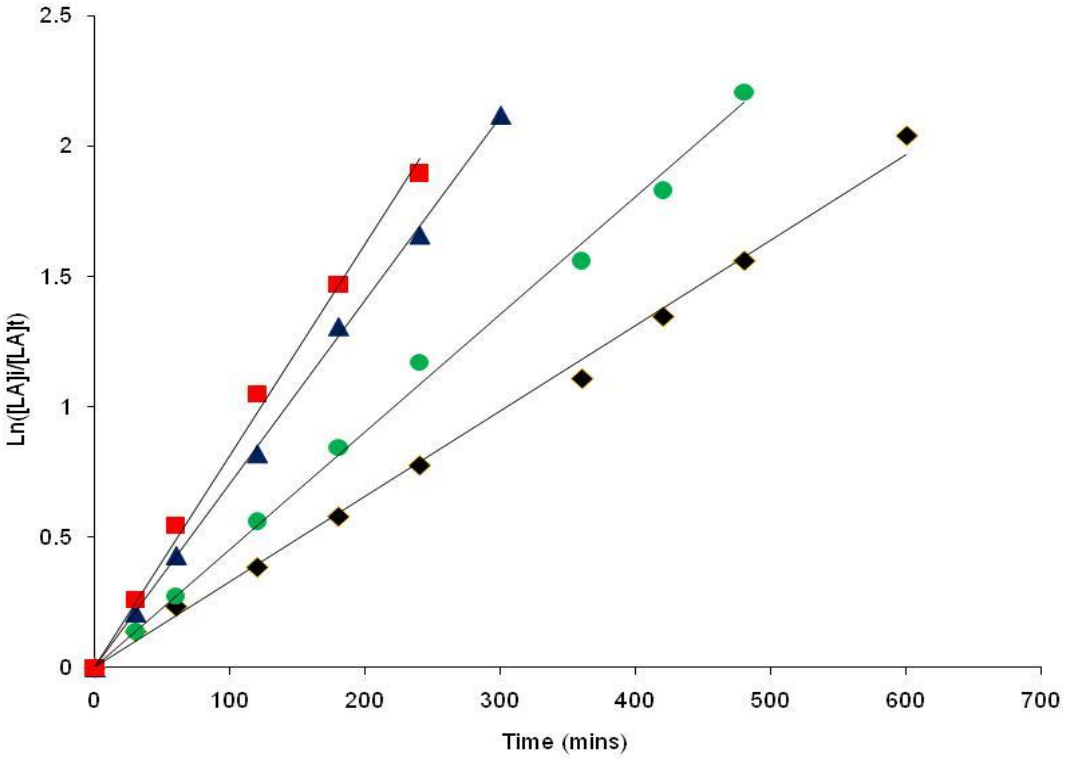
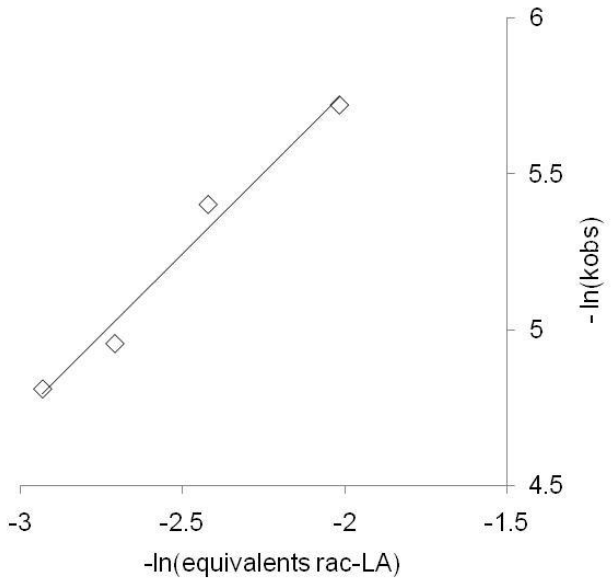


Figure 4.13. A plot of -ln(k_{obs}) against -ln(equivalents *rac*-LA) using 1 equivalent of **26-[BPh$_4$]$_2$** in the presence of 3 equivalents of $BnNH_2$. The gradient of the line of best fit was 1.04(1), R^2 = 0.978.



In a complementary set of experiments, holding the [*rac*-LA]:[Y]$_0$ value constant and varying the equivalents of $BnNH_2$ from 1 to 5 had no effect on the rate of polymerisation (Figure 4.14). The measured rate constants were 0.0026(3), 0.0028(7) and 0.0029(6) min^{-1} for 1, 3 and 5 equivalents of $BnNH_2$ respectively. Furthermore, whilst the rate of polymerisation was shown to be zero order in [$BnNH_2$], the resulting M_n of the polymer was also shown to have a dependence on [$BnNH_2$] (Figure 4.15). The gradients of the lines of best fit of M_n *vs.* conversion using 1, 3 and 5 equivalents of $BnNH_2$ were measured to be 74(2), 42(2) and 23(1) g mol^{-1} (equivs. converted)$^{-1}$. These compare well with the calculated gradients of 72, 36 and 24 g mol^{-1} (equivs. converted)$^{-1}$ respectively.

These data, together with the MALDI-ToF mass spectrum in Figure 4.9 showing PLA with predominantly amine end groups (with only a small proportion with alcohol end groups arising from classical coordination-insertion by the bound ^{i}PrO ligand in **26-[BPh$_4$]$_2$**), suggest that in the presence of Lewis acidic **26^{2+}**, $BnNH_2$ rapidly (with respect to propagation) ring-opens a molecule of *rac*-LA to form BnNH-C(O)CH(Me)OC(O)CH(Me)O-H (**I**) *via* an activated monomer mechanism (Scheme 4.4). This is then followed by metal-mediated immortal chain extension of the so-formed macromolecules by coordination-insertion. Thereafter, **I** acts as a CTA in an analogous manner to ^{i}PrOH, ultimately forming amine-terminated PLA in an immortal fashion. The overall rate law has been shown to be Rate = k_{obs}[Y][*rac*-LA][RNH_2]^0. It is noteworthy that $BnNH_2$ alone does not polymerise *rac*-LA under these conditions.

Figure 4.14. First order rate plots for the ROP of 100 equivalents of *rac*-LA using one equivalent of **26-[BPh$_4$]$_2$** and 1 (red squares), 3 (blue triangles) and 5 (black squares) equivalents of BnNH$_2$. Observed first order rate constants are 0.0026(3), 0.0028(7), and 0.0029(6) min^{-1} respectively. Conditions: 6mL THF, 70^{o}C, 12 hours.

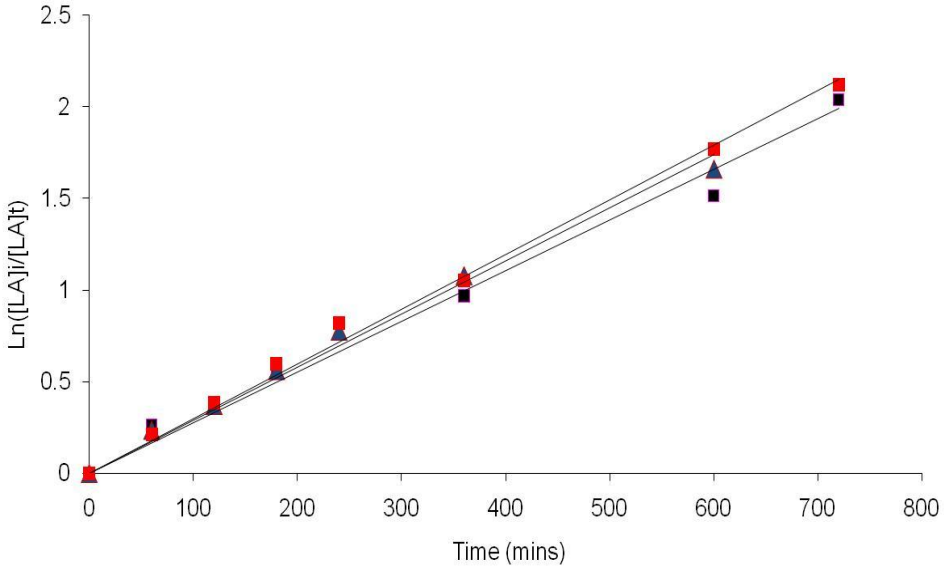
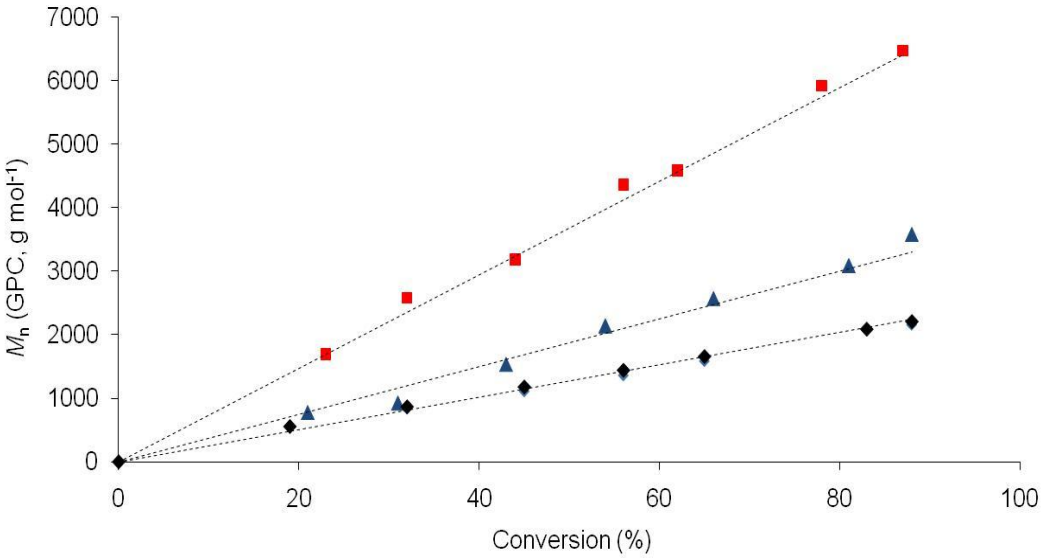
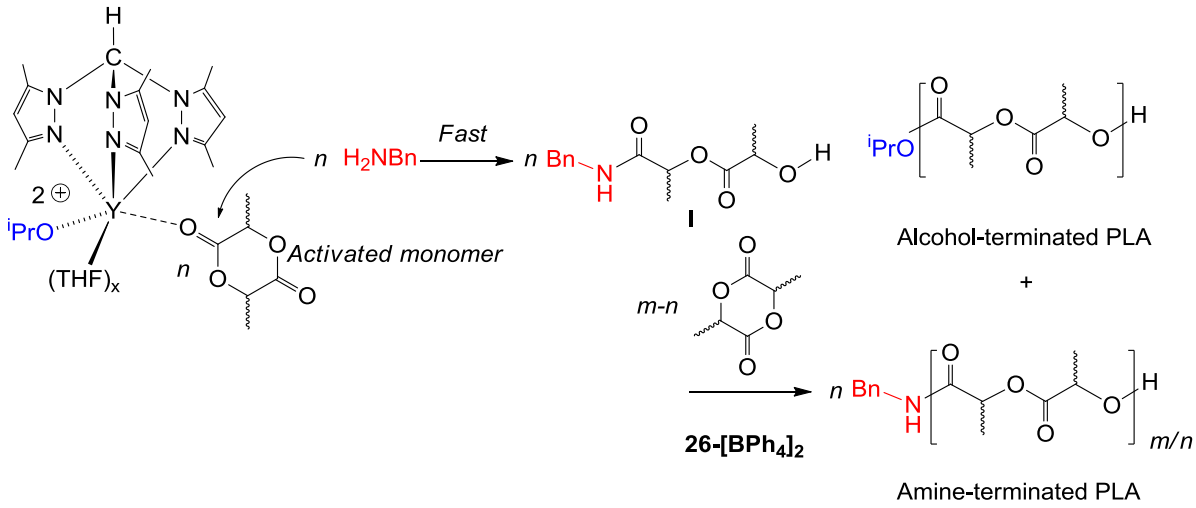


Figure 4.15. M_n (as measured by GPC) *vs.* equivalents % conversion (as measured by ^{1}H NMR) for the ROP of 100 equivalents of *rac*-LA using 1 equivalent of **26-[BPh$_4$]$_2$** in the presence of 1 (red squares), 3 (blue triangles) and 5 (black squares) equivalents of BnNH$_2$. Conditions: 6mL THF, 70^{o}C, 12 hours.



Scheme 4.4. Proposed mechanism for the *i*-ROP of *rac*-LA using **26-[BPh$_4$]$_2$** in the presence of $BnNH_2$



The fact that there is a zero order dependence on [$BnNH_2$] is consistent with the proposed mechanism and implies fast rates of initiation and chain transfer with respect to the rate of propagation (which is independent of [$BnNH_2$] and is therefore likely to be a part of the rate determining step). This has also been observed in related work in the Mountford group using the zwitterionic complex Y(O_2NN´)(HO_2NN´) (H_2O_2NN´ = $Me_2NCH_2CH_2N(CH_2$-2-HO-3,5-$C_6H_2{}^tBu_2)_2$) for the *i*-ROP of *rac*-LA in the presence of $BnNH_2$.[1] It is assumed that an analogous mechanism operates for the *i*-ROP of *rac*-LA using **26-[BPh$_4$]$_2$** in the presence of ^{i}PrOH. This is consistent with the fact that the rate constants using both CTAs are very similar (0.0029(5) and 0.0028(4) min^{-1} for ^{i}PrOH and $BnNH_2$ respectively).

Whilst analogous kinetics experiments with [Y{HC(Me_2pz)$_3$}(CH_2SiMe_3)(THF)$_3$][BPh_4]$_2$ (**25-[BPh$_4$]$_2$**) were inconclusive (for example a partial order in [Y] was shown), it is likely that the CH_2SiMe_3 group undergoes protonolysis with either ^{i}PrOH or $BnNH_2$ to form an amide or alkoxide complex respectively. However the fact that the rate constants for polymerisations using **25-[BPh$_4$]$_2$** are nearly identical (0.0028(6) and 0.003(1) min^{-1} for ^{i}PrOH and $BnNH_2$ respectively) and close to that with no CTA (0.0027(4) min^{-1}) suggest that a similar mechanism may operate also.

NMR scale experiments were carried out in THF-d_8 at 70 °C with 10 equivalents of *rac*-LA, 5 equivalents of $BnNH_2$ and one equivalent of either **25-[BPh$_4$]$_2$** or **26-[BPh$_4$]$_2$**. ^{1}H NMR analysis of the mixture after 12 h showed PLA, a small amount of residual catalyst and almost quantitative formation of uncomplexed HC(Me_2pz)$_3$. Despite this, it is thought that HC(Me_2pz)$_3$ is likely more than merely a spectator ligand. A dicationic yttrium alkoxide species in the absence of a supporting ligand would likely be polymeric and not give the

same degree of excellent M_n control observed in the PLA's formed. It is more likely that $HC(Me_2pz)_3$ is gradually displaced by chelating LA macromolecules in the progression of the polymerisation process. An analogous experiment was carried out with **30-[BPh$_4$]$_2$**. Interestingly, in this case heating in THF-d_8 at 70 °C after 4 h showed the presence of PLA and residual catalyst with no uncomplexed Me_3[9]-aneN_3. This suggests that Me_3[9]aneN_3 remains bound to the yttrium metal centre throughout the polymerisation process (unlike $HC(Me_2pz)_3$). This most likely accounts for the superior activity of **30-[BPh$_4$]$_2$** compared to either **25-[BPh$_4$]$_2$** or **26-[BPh$_4$]$_2$** under the conditions used.

With the aim of developing an improved (higher activity) system, it was attempted to prepare cationic yttrium alkyl and alkoxide species with the monoanionic ligand $Tp^{tBu,Me}$, which was successfully used in Chapter 3. It was reasoned that a monoanionic ligand should remain more tightly bound to the metal centre and the *tert*-butyl groups in the 3-position of the ligand may also provide a degree of stereochemical control over the PLA formed. However, such attempts unfortunately led to C-H activation of the *tert*-butyl group in the ligand.

In related work, the complex $[Y(O^tBu)(Cl)(THF)_5][BPh_4]$ was prepared using the method published by Evans *et al*.[71] However, the attempted preparation of $[(Tp^{tBu,Me})Y(O^tBu)(THF)_x][BPh_4]$ by metathesis between $[Y(O^tBu)(Cl)(THF)_5][BPh_4]$ and $KTp^{tBu,Me}$ proved unsuccessful: no reaction occurred either at RT or 70 °C in THF. Although a surprising result, this is consistent with the lack of reactivity of $[Y(O^tBu)(Cl)(THF)_5][BPh_4]$ reported by Evans *et al*., which was attributed to the halophilicity of the yttrium cation.[71] Perhaps more surprisingly, $[Y(O^tBu)(Cl)(THF)_5][BPh_4]$ was also found to be inactive towards the ROP of *rac*-LA, either at room temperature or 70 °C in THF over a period of 12 h.

4.4 Summary and Conclusions

The work presented in this chapter has developed cationic yttrium alkyl and alkoxide complexes as initiators for the ROP of *rac*-LA. Additionally, **26-[BPh$_4$]$_2$** was the first reported cationic initiator for the ROP of *rac*-LA at the time of publication, and this area is the subject of growing interest. The catalysts presented in this chapter show excellent M_n control of the polymers formed both in the absence of, and together with, ^iPrOH and $BnNH_2$ acting as chain transfer reagents in the *i*-ROP of *rac*-LA, also a subject of growing interest.

The mechanism of *i*-ROP was shown to be coordination-insertion (after an initial activated monomer step to generate amine-capped PLA), as supported by the zero order dependence

on [$BnNH_2$] of the rate of polymerisation and the fact that M_n was shown to be independent of $[Y]_0$ but dependent on [$BnNH_2$], attributed to the fast rate of chain transfer with respect to the rate of propagation.

4.5 References

1. L. Clark, M. G. Cushion, H. E. Dyer, A. D. Schwarz, R. Duchateau and P. Mountford, *Chem. Commun.*, 2010, **46**, 273-275.
2. Z. Hou and Y. Wakatsuki, *Coord. Chem. Rev.*, 2002, **231**, 1-22.
3. B. D. Ward, S. Bellemin-Laponnaz and L. H. Gade, *Angew. Chem. Int. Ed.*, 2005, **44**, 1668-1671.
4. C. Tredget, F. Bonnet, A. Cowley and P. Mountford, *Chem. Commun.*, 2005, 3301-3303.
5. W. E. Piers and D. J. H. Emslie, *Coord. Chem. Rev.*, 2002, **233-234**, 131-155.
6. T. V. Mahrova, G. K. Fukin, A. V. Cherkasov, A. A. Trifonov, N. Ajellal and J. F. Carpentier, *Inorg. Chem.*, 2009, **48**, 4258-4266.
7. E. Grunova, E. Kirillov, T. Roisnel and J. F. Carpentier, *Organometallics*, 2008, **27**, 5691-5698.
8. C.-X. Cai, A. Amgoune, C. W. Lehmann and J. F. Carpentier, *Chem. Commun.*, 2004, 330.
9. A. Amgoune, C. M. Thomas and J. F. Carpentier, *Macromol. Rapid Commun.*, 2007, **28**, 693-697.
10. H. Dyer, S. Huijser, N. Susperregui, F. Bonnet, A. Schwarz, R. Duchateau, L. Maron and P. Mountford, *Organometallics*, 2010, 3602-3621.
11. M. Visseaux and F. Bonnet, *Coord. Chem. Rev.*, 2011, 374-420.
12. R. H. Platel, A. J. P. White and C. K. Williams, *Chem. Commun.*, 2009, 4115-4117.
13. R. H. Platel, L. M. Hodgson, A. J. P. White and C. K. Williams, *Organometallics*, 2007, **26**, 4955-4963.
14. W. E. Piers, P. J. Shapiro, E. E. Bunel and J. E. Bercaw, *Synlett.*, 1990, 74.
15. J. M. Birmingham and G. Wilkinson, *J. Am. Chem. Soc.*, 1956, **78**, 42-44.
16. H. Schumann, J. A. Meese-Marktscheffel and L. Esser, *Chem. Rev.*, 1995, **95**, 865-986.
17. P. J. Chirik, J. E. Bercaw, A. Togni and R. L. Halterman, Eds.;Wiley-VCH, New York, 1998, Vol. 4.
18. J. Okuda, T. Eberle, A. Togni and R. L. Halterman, Eds.; Wiley-VCH, New York, 1998, Vol. 1.

19. R. S. Coutts and P. C. Wailes, *J. Organomet. Chem.*, 1970, **25**, 117-122.
20. J. L. Atwood and K. D. Smith, *J. Chem. Soc. Dalton. Trans.*, 1973, 2487-2490.
21. J. L. Atwood and K. D. Smith, *J. Chem. Soc. Chem. Commun.*, 1972, 593-594.
22. L. E. Manzer, *Inorg. Synth.*, 1982, **21**, 135-140.
23. J. Holton, M. F. Lappert, D. G. H. Ballard, R. Pearce, J. L. Atwood and W. E. Hunter, *J. Chem. Soc., Dalton Trans.*, 1979, 45.
24. W. J. Evans, M. S. Sollberger, J. L. Shreeve, J. M. Olofson, J. H. Hain and J. W. Ziller, *Inorg. Chem.*, 1992, **31**, 2492-2501.
25. S. Arndt and J. Okuda, *Chem. Rev.*, 2002, **102**, 1953.
26. L. D. Henderson, G. D. MacInnis, W. E. Piers and M. Parvez, *Can. J. Chem.*, 2004, **82**, 162.
27. C. J. Schaverien, *Organometallics*, 1994, **13**, 69.
28. P. J. Shapiro, W. D. Cotter, W. P. Schaefer, J. A. Labinger and J. E. Bercaw, *J. Am. Chem. Soc.*, 1994, **116**, 4623 - 4640.
29. K. C. Hultzsch, T. P. Spaniol and J. Okuda, *Organometallics*, 1997, **16**, 4845.
30. S. Arndt, P. Voth, T. P. Spaniol and J. Okuda, *Organometallics*, 2000, **19**, 4690.
31. S. Arndt, A. Trifonov, T. P. Spaniol, J. Okuda, M. Kitamura and T. Takahashi, *J. Organomet. Chem.*, 2002, **647**, 158.
32. A. A. Trifonov, T. P. Spaniol and J. Okuda, *Organometallics*, 2001, **20**, 4869.
33. Y. Mu, W. E. Piers, D. C. MacQuarrie, M. J. Zaworotko and V. G. Young, Jr., *Organometallics*, 1996, **15**, 2720.
34. F. T. Edelmann, D. M. M. Freckmann and H. Schumann, *Chem. Rev.*, 2002, **102**, 1851.
35. P. Mountford and B. D. Ward, *Chem. Commun.*, 2003, 1797.
36. P. G. Hayes, W. E. Piers and R. McDonald, *J. Am. Chem. Soc.*, 2002, **124**, 2132.
37. D. J. H. Emslie, W. E. Piers, M. Parvez and R. McDonald, *Organometallics*, 2002, **21**, 4226.
38. S. Hajela, W. P. Schaefer and J. E. Bercaw, *J. Organomet. Chem.*, 1997, **532**, 45.
39. S. C. Lawrence, B. D. Ward, S. R. Dubberley, C. M. Kozak and P. Mountford, *Chem. Commun.*, 2003, 2880.
40. C. S. Tredget, S. C. Lawrence, B. D. Ward, R. G. Howe, A. R. Cowley and P. Mountford, *Organometallics*, 2005, **24**, 3136.
41. S. Bambirra, A. Meetsma and B. Hessen, *Acta. Crystallogr., Sect. E*, 2006, **E62**, 314.
42. C. S. Tredget, F. Bonnet, A. R. Cowley and P. Mountford, *Chem. Commun.*, 2005, 3301.

43. P. M. Zeimentz, S. Arndt, B. R. Elvidge and J. Okuda, *Chem. Rev.*, 2006, **106**, 2404.
44. C. J. Schaverien, *Organometallics*, 1992, **11**, 3476.
45. S. Arndt, T. P. Spaniol and J. Okuda, *Organometallics*, 2003, **22**, 775.
46. W. J. Evans, T. A. Ulibarri, L. R. Chamberlain, J. W. Ziller and D. Alvarez, Jr., *Organometallics*, 1990, **9**, 2124.
47. W. J. Evans, C. A. Seibel and J. W. Ziller, *J. Am. Chem. Soc.*, 1998, **120**, 6745.
48. P. Voth, Doctoral Thesis , RWTH Aachen University, Aachen, Germany, 2004.
49. C. Cui, A. Shafir, J. A. R. Schmidt, A. G. Oliver and J. Arnold, *Dalton Trans.*, 2005, 1387-1393.
50. L. Lee, D. J. Berg, F. W. Einstein and R. J. Batchelor, *Organometallics*, 1997, **16**, 1819-1821.
51. S. Arndt, T. P. Spaniol and J. Okuda, *Angew. Chem. Int. Ed.*, 2003, **42**, 5075.
52. A. Amgoune, C. M. Thomas and J. F. Carpentier, *Pure. Appl. Chem.*, 2007, **79**, 2013-2030.
53. Y. Sarazin, V. Poirier, T. Roisnel and J. F. Carpentier, *Eur. J. Inorg. Chem.*, 2010, **2010**, 3423-3428.
54. N. Ajellal, J.-F. Carpentier, C. Guillaume, S. M. Guillaume, M. Helou, V. Poirier, Y. Sarazin and A. Trifonov, *Dalton Trans.*, 2010, **39**, 8363-8376.
55. M. Cushion and P. Mountford, *Chem. Commun.*, 2011, 2276-2278.
56. A. Otero, A. Lara-Sánchez, J. Fernández-Baeza, C. Alonso-Moreno, J. A. Castro-Osma, I. Márquez-Segovia, L. F. Sánchez-Barba, A. M. Rodríguez and J. C. Garcia-Martinez, *Organometallics*, 2011, **30**, 1507-1522.
57. I. van der Meulen, E. Gubbels, S. Huijser, R. l. Sablong, C. E. Koning, A. Heise and R. Duchateau, *Macromolecules*, 2011, 4301-4305.
58. C. A. Wheaton and P. G. Hayes, *Chem. Commun.*, 2010, **46**, 8404-8406.
59. Y. Sarazin, B. Liu, T. Roisnel, L. Maron and J. F. Carpentier, *J. Am. Chem. Soc.*, 2011, 9069-9087.
60. Y. Sarazin, M. Schormann and M. Bochmann, *Organometallics*, 2004, **23**, 3296-3302.
61. S. Inoue, *J. Macromol. Sci. A: Chem.*, 1988, **25**, 571 - 582.
62. T. Aida, Y. Maekawa, S. Asano and S. Inoue, *Macromolecules*, 1988, **21**, 1195-1202.
63. M. Okada, *Prog. Polym. Sci.*, 2002, **27**, 87-133.
64. M. G. Kimpel, J. Eppinger, P. Sirsch, W. Scherer and R. Anwander, *Organometallics*, 2002, **21**, 4021.

65. Z. Zhong, P. J. Dijkstra, C. Birg, M. Westerhausen and J. Feijen, *Macromolecules*, 2001, **34**, 3863-3868.
66. H. Ma and J. Okuda, *Macromolecules*, 2005, **38**, 2665-2673.
67. C. S. Tredget, DPhil Thesis and unpublished results, University of Oxford, Oxford, England, 2007.
68. C. S. Tredget, E. Clot and P. Mountford, *Organometallics*, 2008, **27**, 3458-3473.
69. M. U. Kramer, D. Robert, S. Arndt, P. M. Zeimentz, T. P. Spaniol, A. Yahia, L. Maron, O. Eisenstein and J. Okuda, *Inorg. Chem.*, 2008, **47**, 9265-9278.
70. B. R. Elvidge, S. Arndt, T. P. Spaniol and J. Okuda, *Dalton Trans.*, 2006, 890.
71. W. J. Evans, J. M. Olofson and J. W. Ziller, *J. Am. Chem. Soc.*, 1990, **112**, 2308-2314.

Chapter Five

Experimental and Characterising Data

5.0. General methods and instrumentation. All manipulations were carried out using standard Schlenk line or dry-box techniques under an atmosphere of argon or dinitrogen. Solvents were degassed by sparging with dinitrogen and dried by passing through a column of the appropriate drying agent. Toluene was refluxed over sodium and distilled. Deuterated solvents were dried over potassium (C_6H_6, Toluene-d_8 or THF-d_8) or P_2O_5 ($CDCl_3$ and CD_2Cl_2), distilled under reduced pressure and stored under dinitrogen in Teflon valve ampoules. NMR samples were prepared under dinitrogen in 5 mm Wilmad 507-PP tubes fitted with J. Young Teflon valves. ^1H, $^{13}C\{^1H\}$ and $^{11}B\{^1H\}$ NMR spectra were recorded on Varian Mercury-VX 300 and Varian Unity Plus 500 spectrometers at ambient temperature unless stated otherwise and referenced internally to residual protio-solvent (^1H) or solvent (^{13}C) resonances, and are reported relative to tetramethylsilane (δ = 0 ppm). Assignments were confirmed using two dimensional ^1H-^1H and ^{13}C-^1H NMR correlation experiments. Chemical shifts are quoted in δ (ppm) and coupling constants in Hz. IR spectra were recorded on a Nicolet Magna 560 E.S.P. FTIR spectrometer. Samples were prepared in a dry-box either as Nujol mulls between NaCl plates or as solution samples (10 mg per 0.5 mL in the required solvent) and the data are quoted in wavenumbers (cm^{-1}). Elemental analyses were carried out by the Elemental Analysis Service at the London Metropolitan University and Elemental Microanalysis Ltd, Okehampton, Devon.

MALDI-ToF-MS analysis was performed on a Waters MALDI micro equipped with a 337 nm nitrogen laser. An accelerating voltage of 25 kV was applied. The polymer samples were dissolved in THF at a concentration of 1 mg mL^{-1}. The cationization agent used was potassium trifluoroacetate (Fluka, >99%) dissolved in THF at a concentration of 5 mg mL^{-1}. The matrix used was *trans*-2-[3-(4-*tert*-butylphenyl)-2-methyl-2-propenylidene]malononitrile (DCTB) (Fluka) and was dissolved in THF at a concentration of 40 mg mL^{-1}. Solutions of matrix, salt and polymer were mixed in a volume ratio of 4:1:4, respectively. The mixed solution was hand-spotted on a stainless steel MALDI target and left to dry. The spectra were recorded in the refectron mode.

Polymer molecular weights (M_n, M_w) were determined by GPC using a Polymer Laboratories Plgel Mixed-D column (300 mm length, 7.5 mm diameter) and a Polymer Laboratories PL-GPC50 Plus instrument equipped with a refractive index detector. THF (HPLC grade) was used as an eluent at 30 °C with a rate of 1 mL min^{-1}. Linear polystyrenes were used as primary calibration standards, and Mark-Houwink corrections for poly(ε -CL) or poly(*rac*-LA) in THF were applied for the experimental samples.[1-3]

5.1. Literature Preparations.

The compounds $Mg\{N(SiMe_3)_2\}_2$,[4] $Mg\{N(SiHMe_2)_2\}_2$,[5] $Ca\{N(SiMe_3)_2\}_2(THF)_2$,[6] $Zn\{N(SiMe_3)_2\}_2$,[7] $Li\{C(Me_2pz)_3\}(THF)$,[8] $HC(Me_2pz)_3$,[9] $HC(pz)_3$,[9] 4-Etpz,[10] (3-^{t}Bu,5-Mepz),[11] $KTp^{tBu,Me}$,[12] $LiN(SiHMe_2)_2$,[13] $Y(CH_2SiMe_3)_3(THF)$,[14] $Me_3[9]aneN_3$,[15] $[NEt_3H][BPh_4]$[16] and $(Tp^{tBu,Me})Yb(BH_4)(THF)$[17] were prepared according to published procedures. $DC(Me_2pz)_3$ was synthesised by another student in the Mountford group.[18] All other compounds and reagents were purchased from commercial suppliers and used without further purification. ε-CL was dried over freshly ground CaH_2 and distilled before use. *Rac*-LA was recrystallised twice from toluene and then sublimed twice prior to use. Other reagents were obtained commercially and used as received.

5.2. Experimental details and characterising data for Chapter Two

$Mg\{C(Me_2pz)_3\}\{N(SiMe_3)_2\}$ (1). A solution of $Mg\{N(SiMe_3)_2\}_2$ (1.04 g, 3.02 mmol) in benzene (20 mL) was added to a solution of $HC(Me_2pz)_3$ (0.60 g, 2.0 mmol) in benzene (20 mL) at RT. The resulting yellow solution was stirred for 24 h and the volatiles were removed under reduced pressure, leaving an orange solid. This was extracted into pentane (3 x 15mL) and the solution concentrated and cooled to -30 ºC, yielding **1** as a microcrystalline orange solid. Yield: 0.54 g (50%). Diffraction quality crystals were grown from a saturated pentane solution at -30 ºC. ^{1}H NMR (C_6D_6, 299.9 MHz, 293 K): 5.42 (3H, s, $N_2C_3Me_2\underline{H}$), 2.28 (9H, s, 3-$N_2C_3\underline{Me}_2H$), 2.25 (9H, s, 5-$N_2C_3\underline{Me}_2H$) 0.47 (18H, s, $SiMe_3$) ppm. $^{13}C\{^1H\}$ NMR (C_6D_6, 299.9 MHz, 293 K): 149.3 (3-$N_2\underline{C}_3Me_2H$), 147.9 (5-$N_2\underline{C}_3Me_2H$), 104.8 (4-$N_2\underline{C}_3Me_2H$), 72.5 ($\underline{C}(Me_2pz)_3$), 15.1 (3-$N_2C_3\underline{Me}_2H$), 13.3 (5-$N_2C_3\underline{Me}_2H$), 7.3 ($SiMe_3$) ppm. IR (KBr plates, Nujol mull, cm^{-1}): 1570(s), 1259(m), 1004(m), 987 (m), 670(m), 631(m), 550(m), 492(m), 430(s). EI-MS: *m/z* = 481, (6 %), $[\underline{M}]^+$; 312 (100%), $[\underline{M} - N(SiMe_3)_2]^+$. Anal. found (calcd. for $C_{22}H_{39}MgN_7Si_2$): C, 54.75 (54.81); H, 8.11 (8.15); N, 20.29 (20.34) %.

$Mg\{\kappa^2$-*N*-$HC(Me_2pz)_3\}\{N(SiHMe_2)_2\}_2$ (2). A solution of $Mg\{N(SiHMe_2)_2\}_2$ (0.27 g, 1.0 mmol) in toluene (20 mL) was added to a solution of $HC(Me_2pz)_3$ (0.200 g, 0.67 mmol) in toluene (20 mL) at -78 ºC, which was then allowed to warm to RT and stirred for 2 h. Volatiles were removed under reduced pressure from the resulting yellow solution, leaving a yellow solid. This was washed with cold pentane (0 ºC, 3 x 10 mL) and dried *in vacuo*, yielding **2** as a microcrystalline, pale yellow solid. Yield: 0.26 g (65%). Diffraction-quality crystals were grown from a saturated toluene solution at -30 ºC. ^{1}H NMR (CD_2Cl_2, 499.9 MHz, 208 K): 7.57 (1H, s, $\underline{H}C(N_2C_3Me_2H)_3$), 6.15 (2H, s,

$N_2C_3Me_2\underline{H}$ (bound)), 5.85 (1H, s, $N_2C_3Me_2\underline{H}$ (pendant)), 4.60 (1H, br m, $SiMe_2\underline{H}$(3)), 4.29 (2H, br m, $SiMe_2\underline{H}$(1,2)), 3.05 (1H, br m, $SiMe_2\underline{H}$(4)) 2.49 (6H, s, 3-$N_2C_3\underline{Me_2}H$ (bound)), 2.43 (6H, s, 5-$N_2C_3\underline{Me_2}H$ (bound)), 1.97 (3H, s, 3-$N_2C_3\underline{Me_2}H$ (pendant)), 1.38 (3H, s, 5-$N_2C_3\underline{Me_2}H$ (pendant)), -0.01 (6H, br d, Si(3)$\underline{Me_2}H$), -0.30 (12H, br d, Si(1,2)H$\underline{Me_2}$), -0.48 (6H, br d, Si(4)$\underline{Me_2}H$) ppm (atom labels refer to the X-ray structure of **2**). IR (KBr plates, Nujol mull, cm^{-1}): 1548 (s), 1422 (s), 1318 (s), 1222 (s), 1069 (s), 998 (s), 867 (s), 813 (s), 701 (s), 629 (s), 426 (m). EI-MS: *m/z* = 586, (8 %), $[\underline{M}]^+$. Anal. found (calcd. for $C_{24}H_{50}MgN_8Si_4$): Found (Calculated): C, 49.65 (49.10); H, 8.10 (8.58); N, 19.55 (19.10) %. A satisfactory ^{13}C spectrum could not be obtained in the slow exchange limit.

Mg{κ^2*N*-D(Me$_2$pz)$_3$}{N(SiHMe$_2$)$_2$}$_2$ (2-*d*). A solution of $Mg\{N(SiHMe_2)_2\}_2$ (0.27 g, 1.0 mmol) in toluene (20 mL) was added to a solution of $DC(Me_2pz)_3$ (0.20 g, 0.67 mmol) in toluene (20 mL) at -78 ºC, which was then allowed to warm up to RT and stirred for 2 h. The volatiles were then removed under reduced pressure from the resulting yellow solution, leaving a yellow solid. This was washed with cold pentane (0 ºC, 3 x 10 mL) and dried *in vacuo*, yielding **2-*d*** as a microcrystalline pale yellow solid. Yield: 0.26 g (71 %). ^1H NMR (C_6D_6, 299.9 MHz, 293 K): Identical to that for **2** except for the absence of the $\underline{H}(Me_2pz)_3$ resonance. ^2H NMR (C_6H_6, 46.0 MHz, 293 K): 7.49 (s, $\underline{D}C(Me_2pz)_3$).

Mg{C(Me$_2$pz)$_3$}{N(SiHMe$_2$)$_2$} (3). A solution of $Mg\{N(SiHMe_2)_2\}_2$ (0.27 g, 1.0 mmol) in toluene (20 mL) was added to a solution of $HC(Me_2pz)_3$ (0.20 g, 0.67 mmol) in toluene (20 mL) at RT. The resulting yellow solution was stirred at 50 ºC for 3 d, after which time the solution became orange. Volatiles were removed under reduced pressure, leaving an orange solid. This was extracted into pentane (3 x 15 mL) and the solution concentrated and cooled to -30 ºC, yielding **3** as a microcrystalline orange solid. Yield: 0.15 g (49%).^1H NMR (C_6D_6, 299.9 MHz, 293 K): 5.43 (2H, sept, ^3J = 2.7 Hz, $SiMe_2\underline{H}$), 5.38 (3H, s, $N_2C_3Me_2\underline{H}$), 2.30 (9H, s, 3-$N_2C_3\underline{Me_2}H$), 2.26 (9H, s, 5-$N_2C_3\underline{Me_2}H$), 0.56 (12H, d, ^3J = 2.7 Hz, $Si\underline{Me_2}H$) ppm. $^{13}C\{^1H\}$ NMR (C_6D_6, 299.9 MHz, 293 K): 148.8 (3-$N_2\underline{C_3}Me_2H$), 147.1 (5-$N_2\underline{C_3}Me_2H$), 104.0 (4-$N_2\underline{C_3}Me_2H$), 71.9 ($\underline{C}(Me_2pz)_3$), 14.4 (3-$N_2C_3\underline{Me_2}H$), 12.9 (5-$N_2C_3\underline{Me_2}H$), 4.6 ($SiMe_2H$) ppm. IR (KBr plates, Nujol mull, cm^{-1}): 2726(s), 2362(s), 2065(s), 1556(s), 1457(s), 1307(s), 1260(s), 1050(m), 949(s), 890(s), 806(s), 666 (s), 475(m). EI-MS: *m/z* = 453 (5%), $[\underline{M}]^+$; 312 (100 %), $[\underline{M} - N(SiHMe_2)_2]^+$. Anal. found (calcd. for $C_{20}H_{35}MgN_7Si_2$): C, 52.91 (52.91); H, 7.64 (7.77); N, 21.44 (21.60) %.

NMR Tube Scale Synthesis of Mg{C(Me$_2$pz)$_3$}$_2$. From Mg{N(SiMe$_3$)$_2$}$_2$: A solution of Mg{N(SiMe$_3$)$_2$}$_2$ (11.5 mg, 33.6 μmol) and HC(Me$_2$pz)$_3$ (20.0 mg, 67.1 μmol) in C_6D_6 (0.8 mL) was heated at 70 ºC for 4 d to quantitatively form Mg{C(Me$_2$pz)$_3$}$_2$. From Mg{C(Me$_2$pz)$_3$}{N(SiRMe$_2$)$_2$}: A solution of Mg{C(Me$_2$pz)$_3$}{N(SiRMe$_2$)$_2$} (R = Me (**1**) or H (**3**), 67.1 μmol) and HC(Me$_2$pz)$_3$ (20.0 mg, 67.1 μmol) in C_6D_6 (0.8 mL) was heated at 70 ºC for 2 d (R = H) or 3 d (R = Me) to quantitatively form Mg{C(Me$_2$pz)$_3$}$_2$. The ^{1}H NMR resonances for Mg{C(Me$_2$pz)$_3$}$_2$ were identical to those previously reported.[19]

Ca{C(Me$_2$pz)$_3$}{N(SiMe$_3$)$_2$}(THF) (4). THF (20 mL) at -78 °C was added to a solid mixture of Ca{N(SiMe$_3$)$_2$}$_2$(THF)$_2$ (0.25 g, 0.50 mmol) and HC(Me$_2$pz)$_3$ (0.15 g, 0.50 mmol) at -78 ^{o}C which was then allowed to warm to RT and stirred for 2 h. The volatiles were removed under reduced pressure and the residue extracted into benzene (2 x 20 mL) leaving an insoluble beige solid (presumed to be Ca{C(Me$_2$pz)$_3$}$_2$). Volatiles were removed under reduced pressure to yield **4** as a yellow solid which was washed with benzene (2 x 10 mL) and dried *in vacuo*. Yield: 0.24 g (85%). Diffraction-quality crystals were grown from a saturated toluene solution at -30 ºC. ^{1}H NMR (C_6D_6, 299.9 MHz, 293 K): 5.58 (3H, s, $N_2C_3Me_2\underline{H}$), 3.54 (4H, br m, $OC\underline{H_2}CH_2$), 2.43 (9H, s, 3-$N_2C_3\underline{Me_2}H$), 2.26 (9H, s, 5-$N_2C_3\underline{Me_2}H$), 1.22 (4H, br m, $OCH_2C\underline{H_2}$) 0.41 (18H, s, $SiMe_3$) ppm. $^{13}C\{^1H\}$ NMR (C_6D_6, 299.9 MHz, 293 K): 147.0 (3-$N_2\underline{C_3}Me_2H$), 146.8 (5-$N_2\underline{C_3}Me_2H$), 103.2 (4-$N_2\underline{C_3}Me_2H$), 72.4 ($\underline{C}$(Me$_2$pz)$_3$), 69.5 ($OC\underline{H_2}CH_2$), 25.0 ($OCH_2C\underline{H_2}$), 14.8 (3-$N_2C_3\underline{Me_2}H$), 13.1 (5-$N_2C_3\underline{Me_2}H$), 5.9 ($SiMe_3$) ppm. IR (KBr plates, Nujol mull, cm^{-1}): 1553(m), 1423(m), 1391(m), 1246(m), 1236(m), 1217(w), 1155(w), 1057(s), 1037(s), 967(s), 876(m), 829(m), 788(m), 770(m), 745(m), 660(m), 607(m), 590(m). EI-MS: *m/z* = 569, (8 %), $[\underline{M}]^+$. Anal. found (calcd. for $C_{26}H_{47}CaN_7OSi_2$): C, 54.92 (54.79); H, 8.18 (8.31); N, 17.12 (17.20) %.

Ca{C(Me$_2$pz)$_3$}$_2$ (5). Ca{N(SiMe$_3$)$_2$}$_2$(THF)$_2$ (0.20 g, 0.40 mmol) and HC(Me$_2$pz)$_3$ (0.25 g, 0.84 mmol) were stirred together in benzene (20 mL) at RT for 16 h, giving a pale yellow solution and a sparingly soluble beige solid. This was filtered and washed with benzene (2 x 10 mL) and dried *in vacuo* to afford **5**. Yield: 0.16 g (61 %). Diffraction-quality crystals were grown from a saturated benzene solution at RT. ^{1}H NMR (C_6D_6, 299.9 MHz, 293 K): 5.65 (6H, s, $N_2C_3Me_2\underline{H}$),), 2.49 (18H, s, 3- or 5-$N_2C_3\underline{Me_2}H$), 1.95 (18H, s, 3- or 5-$N_2C_3\underline{Me_2}H$) ppm. IR (NaCl plates, Nujol mull, cm^{-1}): 1548(m), 1450(m), 1427(m), 1393(m), 1351(m), 1214(m), 1151(w), 1095(m), 1039(m), 975(w), 872(m), 792(m), 661(m). EI-MS: *m/z* = 634 (6 %), $[\underline{M}]^+$. Anal. found (calcd. for $C_{32}H_{42}CaN_{12}$): C,

60.51 (60.54); H, 6.53 (6.67); N, 26.46 (26.48) %. The compound was too insoluble to obtain a ^{13}C NMR spectrum.

Alternative NMR Tube Scale Synthesis of Ca{C(Me$_2$pz)$_3$}$_2$ (5). Ca{C(Me$_2$pz)$_3$}{N(SiMe$_3$)$_2$}(THF) (18, 38.2 mg, 67.1μmol) and HC(Me$_2$pz)$_3$ (20.0 mg, 67.1 μmol) were dissolved in C_6D_6 (0.8 mL). After 2 h at RT the ^1H NMR spectrum showed quantitative formation of Ca{C(Me$_2$pz)$_3$}$_2$ (**5**), the resonances for which were identical to those reported above.

Zn{C(Me$_2$pz)$_3$}Cl (6). A solution of Li{C(Me$_2$pz)$_3$}(THF) in THF (20 mL) was added to a solution of $ZnCl_2$ (3.52 mL of a 1.0 M solution in Et_2O, 3.52 mmol) in THF (20 mL), giving a pale suspension. The mixture was heated at 70 ºC for 24 h, after which time the volatiles were removed under reduced pressure to leave an orange solid. This was extracted into hot benzene (65 ºC, 3 x 30 mL) and the volatiles were removed under reduced pressure to give **6** as an analytically pure, yellow powder. Yield: 0.51 g (40 %). Diffraction-quality crystals were grown from a pentane-layered THF solution. ^1H NMR (C_6D_6, 299.9 MHz, 293 K): 5.32 (3H, s, $N_2C_3Me_2\underline{H}$), 2.26 (9H, s, 3-$N_2C_3\underline{Me}_2H$), 2.18 (9H, s, 5-$N_2C_3\underline{Me}_2H$). $^{13}C\{^1H\}$ NMR (C_6D_6, 299.9 MHz, 293 K): 148.9 (3-$N_2\underline{C}_3Me_2H$), 146.8 (5-$N_2\underline{C}_3Me_2H$), 104.1 (4-$N_2\underline{C}_3Me_2H$), 73.0 ($\underline{C}$(Me$_2$pz)$_3$), 13.6 (3-$N_2C_3\underline{Me}_2H$), 12.5 (5-$N_2C_3\underline{Me}_2H$) ppm. IR (KBr plates, Nujol mull, cm^{-1}): 1700 (s), 1260 (s), 1100(s), 1057(m), 801(s), 666(s), 465 (s). EI-MS: *m/z* = 396 (5 %), [$\underline{M}$]$^+$; 361 (100 %), [$\underline{M}$ - Cl]$^+$. Anal. found (calcd. for $C_{16}H_{21}ClN_6Zn$): C, 48.16 (48.26); H, 5.30 (5.32); N, 20.93 (21.10) %.

Zn{C(Me$_2$pz)$_3$}{N(SiMe$_3$)$_2$} (7). NaN(SiMe$_3$)$_2$ (0.75 mL of a 1.0 M solution in THF, 0.75 mmol), was added to a solution of Zn{C(Me$_2$pz)$_3$}Cl (0.28 g, 0.70 mmol) in benzene (20 mL). The resulting yellow suspension was stirred at RT for 4 h, after which time the volatiles were removed under reduced pressure, leaving a yellow solid. This was extracted into hot hexanes (70 ºC, 3 x 15 mL) and the solution was concentrated and cooled to -30 ºC, giving **7** as an analytically pure, yellow powder. Yield: 0.25 g (68 %). Diffraction-quality crystals were grown from hexanes at RT. ^1H NMR (C_6D_6, 299.9 MHz, 293 K): 5.59 (3H, s, $N_2C_3Me_2\underline{H}$), 2.29 (18H, br, s, overlapping 3- and 5- $N_2C_3\underline{Me}_2H$), 0.47 (18H, s, Si$\underline{Me}_3$) ppm. $^{13}C\{^1H\}$ NMR (C_6D_6, 299.9 MHz, 293 K): 148.8 (3-$N_2\underline{C}_3Me_2H$), 147.0 (5-$N_2\underline{C}_3Me_2H$), 104.6 (4-$N_2\underline{C}_3Me_2H$), 72.8 ($\underline{C}$(Me$_2$pz)$_3$), 15.4 (3-$N_2C_3\underline{Me}_2H$), 13.2 (5-$N_2C_3\underline{Me}_2H$), 7.4 (SiMe$_3$) ppm. IR (KBr plates, Nujol mull, cm^{-1}): 1558(s), 1260 (s), 1093 (m), 987 (m) 802 (s), 666(s), 472(m). EI-MS: *m/z* = 521 (100 %), [$\underline{M}$]$^+$; 361 (10%), [$\underline{M}$ –

$N(SiMe_3)_2]^+$. Anal. found (calcd. for $C_{22}H_{39}N_7Si_2Zn$): C, 50.64 (50.51); H, 7.58 (7.51); N, 18.92 (18.74) %.

$Zn\{C(Me_2pz)_3\}\{N(SiHMe_2)_2\}$ (8). Benzene (30 mL) was added to a solid mixture of $LiN(SiHMe_2)_2$ (0.11 g, 0.80 mmol) and $Zn\{C(Me_2pz)_3\}Cl$ (0.30 g, 0.75 mmol). The resulting yellow suspension was stirred at RT for 4 h and the volatiles were removed under reduced pressure to give a yellow solid. This was extracted into hot hexanes (70 ºC, 3 x 15 mL), filtered and the solution concentrated and cooled to -30 ºC, giving **8** as an analytically pure, yellow powder. Yield: 0.28 g (75 %). ^{1}H NMR (C_6D_6, 299.9 MHz, 293 K): 5.44 (2H, sept, ^3J = 2.7 Hz, $SiMe_2\underline{H}$), 5.38 (3H, s, $N_2C_3Me_2\underline{H}$), 2.29 (18H, br, s, overlapping 3- and 5- $N_2C_3\underline{Me}_2H$), 0.57 (12H, d, ^3J = 2.7 Hz, $Si\underline{Me}_2H$) ppm. $^{13}C\{^1H\}$ NMR (C_6D_6, 125.7 MHz, 293 K): 148.0 (3-$N_2\underline{C}_3Me_2H$), 146.1 (5-$N_2\underline{C}_3Me_2H$), 103.8 (4-$N_2\underline{C}_3Me_2H$), 71.3 ($\underline{C}(Me_2pz)_3$), 14.3 (3-$N_2C_3\underline{Me}_2H$), 12.3 (5-$N_2C_3\underline{Me}_2H$), 4.2 ($Si\underline{Me}_2H$) ppm. IR (KBr plates, Nujol mull, cm^{-1}): 1559 (s), 1269 (s), 1094 (s), 1020 (s), 883 (s), 802 (s), 666 (s), 469 (m). EI-MS: *m/z* = 493 (6 %), $[\underline{M}]^+$; 361 (100 %), $[\underline{M} - N(SiHMe_2)_2\}]^+$. Anal. found (calcd. for $C_{22}H_{39}N_7Si_2Zn$): C, 48.43 (48.52); H, 7.17 (7.13); N, 19.75 (19.80) %.

$Zn\{C(Me_2pz)_3\}_2$ (9). A solution of $Li\{C(Me_2pz)_3\}(THF)$ (1.20 g, 3.20 mmol) in THF (30 mL) was added to a solution of $ZnCl_2$ (1.59 mL of a 1.0 M solution in Et_2O, 1.59 mmol) in THF (20 mL) and the mixture was heated at 70 ºC for 3 d, forming a dark orange suspension. Volatiles were removed under reduced pressure to leave an orange solid. This was extracted into hot toluene (80 ºC, 3 x 30 mL), filtered, concentrated and cooled to -30 ºC. Compound **9** was isolated as an analytically pure, white powder. Yield: 0.10 g (9 %). Diffraction-quality crystals were grown from hexanes at RT. ^{1}H NMR (C_6D_6, 299.9 MHz, 293 K): 5.63 (6H, s, $N_2C_3Me_2\underline{H}$), 2.52 (18H, s, 3-$N_2C_3\underline{Me}_2H$), 1.68 (18H, s, 5-$N_2C_3\underline{Me}_2H$) ppm. $^{13}C\{^1H\}$ NMR (C_6D_6, 299.9 MHz, 293 K): 147.5 (3-$N_2\underline{C}_3Me_2H$), 145.1 (5-$N_2\underline{C}_3Me_2H$), 102.5 (4-$N_2\underline{C}_3Me_2H$), 72.9 ($\underline{C}(Me_2pz)_3$), 13.1 (3-$N_2C_3\underline{Me}_2H$), 12.8 (5-$N_2C_3\underline{Me}_2H$) ppm. IR (NaCl plates, Nujol mull, cm^{-1}): 1636 (s), 1260 (s), 1100 (m), 1057(m), 809 (m), 665 (w). EI-MS: *m/z* = 658 (8 %), $[\underline{M}]^+$. Anal. found (calcd. for $C_{32}H_{42}N_{12}Zn$): C, 58.12 (58.22); H, 6.31 (6.41); N, 25.48 (25.46) %.

$Mg\{C(Me_2pz)_3\}\{C(pz)_3\}$ (10). A solution of $HC(pz)_3$ (0.13 g, 0.61 mmol) in benzene (20 mL) was added dropwise to a solution of **1** (0.30 g, 0.61 mmol) in benzene (20 mL). The resulting dark red suspension was heated to 70 °C for 24 h. Volatiles were removed under reduced pressure to leave an orange solid. This was extracted into hot hexanes (70 °C, 3 x 15 mL), filtered, concentrated and cooled to -30 °C. Compound **10** was isolated as an off-

white solid. Yield: 0.18 g (55 %). Diffraction-quality crystals were grown from a saturated hexanes solution at RT. ^{1}H NMR (C_6D_6, 299.9 MHz, 293 K): 7.88 (3H, d, ^{3}J = 1.24 Hz, 5-$N_2C_3\underline{H}$), 7.18 (3H, d, ^{3}J = 1.24 Hz, 3-$N_2C_3\underline{H}$), 5.67 (3H, dd, ^{3}J = 1.24, 1.81 Hz, 4-$N_2C_3\underline{H}$), 5.62 (3H, s, $N_2C_3Me_2\underline{H}$), 2.58 (9H, s, 3-$N_2C_3\underline{Me_2}H$), 1.58 (9H, s, 5-$N_2C_3\underline{Me_2}H$) ppm. ^{13}C{^{1}H} NMR (C_6D_6, 75.4 MHz, 293 K): 147.8 (3-$N_2\underline{C_3}Me_2H$), 145.6 (5-$N_2\underline{C_3}Me_2H$), 139.6 (3-$N_2\underline{C_3}H_3$), 137.2 (5-$N_2\underline{C_3}H_3$), 103.6 (4-$N_2\underline{C_3}H_3$), 103.3 (4-$N_2\underline{C_3}Me_2H$), 89.1 ($\underline{C}(pz)_3$), 72.1 ($\underline{C}(Me_2pz)_3$), 13.4 (3-$N_2C_3\underline{Me_2}H$), 12.7 (5-$N_2C_3\underline{Me_2}H$) ppm. IR (KBr plates, Nujol mull, cm^{-1}): 3750 (s), 1558 (s), 1308 (m), 868 (s), 783 (s), 760 (s), 613 (s), 572 (s), 465 (s). EI-MS: *m/z* = 534 (10 %), $[\underline{M}]^+$. Anal. found (calcd. for $C_{26}H_{30}MgN_{12}$): C, 58.34 (58.40); H, 5,76 (5.66); N, 31.36 (31.45) %.

Ca{C(Me$_2$pz)$_3$}{C(pz)$_3$} (11). A solution of $HC(pz)_3$ (0.13 g, 0.60 mmol) in benzene (20 mL) was added dropwise to a solution of **4** (0.35 g, 0.60 mmol) in benzene (20 mL). The resulting dark red suspension was stirred at RT for 24 h. Volatiles were removed under reduced pressure to leave an orange solid. Recrystallisation from a saturated toluene solution at -30 °C yielded **11** as an analytically pure, beige solid. Yield: 0.24 g, (73 %). ^{1}H NMR (C_6D_6, 299.9 MHz, 293 K): 7.95 (3H, d, ^{3}J = 1.21 Hz, 5-$N_2C_3\underline{H}$), 7.21 (3H, s, ^{3}J = 1.21 Hz, 3-$N_2C_3\underline{H}$), 5.75 (3H, dd, ^{3}J = 1.21, 1.82 Hz, 4-$N_2C_3\underline{H}$), 5.65 (3H, s, $N_2C_3Me_2\underline{H}$), 2.55 (9H, s, 3-$N_2C_3\underline{Me_2}H$), 1.90 (9H, s, 5-$N_2C_3\underline{Me_2}H$) ppm. ^{13}C{^{1}H} NMR (C_6D_6, 75.4 MHz, 293 K): 147.7 (3-$N_2\underline{C_3}Me_2H$), 145.5 (5-$N_2\underline{C_3}Me_2H$), 139.6 (3-$N_2\underline{C_3}H_3$), 137.1 (5-$N_2\underline{C_3}EtH$), 103.5 (4-$N_2\underline{C_3}H_3$), 103.2 (4-$N_2\underline{C_3}Me_2H$), 89.0 ($\underline{C}(pz)_3$), 72.8 ($\underline{C}(Me_2pz)_3$, 17.5 ($N_2C_3\underline{C}H_2CH_3$), 13.2 (3-$N_2C_3\underline{Me_2}H$), 12.6 (5-$N_2C_3\underline{Me_2}H$) ppm IR (KBr plates, Nujol mull, cm^{-1}): 1531 (s), 1418 (s), 1220 (s), 1127 (s), 927 (m), 772 (s) , 615 (s), 423 (s). EI-MS: *m/z* = 550 (20 %), $[\underline{M}]^+$. Anal. found (calcd. for $C_{26}H_{30}CaN_{12}$): C, 56.56 (56.70); H, 5.51 (5.49); N, 30.52 (30.54) %.

HC(4-Etpz)$_3$} (12). Distilled water (200 mL) was added to a 1 L flask containing a mixture of 4-ethyl pyrazole (11.1 g, 0.12 mol) and tetra-*n*-butylammonium bromide (2.25g, 7.0 mol). With vigorous stirring, sodium carbonate (64 g, 0.60 mol) was added gradually to the reaction mixture. After cooling to RT, chloroform (100mL) was added and the flask equipped with a reflux condenser. The mixture was heated at gentle reflux for 24 h, during which time it became an orange/ red emulsion. The mixture was allowed to cool to RT, filtered through a Büchner funnel to remove the excess base, and the organic layer separated from the aqueous layer. The organic layer was washed with distilled water (3 x 25 mL) and dried over sodium sulfate. The drying agent was removed by filtration and the solvent was removed by rotary evaporation. The resulting brown

residue was dissolved in CH_2Cl_2 (50 mL) and passed through a silica plug with CH_2Cl_2 (2 x 200 mL). The solvent was removed by rotary evaporation to afford an analytically pure off-white solid. Yield: 6.20 g (54 %). Diffraction-quality crystals were grown from a saturated benzene solution at RT. ^{1}H NMR (C_6D_6, 299.9 MHz, 293 K): 8.43 (1H, s, H$\underline{C}$(4-Etpz)$_3$), 7.38 (3H, s, 5-$N_2C_3Et\underline{H}_2$), 7.29 (3H, s, 3-$N_2C_3Et\underline{H}_2$) 2.13 (6H, q, ^3J = 8.6 Hz, $C\underline{H}_2$), 0.87 (9H, t, ^3J = 8.6 Hz, $C\underline{H}_3$) ppm. ^{13}C{^{1}H} NMR (C_6D_6, 75.4 MHz, 293 K): 140.5 (3-$N_2\underline{C}_3EtH_2$), 126.7 (5-$N_2\underline{C}_3EtH_2$), 124.4 (4-$N_2\underline{C}_3EtH_2$), 83.6 (H$\underline{C}$(4-Etpz)$_3$), 17.1 ($\underline{C}H_2$), 14.5 ($\underline{C}H_3$) ppm. IR (KBr plates, Nujol mull, cm^{-1}): 2726 (s), 2641 (s), 1310 (s), 1165 (s), 918 (s) , 815 (s). EI-MS: *m/z* = 219 (100 %), [$\underline{M}$]$^+$. Anal. found (calcd. for $C_{16}H_{23}N_6$): C, 64.30 (64.40); H, 7.28 (7.43); N, 27.94 (28.16) %.

Mg{C(Me$_2$pz)$_3$}{C(4-Etpz)$_3$} (13). A solution of HC(4-Etpz)$_3$ (**12**) (0.30 g, 1.01 mmol) in benzene (20 mL) was added dropwise to a solution of **1** (0.49 g, 1.01 mmol) in benzene (20 mL). The resulting dark red suspension was stirred at 70 °C for 24 h. Volatiles were removed under reduced pressure to leave an orange solid. Recrystallisation from a saturated toluene:pentane solution (1:3 v/v) at -30 °C yielded **13** as an analytically pure, beige solid. Yield: 0.29 g (46 %). ^{1}H NMR (C_6D_6, 299.9 MHz, 293 K): 7.82 (3H, s, 5-$N_2C_3Et\underline{H}_2$), 6.99 (3H, s, 3-$N_2C_3Et\underline{H}_2$), 5.67 (3H, s, $N_2C_3Me_2\underline{H}$), 2.60 (9H, s, 5-$N_2C_3\underline{Me}_2H$), 2.12 (6H, q, ^3J = 7.5 Hz, $C\underline{H}_2CH_3$), 1.66 (9H, s, 3-$N_2C_3\underline{Me}_2H$), 0.83 (9H, t, ^3J = 7.5 Hz, $CH_2C\underline{H}_3$) ppm. ^{13}C{^{1}H} NMR (C_6D_6, 75.4 MHz, 293 K): 147.7 (3-$N_2\underline{C}_3Me_2H$), 145.4 (5-$N_2\underline{C}_3Me_2H$), 138.3 (3-$N_2\underline{C}_3EtH_2$), 135.1 (5-$N_2\underline{C}_3EtH_2$), 120.5 (4-$N_2\underline{C}_3EtH_2$), 103.4 (4-$N_2\underline{C}_3Me_2H$), 90.0 ($\underline{C}$(4-Etpz)$_3$), 73.1 ($\underline{C}$(Me$_2$pz)$_3$), 17.5 ($\underline{C}H_2CH_3$), 15.4 ($CH_2\underline{C}H_3$) 13.4 (3-$N_2C_3\underline{Me}_2H$), 12.6 (5-$N_2C_3\underline{Me}_2H$) ppm. IR (KBr plates, Nujol mull, cm^{-1}): 2726 (m), 1703 (s), 1663 (w), 1261 (s), 1143 (s), 851 (s). EI-MS: *m/z* = 618 (40 %), [$\underline{M}$]$^+$. Anal. found (calcd. for $C_{32}H_{42}MgN_{12}$): C, 62.03 (62.10); H, 6.96 (6.85); N, 27.27 (27.18) %.

Ca{C(Me$_2$pz)$_3$}{C(4-Etpz)$_3$} (14). A solution of HC(4-Etpz)$_3$ (**12**) (0.13 g, 0.44 mmol) in benzene (20 mL) was added dropwise to a solution of **4** (0.25 g, 0.44 mmol) in benzene (20 mL). The resulting dark red suspension was stirred at RT for 24 h. Volatiles were removed under reduced pressure to leave an orange solid. Recrystallisation from a saturated toluene solution at -30 °C yielded **14** as an analytically pure, beige solid. Yield: 0.19 g (68 %). ^{1}H NMR (C_6D_6, 299.9 MHz, 293 K): 7.97 (3H, s, 5-$N_2C_3Et\underline{H}_2$), 7.25 (3H, s, 3-$N_2C_3Et\underline{H}_2$), 5.79 (3H, s, $N_2C_3Me_2\underline{H}$), 2.69 (9H, s, 5-$N_2C_3\underline{Me}_2H$), 2.29 (6H, q, ^3J = 7.6 Hz, $C\underline{H}_2CH_3$), 2.07 (9H, s, 3-$N_2C_3\underline{Me}_2H$), 1.02 (9H, t, ^3J = 7.6 Hz, $CH_2C\underline{H}_3$) ppm. ^{13}C{^{1}H} NMR (C_6D_6, 75.4 MHz, 293 K): 147.3 (3-$N_2\underline{C}_3Me_2H$), 146.8 (5-$N_2\underline{C}_3Me_2H$),

138.3 (3-$N_2\underline{C}_3EtH_2$), 136.7 (5-$N_2\underline{C}_3EtH_2$), 120.5 (4-$N_2\underline{C}_3EtH_2$), 102.9 (4-$N_2\underline{C}_3Me_2H$), 90.8 ($\underline{C}$(4-Etpz)$_3$), 73.3 ($\underline{C}(Me_2pz)_3$, 17.5 ($\underline{C}H_2CH_3$), 15.1 ($CH_2\underline{C}H_3$), 13.9 (3-$N_2C_3\underline{Me}_2H$), 13.1 (5-$N_2C_3\underline{Me}_2H$) ppm. IR (KBr plates, Nujol mull, cm^{-1}): 2726 (m), 2178 (s), 1685 (s), 1425 (s), 1310 (s), 1260 (s), 1169 (s), 1093 (m), 846 (s), 674 (s). EI-MS: *m/z* = 550 (45 %), $[\underline{M}]^+$. Anal. found (calcd. for $C_{32}H_{42}CaN_{12}$): C, 60.32 (60.57); H, 6.55 (6.71); N, 26.31 (26.51) %.

Mg{HC(^{t}Bu$_2$pz)$_2$SiMe$_2$NPh}{N(SiMe$_3$)$_2$} (15). To a solution of Mg{N(SiMe$_3$)$_2$}$_2$ (0.30 g, 0.87 mmol) in benzene (15 mL) was added slowly HC(^{t}Bu$_2$pz)$_2$SiMe$_2$N(H)Ph (0.45 g, 0.87 mmol) in benzene (15 mL). The mixture was heated to 60 °C and stirred for 6 h. Volatiles were removed under reduced pressure to give a pale yellow solid. Recrystallisation from a saturated pentane solution at -30 °C yielded **15** as an analytically pure, off-white solid. Yield: 0.30 g (49 %). ^{1}H NMR (C_6D_6, 299.9 MHz, 293 K): 7.24 (2 H, app. t, app. ^3J = 7.9 Hz, 3-C_6H_5), 6.98 (2 H, d, ^3J = 7.1 Hz, 2-C_6H_5), 6.83 (1 H, app. t, app. ^3J = 7.9 Hz, 4-C_6H_5), 6.21 (1 H, s, $\underline{H}C(^tBu_2pz)_2$), 6.05 (2 H, s, $N_2C_3\underline{H}^tBu_2$), 1.61 (18 H, s, 3-$N_2C_3H^t\underline{Bu}_2$), 1.07 (18 H, s, 5-$N_2C_3H^t\underline{Bu}_2$), 0.36 (18 H, Si$\underline{Me}_3$), -0.08 (6 H, s, Si$\underline{Me}_2$) ppm. ^{13}C{^{1}H} NMR (C_6D_6, 75.4 MHz, 293 K): 165.4 (3-$N_2\underline{C}_3H^tBu_2$), 156.8 (1-$C_6H_5$), 156.3 (5-$N_2\underline{C}_3H^tBu_2$), 128.4 (3-$C_6H_5$), 126.9 (2-$C_6H_5$), 118.0 (4-$C_6H_5$), 104.8 (4-$N_2\underline{C}_3H^tBu_2$), 68.5 ($H\underline{C}(^tBu_2pz)_2$), 32.8 (5-$N_2C_3H(\underline{C}Me_3)_2$), 32.6 (3-$N_2C_3H(\underline{C}Me_3)_2$), 31.4 (5-$N_2C_3H(C\underline{Me}_3)_2$), 31.2 (3-$N_2C_3H(C\underline{Me}_3)_2$), 6.1 (Si$\underline{Me}_3$), 0.2 (Si$\underline{Me}_2$) ppm. IR (NaCl plates, Nujol, cm^{-1}): 2726 (s), 2670 (m), 1589 (w), 1549 (w), 1196 (w), 1167 (w), 1067 (s), 951 (w), 837 (m). Anal. found (calcd. for $C_{37}H_{68}MgN_6Si_3$): C, 59.07 (62.99); H, 9.19 (9.71); N, 11.21 (11.91) %. This was the best of several attempts.

Mg{HC(^{t}Bu$_2$pz)$_2$SiMe$_2$NPh}{N(SiHMe$_2$)$_2$} (16). To a solution of Mg{N(SiHMe$_2$)$_2$}$_2$ (0.17 g, 0.59 mmol) in benzene (15 mL) was added slowly HC(^{t}Bu$_2$pz)$_2$SiMe$_2$N(H)Ph (0.31 g, 0.59 mmol) in benzene (15 mL). The mixture was heated to 60 °C and stirred for 24 h. Volatiles were removed under reduced pressure to give a pale yellow solid. Recrystallisation from a saturated pentane solution at -30 °C yielded **16** as an analytically pure, off-white solid. Yield: 0.21 g (53 %). Diffraction-quality crystals were grown from a saturated pentane solution at -30 °C. ^{1}H NMR (C_6D_6, 299.9 MHz, 293 K): 7.26 (2 H, app. t, app. ^3J = 7.9 Hz, 3-C_6H_5), 7.01 (2 H, d, ^3J = 7.1 Hz, 2-C_6H_5), 6.84 (1 H, app. t, app. ^3J = 7.9 Hz, 4-C_6H_5), 6.30 (1 H, s, $\underline{H}C(^tBu_2pz)_2$), 6.03 (2 H, s, $N_2C_3\underline{H}^tBu_2$), 5.24 (2H, sept, ^3J = 2.7 Hz, SiMe$_2\underline{H}$), 1.59 (18 H, s, 3-$N_2C_3H^t\underline{Bu}_2$), 1.11 (18 H, s, 5-$N_2C_3H^t\underline{Bu}_2$), 0.38 (12 H, ^3J = 2.7 Hz, SiH$\underline{Me}_2$), -0.05 (6 H, s, Si$\underline{Me}_2$) ppm. ^{13}C{^{1}H} NMR (C_6D_6, 75.4 MHz, 293 K): 165.5 (3-$N_2\underline{C}_3H^tBu_2$), 156.8 (1-$C_6H_5$), 155.9 (5-$N_2\underline{C}_3H^tBu_2$), 128.8 (3-$C_6H_5$), 126.4

(2-C_6H_5), 117.5 (4-C_6H_5), 104.7 (4-$N_2\underline{C}_3H^tBu_2$), 69.0 ($H\underline{C}(^tBu_2pz)_2$), 33.1 (5-$N_2C_3H(\underline{C}Me_3)_2$), 33.0 (3-$N_2C_3H(\underline{C}Me_3)_2$), 31.6 (5-$N_2C_3H(C\underline{Me}_3)_2$), 31.4 (3-$N_2C_3H(C\underline{Me}_3)_2$), 3.7 ($SiH\underline{Me}_2$), 0.4 ($Si\underline{Me}_2$) ppm. IR (NaCl plates, Nujol, cm^{-1}): 2854 (s), 2058 (m), 1586 (w), 1261 (w), 1093 (s), 976 (w), 886 (m), 759 (w). EI-MS: *m/z* 676 [*M*-Mg{N($SiHMe_2)_2$}-NPh]$^+$ (20 %). Anal. found (calcd. for $C_{35}H_{64}MgN_6Si_3$): C, 62.0 (62.09); H, 9.57 (9.54); N, 12.36 (12.42) %.

5.3. Experimental details and characterising data for Chapter Three

[Ca(BH_4)(THF)$_5$][BPh_4] (17-BPh_4). A solution of [Et_3NH][BPh_4] (3.94 g, 9.40 mmol) in THF (20 mL) was added to a solution of $Ca(BH_4)_2(THF)_2$ (2.00 g, 9.40 mmol) in THF (20 mL) at -78 °C. The resulting white suspension was stirred for 30 min at this temperature, then allowed to warm to RT and stirred for a further 2 h (gas evolution was observed). Volatiles were removed under reduced pressure, leaving a white solid. This was extracted into THF (3 x 15 mL), and the solution concentrated and cooled to -30 °C, yielding **17-BPh_4** as a colourless microcrystalline solid. Yield: 3.50 g (51 %). Diffraction-quality crystals were grown from a saturated THF solution at -30 °C. ^{1}H NMR (CD_2Cl_2, 299.9 MHz, 293 K): 7.35 (8 H, m, *o*-B(C_6H_5)$_4$), 7.05 (8 H, t, ^3J = 7.5 Hz, *m*-B(C_6H_5)$_4$), 6.90 (4 H, t, ^3J = 7.5 Hz, *p*-B(C_6H_5)$_4$), 3.83 (20 H, m, $OC\underline{H}_2CH_2$), 1.95 (20 H, m, $OCH_2C\underline{H}_2$), -0.19 (4 H, q, $B\underline{H}_4$, $^1J_{BH}$ = 82 Hz) ppm. ^{13}C{^{1}H} NMR (CD_2Cl_2, 75.5 MHz, 293 K): 164.4 (*i*-B(C_6H_5)$_4$), 153.3 (136.3 (*o*-B(C_6H_5)$_4$), 125.9 (*m*-B(C_6H_5)$_4$), 122.1 (*p*-B(C_6H_5)$_4$), 69.2 ($O\underline{C}H_2CH_2$), 25.7 ($OCH_2\underline{C}H_2$) ppm. ^{11}B{^{1}H} NMR (CD_2Cl_2, 96.2 MHz, 293 K): -6.6 (BPh_4), -36.1 (BH_4). IR (NaCl plates, Nujol mull, cm^{-1}): 2725 (s), 2670 (s), 2336 (s), 2261 (s), 2217 (s), 1261 (s), 1150 (m), 1092 (s), 1023 (s), 870 (m), 705 (s). IR (NaCl cell, THF, ν(B-H), cm^{-1}): 2406 (s, B-H_t of BH_4), 2260 and 2208 (s, B-H_b of BH_4 ; 52 cm^{-1} splitting). ES$^+$-MS (THF): *m/z* = 415 [*M*]$^+$. Anal. found (calcd. for $C_{44}H_{64}B_2CaO_5$): C, 71.75 (71.93); H, 8.72 (8.78) %.

[Ca{HC($Me_2pz)_3$}(BH_4)(THF)$_2$][BPh_4] (18-BPh_4). A solution of $HC(Me_2pz)_3$ (0.30 g, 1.00 mmol) in CH_2Cl_2 (20 mL) was added dropwise to a solution of [Ca(BH_4)(THF)$_5$][BPh_4] (0.67 g, 1.00 mmol) in CH_2Cl_2 (20 mL) at -78 °C. The resulting pale yellow solution was stirred at this temperature for 2 h, then allowed to warm to RT and stirred for a further 2 h. Volatiles were removed under reduced pressure, leaving a spongy yellow solid. Recrystallisation from CH_2Cl_2:pentane (1:3 v/v) at -30 °C, gave **18-BPh_4** as an off-white microcrystalline solid. Yield: 0.61 g (74 %). Diffraction-quality crystals were grown from a hexane-layered CH_2Cl_2 solution at RT. ^{1}H NMR (CD_2Cl_2, 299.9 MHz, 293 K): 7.80 (1 H, s, $\underline{H}C(N_2C_3Me_2H)_3$), 7.33 (8 H, m, *o*-B($C_6H_5$)$_4$), 7.00 (8

H, t, ^{3}J = 7.2 Hz, *m*-B(C_6H_5)$_4$), 6.84 (8 H, t, ^{3}J = 7.2 Hz, *p*-B(C_6H_5)$_4$), 5.98 (3 H, s, $N_2C_3Me_2\underline{H}$), 3.82 (8 H, m, OC$\underline{H}_2CH_2$), 2.41 (9 H, s, 3-$N_2C_3\underline{Me}_2H$), 2.29 (9 H, s, 5-$N_2C_3\underline{Me}_2H$), 1.94 (8 H, $OCH_2C\underline{H}_2$), 0.15 (4 H, q, B$\underline{H}_4$, $^{1}J_{BH}$ = 82 Hz) ppm. $^{13}C\{^{1}H\}$ NMR (CD_2Cl_2, 75.5 MHz, 293 K): 164.5 (*i*-B(C_6H_5)$_4$), 153.3 (3-$N_2\underline{C}_3Me_2H$), 141.5 (5-$N_2\underline{C}_3Me_2H$), 136.3 (*o*-B(C_6H_5)$_4$), 125.9 (*m*-B(C_6H_5)$_4$), 122.1 (*p*-B(C_6H_5)$_4$), 69.2 (overlapping H$\underline{C}$($N_2C_3Me_2H$)$_3$ and O$\underline{C}H_2CH_2$), 25.7 ($OCH_2\underline{C}H_2$), 14.0 (3-$N_2C_3\underline{Me}_2H$), 11.4 (5-$N_2C_3\underline{Me}_2H$) ppm. $^{11}B\{^{1}H\}$ NMR (CD_2Cl_2, 96.2 MHz). $^{11}B\{^{1}H\}$ NMR (CD_2Cl_2, 96.2 MHz, 293 K): δ = -6.9 (BPh_4), -35.6 (BH_4). IR (NaCl plates, Nujol mull, cm^{-1}): 2725 (s), 2670(s), 2336(s), 2269(s), 2214(s), 1306 (s), 1260(s), 1154(m), 1098(m), 1032(s), 977(s), 858(s). IR (NaCl cell, THF, ν(B-H), cm^{-1}): 2410 (s, B-H_t of BH_4), 2270 and 2220 (s, B-H_b of BH_4; 50 cm^{-1} splitting). ES^{+}-MS (THF): *m/z* = 426 ([$\underline{M}$-THF]$^{+}$), 353 ([$\underline{M}$-(THF)$_2$]$^{+}$). Anal. found (calcd. For $C_{52}H_{70}B_2Ca_1N_6O_3$ (**18-BPh$_4$**·THF)): C, 69.98 (70.27); H, 7.93 (7.94); N, 9.43 (9.45) %.

[Ca{HC(Me$_2$pz)$_3$}$_2$][BPh$_4$]$_2$ (19-[BPh$_4$]$_2$). A solution of HC(Me_2pz)$_3$ (0.30 g, 1.00 mmol) in THF (20 mL) was added to a solution of [Ca(BH_4)(THF)$_5$][BPh_4] (0.67 g, 1.00 mmol) in THF (20 mL) at RT. The resulting white suspension was stirred for 2 h. Volatiles were removed under reduced pressure, leaving a white solid. Recrystallisation from THF:pentane (1:2 v/v) at -30 °C, gave **19-[BPh$_4$]$_2$** as a colourless microcrystalline solid. Yield: 0.61 g (52 %). Diffraction-quality crystals were grown from a saturated CH_2Cl_2 solution at RT. ^{1}H NMR (CD_2Cl_2, 299.9 MHz, 293 K): 7.90 (2 H, s, $\underline{H}C(N_2C_3Me_2H)_3$), 7.30 (16 H, m, *o*-B($C_6H_5$)$_4$), 6.96 (16 H, t, ^{3}J = 6.6 Hz, *m*-B(C_6H_5)$_4$), 6.81 (8 H, t, ^{3}J = 6.6 Hz, *p*-B(C_6H_5)$_4$), 6.04 (6 H, s, $N_2C_3Me_2\underline{H}$), 2.44 (18 H, s, 3-$N_2C_3\underline{Me}_2H$), 1.96 (18 H, s, 5-$N_2C_3\underline{Me}_2H$) ppm. $^{13}C\{^{1}H\}$ NMR (CD_2Cl_2, 75.5 MHz, 293 K): 164.4 (*i*-B(C_6H_5)$_4$), 153.6 (3-$N_2\underline{C}_3Me_2H$), 143.4 (5-$N_2\underline{C}_3Me_2H$) 136.3 (*o*-B(C_6H_5)$_4$), 126.0 (*m*-B(C_6H_5)$_4$), 122.1 (*p*-B(C_6H_5)$_4$), 108.7 (4-$N_2\underline{C}_3Me_2H$), 68.1 (H$\underline{C}$($N_2C_3Me_2H$)$_3$), 13.4 (3-$N_2C_3\underline{Me}_2H$), 11.7 (5-$N_2C_3\underline{Me}_2H$) ppm. $^{11}B\{^{1}H\}$ NMR (CD_2Cl_2, 96.2 MHz, 293 K): -6.6 (BPh_4). IR (NaCl plates, Nujol mull, cm^{-1}): 1559(s), 1306(s), 1259(s), 1152(s), 1107(s), 1039(m), 977(m), 898(s), 856(s), 812(m), 706(s). Anal. found (calcd. for $C_{80.8}H_{85.6}B_2CaCl_{1.6}N_{12}$ (**19-[BPh$_4$]$_2$**·0.8(CH_2Cl_2)): C, 72.27 (72.25); H, 6.47 (6.42); N, 12.52 (12.51) %.

(Tp^{tBu,Me})Ca(BH$_4$)(THF) (20). A suspension of KTp^{tBu,Me} (0.50 g, 1.08 mmol) in THF (30 mL) was added dropwise over 30 mins to a solution of Ca(BH_4)$_2$(THF)$_2$ (0.23 g, 1.08 mmol) in THF (20 mL) at RT. The resulting suspension was stirred for 3 h. The suspension was filtered and the volatiles removed under reduced pressure, leaving a white

residue. This was extracted into benzene (3 x 10 mL) and the volatiles removed under reduced pressure to give a spongy white solid. This was recrystallised from THF:pentane (1:3 v/v) to give **20** as a colorless microcrystalline solid. Yield: 0.37 g (65 %). ^{1}H NMR (C_6D_6, 299.9 MHz, 293 K): 5.68 (3 H, s, $N_2C_3{}^{t}$BuMeH), 3.26 (4 H, m, OCH_2CH_2), 2.19 (9 H, s, $N_2C_3{}^{t}$BuMeH), 1.42 (27 H, s, $N_2C_3{}^{t}$BuMeH), 1.17 (4 H, m, OCH_2CH_2), BH of $Tp^{tBu,Me}$ and BH_4 not observed. ^{13}C{^{1}H} NMR (C_6D_6, 75.5 MHz, 293 K): 163.4 (3-$N_2C_3{}^{t}$BuMeH), 145.3 (5-$N_2C_3{}^{t}$BuMeH), 103.1 (4-$N_2C_3{}^{t}$BuMeH), 68.6 (OCH_2CH_2), 32.2 (CMe_3), 31.5 ($C(Me_3$), 25.5 (OCH_2CH_2), 13.5 ($N_2C_3{}^{t}$BuMeH) ppm. ^{11}B{^{1}H} NMR (C_6D_6, 96.2 MHz, 293 K): -7.9 (B-H of $Tp^{tBu,Me}$), -32.1 (BH_4). IR (NaCl plates, Nujol mull, cm^{-1}): 2558 (s), 2396(s), 2255(m), 2214(s), 1541(s), 1334(s), 1240(s), 1199(s), 1178(s), 1068(s), 1027(s), 705(s). IR (NaCl cell, THF), ν(B-H), cm^{-1}) : 2562 (s, B-H of $Tp^{tBu,Me}$), 2416 (s, B-H_t of BH_4), 2223 and 2174 (s, B-H_b of BH_4 ; 49 cm^{-1} splitting). EI-MS: *m/z* = 478 (80 %), [*M*-THF]$^{+}$. Anal. found (calcd. for $C_{28}H_{52}B_2CaON_6$): C, 60.67 (61.10); H, 9.35 (9.52); N, 14.56 (15.27) %.

($Tp^{tBu,Me}$)Ca(I)(THF) (21). A suspension of $KTp^{tBu,Me}$ (1.46 g, 3.16 mmol) in THF (40 mL) was added dropwise over 30 mins to a suspension of CaI_2 (0.93 g, 3.16 mmol) in THF (20 mL) at RT. The resulting suspension was stirred for 24 h, filtered and the volatiles removed under reduced pressure, leaving a white residue. This was extracted into benzene (3 x 10 mL) and the volatiles were removed under reduced pressure to give a spongy white solid which was recrystallised from THF:pentane (1:3 v/v) to give **21** as a colorless microcrystalline solid. Yield: 1.49 g (71 %). ^{1}H NMR (C_6D_6, 299.9 MHz, 293 K): 5.70 (3 H, s, $N_2C_3{}^{t}$BuMeH), 3.36 (4 H, m, OCH_2CH_2), 2.24 (9 H, s, $N_2C_3{}^{t}$BuMeH), 1.49 (27 H, s, $N_2C_3{}^{t}$BuMeH), 1.19 (4 H, m, OCH_2CH_2), BH of $Tp^{tBu,Me}$ not observed. ^{13}C{^{1}H} NMR (C_6D_6, 75.5 MHz, 293 K): 163.5 (3-$N_2C_3{}^{t}$BuMeH), 145.4 (5-$N_2C_3{}^{t}$BuMeH), 102.8 (4-$N_2C_3{}^{t}$BuMeH), 69.1 (OCH_2CH_2), 32.4 (CMe_3), 32.0 ($C(Me_3$), 25.4 (OCH_2CH_2), 13.4 ($N_2C_3{}^{t}$BuMeH) ppm. ^{11}B{^{1}H} NMR (C_6D_6, 96.2 MHz, 293 K): -8.1 (B-H of $Tp^{tBu,Me}$). IR (NaCl plates, Nujol mull, cm^{-1}): 2558 (s), 1538(s), 1461(m), 1336(m), 1261(m), 1068(s), 1020(s), 867(s), 767(m). EI-MS: *m/z* = 590 (20 %), [*M*-THF]$^{+}$. Anal. found (calcd. for $C_{28}H_{52}B_2CaON_6$): C, 50.57 (50.76); H, 7.25 (7.30); N, 12.50 (12.69) %.

($Tp^{tBu,Me}$)Ca(BD_4)(THF) (20-*d_4*). A suspension of $NaBD_4$ (0.19 g, 4.53 mmol) in acetonitrile (10 mL) was added to a solution of **21** (1.00 g, 1.51 mmol) in acetonitrile (20 mL) at RT. The resulting suspension was stirred for 24 h. The suspension was filtered and the volatiles removed under reduced pressure, leaving a white residue. This was extracted

into benzene (3 x 10 mL) and the volatiles were removed under reduced pressure to give a spongy white solid which was recrystallised from THF:pentane (1:3 v/v) to give **20-*d*** as a colourless microcrystalline solid. Yield: 0.58 g (58 %). ^{1}H NMR (C_6D_6, 299.9 MHz, 293 K): Identical to that for **20.** ^{2}H NMR (C_6H_6, 46.0 MHz, 293 K): 0.23 (br, s, B<u>D</u>$_4$. ^{11}B{^{1}H} NMR (C_6D_6, 96.2 MHz, 293 K): -7.2 (B-H of Tp^{tBu,Me}), -32.0 (BD_4). IR (NaCl cell, THF), ν(B-H or B-D), cm^{-1}) : 2558 (s, B-H of Tp^{tBu,Me}), 1807 (s, B-D$_t$ of BD_4) ; ν_H/ν_D = 1.34, 1543 (s, B-D$_b$ of BD_4); ν_H/ν_D = 1.41, other stretching frequency hidden under subtraction artefact. EI-MS: *m/z* = 553 (10 %) [<u>*M*</u>]$^{+}$.

(Tp^{tBu,Me})Mg(BH$_4$) (22). A suspension of KTp^{tBu,Me} (1.00 g, 2.16 mmol) in THF (30 mL) was added dropwise over 30 mins to a solution of $Mg(BH_4)_2$ (0.12 g, 2.16 mmol) in THF (20 mL) at RT. The resulting suspension was stirred for 24 h, and the volatiles removed under reduced pressure, leaving a white residue. This was extracted into benzene (3 x 10 mL) and the volatiles were removed under reduced pressure to give a white solid which was recrystallised from THF:pentane (1:3 v/v) to give **22** as a colourless microcrystalline solid. Yield: 0.57 g (57 %). ^{1}H NMR (C_6D_6, 299.9 MHz, 293 K): 5.62 (3 H, s, $N_2C_3{}^{t}$BuMe<u>H</u>), 2.04 (9 H, s, $N_2C_3{}^{t}$Bu<u>Me</u>H), 1.51 (4 H, q, B<u>H</u>$_4$, $^{1}J_{BH}$ = 83.4 Hz), 1.45 (27 H, s, $N_2C_3{}^{t}$<u>Bu</u>MeH), BH of Tp^{tBu,Me} not observed. ^{13}C{^{1}H} NMR (C_6D_6, 75.5 MHz, 293 K): 165.3 (3-N_2<u>C</u>$_3{}^{t}$BuMeH), 145.0 (5-N_2<u>C</u>$_3{}^{t}$BuMeH), 104.1 (4-N_2<u>C</u>$_3{}^{t}$BuMeH), 32.1 (<u>C</u>Me$_3$), 31.2 (C(<u>Me</u>$_3$), 13.0 ($N_2C_3{}^{t}$Bu<u>Me</u>H) ppm. ^{11}B{^{1}H} NMR (C_6D_6, 96.2 MHz, 293 K): -8.9 (B-H of Tp^{tBu,Me}), -37.6 (BH_4). IR (NaCl cell, THF), ν(B-H), cm^{-1}) : 2564 (s, B-H of Tp^{tBu,Me}), 2439 (s, B-H$_t$ of BH_4), 2229 and 2174 (s, B-H$_b$ of BH_4 ; 55 cm^{-1} splitting). EI-MS: *m/z* = 449 (10 %), [<u>*M*</u>-BH_3]$^{+}$. Anal. found (calcd. for $C_{24}H_{44}B_2MgN_6$): C, 60.67 (62.32); H, 9.35 (9.59); N, 14.56 (18.17) %.

5.4. Experimental details and characterising data for Chapter Four

[Y{HC(Me$_2$pz)$_3$}(CH$_2$SiMe$_3$)$_2$(THF)][BPh$_4$] (23-BPh$_4$). To cold (-78 °C) solid $Y(CH_2SiMe_3)_3$·$(THF)_2$ (0.50 g, 1.01 mmol) and [NEt$_3$H][BPh$_4$] (0.42 g, 1.01 mmol) at -78 °C, THF (15 mL) at -78 °C was added. To this was added a solution of $HC(Me_2pz)_3$ (0.30 g, 1.01 mmol) in cold (-78 °C) THF (10 mL). The solution was stirred at –78 °C for 1.5 h after which time it was allowed to warm to RT and stirred for another 2 h. The solution was concentrated to *ca*. 2 mL and then pentane (10 mL) added. The supernatant was carefully decanted to leave a yellow oil, which upon drying gave **23-BPh$_4$** as a spongy yellow solid. Yield: 0.75 g (78 %). ^{1}H NMR (CD_2Cl_2, 299.9 MHz, 293 K): 7.78 (1 H, s, <u>H</u>C($N_2C_3Me_2H)_3$), 7.31 (8 H, m, *o*-B($C_6H_5)_4$), 6.99 (8 H, t, ^{3}J = 7.4 Hz, *m*-B($C_6H_5)_4$) 6.86

(4 H, t ^3J = 7.4 Hz, *p*-B(C_6H_5)$_4$), 6.05 (3 H, s, $N_2C_3Me_2\underline{H}$), 3.90 (4 H, m, OC$\underline{H}_2CH_2$), 2.47 (9 H, s, 3-$N_2C_3\underline{Me}_2H$), 2.38 (9 H, s, 5-$N_2C_3\underline{Me}_2H$), 1.95 (4 H, m, $OCH_2C\underline{H}_2$), -0.15 (18 H, s, Si$\underline{Me}_3$), -0.43 (2 H, d, J_{HY} = 2.8 Hz, YCH_2) ppm. $^{13}C\{^1H\}$ NMR (CD_2Cl_2, 75.5 MHz, 293 K): 164.5 (*i*-B(C_6H_5)$_4$) 154.7 (3-$N_2\underline{C}_3Me_2H$), 143.0 (5-$N_2\underline{C}_3Me_2H$), 136.4 (*o*-B(C_6H_5)$_4$), 126.1 (*m*-B(C_6H_5)$_4$), 122.5 (*p*-B(C_6H_5)$_4$), 109.2 (4-$N_2\underline{C}_3Me_2H$), 70.7 (O$\underline{C}H_2CH_2$), 68.5 (H$\underline{C}$($N_2C_3Me_2H$)$_3$), 38.7 (d, J_{CY} = 49 Hz, YCH_2) 26.0 ($OCH_2\underline{C}H_2$), 15.2 (3-$N_2C_3\underline{Me}_2H$), 11.7 (5-$N_2C_3\underline{Me}_2H$), 4.1 ($SiMe_3$) ppm. IR (NaCl plates, Nujol mull, cm^{-1}): 2670 (m), 2407 (s), 1819 (m), 1566 (m), 1305 (m), 1304 (m), 1034 (m), 980 (m), 861 (s). Anal. found (calcd. for $C_{52}H_{72}BN_6OSi_2Y$): C, 65.37 (65.52); H, 7.62 (7.62); N, 8.77 (8.82) %.

[Y{HC(Me$_2$pz)$_3$}(O^{i}Pr)$_2$(THF)][BPh$_4$] (24-BPh$_4$). To a stirring solution of [Y{HC(Me_2pz)$_3$}(CH_2SiMe_3)$_2$(THF)][BPh_4] (0.50g, 0.53 mmol) in CH_2Cl_2 (20 mL) ^{i}PrOH (80 μL, 1.05 mmol) was added. The solution was stirred at RT for 2 h after which time the volatiles were removed under reduced pressure to leave **24-BPh$_4$** as a spongy pale yellow solid. This was dissolved in the minimum amount of THF and then pentane added dropwise until the solution turned cloudy. The minimum amount of THF was then added dropwise until the solution became transparent. The solution was then cooled to -78 ºC, yielding **24-BPh$_4$** as a microcrystalline, off-white solid. Yield: 0.37 g (79 %). ^1H NMR (CD_2Cl_2, 299.9 MHz, 293 K): 7.77 (1 H, s, $\underline{H}C(N_2C_3Me_2H)_3$), 7.24 (8 H, m, *o*-B($C_6H_5$)$_4$), 6.98 (8 H, t, ^3J = 7.5 Hz, *m*-B(C_6H_5)$_4$), 6.83 (4 H, t ^3J = 7.5 Hz, *p*- B($C_6\underline{H}_5$)$_4$), 6.02 (3 H, s, $N_2C_3Me_2\underline{H}$), 4.11 (2 H, sept., ^2J = 6.5 Hz, OC$\underline{H}$(CH_3)$_2$), 3.79 (4 H, m, OC$\underline{H}_2CH_2$), 2.47 (9 H, s, 3-$N_2C_3\underline{Me}_2H$), 2.38 (9 H, s, 5-$N_2C_3\underline{Me}_2H$), 2.09 (4 H, m, $OCH_2C\underline{H}_2$), 1.14 (12 H, d, ^2J = 5.9 Hz, OCH(C$\underline{H}_3$)$_2$) ppm. $^{13}C\{^1H\}$ NMR (CD_2Cl_2, 75.5 MHz, 293 K): 164.8 (*i*-B(C_6H_5)$_4$) 154.2 (3-$N_2\underline{C}_3Me_2H$), 141.4 (3-$N_2\underline{C}_3Me_2H$), 136.0 (*o*-B(C_6H_5)$_4$), 125.7 (*m*-B(C_6H_5)$_4$), 121.8 (*p*-B(C_6H_5)$_4$), 108.1 (4-$N_2\underline{C}_3Me_2H$), 68.3 (O$\underline{C}$H(CH_3)$_2$), 67.1 (H$\underline{C}$($N_2C_3Me_2H$)$_3$), 67.8 (O$\underline{C}H_2CH_2$), 27.5 (OCH($\underline{C}H_3$)$_2$), 25.6 ($OCH_2\underline{C}H_2$), 14.4 (3-$N_2C_3\underline{Me}_2H$), 11.2 (5-$N_2C_3\underline{Me}_2H$). IR (NaCl plates, Nujol Mull, cm^{-1}): 2670 (m), 2410 (s), 1580 (s), 1565 (s), 1099 (m), 1032 (m), 859 (m), 800 (s), 703 (m). Anal. Found (calcd. for $C_{50}H_{64}B_1N_6O_3Y_1$): C, 66.83 (66.93); H, 7.21 (7.20); N, 9.27 (9.37) %.

[Y{HC(Me$_2$pz)$_3$}(CH$_2$SiMe$_3$)(THF)$_3$][BPh$_4$]$_2$ (25-[BPh$_4$]$_2$). To cold (-78 °C) solid $Y(CH_2SiMe_3)_3(THF)_2$ (0.50 g, 1.01 mmol) and [NEt_3H][BPh_4] (0.85 g, 2.02 mmol), THF (15 mL) was added. To this was added a solution of $HC(Me_2pz)_3$ (0.30 g, 1.01 mmol) in cold (-78 °C) THF (10 mL). The solution was stirred at –78 °C for 1.5 h after which time

it was allowed to warm to RT and stirred for another 2 h. The solution was concentrated to *ca*. 2 mL and then pentane (10 mL) added. The supernatant was carefully decanted to leave a yellow oil which, upon drying, gave **25-[BPh_4]$_2$** as a spongy yellow solid. Yield: 1.03 g (77 %). ^{1}H NMR (CD_2Cl_2, 299.9 MHz, 293 K): 7.65 (1 H, s, $\underline{H}C(N_2C_3Me_2H)_3$), 7.33 (16 H, m, *o*-$B(C_6\underline{H}_5)_4$), 6.98 (16 H, t, ^3J = 7.5 Hz, *m*-$B(C_6\underline{H}_5)_4$), 6.83 (8 H, t ^3J = 7.5 Hz, *p*-$B(C_6\underline{H}_5)_4$), 5.96 (3 H, s, $N_2C_3Me_2\underline{H}$), 3.75 (12 H, m, $OC\underline{H}_2CH_2$), 2.24 (9 H, s, 3-$N_2C_3\underline{Me}_2H$), 2.21 (9 H, s, 5-$N_2C_3\underline{Me}_2H$), 1.88 (12 H, m, $OCH_2C\underline{H}_2$), -0.11 (9 H, s, $SiMe_3$), -0.19 (2 H, d, J_{HY} = 2.9 Hz, YCH_2) ppm. $^{13}C\{^1H\}$ NMR (CD_2Cl_2, 75.5 MHz, 293 K): 164.3 (*i*-$B(C_6\underline{H}_5)_4$) 155.1 (3-$N_2\underline{C}_3Me_2H$), 145.4 (5-$N_2\underline{C}_3Me_2H$), 136.8 (*o*-$B(C_6\underline{H}_5)_4$), 126.2 (*m*-$B(C_6\underline{H}_5)_4$), 122.3 (*p*-$B(C_6\underline{H}_5)_4$), 110.1 (4-$N_2\underline{C}_3Me_2H$), 71.3 ($O\underline{C}H_2CH_2$), 68.5 ($H\underline{C}(N_2C_3Me_2H)_3$), 47.8 (d, J_{CY} = 40 Hz, YCH_2), 26.0 ($OCH_2\underline{C}H_2$), 14.6 (3-$N_2C_3\underline{Me}_2H$), 11.7 (5-$N_2C_3\underline{Me}_2H$), 3.9 ($SiMe_3$) ppm. IR (NaCl plates, Nujol mull, cm^{-1}): 2727 (m), 2670 (m), 1943 (s), 1616 (w), 1563 (m), 1302 (m), 1151 (s), 1037 (m), 859 (m), 703 (s), 668 (s). Anal. found (calcd. for $C_{80}H_{97}B_2N_6O_3SiY$): C, 72.75 (72.88); H, 7.38 (7.42); N, 6.27 (6.38) %.

[Y{HC(Me$_2$pz)$_3$}(O^{i}Pr)(THF)$_3$][BPh$_4$]$_2$ (26-[BPh$_4$]$_2$). To a stirring solution of [Y{HC(Me_2pz)$_3$}(CH_2SiMe_3)(THF)$_3$][BPh_4]$_2$ (0.50 g, 0.38 mmol) in CH_2Cl_2 (20 mL), ^{i}PrOH (30 μL, 0.38 mmol) was added. The solution was stirred at RT for 2 hours, after which time the volatiles were removed under reduced pressure to leave **26-[BPh_4]$_2$** as a spongy pale yellow solid. This was dissolved in the minimum amount of THF and pentane added dropwise until the solution turned cloudy. The minimum amount of THF was then added dropwise until the solution became transparent. The solution was then cooled to -78 ^{o}C, yielding **26-[BPh_4]$_2$** as a microcrystalline off-white solid. Yield: 0.33 g (67%). ^{1}H NMR (CD_2Cl_2, 299.9 MHz, 293 K): 7.76 (1 H, s, $\underline{H}C(N_2C_3Me_2H)_3$), 7.33 (16 H, m, *o*-$B(C_6\underline{H}_5)_4$), 6.97 (16 H, t, ^3J = 7.5 Hz, *m*-$B(C_6\underline{H}_5)_4$) 6.81 (8 H, t ^3J = 7.5 Hz, *p*-$B(C_6\underline{H}_5)_4$), 6.02 (3 H, s, $N_2C_3Me_2\underline{H}$), 4.07 (1 H, sept., ^3J = 6.5 Hz, $OC\underline{H}(CH_3)_2$), 3.73 (12 H, m, $OC\underline{H}_2CH_2$), 2.29 (9 H, s, 3-$N_2C_3\underline{Me}_2H$), 2.24 (9 H, s, 5-$N_2C_3\underline{Me}_2H$), 1.89 (12 H, m, $OCH_2C\underline{H}_2$), 1.16 (6 H, d, ^3J = 5.9 Hz, $OCH(C\underline{H}_3)_2$) ppm. $^{13}C\{^1H\}$ NMR (CD_2Cl_2, 75.5 MHz, 293 K): 165.2 (*i*-$B(C_6\underline{H}_5)_4$) 163.9 (3-$N_2\underline{C}_3Me_2H$), 139.5 (5-$N_2\underline{C}_3Me_2H$), 136.8 (*o*-$B(C_6\underline{H}_5)_4$), 129.2 (5-$N_2\underline{C}_3Me_2H$), 126.5 (*m*-$B(C_6\underline{H}_5)_4$), 122.7 (*p*-$B(C_6\underline{H}_5)_4$), 70.3 ($O\underline{C}H(CH_3)_2$), 69.1 ($H\underline{C}(N_2C_3Me_2H)_3$), 67.8 ($O\underline{C}H_2CH_2$), 27.3 ($OCH(\underline{C}H_3)_2$), 26.4 ($OCH_2\underline{C}H_2$), 14.4 (3-$N_2C_3\underline{Me}_2H$), 12.0 (5-$N_2C_3\underline{Me}_2H$). IR (NaCl plates, Nujol mull, cm^{-1}): 2726 (m), 1460 (m), 1304 (m), 1261 (s), 1093 (m), 1018 (m), 799 (s). Anal. found (calcd. for $C_{79}H_{93}B_2N_6O_4Y$): C, 72.83 (72.88); H, 7.09 (7.21); N, 6.51 (6.46) %.

[Y(Me$_3$[9]aneN$_3$)(CH$_2$SiMe$_3$)$_2$(THF)][BPh$_4$] (27-BPh$_4$). To cold (-78 °C) solid Y(CH$_2$SiMe$_3$)$_3$(THF)$_2$ (0.40 g, 0.80 mmol) and [NEt$_3$H][BPh$_4$] (0.34 g, 0.80 mmol), cold (-78 °C) THF (15 mL) was added. To this was added Me$_3$[9]aneN$_3$ (156 μl, 0.800 mmol). The solution was stirred at –78 °C for 1.5 h after which time it was allowed to warm to RT, stirred for another 2 h and concentrated to *ca*. 2 mL. Pentane (10 mL) was added and the supernatant carefully decanted to leave a yellow oil, which, upon drying gave **27-BPh$_4$** as a yellow solid. Yield: 0.47 g (71 %). ^{1}H NMR (CD$_2$Cl$_2$, 299.9 MHz, 293 K): 7.36 (8 H, m, *o*-B(C$_6$H$_5$)$_4$), 7.06 (8 H, t, ^3J = 7.5 Hz, *m*-B(C$_6$H$_5$)$_4$), 6.93 (8 H, t ^3J = 7.5 Hz, *p*-B(C$_6$H$_5$)$_4$), 4.19 (3 H, s, NMe, *trans* to THF), 3.81 (4 H, m, OCH$_2$CH$_2$), 2.53-2.46 (12 H, m, NCH$_2$, 2.40 (6 H, s, NMe, *trans* to CH$_2$SiMe$_3$), 1.92 (4 H, m, OCH$_2$CH$_2$) , -0.02 (18 H, s, SiMe$_3$), -0.76 (4 H, br, s, YCH$_2$) ppm. ^{13}C{^{1}H} NMR (CD$_2$Cl$_2$, 75.5 MHz, 293 K): 164.2 (*i*-B(C$_6$H$_5$)$_4$), 136.3 (*o*-B(C$_6$H$_5$)$_4$), 126.1 (*m*-B(C$_6$H$_5$)$_4$), 122.3 (*p*-B(C$_6$H$_5$)$_4$), 71.2 (OCH$_2$CH$_2$), 47.8 (NMe *trans* to CH$_2$SiMe$_3$), 40.9 (d, J_{CY} = 45 Hz, YCH$_2$), 41.1 ((NMe, *trans* to THF), 25.8 (OCH$_2$CH$_2$), 3.7 (SiMe$_3$) ppm. NCH$_2$ resonances obscured by CD$_2$Cl$_2$. IR (NaCl plates, Nujol mull, cm^{-1}): 1580 (m), 1366 (m), 1304 (m), 1237 (s), 1209 (m), 1003 (m), 862 (s). Anal. found (calcd. for C$_{45}$H$_{71}$B$_1$N$_3$O$_1$Si$_2$Y): C, 65.83 (65.44); H, 8.17 (8.66); N, 5.24 (5.09) %.

[Y(Me$_3$[9]aneN$_3$)(O^{i}Pr)$_2$(THF)][BPh$_4$] (28-BPh$_4$). To a stirring solution of [Y(Me$_3$[9]aneN$_3$)(CH$_2$SiMe$_3$)$_2$(THF)][BPh$_4$] (0.40g, 0.48 mmol) in CH$_2$Cl$_2$ (20 mL), ^{i}PrOH (74 μL, 0.96 mmol) was added. The solution was stirred at RT for 2 h after which time the volatiles were removed under reduced pressure to leave **28-BPh$_4$** as a pale yellow solid. This was dissolved in the minimum amount of THF and pentane added dropwise until the solution turned cloudy. The minimum amount of THF was then added dropwise until the solution became transparent. The solution was then cooled to -78 ºC, yielding **28-BPh$_4$** as a microcrystalline yellow solid. Yield: 0.23 g (62 %). ^{1}H NMR (CD$_2$Cl$_2$, 299.9 MHz, 293 K): 7.38 (8 H, m, *o*-B(C$_6$H$_5$)$_4$), 7.06 (8 H, t, ^3J = 7.5 Hz, *m*-B(C$_6$H$_5$)$_4$), 6.94 (8 H, t ^3J = 7.5 Hz, *p*-B(C$_6$H$_5$)$_4$), 4.07 (2 H, sept., ^3J = 6.7 Hz, OCHMe$_2$), 4.02 (3 H, s, NMe, *trans* to THF), 3.77 (4 H, m, OCH$_2$CH$_2$), 2.56 (6 H, s, NMe, *trans* to CH$_2$SiMe$_3$), 2.28-2.21 (12 H, m, NCH$_2$), 1.88 (4 H, m, OCH$_2$CH$_2$), 1.19 (12 H, d, ^3J = 5.9 Hz, OCHMe$_2$) ppm. ^{13}C{^{1}H} NMR (CD$_2$Cl$_2$, 75.5 MHz, 293 K): 163.8 (*i*-B(C$_6$H$_5$)$_4$), 136.2 (*o*-B(C$_6$H$_5$)$_4$), 126.3 (*m*-B(C$_6$H$_5$)$_4$), 121.8 (*p*-B(C$_6$H$_5$)$_4$), 70.6 (OCH(CH$_3$)$_2$), 69.2 (OCH$_2$CH$_2$), 54.7 (NCH$_3$ *trans* CH$_2$SiMe$_3$), 42.6 ((NCH$_3$, *trans* THF), 26.2 (OCH(CH$_3$)$_2$), 25.8 (OCH$_2$CH$_2$) ppm. NCH$_2$ resonances obscured by CD$_2$Cl$_2$. IR (NaCl plates, Nujol mull, cm^{-1}): 2854 (m), 1457 (m), 1419 (m), 1261 (s), 1063 (m), 1022 (m), 816 (s), 668 (s). Anal. found

(calcd. for $C_{72}H_{92}B_2N_3O_4Y$): C, 63.56 (67.10); H, 6.88 (8.25); N, 4.79 (5.46) %. This was the best of several attempts.

[Y(Me$_3$[9]aneN$_3$)(CH$_2$SiMe$_3$)(THF)$_3$][BPh$_4$]$_2$ (29-[BPh$_4$]$_2$). To cold (-78 °C) solid containing Y(CH$_2$SiMe$_3$)$_3$(THF)$_2$ (0.40 g, 0.80 mmol) and [NEt$_3$H][BPh$_4$] (0.68 g, 1.60 mmol), cold (-78 °C) THF (15 mL) was added, followed by Me$_3$[9]aneN$_3$ (156 μl, 0.800 mmol). The solution was stirred at -78 °C for 1.5 h after which time it was allowed to warm to RT, then stirred for another 2 h. The solution was concentrated to *ca*. 2 mL and then pentane (10 mL) added. The supernatant was carefully decanted to leave a yellow oil, which, upon drying gave **29-[BPh$_4$]$_2$** as an off-whtie solid. Yield: 0.65 g (68 %). ^{1}H NMR (CD$_2$Cl$_2$, 299.9 MHz, 293 K): 7.34 (16 H, m, *o*-B(C$_6$H$_5$)$_4$), 7.05 (16 H, t, ^3J = 7.5 Hz, *m*-B(C$_6$H$_5$)$_4$), 6.90 (8 H, t ^3J = 7.5 Hz, *p*-B(C$_6$H$_5$)$_4$), 4.22 (3 H, s, NMe, *trans* to THF), 3.73 (12 H, m, OCH$_2$CH$_2$), 2.58 (6 H, s, NMe, *trans* to CH$_2$SiMe$_3$), 2.32-2.18 (12 H, m, NCH$_2$, 1.88 (12 H, m, OCH$_2$CH$_2$), -0.05 (9 H, s, SiMe$_3$), -0.78 (4 H, br, s, YCH$_2$) ppm. ^{13}C{^{1}H} NMR (CD$_2$Cl$_2$, 75.5 MHz, 293 K): 164.4 (*i*-B(C$_6$H$_5$)$_4$), 136.3 (*o*-B(C$_6$H$_5$)$_4$), 126.0 (*m*-B(C$_6$H$_5$)$_4$), 122.3 (*p*-B(C$_6$H$_5$)$_4$), 69.1 (OCH$_2$CH$_2$), 51.1 (NMe *trans* to CH$_2$SiMe$_3$), 47.1 (d, J_{CY} = 43 Hz, YCH$_2$), 43.1 ((NMe, *trans* to THF), 25.9 (OCH$_2$CH$_2$), -0.2 (SiMe$_3$) ppm. NCH$_2$ resonances obscured by CD$_2$Cl$_2$. IR (NaCl plates, Nujol mull, cm^{-1}): 1943 (m), 1581 (m), 1307 (m), 1285 (m), 1031 (s), 893 (m), 850 (m), 775 (s). Anal. found (calcd. for $C_{73}H_{96}B_2N_3O_3SiY$): C, 72.98 (72.90); H, 8.00 (8.05); N, 3.57 (3.50) %.

[Y(Me$_3$[9]aneN$_3$)(O^{i}Pr)(THF)$_3$][BPh$_4$]$_2$ (30-[BPh$_4$]$_2$) To a stirring solution of [Y(Me$_3$[9]aneN$_3$)(CH$_2$SiMe$_3$)(THF)$_3$][BPh$_4$]$_2$ (0.60 g, 0.50 mmol) in CH$_2$Cl$_2$ (20 mL), ^{i}PrOH (40 μL, 0.50 mmol) was added. The solution was stirred at RT for 2 h after which time the volatiles were removed under reduced pressure to leave **30-[BPh$_4$]$_2$** as a pale yellow solid. This was dissolved in the minimum amount of THF and pentane added dropwise until the solution turned cloudy. The minimum amount of THF was then added dropwise until the solution became transparent. The solution was then cooled to -80 ºC, yielding **30-[BPh$_4$]$_2$** as a microcrystalline off-white solid. Yield: 0.37 g (63 %). ^{1}H NMR (CD$_2$Cl$_2$, 299.9 MHz, 293 K): 7.29 (16 H, m, *o*-B(C$_6$H$_5$)$_4$), 6.96 (16 H, t, ^3J = 7.5 Hz, *m*-B(C$_6$H$_5$)$_4$), 6.82 (8 H, t ^3J = 7.5 Hz, *p*-B(C$_6$H$_5$)$_4$), 4.11 (1 H, br, m, OCHMe$_2$), 3.99 (3 H, s, NMe, *trans* to THF), 3.68 (12 H, m, OCH$_2$CH$_2$), 2.47 (6 H, s, NMe, *trans* to CH$_2$SiMe$_3$), 2.18 (12 H, m, NCH$_2$), 1.80 (12 H, m, OCH$_2$CH$_2$), 1.09 (6 H, br, m, OCHMe$_2$ ppm. ^{13}C{^{1}H} NMR (CD$_2$Cl$_2$, 75.5 MHz, 293 K): 164.2 (*i*-B(C$_6$H$_5$)$_4$), 136.9 (*o*-B(C$_6$H$_5$)$_4$), 127.7 (*m*-B(C$_6$H$_5$)$_4$), 122.8 (*p*-B(C$_6$H$_5$)$_4$), 70.3 (OCHMe$_2$), 69.4 (OCH$_2$CH$_2$), 54.5 (NMe *trans* to CH$_2$SiMe$_3$), 43.3 (NMe, *trans* to THF), 26.3 (OCHMe$_2$), 25.9 (OCH$_2$CH$_2$) ppm.

$NC\underline{H}_2$ resonances obscured by CD_2Cl_2. IR (NaCl plates, Nujol mull, cm^{-1}): 1942 (m), 1885 (s), 1821 (s), 1650 (s), 1580 (s), 1427 (m), 1286 (s), 1155 (m), 1030 (m), 982 (s), 744 (s), 704 (s). Anal. found (calcd. for $C_{72}H_{92}B_2N_3O_4Y_1$): C, 73.46 (73.62); H, 7.85 (7.90); N, 3.62 (3.58) %.

5.5. Polymerisation procedures for Chapters Two, Three and Four.

General procedure for the polymerisation of ε-CL. A solution of ε-CL (3.3 mmol) in solvent (toluene or THF, 2.0 mL, heated to 70 ºC or at RT) was added to a solution of catalyst (0.033 mmol) in solvent (toluene or THF, 1.4 mL, heated to 70 ºC or at RT). Upon completion, the reaction was quenched by addition of wet THF (5 mL) and an aliquot was taken. The percentage conversion was recorded by ^1H NMR in $CDCl_3$. Isolated yields were obtained by precipitation of polymer from the remaining mixture by addition to hexanes (100 mL) with vigorous stirring. The polymer was filtered and dried to constant weight *in vacuo*.

General procedure for the polymerisation of *rac*-LA. A solution of *rac*-LA (3.00 mmol) in solvent (toluene or THF) (3.0 mL, heated to 70 ºC or at RT) was added to a solution of catalyst (0.03 mmol) in solvent (toluene or THF) (3.0 mL, heated to 70 ºC or at RT). The resultant solution was stirred (at 70 ºC or RT) and aliquots were taken at the respective time intervals. Upon completion of the reaction, wet THF (10 mL) was added and the solution evaporated to dryness to give PLA. Conversions were determined by ^1H NMR integration of the $OC\underline{H}Me$ resonance relative intensities of the residual *rac*-LA and PLA.

Procedure for solution polymerization of *rac*-LA in the presence of co-initiators (Chapter four). *Rac*-LA (3.00 mmol) was dissolved in THF (3.0 mL) and the required amount (e.g. 0.15 mmol for a standard 5 equivalents of co-initiator test) of co-initiator (^iPrOH or $BnNH_2$) was added. This was heated to 70 ºC and was added to a THF solution (3 mL) of catalyst (0.03 mmol) at 70 ºC. The resultant solution was stirred at 70 ºC and aliquots were taken at the respective time intervals. Upon completion of the reaction, wet THF (10 mL) was added and the solution evaporated to dryness to give PLA. Conversions were determined by ^1H NMR integration of the $OC\underline{H}Me$ resonance relative intensities of the residual *rac*-LA and PLA.

5.6. X-ray data collection and processing parameters.

Crystal structure determinations of 1, 2, 4, 5, 6, 7, 9, 10, 12, 15, 16, 17-BPh_4, 18-$[BPh_4]_2$, 19-BPh_4, 20, 21, and 26-$[BPh_4]_2$. Crystal data collection and processing parameters are given in Table **5.0**. In order to avoid degradation, the single crystals were mounted on glass fibres using perfluoropolyether oil and cooled rapidly in a stream of cold N_2 using an Oxford Cryosystems Cryostream unit. Diffraction data were measured using an Enraf-Nonius KappaCCD and graphite-monochromated $Mo_{K\alpha}$ (0.71073 Å) radiation. As appropriate, absorption and decay corrections were applied to the data and equivalent reflections merged.[20] All calculations were performed using SHELXL-97,[21] SIR92[22] or the CRYSTALS program suite.[23] The structures were solved by direct methods and successive interpretation of the difference Fourier maps, followed by full matrix least-squares refinement (against *F*). All non-hydrogen atoms were refined anisotropically. The contribution of the hydrogen atoms, in their calculated positions, was included in the refinement using a riding model. Upon convergence, the final Fourier difference map of the X-ray structures showed no significant peaks.

Table 5.0. X-ray data collection and processing parameters for Mg{C(Me$_2$pz)$_3$}{N(SiMe$_3$)$_2$} (**1**), Mg{κ^2*N*-HC(Me$_2$pz)$_3$}{N(SiHMe$_2$)$_2$}$_2$ (**2**), Ca{C(Me$_2$pz)$_3$}{N(SiMe$_3$)$_2$}(THF) (**4**), Ca{C(Me$_2$pz)$_3$}$_2$ · 2 C$_6$H$_6$ (**5** · 2 C$_6$H$_6$), Zn{C(Me$_2$pz)$_3$}Cl (**6**), Zn{C(Me$_2$pz)$_3$}{N(SiMe$_3$)$_2$} (**7**), Zn{C(Me$_2$pz)$_3$}$_2$ (**9**), Mg{C(Me$_2$pz)$_3$}{C(pz)$_3$} (**10**), HC(4-Etpz)$_3$ (**12**), Mg{HC(^{t}Bu$_2$pz)$_2$SiMe$_2$NPh}N(SiMe$_3$)$_2$ (**15**) and Mg{HC(^{t}Bu$_2$pz)$_2$SiMe$_2$NPh}N(SiHMe$_2$)$_2$ (**16**).

compound	**1**	**2**	**4**	**5**
empirical formula	$C_{22}H_{39}MgN_7Si_2$	$C_{24}H_{50}MgN_8Si_4$	$C_{26}H_{47}CaN_7OSi_2$	$C_{32}H_{42}CaN_{12}\cdot 2C_6H_6$
fw	482.08	587.36	569.96	791.07
temp / K	150	150	150	150
wavelength / Å	0.71073	0.71073	0.71073	0.71073
space group	*P* 2$_1$/*n*	*P* 2$_1$/*n*	*C* 2/*c*	*P* 2$_1$/*c*
a / Å	16.3849(2)	11.3901(3)	39.3059(4)	8.4830(2)
b / Å	24.5357(4)	18.6622(5)	8.599(2)	10.2774(3)
c / Å	16.1402(2)	16.4869(4)	20.6529(8)	24.3896(9)
α / deg	90	90	90	90
β / deg	119.546(1)	104.834(1)	110.691(2)	93.248(1)
γ / deg	90	90	90	90
V / Å^3	5644.8(2)	3387.7(2)	6530(1)	2123.0(1)
Z	8	4	8	2
d (calcd) / Mg·m^{-3}	1.134	1.152	1.159	1.237
abs coeff / mm^{-1}	0.170	0.221	0.295	0.195
R indices: R_1 =	0.0427 [I>3σ(*I*)][a]	0.0464 [I>3σ (*I*)][a]	0.098 [I>2σ (*I*)][a]	0.0583 [I>3σ (*I*)][a]
R_w or w*R*2 =	0.0413 [I>3σ (*I*)][b]	0.0457 [I>3σ (*I*)][b]	0.317 [all data][c]	0.0632 [I>3σ (*I*)][b]

Table 5.0 (Continued)

compound	**6**	**7**	**9**	**10**
empirical formula	$C_{16}H_{21}ClN_6Zn$	$C_{22}H_{39}N_7Si_2Zn$	$C_{32}H_{42}N_{12}Zn$	$C_{26}H_{30}MgN_{12}$
fw	398.22	523.15	660.15	534.91
temp / K	150	200	100	150
wavelength / Å	0.71073	0.71073	0.71073	0.71073
space group	$P\,2_1$	$P\,2_1/n$	$P\,\bar{1}$	$C\,2/m$
a / Å	7.8808(3)	8.065(2)	8.665(2)	35.684(1)
b / Å	17.5757(6)	24.312(5)	9.833(2)	13.3948(4)
c / Å	13.2885(5)	14.299(3)	10.499(2)	8.0750(3)
α / deg	90	90	67.21(3)	90
β / deg	90.282(2)	90.57(3)	86.58(3)	94.313(2)
γ / deg	90	90	81.81(3)	90
V / Å^3	1840.6(1)	2803.4(10)	816.3(3)	3848.7(2)
Z	4	4	1	4
d (calcd) / Mg·m^{-3}	1.437	1.240	1.343	0.923
abs coeff / mm^{-1}	1.489	0.984	0.795	0.075
R indices: R_1 =	0.0703 [I>3σ(I)][a]	0.0748 [I>2σ(I)][a]	0.0278 [I>2σ(I)][a]	0.0787 [I>3σ(I)][a]
R_w or wR2 =	0.0721 [I>3σ(I)][b]	0.2077 [all data][c]	0.0794 [all data][c]	0.0817 [I>3σ(I)][b]

Table 5.0 (Continued)

compound	**12**	**15**	**16**
empirical formula	$C_{16}H_{22}N_6$	$C_{37}H_{68}Mg_1N_6Si_3$	$C_{35}H_{64}Mg_1N_6Si_3 \cdot 0.75C_5H_{12}$
fw	298.39	705.55	731.61
temp / K	150	150	150
wavelength / Å	0.71073	0.71073	0.71703
space group	*P* $2_1/c$	*P* $2_1\ 2_1\ 2_1$	*P* $2_1/c$
a / Å	17.6995(8)	13.9372(2)	19.7490(9)
b / Å	9.3405(3)	15.2750(2)	11.0055(5)
c / Å	9.7378(4)	20.1552(2)	22.6313(10)
α / deg	90	90	90
β / deg	95.4160(10)	90	110.253(2)
γ / deg	90	90	90
V / Å^3	1602.69(11)	4290.85(9)	4614.7(4)
Z	4	4	4
d (calcd) / Mg·m^{-3}	1.237	0.092	1.053
abs coeff / mm^{-1}	0.079	0.157	0.148
R indices: R_1 =	0.0553 [I>2σ(*I*)][a]	0.0357 [I>2σ(*I*)][a]	0.0619 [I>3σ(*I*)][a]
R_w or w*R*2 =	0.0565 I>2σ(*I*)][b]	0.0372 [all data][b]	0.0591 [I>3σ(*I*)][b]

[a] $R_1 = \Sigma||F_o|-|F_c|| / \Sigma|F_o|$; [b] $R_w = \sqrt{\{\Sigma w\ (|F_o|-|F_c|)^2 / \Sigma w|F_o|^2\}}$; [c] $wR2 = \sqrt{\{\Sigma w(F_o^2-F_c^2)^2 / \Sigma w(F_o)^2\}}$

Table 5.1. X-ray data collection and processing parameters for [Ca(BH$_4$)(THF)$_5$][BPh$_4$] (**17-BPh$_4$**), [Ca{HC(3,5-Me$_2$pz)$_3$}$_2$][BPh$_4$]$_2$ (**18-[BPh$_4$]$_2$**), [Ca{HC(3,5-Me$_2$pz)$_3$}(BH$_4$)(THF)$_2$][BPh$_4$] (**19-BPh$_4$**), (Tp^{tBu,Me})Ca(BH$_4$)(THF) (**20**), Tp^{tBu,Me})Ca(I)(THF) (**21**) and [Y{HC(3,5-Me$_2$pz)$_3$}(O^{i}Pr)(THF)$_3$][BPh$_4$]$_2$ (**26-[BPh$_4$]$_2$**).

compound	**17-BPh$_4$**	**18-[BPh$_4$]$_2$**	**19-BPh$_4$**	**20**
empirical formula	$C_{44}H_{64}B_2Ca_1O_5$	$C_{56}H_{64}B_1Ca_1N_{12}$ ·2CH_2Cl_2	$C_{48}H_{62}B_2Ca_1N_6O_2$ ·2C_4H_8O	$C_{28}H_{52}B_2Ca_1N_6O_1$ ·0.5C_5H_{12}
fw	734.69	587.36	960.98	586.54
temp / K	150	150	150	150
wavelength / Å	0.71073	0.71073	0.71073	0.71073
space group	*P* $\bar{1}$	*P* 2$_1$/*n*	*P* $\bar{1}$	*I* 2$_1$/*a*
a / Å	9.6080(2)	11.3901(3)	10.3958(2)	20.9226(3)
b / Å	14.8383(3)	18.6622(5)	15.0936(4)	16.1574(2)
c / Å	15.2496(3)	16.4869(4)	17.5126(4)	21.6436(3)
α / deg	94.1835(10)	90	82.3488(12)	90
β / deg	103.4250(9)	104.834(1)	82.0004(12)	95.5320(8)
γ / deg	92.0870(10)	90	80.4508(7)	90
V / Å^3	2105.85(7)	3387.7(2)	2666.36(11)	7282.65(17)
Z	2	4	2	8
d (calcd) / Mg·m^{-3}	1.159	1.152	1.197	1.070
abs coeff / mm^{-1}	0.191	0.221	0.168	0.202
R indices: R_1 =	0.0723 [I>3σ(*I*)][a]	0.0464 [I>3σ (*I*)][a]	0.0440 [I>3σ (*I*)][a]	0.0571 [I>2σ (*I*)][a]
R_w or w*R*2 =	0.0815 [I>3σ (*I*)][b]	0.0457 [I>3σ (*I*)][b]	0.0464 [all data][c]	0.0639 [I>2σ (*I*)][b]

Table 5.1 (Continued)

compound	**21**	**26-[BPh$_4$]$_2$**
empirical formula	$C_{28}H_{48}B_1Ca_1I_1N_6O_1$	$C_{79}H_{92}B_2N_6O_4Y_1 \cdot 0.75C_4H_8O$
fw	662.52	1354.24
temp / K	150	150
wavelength / Å	0.71073	0.71073
space group	$P\,2_1\,2_1\,2_1$	$P\,\bar{1}$
a / Å	12.2288(3)	18.7867(2)
b / Å	15.6173(4)	20.3526(2)
c / Å	17.3602(5)	22.6804(3)
α / deg	90	111.9457(6)
β / deg	90	107.6075(5)
γ / deg	90	94.1956(7)
V / Å^3	3315.47(15)	7494.82(16)
Z	4	4
d (calcd) / Mg·m^{-3}	1.327	1.200
abs coeff / mm^{-1}	1.150	0.832
R indices: R_1 =	0.0496 [I>2σ(*I*)][a]	0.0651 [I>2σ(*I*)][a]
R_w or w*R*2 =	0.0541 [I>2σ(*I*)][b]	0.0633 [I>2σ(*I*)]][b]

[a] $R_1 = \Sigma||F_o|-|F_c|| / \Sigma|F_o|$; [b] $R_w = \sqrt{\{\Sigma w\,(|F_o|-|F_c|)^2 / \Sigma w|F_o|^2\}}$; [c] $wR2 = \sqrt{\{\Sigma w(F_o^2-F_c^2)^2 / \Sigma w(F_o)^2}$

5.7 References

1. A. Rudin and H. L. W. Hoegy, *J. Polym. Sci. Part A: Polym. Chem.*, 1972, **10**, 217-235.
2. I. Barakat, P. Dubois, R. Jérôme and P. Teyssié, *J. Polym. Sci. Part A: Polym. Chem.*, 1993, **31**, 505-514.
3. J. R. Dorgan, J. Janzen, D. M. Knauss, S. B. Hait, B. R. Limoges and M. H. Hutchinson, *J. Poly. Sci. Part B: Polym. Phys.*, 2005, **43**, 3100-3111.
4. M. Westerhausen, *Inorg. Chem.*, 1991, **30**, 96-101.
5. C. Zapilko, Y. Liang and R. Anwander, *Chem. Mater.*, 2007, **19**, 3171-3176.
6. Y. Sarazin, R. H. Howard, D. L. Hughes, S. M. Humphrey and M. Bochmann, *Dalton Trans.*, 2006, 340-350.
7. H. Bürger, W. Sawodry and U. Wannagat, *J. Organomet. Chem.*, 1965, **3**, 113-120.
8. F. Breher, J. Grunenberg, S. C. Lawrence, P. Mountford and H. Rüegger, *Angew. Chem. Int. Ed.*, 2004, **43**, 2521-2524.
9. D. L. Reger, T. C. Grattan, K. J. Brown, C. A. Little, J. J. S. Lamba, A. L. Rheingold and R. D. Sommer, *J. Organomet. Chem.*, 2000, **607**, 120.
10. D. L. Reger, J. R. Gardinier, T. Christian Grattan, M. R. Smith and M. D. Smith, *New J. Chem.*, 2003, **27**, 1670-1677.
11. F. W. Swamer and C. R. Hauser, *J. Am. Chem. Soc.*, 1950, **72**, 1352-1356.
12. S. Trofimenko, J. C. Calabrese, J. K. Kochi, S. Wolowiec, F. B. Hulsbergen and J. Reedijk, *Inorg. Chem.*, 1992, **31**, 3943-3950.
13. J. Eppinger, E. Herdtweck and R. Anwander, *Polyhedron*, 1998, **17**, 1195-1201.
14. M. F. Lappert and R. Pearce, *J. Chem. Soc., Chem. Commun.*, 1973, 126.
15. *United States Patent; 5, 284, 944 Pat.*, 93-EP15509400439, 1994.
16. D. Robert, M. Kondracka and J. Okuda, *Dalton Trans.*, 2008, 2667-2669.

17. K. O. Saliu, G. H. Maunder, M. J. Ferguson, A. Sella and J. Takats, *Inorg. Chim. Acta*, 2009, **362**, 4616-4622.

18. A. Heath, DPhil thesis and unpublished results, University of Oxford, Oxford, England, 2011.

19. H. Bigmore, J. Meyer, I. Krummenacher, H. Rugger, E. Clot, P. Mountford and F. Breher, *Chem. Eur. J.*, 2008, 5918-5934.

20. Z. Otwinowski and W. Minor, *Processing of X-ray Diffraction Data Collected in Oscillation Mode*, Academic press, New York, 1997.

21. G. M. Sheldrick, *Acta Cryst.Sect. A*, 2008, **64**, 112.

22. A. Altomare, G. Cascarano, G. Giacovazzo, A. Guagliardi, M. C. Burla, G. Polidori and M. Camalli, *J. Appl. Crystallogr.*, 1994, **27**, 435.

23. P. W. Betteridge, J. R. Cooper, R. I. Cooper, K. Prout and D. J. Watkin, *J. Appl. Cryst.*, 2003, **36**, 1487.